NONLINEAR CONVECTION OVER AN INCLINED PLATE IN MICROPOLAR AND POWER-LAW FLUIDS

A THESIS SUBMITTED TO
NATIONAL INSTITUTE OF TECHNOLOGY WARANGAL, (T.S.)
FOR THE AWARD OF THE DEGREE OF
DOCTOR OF PHILOSOPHY
IN
MATHEMATICS

BY
PADIGEPATI NAVEEN
(Roll No. 716050)

UNDER THE SUPERVISION OF
Dr. CH. RAMREDDY

DEPARTMENT OF MATHEMATICS
NATIONAL INSTITUTE OF TECHNOLOGY
WARANGAL-506004, INDIA

MAY 2019

C E R T I F I C A T E

This is to certify that the thesis entitled "**Nonlinear Convection over an Inclined Plate in Micropolar and Power-Law Fluids**" submitted to National Institute of Technology Warangal, for the award of the degree of ***Doctor of Philosophy***, is the bonafide research work done by **Mr. PADIGEPATI NAVEEN** under my supervision. The contents of this thesis have not been submitted elsewhere for the award of any degree.

Dr. Ch. Ramreddy
Assistant Professor
Department of Mathematics
National Institute of Technology Warangal
Telangana State, INDIA

.

DECLARATION

This is to certify that the work presented in the thesis entitled **"Nonlinear Convection over an Inclined Plate in Micropolar and Power-Law Fluids"**, is a bonafide work done by me under the supervision of **Dr. CH. RAMREDDY** and has not been submitted elsewhere for the award of any degree.

I declare that this written submission represents my ideas in my own words and where others' ideas or words have been included, I have adequately cited and referenced the original sources. I also declare that I have adhered to all principles of academic honesty and integrity and have not misrepresented or fabricated or falsified any idea / data / fact /source in my submission. I understand that any violation of the above will be a cause for disciplinary action by the Institute and can also evoke penal action from the sources which have thus not been properly cited or from whom proper permission has not been taken when needed.

Padigepati Naveen

Roll No. 716050

Date:_____

Dedicated to

My Family, My Teachers

&
Sri Venkateshwara Swamy

ACKNOWLEDGEMENTS

It is a rare privilege and boon that I could associate myself for pursuing my research work with Dr. Ch. Ramreddy, Assistant Professor of Mathematics, National Institute of Technology Warangal, India. I sincerely record my gratitude for his invaluable guidance and constant encouragement throughout the preparation of this thesis and his involvement and meticulous supervision while my work was in progress. With his inimitable qualities as a good teacher, he chiseled my path towards perfection. Ever since I met him, he has been a perpetual source of motivation, inspiration, encouragement and enlightenment. He is responsible for making the period of my research work as an educative and enjoyable learning experience. The thesis would not have seen the light of the day without his unrelenting support and cooperation. I deem it a privilege to have worked under his amiable guidance. My vocabulary is inadequate to express my gratitude. I also thank to his wife Smt. Ch. Geetha Ramreddy, for her hospitality and her patience during our elongated discussions.

I am greatly indebted to the dynamic personality Prof. D. Srinivasacharya, Head, Department of Mathematics for his affectionate support, encouragement and for sparing his valuable time in bringing a proper form for presentation of the results in the thesis. It is not an exaggeration to state that without his assistance and suggestions, this thesis would not have taken this form.

I am grateful to Prof. T.K.V. Iyengar (Late), Prof. G. Radhakrishnamacharya (Retd.), Prof. Y. N. Reddy and Prof. K.N.S. Kasi Viswanadham, Department of Mathematics for their help and support throughout my research period.

I take this opportunity to former Heads, Prof. J. V. Ramana Murthy and Prof. Debashis Dutta, Department of Mathematics for providing necessary help and support throughout my research period. Also, I thank all the Faculty members and the office non-teaching staff of the Department of Mathematics, for their help and constant encouragement.

I thank the members of the Doctoral Scrutiny Committee, Prof. D. Srinivasacharya, Dr. J. Pranitha, Department of Mathematics and Prof. V. Suresh Babu, Department of Mechanical Engineering for their valuable suggestions, moral support and encouragement while my work was in progress.

I acknowledge that, this work was supported by of Council of Scientific and Industrial Research (CSIR), New Delhi, India (Project No 25 (0246)/15 /EMR-II).

I place on record my gratitude to Prof. N.V. Ramana Rao, Director, National Institute of Technology, Warangal for his kind support and encouragement at every stage of this endeavor.

I express my sincere thanks to Prof. Y. Pydisetty, Dean(Academic), National Institute of Technology, Warangal and his staff for there valuable support through out my research work.

I owe my special thanks to Dr. K. Kaladhar, Dr. M. Krishna Prasad, Dr. M. Upendar, Dr. O. Surender, Dr. P. Vijay Kumar, Dr. G. Madhava Rao, Dr. K. Hima Bindu, Dr. T. Pradeepa, Dr. Md. Shafeeurrahaman, Dr. P. Jagadeeshwar, Dr. Ch. Venkata Rao, and Dr. G. Venkata Suman, for their support. I thank Mr. I. Sreenath, Mr. K. Sita Ramana, Mr. Abhinava Srivastav and all other research colleagues in the Department of mathematics and my friends, who helped me during my Ph.D. for being cooperative and also for making my stay in the NITW campus fruitful and enjoyable every moment.

My deepest gratitude to my Parents, P. Anjireddy and P. Ramana and in-laws, S. Satyanarayana Reddy and S. Padma, and other family members for their continuous support and constant encouragement over the years.

Last but not least, I would like to thank my better half S. Sindhuja and my innocent daughter P. Raagavarshini for their prayers, patience, encouragement and understanding that were vital to complete this dissertation. I also thank my new born baby for boosting my energy with her cute smiles at the end of my work. All of their love and affection have been motivating force behind what I am today. Without their help and encouragement, I would not have been finished this thesis.

Padigepati Naveen

A B S T R A C T

The prediction of heat or mass transfer characteristics about natural/mixed convection of non-Newtonian fluids (particularly micropolar fluid or power-law fluids) has received considerable attention because of its important applications in engineering. Micropolar fluids are defined as fluids consisting of randomly oriented molecules whose fluid elements undergo translational as well as rotational motions. Further, the micropolar theory is used to characterize the fluid flow pattern of animal blood, polymeric additives, liquid crystals, colloidal suspensions, lubricants, etc. On the other hand, fluids like molten plastics, glues, pulp, slurries, and others are described by the Ostwald-de Waele power-law fluid model. The heat transfer problems in micropolar fluid and power-law fluids subject to the convective boundary condition are more extensive and it occurs in realistic situations. It is relevant here to analyze the effect of of nonlinear convection (also known as, nonlinear Boussinesq approximation) on the convective flow of non-Newtonian fluids in a porous medium. In all mathematical models of a micropolar fluid and power-law fluids, the physical systems become slightly more complicated leading to the complex interactions of the flow, heat, and mass transfer mechanism. An attempt has been made to analyze the nonlinear convective flow of micropolar fluid and power-law fluids over a convectively heated inclined plate saturated porous medium in the presence or absence of cross-diffusion and double dispersion effects.

The thesis consists of FOUR parts and EIGHT chapters. *Part-I* consists of a single chapter (Chapter-1), which provides an introduction to the concepts in a micropolar fluid, power-law fluids, convective boundary condition, porous medium and also gives a review of the pertinent literature. *Part II* consists of three Chapters (i.e., Chapters 2-4) and the significance of nonlinear convective flow over an inclined plate in a micropolar fluid saturated non-Darcy porous medium under the convective boundary condition is considered in Chapter-2 whereas chapter-3 is an extension of chapter-2 in which cross-diffusion effects are considered. Chapters-4 examines the double dispersion and Biot number effects on the nonlinear convective flow of a micropolar fluid over an inclined plate embedded in a non-Darcy porous medium. *Part III* deals with the non-similarity solution of power-law fluid flows over an inclined flat plate embedded in a non-Darcy porous medium subject to the convective boundary condition in the presence or absence of cross-diffusion and double dispersion effects. This part consists of three Chapters (i,e., Chapters 5-7), in which the nonlinear Boussinesq approximation is also taken into consideration to address the heat and mass transfer phenomena of power-law fluids. The final *Part-IV* consists of only one chapter (Chapter - 8) which gives a summary, overall conclusions and scope for future work.

NOMENCLATURE

b	Coefficient of Forchheimer term
Bi	Biot number
$\mathcal{B}$	Buoyancy ratio
C	Concentration
C_f	Skin friction coefficient
C_p	Specific heat capacity
C_s	Concentration susceptibility
C_w	Wall concentration
C_∞	Ambient concentration
d	Pore diameter
D	Molecular solutal diffusivity
Da	Darcy number
Du	Dufour number
D_d	Dispersion solutal diffusivity
D_e	Effective solutal diffusivity
D_c	Solutal dispersion parameter
D_s	Thermal dispersion parameter
f	Dimensionless stream function
Fs	Non-Darcy parameter (Forchheimer number)
g	Dimensionless microrotation
g^*	Gravitational acceleration
Gr	Thermal Grashof number
Gr^*	Modified Grashof number
h_f	Convective heat transfer coefficient
j	Micro-inertia density
k_d	Dispersion thermal conductivity
k_e	Effective thermal conductivity of the medium
k_f	Molecular thermal conductivity
K_p	Permeability
K_T	Thermal diffusion ratio
L	Characteristic length
Le	Diffusivity ratio
M_w	Dimensionless wall couple stress
m_w	Wall couple stress
N	Coupling number
Nu_x	Local Nusselt number
n	Power-law index
Pe	Global Peclet's number
Pr	Prandtl number
Pe_d	Pore diameter-dependent Peclet's number
Ra	Global Rayleigh number

Re	Global Reynold's number
Ri	Mixed convection parameter
Sc	Schmidt number
Sh_x	Local Sherwood number
Sr	Soret number
T	Temperature
T_f	Convective wall temperature
T_m	Mean fluid temperature
T_∞	Ambient temperature
u_∞	Free stream velocity
u, v	Darcy velocity components in the x and y directions

Greek Symbols

α	Molecular thermal diffusivity
α_e	Effective thermal diffusivity
α_1	Nonlinear density-temperature (NDT) parameter
α_2	Nonlinear density-concentration (NDC) parameter
β_0, β_1	First and second order thermal expansion coefficients
β_2, β_3	First and second order solutal expansion coefficients
$\mathcal{J}$	Dimensionless micro-inertia density
η	Similarity variable
γ	Spin-gradient viscosity
ε	Porosity
κ	Vortex viscosity
χ	Thermal dispersion coefficient
λ	Dimensionless spin-gradient viscosity
ω	Component of microrotation
Ω	Angle of inclination
θ	Dimensionless temperature
ϕ	Dimensionless concentration
μ^*	Consistency index of power-law fluid
μ	Dynamic viscosity
ζ	Solutal dispersion coefficient
ν	Kinematic viscosity
ρ	Density of the fluid
ψ	Stream function
τ_w	Wall shear stress
ξ	Stream-wise coordinate

Superscripts

w	Wall condition
∞	Ambient condition

Superscripts

$'$	Differentiation with respect to η

Contents

Certificate i

Declaration ii

Dedication iii

Acknowledgements iv

Abstract vi

Nomenclature vii

I INTRODUCTION 1

1 Preliminaries and Review 2

1.1 Introduction 2

1.2 Porous Medium 4

1.3 Non-Newtonian Fluids 6

1.3.1 Micropolar Fluid 7

1.3.2 Power-law Fluids 8

1.4 Convective Boundary Condition 9

1.5 Solution Procedure 9

1.6 Literature Review 11

1.7 Aim and Scope 15

1.8 Outline of the Thesis 16

II NONLINEAR CONVECTION IN MICROPOLAR FLUID 21

2 Effect of Biot Number in a Non-Darcy Porous Medium Saturated with a Micropolar Fluid [1] 22

2.1 Introduction 22

2.2 Mathematical Formulation 23

2.2.1 Case(a): Natural Convection 26

2.2.2 Case(b): Mixed Convection 46

2.3 Conclusions 62

3 Effect of Cross-Diffusion in a Micropolar Fluid Saturated Non-Darcy Porous Medium with Convective Boundary Condition [2] 63

3.1 Introduction 63

3.2 Mathematical Formulation 64

3.2.1 Case(a): Natural Convection 65

3.2.2 Case(b): Mixed Convection 78

3.3 Conclusions 90

4 Double Dispersion Effects on Nonlinear Convective Flow along an Inclined Plate in a Micropolar Fluid Saturated Non-Darcy Porous Medium [3] 91

4.1 Introduction 91

4.2 Mathematical Formulation 92

4.2.1 Case(a): Natural Convection 93

4.2.2 Case(b): Mixed Convection 105

4.3 Conclusions 117

[1]Case(a): Published in "**Frontiers in Heat and Mass Transfer**" 9(35) (2017) 1–10, Case(b): Published in "**Nonlinear Engineering - Modeling and Application**" 6(2) (2017) 139–152.

[2]Case(a): Published in "**International Journal of Pure and Applied Mathematics**" 113 (8) (2017) 46–53, Case(b): Published in "**Computational Thermal Sciences: An International Journal**" 11(3) (2019) 205–218

[3]Case(a): Published in "**Heat Transfer - Asian Research**" 48 (2019) 414–434, Case(b): Published in "**Engineering Science and Technology, an International Journal**" 21(5) (2018) 984–995.

III NONLINEAR CONVECTION IN POWER-LAW FLUIDS 118

5 Nonlinear Convective Flow of a Power-law Fluid past an Inclined Plate with Convective Boundary Condition [4] 119

5.1 Introduction 119

5.2 Mathematical Formulation 120

5.2.1 Case(a): Natural Convection 123

5.2.2 Case(b): Mixed Convection 135

5.3 Conclusions 146

6 Effects of Biot Number and Cross-Diffusion on Nonlinear Convective Flow of a Power-law Fluid in a Non-Darcy Porous Medium [5] 147

6.1 Introduction 147

6.2 Mathematical Formulation 148

6.2.1 Case(a): Natural Convection 149

6.2.2 Case(b): Mixed Convection 159

6.3 Conclusions 169

7 Effects of Double Dispersion in a Non-Darcy Porous Medium Saturated with a Power-law Fluid subject to Convective Boundary Condition [6] 170

7.1 Introduction 170

7.2 Mathematical Formulation 171

7.2.1 Case(a): Natural Convection 172

7.2.2 Case(b): Mixed Convection 182

7.3 Conclusions 191

[4]Case(a): Published in "**Nonlinear Engineering**" 8(1) (2019) 94–106, Case(b): Published in "**International Journal of Applied and Computational Mathematics**" 4(51) (2018) 1–18.

[5]Case(a): Published in "**Journal of Nanofluids**" 7(4) (2018) 766–775, Case(b): Published in "**Advanced Science, Engineering and Medicine**" 10 (2018) 1–8.

[6]Case(a): Published in "**Journal of Nanofluids**" 7(6) (2018) 1247–1257, Case(b): Accepted by "**4th Thermal and Fluids Engineering Conference (TFEC) April 14–17, 2019 Las Vegas, NV, USA**".

IV SUMMARY AND CONCLUSIONS 192

8 Summary and Conclusions 193

References 198

Part I

INTRODUCTION

Chapter 1

Preliminaries and Review

1.1 Introduction

The science of fluid dynamics encompasses the motion of gases and liquids, the forces that are responsible for this motion and the interaction of the fluid with solids. This field stands central to much of science and engineering and touches almost every aspect of our daily life. Fluid dynamics, one way or other, impact defense, transportation, manufacturing, environment, medicine, energy, etc. From predicting the aerodynamic behavior of moving vehicles to the movement of biological fluids in the human body, the weather predictions, cooling of electronic components, the performance of microfluidic devices, all demand a detailed understanding of the subject of fluid dynamics and substantial research, thereof. Due to the complexity of the subject and breadth of its applications, fluid dynamics is proven to be a highly exciting and challenging subject of modern sciences. The quest for deeper understanding of the subject has not only inspired the development of the subject itself but has also suggested the progress in the supporting areas, such as applied mathematics, numerical computing and experimental techniques. The fundamental axioms of fluid dynamics are the conservation laws namely conservation of mass, Newton's second law of motion (known as conservation of linear momentum) and first law of thermodynamics (known as conservation of energy) which states that energy and mass can neither be created nor destroyed. A large

number of problems in fluid dynamics have claimed the attention of mathematicians, physicists, and engineers for many years. As a result, an enormous body of established results has accumulated steadily but remains scattered in the literature.

Convective heat transfer, or simply, convection is the study of heat transport processes affected by the flow of fluids and has gained significant importance in recent times. The convective mode of heat transfer is generally divided into two basic processes. If the motion of the fluid arises from an external agent, then the process is termed as forced convection. If, on the other hand, no such externally induced flow is provided and the flow arises from the effect of a density difference resulting from temperature variations in a body force field such as the gravitational field, then the process is termed natural or free convection. When both free and forced convection effects are significant and neither of the two can be neglected, the process is called mixed convection. The phenomenon of free and mixed convection occurs in many technical and industrial problems such as cooling of electronic equipment, materials processing, and drilling operations. Apart from these applications, the free convection has also been used to explain the connection between skin disease and respiratory disease such as eczema and asthma respectively whereas the mixed convection has an important role in controlling the temperature of a medium. Both free and mixed convection processes may be divided into external flows over immersed bodies (such as flat plates, cones, cylinders and wires, spheres or other bodies), free boundary flows (such as plumes, jets and wakes), and internal flow in ducts (such as pipes, channels and enclosures).

The involvement and applications of mass transfer process go to a greater length in multiple fields of science, engineering, and technology. The transport of a component in a mixture from a region of high concentration to a region of low concentration is called mass transfer. It is used by different scientific disciplines for different processes and mechanisms. Coupled heat and mass transfer flows constitute a major area of research in modern fluid dynamics. Such flows arise in electronic cooling, drying processes, manufacture of electric cable insulations, curing of plastics, solar energy system, and purification processes. There are two modes of mass transfer: mass transfer by diffusion and convective mass transfer. The transport of mass by random molecular motion in laminar flowing fluids is known as

a mass transfer by diffusion, which occurs due to the concentration gradient, temperature gradient, and hydrostatic pressure difference. The rate of molecular diffusion of mass can be accelerated by the bulk motion of the fluid. Mass can be transported between the boundary of a surface and a moving fluid or between two moving fluids which are relatively inhomogeneous. This mechanism of mass transfer is called convective mass transfer and is analogous to heat transfer by convection (free or forced). For more details on the convective heat and mass transfer, one can refer the text book by Bejan [19].

1.2 Porous Medium

A porous medium may be defined as a solid matrix containing holes either connected or non-connected, dispersed within the medium in a regular or random manner provided such holes occur frequently in the medium. If these pores are saturated with fluid, then the solid matrix with the fluid is called a fluid-saturated porous medium. This type of analysis in porous media plays an essential role in many fields of science and engineering, for instance, petroleum engineering, groundwater hydrology, agricultural engineering, and soil mechanics. But, the flow of the fluid in a porous medium is possible only when some of the pores are interconnected.

To study the motion of fluids through porous media, one must have sufficient understanding of the governing equations for the fluid flow through a porous medium. Owing to the intricate structure of the porous medium, several models have been proposed to explain its mathematical and physical aspects. Among these, the Darcy model and a series of its modifications have attained much acceptance. Further, the boundary layer assumptions have been successfully applied to these models and much work over the last few decades has been done on them for a wide variety of geometries.

Darcy Model

The governing equation of fluid motion in a vertical porous column was first given by Darcy [34] in 1856. It represents a balance of viscous force and pressure gradient. In mathematical

form, it is written as

$$\overrightarrow{q} = -\frac{K_p}{\mu}(\nabla p - \rho\, g^*) \tag{1.1}$$

where $\overrightarrow{q}$ is the space-averaged velocity (also, known as Darcian velocity), K_p is the (intrinsic) permeability of the medium, p is the fluid pressure, ρ is the density, g^* is the acceleration due to gravity and μ is the coefficient of viscosity. For one-dimensional flow and low porosity system, the above law appears to provide good agreement with experimental results. As this model does not take inertial effects into consideration, it is valid only for seepage flows, i.e., for flows with low Reynolds number $[O(Re) < 1]$.

Darcy-Brinkman Model

It is assumed that the flow through an anisotropic porous medium with high permeability must reduce to the viscous flow in a limit. In view of this, Brinkman felt the need to account for the viscous force exerted by a flowing fluid on a dense swarm of spherical particles embedded in a porous mass and added the term $\mu'\,\nabla^2 V$ to balance the pressure gradient. Here μ' is the effective viscosity given by $\mu' = \mu[1 - 2.5(1 - \varepsilon)]$, in which ε is porosity. The validity of the Brinkman model is restricted to the high porosity medium (as confirmed by the experiments) and its governing equation is given by

$$-\left[\nabla p - \rho g^*\right] = \frac{\mu}{K_p}\overrightarrow{q} - \mu'\nabla^2\overrightarrow{q} \tag{1.2}$$

Darcy-Forchheimer Model

In 1901, Forchheimer conducted experiments and proposed that inertial effects can be accounted for by the addition of the square of velocity in the momentum equation. The modification to Darcy′s equation is

$$\left[1 + \frac{\rho\, c\,\sqrt{K_p}}{\mu}|\overrightarrow{q}|\right]\overrightarrow{q} = -\frac{K_p}{\mu}\left[\nabla p - \rho g^*\right] \tag{1.3}$$

where c is the dimensionless form drag coefficient and it varies with the nature of the porous medium. The coefficients of Darcy and Forchheimer terms contain both fluid properties and the microstructure of the porous medium. Several other models are found in the literature related to porous media, and the validity and limitations of these models are well discussed in the textbook by Nield and Bejan [75].

A Newtonian fluid is the fluid which exhibits a viscosity that remains constant regardless of any external stress that is placed upon it, such as mixing or a sudden application of force. One example is water, since it flows the same way, in spite of whether it is left alone or agitated vigorously. Another way to describe these fluids is that they have a linear relationship between viscosity and shear stress. Regardless of the shear stress applied to these fluids, the coefficient of viscosity will not change. Further, Newtonian fluids are those that obey Newtons law relating shear stress and shear rate with a simple material property (the viscosity) dependent on basic thermodynamic variables such as temperature, concentration, and pressure, but independent of flow parameters such as shear rate and time. This can be contrasted with the non-Newtonian fluids, which can become thicker or thinner when stress is applied.

1.3 Non-Newtonian Fluids

A great deal of involvement has been brought forth to illustrate the nonlinear relationship between the rate of strain and stress in non-Newtonian fluid models. But there is no single fluid flow model which undoubtedly exhibits all the properties of real fluids. Therefore, during the last century, several fluid models are proposed to characterize the real fluid behavior. Among these, the micropolar fluid and power-law fluids gained much importance. Micropolar fluid introduced by Eringen [40] has distinct features such as micro inertial effect, the presence of couple stresses, body couples and non-symmetric stress tensor. Whereas, Ostwald-de Waele power-law fluid model is proposed by Ostwald [76] and de Waele [35] and it is one which characterizes the flow pattern of polymer melt, glass, cosmetic products, grease, and much more, and it has substantial applications in many engineering industries such as manufacturing processes, oil reservoir and chemical engineering, etc.

1.3.1 Micropolar Fluid

Micropolar fluid is the subclass of micro-fluids and deal with a class of fluids which exhibit some microscopic effects arising from the local structure and micromotion of the fluid elements. Compared to the classical Newtonian fluids, the flow motion of micropolar fluid is distinguished by two supplementary variables, (i.e.,) the spin vector, responsible for the micro-rotations, and the micro-inertia tensor that describes the distribution of atoms and molecules inside the fluid elements in addition to the velocity vector. Physically, micropolar fluid is the fluid which comprises of rigid randomly oriented (spherical) particles where the deformation of the particles is ignored. Some common examples of micropolar fluid are sediments in rivers, human blood, liquid crystal, drug suspension in pharmacology, plasma, colloidal fluids, etc. These fluids may have immense applications in diverse areas such as engineering sciences, lubrication theory, short waves for heat conducting fluids, etc. A deep monograph to the micropolar fluid theory and its applications has been reported by Ariman *et al.* [8, 9], Lukaszewicz [60] and Eremeyev *et al.* [39].

The governing equations of micropolar fluid are represented in terms of the velocity and the microrotation vectors associated with each particle present in the fluid medium. The microrotation vector explores the rotation in an average sense of the rigid particles centered in a small volume element about the centroid of the element. The governing equations of the an incompressible micropolar fluid [40], are given by

$$\frac{d\rho}{dt} + \rho(\nabla \cdot \overline{q}) = 0 \tag{1.4}$$

$$\rho \, \frac{d\overline{q}}{dt} = \rho\overline{f} - \nabla p + \kappa(\nabla \times \overline{\nu}) - (\mu + \kappa)[\nabla \times (\nabla \times \overline{q})] + (\lambda + 2\mu + \kappa) \, \nabla(\nabla \cdot \overline{q}) \tag{1.5}$$

$$\rho j \, \frac{d\overline{\nu}}{dt} = \rho\overline{l} - 2k\overline{\nu} + \kappa(\nabla \times \overline{q}) - \gamma[\nabla \times (\nabla \times \overline{\nu})] + (\alpha_1 + \beta_1 + \gamma)\nabla(\nabla \cdot \overline{\nu}) \tag{1.6}$$

where $\overline{q}$ is the velocity vector, $\overline{\nu}$ is the microrotation vector, j is the micro-gyration parameter or micro-inertia density of the fluid, $\overline{f}$ is the body force per unit mass, $\overline{l}$ is the body couple per unit mass, κ is the vortex viscosity, γ is the spin-gradient viscosity and t is the time variable. Also, the material constants $\{ \mu, \kappa, \alpha_1 \}$ and $\{\alpha_1, \beta_1, \gamma\}$ denote the viscosity and gyro-viscosity coefficients respectively and satisfy the following inequalities:

$$\kappa \geq 0, \; 2\mu + \kappa \geq 0, \; 3\alpha_1 + \beta_1 + \gamma \geq 0, \; 3\lambda + 2\mu + \kappa \geq 0, \;\; |\gamma| \geq 0, \; \gamma \geq |\beta| \, .$$

The force stress tensor τ_{ij} and the couple stress tensor m_{ij} are respectively given by

$$\tau_{i,j} = (-p + \lambda_1 \ \nabla\overline{q})\,\delta_{ij} + (2\mu + \kappa)\ e_{ij} + \kappa\ \varepsilon_{ijm}\ (\Omega_m - \nu_m) \tag{1.7}$$

and

$$m_{ij} = \alpha_1\ (\nabla\overline{\nu})\ \delta_{ij} + \beta_1\ \overline{\nu}_{i,j} + \gamma\ \overline{\nu}_{j,i} \tag{1.8}$$

where ν_i and $2\Omega_i$ are the components of microrotation and the vorticity vector respectively, δ_{ij} is the Kronecker delta, e_{ij} is the component of the rate of strain, ε_{ijm} is the alternative symbol and comma in suffix represents covariant differentiation. The boundary conditions are treated for microrotation such that there is no relative spin on the boundary, this condition is the generalization of classical no-slip condition to require that the fluid particles nearest to a solid boundary stick to it and neither translating nor rotating.

In the special case where the fluid has constant physical properties, no external body force exists and for the steady-state flow, the conservation equations can be extremely simplified. Apart from the previous case, when $\kappa = \alpha_1 = \beta_1 = \gamma = 0$ and with vanishing $\bar{l}$, the gyration vector disappears and angular momentum equation (1.6) vanishes identically and the equation (1.5) reduces to the classical Navier-Stokes equations. We also noticed that in the case of zero vortex viscosity ($\kappa = 0$) only, the velocity vector $\overline{q}$ and the microrotation vector $\overline{\nu}$ are decoupled and the global motion is unchanged by the microrotation.

1.3.2 Power-law Fluids

A power-law fluid is a type of generalized non-Newtonian fluids for which the shear stress τ_{xy} can be expressed as

$$\tau_{xy} = \mu^* \left|\frac{\partial u}{\partial y}\right|^{n-1} \frac{\partial u}{\partial y} \tag{1.9}$$

Here, μ^* is called the consistency coefficient and n is the power-law index. The dimension of μ^* depends on the value of n which is non-dimensional. When $n = 1$, the equation represents a Newtonian fluid with a dynamic coefficient of viscosity μ^*. Therefore, the deviation of n from unity indicates the degree of deviation from Newtonian behavior. One may interpret the physical behavior of the fluid by appealing to an effective viscosity. For $n > 1$, the fluid is dilatant (e.g., suspensions of sand) or shear-thickening fluids in which apparent viscosity at high shear rates. For

$n < 1$, the fluid is pseudo-plastic (e.g., polymer solutions) or shear-thinning fluids that have a lower apparent viscosity at higher shear rates. Shenoy [91, 92] presented many interesting studies on convective heat transport in non-Newtonian power-law fluids saturated porous media in connection with geothermal and oil reservoir engineering applications.

1.4 Convective Boundary Condition

In the analysis of convective heat transfer problems, a novel mechanism for the heating process (known as Convective Boundary Condition) has drawn the involvement of many researchers (for more details, see Aziz [13]). Because the convective flow of fluids with either wall temperature or heat flux condition cannot explain the supply of heat with a finite heat capacity to the convecting fluid through a bounding surface. Further, the heat transfer with a convective boundary condition is more general and realistic especially with respect to various engineering and industrial processes including material drying, laser pulse heating and transpiration cooling. Also, it occurs when a solid substrate is in contact with a fluid at a different temperature and involves relative motion between the fluid and the substrate. The magnitude of heat exchange is described in terms of Newton's law of cooling, for which the relevant constitutive property of the system is the convective heat transfer coefficient. The convective boundary condition for heat transfer involves equating Fourier's law of conduction at the solid surface with Newton's law of cooling in the fluid, as given below

$$-k_f \frac{\partial T}{\partial y} = h_f (T_f - T) \tag{1.10}$$

where h_f is the convective heat transfer coefficient and k_f is the thermal conductivity of the fluid.

1.5 Solution Procedure

The **r** number of dimensionless coupled nonlinear partial differential equations and their associated boundary conditions are numerically solved using a novel Successive Linearization Method (SLM) [64, 11, 56] together with the local similarity and non-similarity procedures [95, 65]. A brief details of this procedure given in the following steps:

1. First, by following local similarity and non-similarity approaches,

   - Reduce the **r** number of dimensionless coupled nonlinear partial differential equations into a system of nonlinear ordinary differential equations by introducing the auxiliary variables to the partial derivatives of the unknown functions.
   - With these approaches, one can obtain 2**r** number of coupled nonlinear ordinary differential equations that need to be solved simultaneously in conjunction with the set of respective boundary conditions.

2. Next, these resulting 2**r** number of set of nonlinear ordinary differential equations is linearized using the successive linearization. For this,

   - Consider the unknown functions as a combination of i^{th} stage unknown function and sum of the known functions from initial to $(i-1)^{th}$ stage, as given below

   $$\mathbb{Q}(\eta) = \mathbb{Q}_i(\eta) + \sum_{m=0}^{i-1} \mathbb{Q}_m(\eta),\ i = 1, 2, 3...$$

     where $\mathbb{Q}$ is the notation for one of the unknown functions.
   - Choose the initial guesses $\mathbb{Q}_0(\eta)$ in such a way that these satisfy the set of boundary conditions.
   - Linearize the resulting 2**r** coupled nonlinear ordinary differential equations successively by substituting the above assumed unknown functions and neglecting the nonlinear terms containing $\mathbb{Q}_i(\eta)$ $(i \geq 1)$ and its derivatives to obtain set of linearized equations.

3. Later, use the Chebyshev spectral collocation method [21] to solve the system of 2**r** linearized equations which are obtained in the previous step. In this method, we use the following steps:

   - The transformation $\dfrac{\eta}{S} = \dfrac{\tau + 1}{2}$, $-1 \leq \tau \leq 1$, is used to transform the domain $[0, S]$.
   - Discretized the transformed domain $[-1, 1]$ using the Gauss-Lobatto collocation points.
   - Approximate the unknown functions and its derivatives in terms of Chebyshev polynomials $T_w(\tau) = \cos[w\ \cos^{-1}\tau]$ at the collocation points.
   - Substitute these expressions in the system of linearized differential equations to obtain the matrix system.

4. Finally, solve the resultant matrix system iteratively by starting with the initial approximations $\mathbb{Q}_0(\eta)$.

1.6 Literature Review

The study of free and mixed convection due to a heated or cooled vertical surface provides one of the basic scenarios for heat and mass transfer theory and thus, is of considerable theoretical and practical interest. Free convection of heat and mass transfer occurs simultaneously in the fields of design of chemical processing equipment, formation and dispersion of fog, distributions of temperature, moisture over agricultural fields and groves of fruit trees. It also occurs in the context of damage to crops due to freezing and pollution of the environment. The phenomenon of mixed convection occurs in many technical and industrial problems such as electronic devices cooled by fans, nuclear reactors cooled during an emergency shutdown, a heat exchanger placed in a low-velocity environment, solar collectors, and so on.

Convective flow along a vertical surface embedded in a porous medium is one of the fundamental and classical problems in the heat and mass transfer theory. It has attracted a great deal of interest from many investigators owing to the broad applications such as geothermal systems, energy-storage units, heat insulation, heat exchangers, drying technology, catalytic reactors, nuclear waste repositories, etc. The literature relevant to the convective flows over different surface geometries in Darcy and non-Darcy porous media has been reported by Ingham and Pop [47], Nield and Bejan [75] and Vafai [105] (also see the citations therein).

Heat transfer analysis with convective thermal boundary condition is an essential and useful consideration in the gas turbines, nuclear plants and heat exchangers related industries due to its realistic nature. Also, it occurs when a solid substrate is in contact with the fluid at a different temperature and involves relative motion between the fluid and the substrate. In many practical applications involving cooling or heating of the surface, the presence of convective heat exchange between the surface and the surrounding fluid cannot be neglected, and this is a very crucial aspect in thermal materials processing industries. In this mechanism, heat is supplied to the convecting fluid through a bounding surface with a finite heat capacity, which provides a convective heat transfer coefficient. To address some of these applications, Makinde and Aziz [62] considered the

convective thermal boundary condition for the analysis of magnetohydrodynamics cold fluid flow along a vertical surface, whereas Hayat *et al.* [43] analyzed the effect of thermal radiation on the stagnation point flow over a moving surface subject to the convective boundary condition. Influence of magnetic field under the convective thermal condition has been analyzed by Murthy *et al.* [68] for a thermally stratified nanofluid flow over a vertical surface in a non-Darcy porous medium. Sivasankaran *et al.* [94] examined the effects of chemical reaction, heat generation/absorption and radiation on the magnetohydrodynamic flow near a stagnation point in the presence of convective boundary condition and slip effects.

Several investigators have shown much attention to non-Newtonian fluids in view of their applications in various aspects of industrial processing, the design of equipment, chemical and allied processes such as cosmetics, synthetic polymers, biological fluids, synthetic lubricants etc. These fluids reveal complex rheological nature which is not accomplished by Newtonian fluids. Among the non-Newtonian fluids, the micropolar fluid is the one which takes care of the rotation of fluid particles by means of independent kinematic vector known as the microrotation vector. The subject of free and mixed convective boundary layer flow of a micropolar fluid has been keyed out by several investigators due to its immense applications in many engineering problems such as solar energy collecting devices, air conditioning of a room, material processing, passive cooling of nuclear reactors etc. The boundary layer flow over a semi-infinite flat plate is considered for a deep understanding of the micropolar fluid theory and its application to low concentration suspension flow by Ahmadi [3]. Jena and Mathur [48] analyzed the mixed convection over an isothermal vertical plate in a micropolar fluid and this work extended by the Wang [107] with the addition of wall conduction. Hayat *et al.* [41] presented the laminar mixed convective flow of micropolar fluid along a stretching sheet, whereas the influences of thermal stratification and uniform heat flux on the natural convective flow of micrpolar fluid along a vertical plate have been discussed by Chang and Lee [24]. Srinivasacharya and RamReddy [98] analyzed the effect of double stratification on mixed convective flow of an incompressible micropolar fluid along a vertical plate and pointed out some useful results. In recent times, the influences of Joule heating and thermal radiation on MHD micropolar fluid have been discussed by Ramzan *et al.* [84] by taking the partial slip and convective boundary conditions into account.

On the other hand, non-Newtonian power-law fluids are so widespread in industrial processes and in the environment that it would be no exaggeration to affirm that Newtonian shear flows

are the exceptions rather than the rule. Combined free and forced convective flows of power-law fluid-saturated porous medium has been studied by Nakayama and Shenoy [72]. Non-Darcy mixed convective flow of power-law fluids over an isothermal vertical plate with suction/injection effects has been examined by Ibrahim *et al.* [46]. Kumari and Nath [58] studied power-law fluid flow along a horizontal impermeable surface with variable surface temperature. Free convection from a cone/flat plate in a non-Darcy porous medium saturated by the power-law fluid, has been analyzed by Kairi and Murthy [52]. Further, Srinivasacharya and Reddy [100] discussed the importance of chemical reaction and radiation on the power-law fluid flow along a vertical plate embedded in a porous medium with the variable temperature and concentration wall conditions.

The analysis of convective flows over various geometries in non-Newtonian fluids in a porous medium, has been provided because of its emerging applications in discrete aspects of engineering, science and industry like solar energy collecting devices, air conditioning of a room, material processing, cooling of molten metals and so on. Fluid flow, heat and mass transfer along an inclined surface embedded in a porous medium with different boundary conditions is one of the thrust areas of research in engineering. However, free/mixed convection along an inclined surface has received less attention than the cases of vertical and horizontal plates. This concept has a wide range of applications in the ash or scrubber waste treatment, chemical processing, electrical systems, brine clarification, iron removal, food and dairy processing, coal and other mineral separation. Due to this importance, Cheng [32] discussed the combined free and forced convective boundary-layer flow along inclined surfaces embedded in porous media, whereas free convection from an arbitrary inclined isothermal plate embedded in a porous medium has been presented by Pop and Na [80]. Chamkha *et al.* [23] analyzed the influences of the external magnetic field and internal heat generation or absorption effects on the convective flow along an inclined plate. Numerical simulations are performed by Rahman *et al.* [81] to investigate the effects of the non-uniform heat source (or sink) and the fluid electric conductivity on the convective flow of micropolar fluid flow along an inclined flat plate. Further, Murthy *et al.* [70] discussed the double-diffusive convective flow of a nanofluid past an inclined plate in a non-Darcy porous medium.

The Soret effect (thermal diffusion), the existence of a diffusion flux in view of a temperature gradient, becomes very noteworthy when the thermal gradient is very large. The energy flux caused by a concentration gradient is termed as the Dufour effect (diffusion-thermo). Generally, these effects are considered as a second-order phenomenon and may become significant in areas

such as petrology, hydrology, geosciences, etc. Eckert and Drake [37] recognized many instances when the importance of these effects cannot be neglected. Significance of cross-diffusion effects is examined by Dursunkaya and Worek [36] for the transient and steady natural convection over a vertical surface, whereas Alam and Rahman [5] studied the same effects with variable suction on mixed convective flow past the vertical porous plate. Beg *et al.* [16] obtained a numerical solution to investigate the influence of Soret and Dufour effects on the mixed convective flow of micropolar fluid in a Darcy-Forchheimer porous medium. Tai and Char [103] employed the differential quadrature method to examine the thermal radiation and cross-diffusion effects on the free convective flow of a power-law fluid in a porous medium. Very recently, Reddy and Krishna [87] discussed micropolar fluid flow towards a linearly stretching sheet in the presence of Soret and Dufour effects along with the thermal radiation.

The double dispersion effects are more important in the flow region of a porous medium under the condition that the inertial effects are not negligible (refer Nield and Bejan [75] and citations therein). The double dispersion plays an important role in a steady fluid flow due to the combined action of convection and molecular diffusion, and this concept helps to explain the differences often observed between transport parameters measured along and across the principal directions of the fluid flow over the considered geometries. The development of double dispersion has been mainly related to miscible displacement and solute spreading in porous media. These kinds of effects have notable importance in many engineering areas such as ceramic processing, oil reservoir, heat storage beds, etc. In irregular geometries, especially in the packed beds, the transportation of fluid through tortuous paths will lead to double dispersion effects at the pore level of porous media. With this consideration, many authors to point out few, Murthy [67], Kairi and Murthy [51], have exhibited the significance of double dispersion on the characteristics of the fluid flow through a porous medium.

From the literature, it seems that the Boussinesq approximation is applicable for some flows in which the temperature and concentration gradients vary a little. Therefore, the density variation is less and the buoyancy drives the motion. In this approximation, the density is considered as constant everywhere except in the buoyancy force term. When the temperature and concentration differences between ambient fluid and inclined surface are appreciably large, the mathematical model developed by using a linear density relation becomes more inaccurate. For instant, some of the thermal systems, e.g., areas of reactor safety, combustion, solar collectors, layered porous media

of high thermal conductivity architecture (metallic foams and sponges), are operated at moderate and very high temperatures. In such special cases, the temperature-concentration-dependent relation becomes nonlinear. Also, the heat produced by the viscous dissipation and inertia, or the presence of different densities are other reasons for the nonlinear density-temperature-concentration relationship. This nonlinear variation in temperature-concentration-dependent density relation (to be specific, nonlinear Boussinesq approximation or nonlinear convection) gives a strong influence to the fluid flow characteristics (for more details, one can see the works of Barrow and Sitharamarao [15], Vajravelu and Sastri [106]). Partha [79] examined the effects of cross-diffusion and double dispersion with the nonlinear convection to the viscous fluid flow, whereas this work has been extended by Kameswaran *et al.* [54] in which thermophoretic effect is discussed in the absence of cross-diffusion effects. Nonlinear convection over an impulsive stretching sheet has been examined numerically by Motsa *et al.* [66] (and also see the citations therein).

This limited literature shows that the analysis of micropolar fluid or power-law fluids flow over an inclined plate in a porous medium under different conditions has not received significant attention so far. Also, it seems that the similarity solution does not exist for this kind of complex fluid flow problems by using either Lie scaling group or other transformations. Hence, one has to use appropriate non-dimensional transformations to find an approximate solution of the governing partial differential equations.

Owing to the important applications of the micropolar fluid or power-law fluids saturated porous medium, the convective flow over an inclined plate has been analyzed in this thesis. In addition, the nonlinear Boussinesq approximation and convective boundary condition are incorporated into the analysis. The problems that we studied are outlined in the next section.

1.7 Aim and Scope

The objective of the present thesis is to study the influence of nonlinear Boussinesq approximation, double dispersion, Soret and Dufour effects on the free and mixed convective flows along an inclined plate in a micropolar fluid or power-law fluids saturated non-Darcy porous medium in the presence of convective boundary condition. This study focuses on the attributes of various effects such as nonlinear convection parameters, Soret and Dufour numbers, Darcy and non-Darcy (Forchheimer)

numbers, Biot number, thermal and solutal dispersion parameters. The problems considered in this thesis deal with a semi-infinite inclined flat plate for the two cases: (i) free convection, (ii) mixed convection.

1.8 Outline of the Thesis

This thesis is arranged in four parts with a total of eight chapters.

Part I consists of single Chapter (i.e., Chapter-1). It is introductory in nature and gives motivation to the investigations carried out in the thesis. A survey of pertinent literature is presented here to show the significance of the problems considered. The equations which govern the flow, heat and mass transfers of a micropolar and power-law fluids along with the details of numerical procedure (viz., local similarity and non-similarity technique, and successive linearisation method) are given in this chapter.

Part II presents the boundary layer analysis to study the effects of cross-diffusion, thermal and solutal dispersion on the nonlinear convective flow of a micropolar fluid along an inclined plate embedded in a non-Darcy porous medium with convective boundary condition. This part consists of three Chapters (i.e., Chapters 2-4). The details of these chapters are given below.

In Chapter-2, a mathematical model is presented to investigate the nonlinear variation in temperature-concentration-dependent density relation on the free and mixed convective flows of a micropolar fluid over an inclined flat plate in a non-Darcy porous medium in the presence of convective boundary condition. The effects of the angle of inclination, Biot number, nonlinear convection, non-Darcy and micropolar parameters on the fluid flow, heat and mass transfer rates are exhibited graphically. Further, the skin friction and wall couple stress are presented quantitatively for the above-said parameters.

The combined effects of diffusion-thermal and thermal-diffusion on the free and mixed convective flows along an inclined plate in a non-Darcy porous medium saturated by a micropolar fluid subject to the convective boundary condition, are examined in Chapter-3. The effects of physical parameters on the velocity, microrotation, temperature, concentration, skin friction, wall couple stress, heat and mass transfer rates along an inclined plate are given and the salient features are

discussed.

In Chapter-4, the significance of Biot number and double dispersion effects on the natural and mixed convective flows of an incompressible micropolar fluid saturated non-Darcy porous medium in the presence of nonlinear Boussinesq approximation, is analyzed. The effects of various parameters on the velocity, microrotation, temperature, concentration, skin friction, wall couple stress, heat and mass transfer rates are presented through graphs.

Part III deals with the non-similarity solution of an Ostwald-de Waele power-law fluid flow over an inclined flat plate in a non-Darcy porous medium subject to the convective boundary condition in the presence or absence of cross-diffusion and double dispersion effects. This part consists of three Chapters (i,e., Chapters 5-7), in which the nonlinear Boussinesq approximation (known as the nonlinear convection) is also taken into consideration to address the heat and mass transfer phenomena of power-law fluids. The details of these chapters are given below:

Chapter-5 discusses the significance of nonlinear Boussinesq approximation on the free and mixed convective flows of Ostwald-de Waele power-law fluids along an inclined plate in a non-Darcy porous medium in the presence of convective thermal boundary condition. This numerical study explores the impact of pertinent parameters on the fluid flow characteristics through graphs and the salient features are discussed in detail.

The non-similarity solution for the nonlinear convective flow of non-Newtonian power-law fluids along an inclined plate in a non-Darcy porous medium, is obtained in Chapter-6. In addition, the convective thermal boundary condition, diffusion-thermal and thermal-diffusion effects are taken into account. The effects of the angle of inclination, Soret number, Dufour number, Biot number and nonlinear convection parameters on the velocity, temperature and concentration profiles are presented graphically for all three kinds of fluids (pseudo-plastic, Newtonian and dilatant fluids). Moreover, the non-dimensional Nusselt and Sherwood numbers against stream-wise coordinate for various values of the pertinent parameters are also analyzed through graphs.

In Chapter-7, an attempt has been made to study the effects of thermal and solutal dispersion on free and mixed convective flows of Ostwald-de Waele power-law fluids over an inclined plate embedded in a non-Darcy porous medium subject to the convective boundary condition, are discussed. Additionally, the nonlinear Boussinesq approximation is incorporated in the momentum equation. The effects of various parameters, namely thermal dispersion, solutal dispersion, Biot

number, nonlinear convective parameters and power-law index on physical quantities of the flow are explored in detail and some interesting results have been obtained.

In all the above chapters (i.e., Chapter-2 to Chapter-7), the nonlinear governing partial differential equations and their associated boundary conditions are initially cast into dimensionless forms by using suitable non-similarity transformations. First, the resultant system of nonlinear partial differential equations is transformed into system of nonlinear ordinary differential equations using local similarity and non-similarity approaches. Next, the obtained system of nonlinear ordinary differential equations are converted into an iterative sequence of linearized ordinary differential equations by using successive linearization procedure. Finally, the Chebyshev collocation method is used to solve the resultant iterative sequence of linearized ordinary differential equations. In order to check the accuracy and validity of these problems, the obtained results are compared against previously published work wherever possible on special cases and are found to be in good agreement.

Lastly, *Part IV* consists of a single Chapter (i.e., Chapter-8). The main conclusions of the earlier chapters are recorded and the directions in which further investigations may be carried out, are indicated in this chapter.

List of references is given at the end of the thesis. The references are arranged in alphabetical order and according to this order, citations appear in the text. In the individual Chapters, in some of the Chapters, details which are already presented in the earlier Chapters are avoided. As a review of the existing literature is presented in the introductory Chapter itself, in each of the Chapters only a brief introduction to the concerned problem is given. Also, the physical meaning of the various parameters is given in the Chapters repeatedly for the easy readability of readers.

All problems undertaken in the present thesis are published/accepted for publication in the reputed journals. The details are presented below:

List of papers published

1. "Quadratic Convective Flow of a Micropolar Fluid along an Inclined Plate in a Non-Darcy Porous Medium with Convective Boundary Condition", *Nonlinear Engineering–Modeling and Application*, Vol.6(2) (2017), pp. 139–152.

2. "Nonlinear Convective Transport along an Inclined Plate in Non-Darcy Porous Medium Saturated by a Micropolar Fluid with Convective Boundary Condition", *Frontiers in Heat and Mass Transfer*, Vol.9(35) (2017), pp. 1–10.

3. "Cross-Diffusion Effects on Nonlinear Convective Flow of Micropolar Fluid under Convective Boundary Condition: A Darcy-Forchheimer Model", *International Journal of Pure and Applied Mathematics*, Vol.113 (8) (2017), pp. 46–53.

4. "Nonlinear Convective Flow of Non-Newtonian Fluid over an Inclined Plate with Convective Surface Condition: A Darcy-Forchheimer Model", *International Journal of Applied and Computational Mathematics*, Vol.4(51) (2018), pp. 1–18.

5. "Non-Linear Boussinesq Approximation and Cross-Diffusion Effects on an Ostwald-de-Waele Power-Law Fluid Flow with Convective Boundary Condition", *Advanced Science, Engineering and Medicine*, Vol.10 (2018), pp. 1–8.

6. "Nonlinear Boussinesq Approximation in an Ostwald-de-Waele Power-law Fluid subject to Cross-Diffusion Effects and Convective Thermal Condition", *Journal of Nanofluids*, Vol.7 (2018), pp. 766–775.

7. "Effects of Nonlinear Boussinesq Approximation and Double Dispersion on Free Convective Flow of an Ostwald-de Waele Power-Law Fluid Along an Inclined Plate Under Convective Thermal Condition", *Journal of Nanofluids*, Vol.7(6) (2018), pp. 1247–1257.

8. "Double Dispersion Effect on Nonlinear Convective Flow over an Inclined Plate in a Micropolar Fluid saturated non-Darcy Porous Medium", *Engineering Science And Technology, An International Journal*, Vol.21(5) (2018), pp. 984–995.

9. "Effects of Nonlinear Boussinesq Approximation and Double Dispersion on a Micropolar Fluid Flow under Convective Thermal Condition", *Heat TransferAsian Research*, Vol.48(1) (2019), pp. 414–434.

10. "Effects of Nonlinear Convection and Cross-Diffusion for the Flow of Darcy-Forchheimer Model Micropolar Fluid with Convective Boundary Condition", *Computational Thermal Sciences: An International Journal*, Vol.11(3) (2019), pp. 205–218.

11. "Influence of Non-linear Boussinesq Approximation on Natural Convective Flow of a Power-Law Fluid along an Inclined Plate under Convective Thermal Boundary Condition", *Nonlinear Engineering - Modeling and Application*, Vol.8(1) (2019), pp. 94–106.

List of papers accepted

1. "Double Dispersion and Nonlinear Boussinesq Approximation in an Ostwald-de Waele Power-law Fluid Flow subject to Convective Thermal Condition", This paper is accepted for oral presentation and proceedings of the "4^{th} Thermal and Fluids Engineering Conference (TFEC)" to be held 14^{th}–17^{th} April 2019, at Las Vegas, NV, USA.

Part II

NONLINEAR CONVECTION IN MICROPOLAR FLUID

Chapter 2

Effect of Biot Number in a Non-Darcy Porous Medium Saturated with a Micropolar Fluid [1]

2.1 Introduction

One of the best established theories of fluids with microstructure is the theory of micropolar fluids. The micropolar fluids may be treated as non-Newtonian fluids consisting of dumbbell molecules or rigid cylindrical elements. The analysis of free and/or mixed convection in a micropolar fluid saturated porous medium has received a considerable interest from theoretical and practical point of view. Several authors, to mention few, Rawat *et al.* [85], Shafie [88] and Srinivasacharya and RamReddy [97], examined the heat and mass transfer characteristics of micropolar fluid in a non-Darcy porous medium.

Convective boundary condition plays a vital role in the mechanism of supplying heat to the convecting fluid through a bounding surface with a finite heat capacity. It is because of its universal and realistic nature particularly in diverse technologies and industrial operations such as transpiration cooling process, textile drying, laser pulse heating etc. In view of these applications,

[1] Case(a): Published in "**Frontiers in Heat and Mass Transfer**" 9(35) (2017) 1–10, Case(b): Published in "**Nonlinear Engineering - Modeling and Application**" 6(2) (2017) 139–152.

Yacob and Ishak [108] investigated the stagnation point flow towards a stretching/shrinking sheet immersed in a micropolar fluid with the convective boundary condition. In recent times, the influence of homogeneous-heterogeneous reactions on convective heat flow of a micropolar fluid along a vertical plate in a porous medium under the convective boundary condition, has been discussed by Ramreddy *et al.* [83] (also refer the references given therein).

The concept of nonlinear convection in the study of boundary layer fluid flow problems is of great importance in a variety of disciplines such as astrophysics, geophysics, geothermal and engineering applications. Mallikarjuna *et al.* [14] analyzed the effect of thermophoresis on the viscous fluid flow past a rotating cone in the presence of nonlinear convection. Recently, the effect of nonlinear thermal convection on the boundary layer flow of a micropolar fluid over a vertical plate subject to the convective boundary condition, has been investigated by RamReddy and Pradeepa [82].

From the literature survey, it seems that the problem of nonlinear convection along an inclined plate in a micropolar fluid with the convective boundary condition has not been investigated so far. Hence, the aim of the present chapter is to analyze the effect of nonlinear convective flow of a micropolar fluid along an inclined plate in a non-Dacy porous medium with the convective boundary condition. But, this type of mathematical modeling becomes slightly more complicated leading to the complex interactions in flow, heat and mass transfer mechanisms. The governing system of nonlinear partial differential equations is transformed to a set of nonlinear ordinary differential equations by local similarity and non-similarity procedures and then the successive linearization method is used to solve the resulting boundary value problem. Also, the influences of important parameters on the physical quantities of the flow, heat and mass transfer rates are analyzed under different flow situations.

2.2 Mathematical Formulation

Consider the steady, laminar and two-dimensional flow of an incompressible micropolar fluid along a semi-infinite inclined flat plate in a non-Darcy porous medium. Choose the coordinate system such that the x-axis is along the plate and y-axis is normal to the plate. The semi-infinite plate is inclined about vertical direction with an acute angle Ω as depicted in Fig.(2.1). In the figure, **M.B.L** is used to represent the momentum boundary layer, while **T.B.L** and **C.B.L** are used to

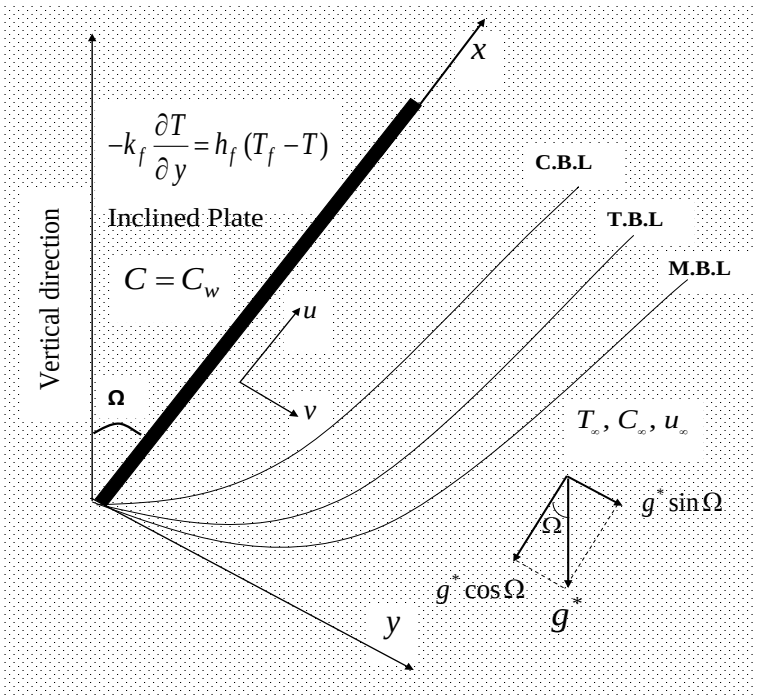

Figure 2.1: *Physical model and coordinate system.*

represent the thermal and concentration boundary layers respectively. The velocity of the outer flow is assumed to be u_∞ whereas the free stream temperature and concentration are taken as T_∞ and C_∞ respectively. The plate is either heated or cooled from a flow field of temperature T_f to the left by convection with $T_f > T_\infty$ relating to a heated surface (assisting flow) and $T_f < T_\infty$ relating to a cooled surface (opposing flow) respectively. On the wall, the solutal concentration is taken to be C_w which is a constant quantity. The porous medium is taken to be uniform with a constant permeability and porosity, and is saturated by a micropolar fluid which is in the local thermodynamic equilibrium with the solid matrix. Further, the temperature difference and concentration difference between the surface of the plate and the ambient fluid are assumed to be significantly larger. Hence, the linear Boussinesq approximation becomes inaccurate in the present analysis.

Under the consideration of usual boundary layer assumptions together with the nonlinear Boussinesq approximation, the governing equations for the micropolar fluid flow in an isotropic and homogeneous non-Darcy (Darcy-Forchheimer model) porous medium can be represented as

$$\frac{\partial u}{\partial x} + \frac{\partial v}{\partial y} = 0 \tag{2.1}$$

$$\frac{\rho}{\varepsilon^2}\left(u\frac{\partial u}{\partial x}+v\frac{\partial u}{\partial y}\right)=\frac{1}{\varepsilon}\left(\mu+\kappa\right)\frac{\partial^2 u}{\partial y^2}+\kappa\frac{\partial \omega}{\partial y}+\frac{\mu}{K_p}(u_\infty-u)+\frac{\rho\, b}{K_p}(u_\infty^2-u^2)$$
$$+\rho g^*\left[\beta_0\left(T-T_\infty\right)+\beta_1\left(T-T_\infty\right)^2+\beta_2\left(C-C_\infty\right)+\beta_3\left(C-C_\infty\right)^2\right]\cos\Omega \tag{2.2}$$

$$\frac{\rho j}{\varepsilon}\left(u\frac{\partial \omega}{\partial x}+v\frac{\partial \omega}{\partial y}\right)=\gamma\frac{\partial^2 \omega}{\partial y^2}-\kappa\left(2\omega+\frac{1}{\varepsilon}\frac{\partial u}{\partial y}\right) \tag{2.3}$$

$$u\frac{\partial T}{\partial x}+v\frac{\partial T}{\partial y}=\alpha\frac{\partial^2 T}{\partial y^2} \tag{2.4}$$

$$u\frac{\partial C}{\partial x}+v\frac{\partial C}{\partial y}=D\frac{\partial^2 C}{\partial y^2} \tag{2.5}$$

where u and v are the Darcy velocity components in x and y directions respectively, ω is the component of micro-rotation whose direction of rotation lies in the xy-plane, T is the temperature, C is the concentration, g^* is the acceleration due to gravity, ρ is the density, μ is the dynamic coefficient of viscosity, b is the empirical constant, K_p is the permeability, κ is the vortex viscosity, j is the micro-inertia density, γ is the spin-gradient viscosity, ε is the porosity, Ω is the angle of inclination, α is the thermal diffusivity and D is the solutal diffusivity of the medium. Further, β_0 and β_1 are used to represent the first and second order thermal expansion coefficients respectively. Further more, β_2 and β_3 are used to represent the first and second order solutal expansion coefficients respectively.

The corresponding boundary conditions are

$$\begin{gathered}u=0,\ v=0,\ \omega=0,\ -k_f\frac{\partial T}{\partial y}=h_f(T_f-T),\ C=C_w\ \text{ at }\ y=0\\ u=u_\infty,\ \omega=0,\ T=T_\infty,\ C=C_\infty\ \text{as}\ y\to\infty\end{gathered} \tag{2.6}$$

where the subscripts w and ∞ indicate conditions at the wall and at the outer edge of the boundary layer respectively. Generally, $\omega=0$ represents the case of concentrated particle flows in which the micro-elements close to the wall are not able to rotate. Further, the assumption $\gamma=\left(\mu+\frac{\kappa}{2}\right)j$ is incorporated to allow the field equations to predict the correct behavior in the limiting case when the micro-structure effects become negligible and the total spin ω reduces to the angular velocity [3]. Furthermore, h_f is the convective heat transfer coefficient and k_f is the thermal conductivity of the fluid. The same symbols are used throughout the thesis unless otherwise specified.

Now, we introduce the stream function ψ such that it satisfies the continuity equation (2.1)

automatically, and it is defined as

$$u = \frac{\partial \psi}{\partial y}, \quad v = -\frac{\partial \psi}{\partial x} \tag{2.7}$$

In this chapter, two types (cases) of problems are considered: (a) free/natural convection and (b) mixed convection.

2.2.1 Case(a): Natural Convection

The flow is assumed to be a natural convective flow which is caused by only buoyancy forces and without any external agent. Hence, the velocity of the external flow becomes zero (*i.e.*, $u_\infty = 0$). Initially, we introduce the following dimensionless variables

$$\begin{aligned} &\xi = \frac{x}{L}, \ \eta = \frac{y}{L}\left(\frac{Gr}{\xi}\right)^{\frac{1}{4}}, \ \psi = \frac{\mu\, Gr^{\frac{1}{4}}\ \xi^{\frac{3}{4}}}{\rho}\, f(\xi,\eta) \ \ \omega = \frac{\mu\, Gr^{\frac{3}{4}}\ \xi^{\frac{1}{4}}}{\rho L^2}\, g(\xi,\eta), \\ &\theta(\xi,\eta) = \frac{T - T_\infty}{T_f - T_\infty}, \ \ \phi(\xi,\eta) = \frac{C - C_\infty}{C_w - C_\infty} \end{aligned} \tag{2.8}$$

where ξ is the stream-wise coordinate, $Gr = \dfrac{g^* \beta_0 (T_f - T_\infty) L^3}{\nu^2}$ is the global thermal Grashof number, L is the characteristics length, f is the dimensionless stream function, g is the dimensionless microrotation, θ is the dimensionless temperature and ϕ is the dimensionless concentration.

Substituting the stream function (2.7) and the transformations (2.8) into Eqs.(2.1)-(2.5), the governing equations reduce to the following form:

$$\begin{aligned} \frac{1}{\varepsilon}\left(\frac{1}{1-N}\right) f''' + \frac{3}{4\varepsilon^2} f f'' - \frac{1}{2\varepsilon^2} f'^2 + \left(\frac{N}{1-N}\right) g' - \frac{Fs}{Da}\xi\, f'^2 - \frac{\xi^{\frac{1}{2}}}{Da\, Gr^{\frac{1}{2}}} f' \\ + [\theta(1+\alpha_1\theta) + \mathcal{B}\phi(1+\alpha_2\phi)]\cos\Omega = \frac{\xi}{\varepsilon^2}\left(f'\frac{\partial f'}{\partial \xi} - f''\frac{\partial f}{\partial \xi}\right) \end{aligned} \tag{2.9}$$

$$\lambda g'' + \frac{3}{4\varepsilon} f g' - \frac{1}{4\varepsilon} f' g - \left(\frac{N}{1-N}\right)\mathcal{J}\xi^{\frac{1}{2}}\left(2g + \frac{1}{\varepsilon} f''\right) = \frac{\xi}{\varepsilon}\left(f'\frac{\partial g}{\partial \xi} - \frac{\partial f}{\partial \xi} g'\right) \tag{2.10}$$

$$\frac{1}{\mathrm{Pr}}\theta'' + \frac{3}{4} f\theta' = \xi\left(f'\frac{\partial \theta}{\partial \xi} - \frac{\partial f}{\partial \xi}\theta'\right) \tag{2.11}$$

$$\frac{1}{Sc}\phi'' + \frac{3}{4} f\phi' = \xi\left(f'\frac{\partial \phi}{\partial \xi} - \frac{\partial f}{\partial \xi}\phi'\right) \tag{2.12}$$

In the above equations, the primes represent partial derivative with respect to η alone. Fur-

ther, $N = \left(\frac{\kappa}{\mu+\kappa}\right)$ is the coupling number $(0 \leq N < 1)$ (Ref., Cowin [33]), $Da = \frac{K_p}{L^2}$ is the Darcy number, $Fs = \frac{b}{L}$ is the Forchheimer number, $\mathcal{B} = \frac{\beta_2(C_w - C_\infty)}{\beta_0(T_f - T_\infty)}$ is the buoyancy ratio, $\alpha_1 = \frac{\beta_1(T_f - T_\infty)}{\beta_0}$ is the nonlinear density-temperature parameter (NDT), $\alpha_2 = \frac{\beta_3(C_w - C_\infty)}{\beta_2}$ is the nonlinear density-concentration parameter (NDC), $\lambda = \frac{\gamma}{j\rho\nu}$ is the spin-gradient viscosity, $\mathcal{J} = \frac{L^2}{jGr^{\frac{1}{2}}}$ is the micro-inertia density, $\Pr = \frac{\nu}{\alpha}$ is the Prandtl number and $Sc = \frac{\nu}{D}$ is the Schmidt number.

The boundary conditions (2.6) become

$$\begin{gathered} f'(\xi,0) = 0,\ f(\xi,0) = -\frac{4}{3}\xi\left(\frac{\partial f}{\partial \xi}\right)_{\eta=0},\ g(\xi,0) = 0, \theta'(\xi,0) = -Bi\xi^{\frac{1}{4}}\left[1-\theta(\xi,0)\right], \\ \phi(\xi,0) = 1,\ f'(\xi,\infty) = 0,\ \ g(\xi,\infty) = 0,\ \ \theta(\xi,\infty) = 0,\ \ \phi(\xi,\infty) = 0, \end{gathered} \tag{2.13}$$

where $Bi = \frac{h_f L}{k_f\ Gr^{\frac{1}{4}}}$ is the Biot number and physically, it is the ratio of internal thermal resistance of the plate to the boundary layer thermal resistance of the hot fluid at the bottom of the surface.

The wall shear stress and wall couple stress are given by

$$\tau_w = \left[(\mu+\kappa)\frac{\partial u}{\partial y} + \kappa\omega\right]_{y=0} \text{ and } m_w = \gamma\left[\frac{\partial \omega}{\partial y}\right]_{y=0}, \tag{2.14}$$

and the heat and mass transfer rates from the plate are given by

$$q_w = -k_f\left[\frac{\partial T}{\partial y}\right]_{y=0} \text{ and } q_m = -D\left[\frac{\partial C}{\partial y}\right]_{y=0}. \tag{2.15}$$

The non-dimensional skin friction $C_f = \frac{2\tau_w}{\rho u_*^2}$, wall couple stress $M_w = \frac{m_w}{\rho u_*^2 x}$, local Nusselt number $Nu_x = \frac{q_w x}{k_f(T_f - T_\infty)}$ and the local Sherwood number $Sh_x = \frac{q_m x}{D(C_w - C_\infty)}$, are given by

$$\begin{gathered} C_f Gr^{\frac{1}{4}} = \left(\frac{2}{1-N}\right)\xi^{\frac{-3}{4}} f''(\xi,0),\ M_w Gr^{\frac{1}{2}} = \left(\frac{\lambda}{\xi\ \mathcal{J}}\right) g'(\xi,0), \\ Nu_x\, Gr^{\frac{-1}{4}} = -\xi^{\frac{3}{4}}\ \theta'(\xi,0),\ Sh_x\, Gr^{\frac{-1}{4}} = -\xi^{\frac{3}{4}}\ \phi'(\xi,0), \end{gathered} \tag{2.16}$$

where u_* is the characteristic velocity.

Numerical Solution

The governing Eqs.(2.9)-(2.12) along with the boundary conditions (2.13) are solved numerically using successive linearization method (SLM) together with the local similarity and non-similarity approaches. The details are given below:

Local similarity and non-similarity approaches:

It is used to convert the set of nonlinear partial differential equations (2.9)-(2.12) along with the boundary conditions (2.13) into a set of nonlinear ordinary differential equations along with the associated boundary conditions (for more details, one can refer [95, 65]).

Before proceeding to the local non-similarity procedure, it is useful to examine the boundary-layer equations (2.9)-(2.13) from the perspective of local similarity concept.

Local similarity model

To derive the equations for local similarity model, one can assume that the terms on the right side of Eqs.(2.9)-(2.13) are sufficiently small so that they may be neglected. This can be true for a particular case of $\xi << 1$. Under this assumption, the local similarity equations are given by

$$\frac{1}{\varepsilon}\left(\frac{1}{1-N}\right)f''' + \frac{3}{4\varepsilon^2}f f'' - \frac{1}{2\varepsilon^2}f'^2 + \left(\frac{N}{1-N}\right)g' - \frac{Fs}{Da}\xi\, f'^2 - \frac{1}{Da\, Gr^{\frac{1}{2}}}\xi^{\frac{1}{2}}f' + [\theta(1+\alpha_1\theta) + \mathcal{B}\phi(1+\alpha_2\phi)]\cos\Omega = 0 \tag{2.17}$$

$$\lambda g'' - \frac{1}{4\varepsilon}g\, f' + \frac{3}{4\varepsilon}g'\, f - \left(\frac{N}{1-N}\right)\mathcal{J}\,\xi^{\frac{1}{2}}\left(\frac{1}{\varepsilon}f'' + 2g\right) = 0 \tag{2.18}$$

$$\frac{1}{\mathrm{Pr}}\theta'' + \frac{3}{4}f\theta' = 0 \tag{2.19}$$

$$\frac{1}{Sc}\phi'' + \frac{3}{4}f\phi' = 0 \tag{2.20}$$

The associated boundary conditions (2.13) become

$$\begin{aligned} f'(\xi,0) = f(\xi,0) = g(\xi,0) = 0,\ \theta'(\xi,0) + Bi\,\xi^{\frac{1}{4}}\left[1-\theta(\xi,0)\right] = 0, \\ \phi(\xi,0) = 1, f'(\xi,\infty) = g(\xi,\infty) = \theta(\xi,\infty) = \phi(\xi,\infty) = 0. \end{aligned} \tag{2.21}$$

The parameter ξ contained in the governing equations and boundary conditions can be regarded as assigned constant at any stream-wise location along the plate. As a result, the governing equations transformed by the local similarity method can be treated as a system of ordinary differential equations with partial non-similar effects retained in the linear momentum equation, angular momentum equation and the boundary conditions. Here, the solutions are different for different values of the stream-wise coordinate ξ. This can be seen by assigning different values to ξ along the plate and plotting the respective boundary layer distributions.

On the other hand, the non-similar terms on the right hand side of Eqs.(2.9)-(2.13) are vanished in the local-similarity procedure. The local similarity postulation requires ξ to be close to zero. Otherwise, the whole term in the bracket on the right hand side of Eqs.(2.9)-(2.13) must be minimal to justify the exclusion of non-similar terms. The validity of the latter assumption, however, is subject to uncertainty and this is a weakness of the local-similarity procedure.

Local non-similarity model

In order to overcome the limitations imposed by local-similarity procedure, the local non-similar equations will now be derived. For this, consider the auxiliary variables U, V, H and K as $\dfrac{\partial f}{\partial \xi} = U$, $\dfrac{\partial g}{\partial \xi} = V$, $\dfrac{\partial \theta}{\partial \xi} = H$ and $\dfrac{\partial \phi}{\partial \xi} = K$ to recover the omitted expressions in the previous model. Introducing these functions into Eqs.(2.9)-(2.13), we get the first set of auxiliary equations as given below

$$\begin{aligned} \frac{1}{\varepsilon}\left(\frac{1}{1-N}\right) f''' + \frac{3}{4\varepsilon^2} f f'' - \frac{1}{2\varepsilon^2} f'^2 + \left(\frac{N}{1-N}\right) g' - \frac{Fs}{Da}\xi\, f'^2 - \frac{1}{Da\, Gr^{\frac{1}{2}}}\xi^{\frac{1}{2}} f' \\ + \left[\theta(1+\alpha_1\theta) + \mathcal{B}\phi(1+\alpha_2\phi)\right]\cos\Omega = \frac{\xi}{\varepsilon^2}\left(f'\,U' - f''\,U\right) \end{aligned} \tag{2.22}$$

$$\lambda g'' + \frac{3}{4\varepsilon} f g' - \frac{1}{4\varepsilon} f' g - \left(\frac{N}{1-N}\right)\mathcal{J}\xi^{\frac{1}{2}}\left(2g + \frac{1}{\varepsilon} f''\right) = \frac{\xi}{\varepsilon}\left(f'\,V - g'\,U\right) \tag{2.23}$$

$$\frac{1}{\mathrm{Pr}}\theta'' + \frac{3}{4} f\theta' = \xi\left(f'\,H - \theta'\,U\right) \tag{2.24}$$

$$\frac{1}{Sc}\phi'' + \frac{3}{4}f\phi' = \xi\left(f'\,K - \phi'\,U\right) \tag{2.25}$$

along with the boundary conditions

$$\begin{aligned} f(\xi,0) + \frac{4}{3}\xi\,U(\xi,0) = f'(\xi,0) = g(\xi,0) = 0,\ \theta'(\xi,0) = -Bi\xi^{\frac{1}{4}}\left[\theta(\xi,0) - 1\right], \\ \phi(\xi,0) = 1,\ f'(\xi,\infty) = g(\xi,\infty) = \theta(\xi,\infty) = \phi(\xi,\infty) = 0. \end{aligned} \tag{2.26}$$

Differentiating the above Eqs.(2.22)- (2.25) along with the boundary condition (2.26) with respect to ξ and neglecting the terms involving the derivative functions U, V, H and K with respect to ξ, we obtain the second set of auxiliary equations which are given as

$$\begin{aligned} \frac{1}{\varepsilon}\left(\frac{1}{1-N}\right)U''' + \frac{7}{4\varepsilon^2}Uf'' + \frac{3}{4\varepsilon^2}fU'' + \left(\frac{N}{1-N}\right)V' - \frac{\xi^{\frac{-1}{2}}}{2\,Da\,Gr^{\frac{1}{2}}}f' - \frac{\xi^{\frac{1}{2}}}{DaGr^{\frac{1}{2}}}U' - \frac{Fs}{Da}f'^2 \\ + \left[H(1+2\alpha_1\theta) + \mathcal{B}K(1+2\alpha_2\phi)\right]\cos\Omega - 2\left[\frac{Fs}{Da}\xi + \frac{1}{\varepsilon^2}\right]f'U' = \frac{\xi}{\varepsilon^2}\left(U'^2 - U''U\right) \end{aligned} \tag{2.27}$$

$$\begin{aligned} \lambda V'' + \frac{7}{4\varepsilon}Ug' - \frac{1}{2}\left(\frac{N}{1-N}\right)\mathcal{J}\xi^{\frac{-1}{2}}\left(2g + \frac{1}{\varepsilon}f''\right) - \left(\frac{N}{1-N}\right)\mathcal{J}\xi^{\frac{1}{2}}\left(2V + \frac{1}{\varepsilon}U''\right) \\ + \frac{3}{4\varepsilon}fV' - \frac{1}{4\varepsilon}U'g - \frac{5}{4\varepsilon}Vf' = \frac{\xi}{\varepsilon}\left(VU' - V'U\right) \end{aligned} \tag{2.28}$$

$$\frac{1}{\mathrm{Pr}}H'' + \frac{7}{4}U\theta' + \frac{3}{4}fH' - f'H = \xi\left(HU' - H'U\right) \tag{2.29}$$

$$\frac{1}{Sc}K'' + \frac{7}{4}U\phi' + \frac{3}{4}fK' - f'K = \xi\left(KU' - K'U\right) \tag{2.30}$$

along with the boundary conditions

$$\begin{aligned} U'(\xi,0) = U(\xi,0) = V(\xi,0) = 0; H'(\xi,0) - Bi\xi^{\frac{1}{4}}H(\xi,0) + \frac{1}{4}Bi\xi^{\frac{-3}{4}}[1-\theta(\xi,0)] = 0; \\ K(\xi,0) = U'(\xi,\infty) = V(\xi,\infty) = H(\xi,\infty) = K(\xi,\infty) = 0. \end{aligned} \tag{2.31}$$

The two-equation model involves eight coupled equations [i.e., (2.22)-(2.25) and (2.27)-(2.30)] that need to be solved simultaneously in conjunction with the two sets of boundary conditions [(2.26) and (2.31)]. Therefore, the local non-similarity procedure preserves the non-similar terms in original governing equations and boundary conditions because we are dropping the non-similar terms from its auxiliary equations only. Since the original governing equations remain intact, the local non-similarity solution is expected to be more accurate than the local-similarity solution.

Successive linearization method:

In this section, the resulting system of ordinary differential equations (2.22) to (2.25) and (2.27) to (2.30) along with the boundary conditions (2.26) and (2.31) is solved using the Successive Linearization Method (SLM) (for more details, one can refer the works of Makukula *et al.* [64], Awad *et al.* [11] and Khidir *et al.* [56]). This method utilizes the successive linearization initially and then the Chebyshev spectral collocation scheme (see., Canuto *et al.* [21]) to solve the system of nonlinear ordinary differential equations.

In this method, a notation $\mathbb{Q}(\eta)$ is used to represents one of the unknown functions $f(\eta)$, $g(\eta)$, $\theta(\eta)$, $\phi(\eta)$, $U(\eta)$, $V(\eta)$, $H(\eta)$ and $K(\eta)$ and it is assumed as given below

$$\mathbb{Q}(\eta) = \mathbb{Q}_i(\eta) + \sum_{m=0}^{i-1} \mathbb{Q}_m(\eta), \quad i = 1, 2, 3, ... \tag{2.32}$$

where $\mathbb{Q}_i(\eta)$ is the unknown function, and $\mathbb{Q}_m(\eta)$ $(m \geq 1)$ are successive approximations which are obtained by recursively solving the linear part of the system that results from substituting (2.32) into the Eqs.(2.22) to (2.25) and (2.27) to (2.30) along with boundary conditions (2.26) and (2.31).

The main assumption of successive linearization is that $\mathbb{Q}_i$ become increasingly smaller when i becomes large, that is

$$\lim_{i \to \infty} \mathbb{Q}_i = 0 \tag{2.33}$$

The initial guesses $\mathbb{Q}_0(\eta)$ are chosen in such a way that these guesses satisfy the boundary conditions (2.26) and (2.31). Thus, starting from the initial guesses, the subsequent solutions $\mathbb{Q}_i(\eta)$ are obtained by successively solving the linearized form of the equations which are obtained by substituting equation (2.32) in Eqs.(2.22) to (2.25) and (2.27) to (2.30) and neglecting the nonlinear terms containing $\mathbb{Q}_i(\eta)$ $(i \geq 1)$ and its derivatives. Therefore, the resultant linearized equations (which are obtained by expressing in terms of unknown functions f, g, θ, ϕ, U, V, H and K) which has to be solved, are as following

$$\begin{aligned} \tilde{p}_{1,i-1} f_i''' + \tilde{p}_{2,i-1} f_i'' + \tilde{p}_{3,i-1} f_i' + \tilde{p}_{4,i-1} f_i + \tilde{p}_{5,i-1} g_i' + \tilde{p}_{6,i-1} \theta_i + \tilde{p}_{7,i-1} \phi_i \\ + \tilde{p}_{8,i-1} U_i' + \tilde{p}_{9,i-1} U_i = \tilde{\mathbf{r}}_{1,i-1} \end{aligned} \tag{2.34}$$

$$\tilde{q}_{1,i-1}f_i''' + \tilde{q}_{2,i-1}f_i'' + \tilde{q}_{3,i-1}f_i + \tilde{q}_{4,i-1}g_i'' + \tilde{q}_{5,i-1}g_i' + \tilde{q}_{6,i-1}g_i + \tilde{q}_{7,i-1}U_i + \tilde{q}_{8,i-1}V_i = \tilde{\mathbf{r}}_{2,i-1} \tag{2.35}$$

$$\tilde{s}_{1,i-1}f_i' + \tilde{s}_{2,i-1}f_i + \tilde{s}_{3,i-1}\theta_i'' + \tilde{s}_{4,i-1}\theta_i' + \tilde{s}_{5,i-1}U_i + \tilde{s}_{6,i-1}H_i = \tilde{\mathbf{r}}_{3,i-1} \tag{2.36}$$

$$\tilde{t}_{1,i-1}f_i' + \tilde{t}_{2,i-1}f_i + \tilde{t}_{3,i-1}\phi_i'' + \tilde{t}_{4,i-1}\phi_i' + \tilde{t}_{5,i-1}U_i + \tilde{t}_{6,i-1}K_i = \tilde{\mathbf{r}}_{4,i-1} \tag{2.37}$$

$$\tilde{a}_{1,i-1}f_i''' + \tilde{a}_{2,i-1}f_i'' + \tilde{a}_{3,i-1}f_i + \tilde{a}_{4,i-1}\theta_i + \tilde{a}_{5,i-1}\phi_i + \tilde{a}_{6,i-1}U_i''' + \tilde{a}_{7,i-1}U_i'' + \tilde{a}_{8,i-1}U_i' + \tilde{a}_{9,i-1}U_i + \tilde{a}_{10,i-1}V_i' + \tilde{a}_{11,i-1}H_i + \tilde{a}_{12,i-1}K_i = \tilde{\mathbf{r}}_{5,i-1} \tag{2.38}$$

$$\tilde{b}_{1,i-1}f_i'' + \tilde{b}_{2,i-1}f_i' + \tilde{b}_{3,i-1}f_i + \tilde{b}_{4,i-1}g_i' + \tilde{b}_{5,i-1}g_i + \tilde{b}_{6,i-1}U_i'' + \tilde{b}_{7,i-1}U_i' + \tilde{b}_{8,i-1}U_i + \tilde{b}_{9,i-1}V_i'' + \tilde{b}_{10,i-1}V_i' + \tilde{b}_{11,i-1}V_i = \tilde{\mathbf{r}}_{6,i-1} \tag{2.39}$$

$$\tilde{c}_{1,i-1}f_i' + \tilde{c}_{2,i-1}f_i + \tilde{c}_{3,i-1}\theta_i' + \tilde{c}_{4,i-1}U_i' + \tilde{c}_{5,i-1}U_i + \tilde{c}_{6,i-1}H_i'' + \tilde{c}_{7,i-1}H_i' + \tilde{c}_{8,i-1}H_i = \tilde{\mathbf{r}}_{7,i-1} \tag{2.40}$$

$$\tilde{d}_{1,i-1}f_i' + \tilde{d}_{2,i-1}f_i + \tilde{d}_{3,i-1}\phi_i' + \tilde{d}_{4,i-1}U_i' + \tilde{d}_{5,i-1}U_i + \tilde{d}_{6,i-1}K_i'' + \tilde{d}_{7,i-1}K_i' + \tilde{d}_{8,i-1}K_i = \tilde{\mathbf{r}}_{8,i-1} \tag{2.41}$$

together with the reduced boundary conditions

$$\begin{aligned} f_i(0) = f_i'(0) = f_i'(\infty) = 0,\ g_i(0) = g_i(\infty) = 0,\ \theta_i'(0) - Bi\,\xi^{\frac{1}{4}}\theta_i(0) = 0,\ \theta_i(\infty) = 0, \\ \phi_i(0) = \phi_i(\infty) = 0,\ U_i(0) = U_i'(0) = U_i'(\infty) = 0, V_i(0) = V_i(\infty) = 0, \\ H_i'(0) - Bi\,\xi^{\frac{1}{4}}H_i(0) - \frac{1}{4}Bi\,\xi^{\frac{-3}{4}}\theta_i(0) = 0,\ H_i(\infty) = 0,\ K_i(0) = K_i(\infty) = 0. \end{aligned} \tag{2.42}$$

Here the coefficient parameters $\tilde{p}_{e,i-1}$, $\tilde{q}_{e,i-1}$, $\tilde{s}_{e,i-1}$, $\tilde{t}_{e,i-1}$, $\tilde{a}_{e,i-1,}$, $\tilde{b}_{e,i-1}$, $\tilde{c}_{e,n-1}$, $\tilde{d}_{e,i-1}$ and $\tilde{\mathbf{r}}_{e,i-1}$ depend on the initial guesses $\mathbb{Q}_0(\eta)$ and on their derivatives. Once each solution for $\mathbb{Q}_i$ has been obtained by iteratively solving Eqs.(2.34) - (2.41) for each i, the approximate solutions for $\mathbb{Q}(\eta)$ are obtained as

$$\mathbb{Q}(\eta) \approx \sum_{m=0}^{M} \mathbb{Q}_m(\eta), \tag{2.43}$$

where M is the order of successive linearization approximations. Since the coefficient parameters and the right-hand side of Eqs.(2.34)-(2.41) for $i = 1, 2, 3...$ are known (from previous iterations), the system of Eqs.(2.34)-(2.41) along with the boundary conditions (2.42) can be solved easily using any suitable numerical method.

But, the resultant linearized Eqs.(2.34)-(2.41) are solved by an established procedure, namely Chebyshev spectral collocation method (Canuto *et al.* [21]). This method is based on the Chebyshev polynomials which are defined on the interval $[-1, 1]$. So, the physical region $[0, \infty)$ is transformed into the region $[-1, 1]$ using the domain truncation technique in which the problem is solved on the interval $[0, S]$ instead of $[0, \infty)$. This leads to the mapping

$$\frac{\eta}{S} = \frac{\tau + 1}{2}, \qquad -1 \leq \tau \leq 1 \tag{2.44}$$

where S is the scaling parameter which is used to invoke the boundary condition at ∞.

The unknown functions $\mathbb{Q}_i$ are approximated, as will be discussed below, by the Chebyshev interpolating polynomials in such a way that they are collocated at the Gauss-Lobatto collocation points defined as

$$\tau_m = \cos\frac{\pi m}{\mathcal{N}}, \qquad m = 0, 1, ..., \mathcal{N} \tag{2.45}$$

where $\mathcal{N}$ is the number of collocation points.

The unknown functions $\mathbb{Q}_i$ are approximated at the Gauss-Lobatto collocation points as

$$\mathbb{Q}_i(\tau) = \sum_{k=0}^{\mathcal{N}} \mathbb{Q}_i(\tau_k) T_k(\tau_m), \;\; \frac{d^{\mathbb{Z}}}{d\eta^{\mathbb{Z}}}\mathbb{Q}_i(\tau) = \sum_{k=0}^{\mathcal{N}} \mathbf{D}_{km}^{\mathbb{Z}} \mathbb{Q}_i(\tau_k), \quad m = 0, 1, ..., \mathcal{N} \tag{2.46}$$

where T_k is the k^{th} Chebyshev polynomial given by $T_k(\tau) = \cos[k \;\cos^{-1}\tau]$, $\mathcal{D}$ is the Chebyshev spectral derivative matrix such that $\mathbf{D} = (2/S)\mathcal{D}$ and $\mathbb{Z}$ is the order of differentiation.

After substituting (2.44)-(2.46) into the linearized form of equations (2.34)-(2.41), the required solution is given by

$$\tilde{\mathbf{Y}}_i = \tilde{\mathbf{B}}_{i-1}^{-1} \tilde{\mathbf{R}}_{i-1}, \tag{2.47}$$

In Eq.(2.47), $\tilde{\mathbf{B}}_{i-1}$ is a square matrix of order $(8\mathcal{N} + 8)$ and $\tilde{\mathbf{Y}}_i$, $\tilde{\mathbf{R}}_{i-1}$ are column matrices of order $(8\mathcal{N} + 1)$, which are defined by

$$\begin{gathered} \tilde{\mathbf{B}}_{i-1} = \left[\tilde{\mathbf{B}}_{kj}\right], \text{ for } k, j = 1, 2, ...8, \;\; \tilde{\mathbf{Y}}_i = \left[\tilde{\mathbb{F}}_i \; \tilde{\mathbb{G}}_i \; \tilde{\Theta}_i \; \tilde{\Phi}_i \; \tilde{\mathbb{U}}_i \; \tilde{\mathbb{V}}_i \; \tilde{\mathbb{H}}_i \; \tilde{\mathbb{K}}_i\right]^T, \\ \tilde{\mathbf{R}}_{i-1} = [\tilde{\mathbf{z}}_{1,i-1} \; \tilde{\mathbf{z}}_{2,i-1} \; \tilde{\mathbf{z}}_{3,i-1} \; \tilde{\mathbf{z}}_{4,i-1} \; \tilde{\mathbf{z}}_{5,i-1} \; \tilde{\mathbf{z}}_{6,i-1} \; \tilde{\mathbf{z}}_{7,i-1} \; \tilde{\mathbf{z}}_{8,i-1}]^T. \end{gathered} \tag{2.48}$$

Validation with Shooting Method

The shooting method is employed to validate the present SLM computations. Therefore, the system of ordinary differential equations (2.17)- (2.20) along with the boundary conditions (2.21) has also been solved with the shooting method. The major steps of this method are as follows:

- Convert the boundary value problem into the initial value problem;
- Reduce the initial value problem into a system of first order differential equations;
- Identify the missing initial values using the Newton-Raphson method;
- Solve the first order system of resultant ordinary differential equations using the Runge-Kutta method of fourth-order;
- Update the obtained information until all the free stream boundary conditions are satisfied asymptotically.

Algebraic details of the shooting method are omitted here for the sake of brevity and there are many references (to mention few, Ref. [67, 52]) in which these details have been documented.

It is noticed that the present problem reduces to free convection heat transfer over an isothermal vertical plate in a viscous fluid in the absence of coupling number, buoyancy ratio and nonlinear convection parameters with $\varepsilon = 1$, $Da \to \infty$, $\lambda = 0$, $\xi = 1$, $Bi \to \infty$ and $\Omega = 0$. In order to assess the accuracy and validity of the present investigation, the results of the local similarity equations (2.17)-(2.20) have been compared with the results reported in the Tab.(4.2) of Bejan [19], as exhibited in Tab. (2.1). Also, the comparison between the SLM computations and shooting method results has been made for certain values of the physical parameters as shown in the Tab.(2.2). It shows an excellent agreement with the existing results.

The numerical computations are carried out by following the fixed values of parameters: $\lambda = 5.0$, $\mathcal{B} = 1.0$, $\mathrm{Pr} = 0.7$, $Sc = 0.22$, $Gr = 10$, $\varepsilon = 0.5$ and $Da = 0.1$. The value of dimensionless micro-inertia density $\mathcal{J} = 5.0$ is chosen to satisfy the thermodynamic restrictions on the material parameters given by Eringen [40]. These values are continued same throughout the evaluation, unless otherwise mentioned.

Table 2.1: *Comparison of* $-\theta'(\xi, 0)$ *for the natural convection along a vertical flat plate in a viscous fluid when* $N = 0$, $\mathcal{B} = 0$, $\alpha_1 = 0$, $\alpha_2 = 0$, $\varepsilon = 1$, $Da \to \infty$, $\lambda = 0$, $\xi \to 0$, $Bi \to \infty$, $\Omega = 0$ *and* $\Pr = 1$.

Bejan [19]	Present
0.401	0.40103

Table 2.2: *Comparison of* $f''(\xi, 0), -g'(\xi, 0), -\theta'(\xi, 0), -\phi'(\xi, 0)$ *using the SLM and Shooting method for different values of* N *with* $\mathcal{B} = 0.5$, $\varepsilon = 0.3$, $\alpha_1 = 0$, $\alpha_2 = 0$, $Da \to \infty$, $\lambda = 5.0$, $J = 5.0$, $Bi \to \infty$, $\Omega = 0$, $\Pr = 0.7$, $\xi \to 0$ *and* $Sc = 0.22$.

	SLM				Shooting Method			
N	f''	$-g'$	$-\theta'$	$-\phi'$	f''	$-g'$	$-\theta'$	$-\phi'$
0.1	0.44697	0.028502	0.25942	0.13309	0.44697	0.028502	0.25942	0.13309
0.3	0.38280	0.114050	0.25303	0.13114	0.38280	0.114050	0.25303	0.13114
0.6	0.26376	0.295950	0.23859	0.12661	0.26376	0.295950	0.23859	0.12661
0.9	0.09660	0.491030	0.20265	0.11428	0.09660	0.491030	0.20265	0.11428

Results and Discussions

Figures 2.2(a)-2.8(d) displays the influence of various parameters on the fluid flow velocity, microrotation, temperature and concentration profiles. The effects of non-Darcy parameter, micropolar parameter, Biot number, angle of inclination and nonlinear density-temperature (NDT) and nonlinear density-concentration (NDC) parameters on the skin friction, gradient of microrotation (wall couple stress), heat and mass transfer rates of the micropolar fluid have been discussed and portrayed through the Figs.2.6(a) -2.8(d).

The effect of nonlinear density-temperature (NDT) parameter α_1 on the velocity, microrotation, temperature and the concentration profiles, is displayed in Figs.2.2(a)-2.2(d). As NDT parameter α_1 increases, the variation of fluid velocity is changed from increasing to decreasing far away from the surface of the wall (i.e., nearer to the free stream condition), as shown in Fig.2.2(a). Physically, $\alpha_1 > 0$ implies that $T_f > T_\infty$; hence, the surface of the wall will induce some amount of heat to the fluid flow region. Similarly, there is a possibility for heat transfer of fluid flow to the wall in the case of $\alpha_1 < 0$. It is clearly noticed from Fig.2.2(b) that the effect of the NDT parameter α_1 on the microrotation is notable in every part of the boundary layer, but more significant away from the

plate and also the rise in α_1 changes the sign of microrotation. The magnitudes of the temperature and concentration are more in the absence of α_1 in comparison with the presence of α_1, as plotted in Figs.2.2(c) - 2.2(d).

Figures 2.3(a) to 2.3(d) depict the influences of the nonlinear density-concentration (NDC) parameter α_2 for a fixed value of α_1 on the velocity, microrotation, temperature and concentration. Usually, the motion of the fluid flow increases sequentially away from the plate so that it reaches maximum position within the boundary layer and then drops to fulfill the free stream value, as portrayed in Fig.2.3(a). However, the rise in NDC parameter α_2 changes the sign of microrotation within the boundary layer from negative to positive and also the trend of microrotation is modified from increasing to decreasing nearer to the free stream value $\eta = 5$, as shown in Fig.2.3(b). The temperature and concentration boundary layer thicknesses decrease with the increase of α_2 and the same result is displayed in Figs.2.3(c) and 2.3(d). In the case of thermal and solutal distributions, present results match with the findings of the work by Partha [79]. This is due to the enhancement of thermal and solutal gradients by nonlinear terms in the momentum equation. By the experience of these two (i.e., NDT and NDC) parameters, one can conclude that the influence of NDC parameter α_2 is more prominent compared with that of NDT parameter α_1.

The profiles of fluid flow for different values of conductive-convective parameter Bi have been displayed in Figs.2.4(a) - 2.4(d). It is noteworthy from Fig.2.4(a) that, as the Biot number increases, the velocity of flow field attains peak position in the neighborhood of the plate due to the reduction in the thermal resistance of inclined plate. It is clear from the Fig.2.4(b) that, the microrotation changes from increasing to decreasing values within the boundary layer as the Biot number increases. Figure 2.4(c) displays the impact of Biot number on the temperature distribution and show results for isothermal and non-isothermal boundary conditions. This condition is changing into wall condition when the Biot number tends to infinity as depicted in Fig.2.4(c). As Bi increases from thermally thin case ($Bi < 0.1$) to thermally thick case ($Bi > 0.1$), the temperature distribution increases on the surface of the plate. The effect of Biot number on the concentration profile is displayed by Fig.2.4(d) and it reveals that the concentration profile decreases within the boundary layer with the increase of Biot number.

The influence of inclination angle (Ω) on the tangential velocity profile is displayed in Fig.2.5(a). An increase in the angle of inclination leads to decrease the velocity distribution within the boundary layer region. From Fig.2.5(b), one can notice that the microrotation increases near the plate and

it shows a reverse trend far away from the plate, when the position of a plate is changed from vertical to horizontal. Similar to the results of Chamkha *et al.* [23] and Chen [27], the thicknesses of temperature and concentration boundary layers enhance with the increase of inclination angle. The displacement of the plate from vertical position to horizontal induces a reduction in the buoyancy force and the same result is portrayed in Figs.2.5(c) and 2.5(d). Also, one can observe that the maximum buoyancy force for the same temperature and concentration differences occurs for $\Omega = 0^0$ (vertical plate) and this is shown in the Figs.2.5(a) - 2.5(d).

The effects of nonlinear density-temperature (NDT) and nonlinear density-concentration (NDC) parameters α_1 and α_2 respectively, on the skin friction, wall couple stress, heat and mass transfer rates the stream-wise coordinate ξ, are shown in Figs.2.6(a) - 2.6(d). As expected, both the heat and mass transfer rates increase with α_1 when other parameters are fixed. The effect of α_2 on the heat and mass transfer rates shows the same behavior like that of α_1. But, along the stream-wise coordinate ξ, the nature of mass transfer rate is reverse to the heat transfer rate. The skin friction and wall couple stresses are enhanced by α_1 and α_2 parameters, as depicted in Figs.2.6(c)-2.6(d).

The effects of Forchheimer number (Fs) and coupling number (N) on the skin friction, wall couple stress, heat and mass transfer rates are presented in Figs.2.7(a) - 2.7(d). The results point out that the heat and mass transfer rates decrease for an increase in Fs. A rise in the coupling number falls down the heat and mass transfer rates. Since, the microrotation tends to zero as $N \to 0$ i.e., $\kappa \to 0$, the Eq.(2.2) is uncoupled with Eq.(2.3) and they reduce to viscous fluid flow equations. Therefore, an increase in the coupling number tends to decrease the skin friction and the opposite change is noticed in the wall couple stress. Moreover, the surface drag and the wall couple stress of a micropolar fluid reduce with the enhancement of Forchheimer number and this is displayed in Figs.2.7(c) - 2.7(d).

Figures 2.8(a) - 2.8(d) demonstrate the influences of Biot number (Bi) and inclination angle (Ω) on the skin friction, wall couple stress, heat and mass transfer rates. It is found that the heat and mass transfer rates diminish when the inclined plate is displaced from vertical to horizontal, and it is easily perceived from the fact that there is a reduction in the buoyancy force by a function of Ω with the enhancement in inclination angle. With the increase of Biot number, there is a considerable enhancement in the heat and mass transfer rates. A modification in the Biot number ceases the rate of heat conduction inside the inclined plate drastically as compared to thermal convection away from its surface and these results are confined to the work of Anwar Beg *et al.*

[18]. One can notice that the effect of inclination angle is more on mass transfer rate as compared with that of the heat transfer rate. Furthermore, it is observed that an enhancement in the Biot number leads to increase the skin friction and couple stress, whereas with the increase of inclination angle, these show the opposite trend. Nominal influence on the wall couple stress and considerable increment in the skin friction are experienced for high enough values of Biot number as depicted in Figs.2.8(c) - 2.8(d).

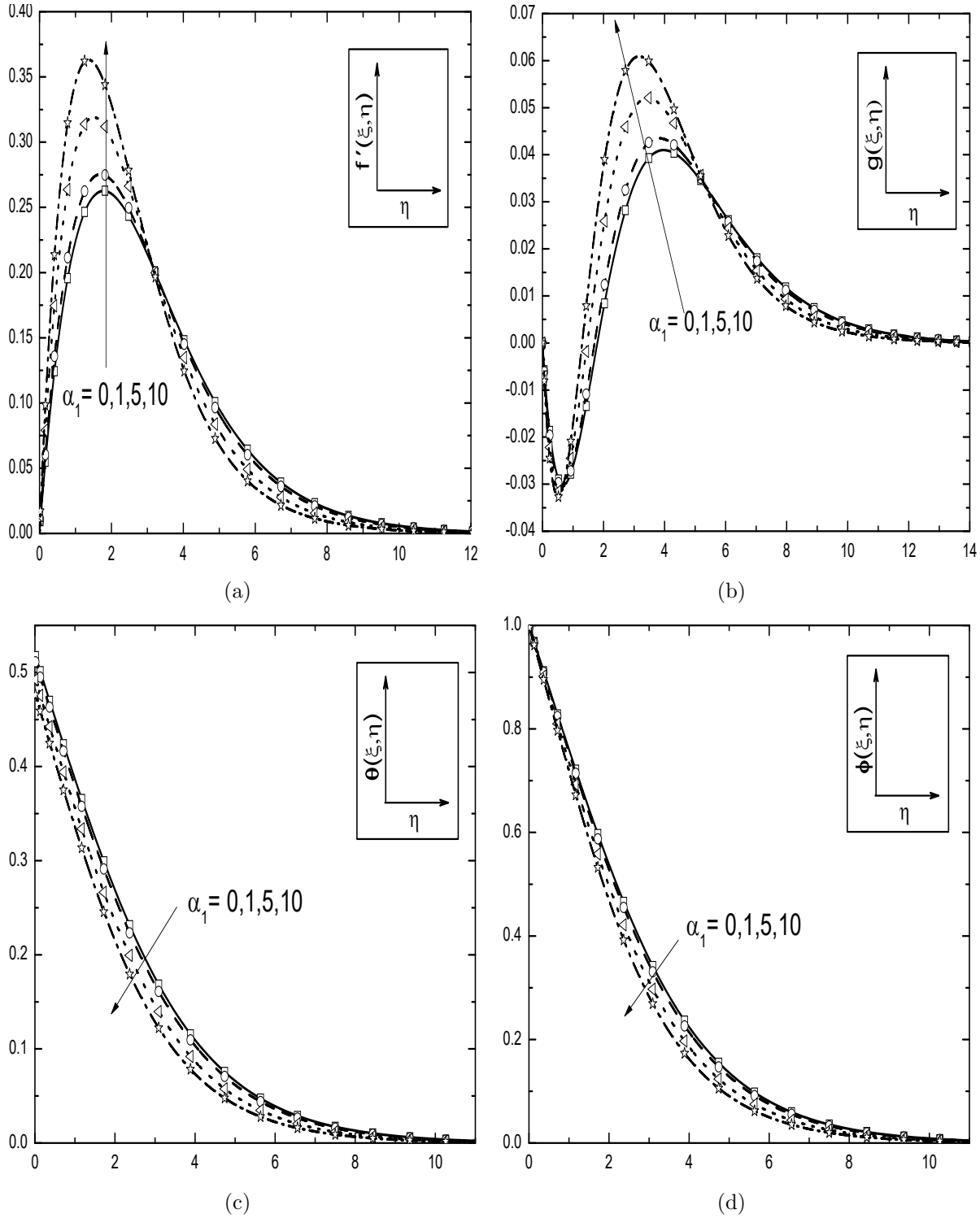

Figure 2.2: *Effect of* α_1 *on the (a) velocity, (b) microrotation, (c) temperature and (d) concentration along* η *with the fixed values of* $\xi = 0.1$, $\alpha_2 = 0.5$, $\Omega = 30^0$, $N = 0.5$, $Bi = 0.5$ *and* $Fs = 0.5$.

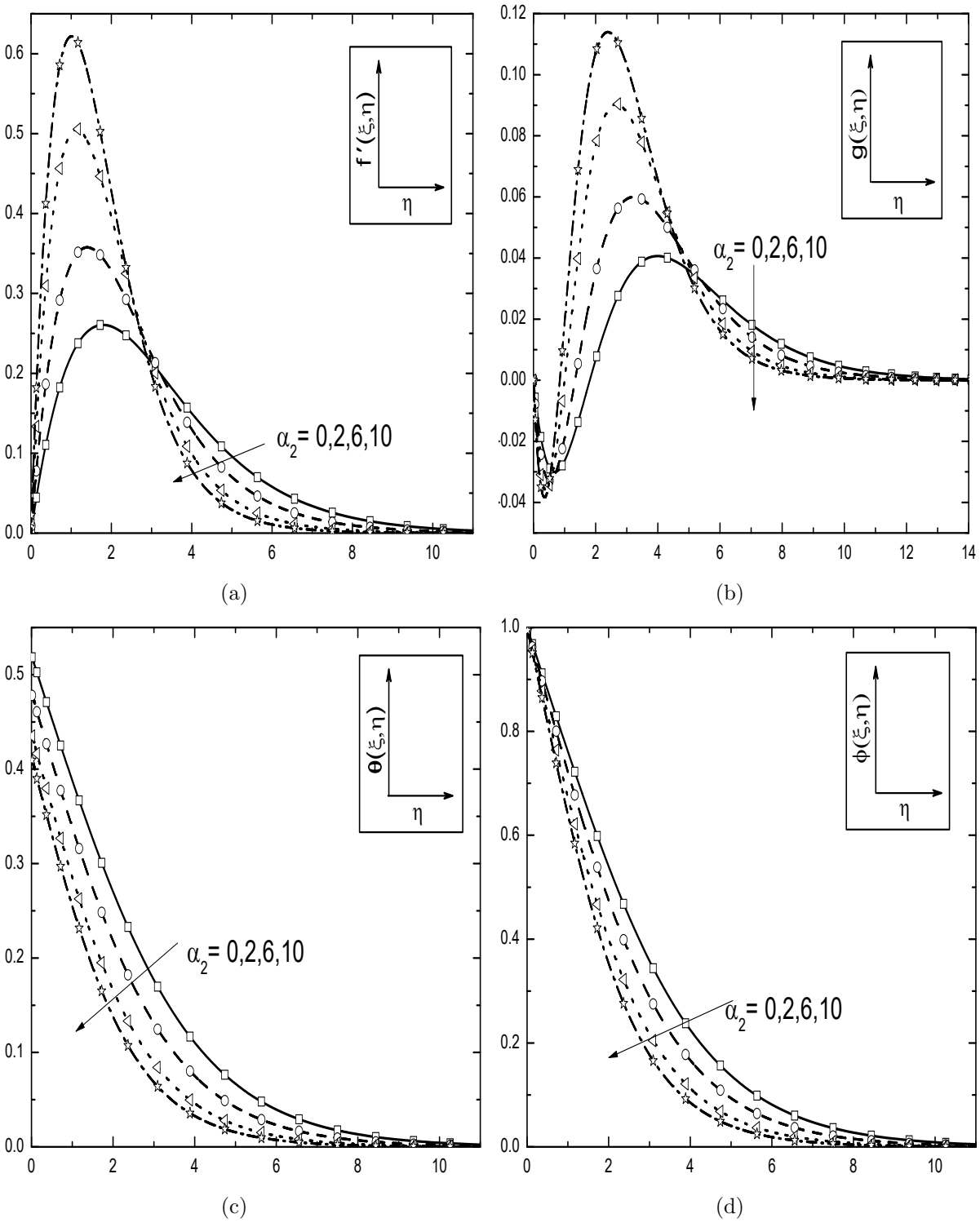

Figure 2.3: *Effect of* α_2 *on the (a) velocity, (b) microrotation, (c) temperature and (d) concentration along* η *with the fixed values of* $\xi = 0.1$, $\alpha_1 = 1$, $\Omega = 30^0$, $N = 0.5$, $Bi = 0.5$ *and* $Fs = 0.5$.

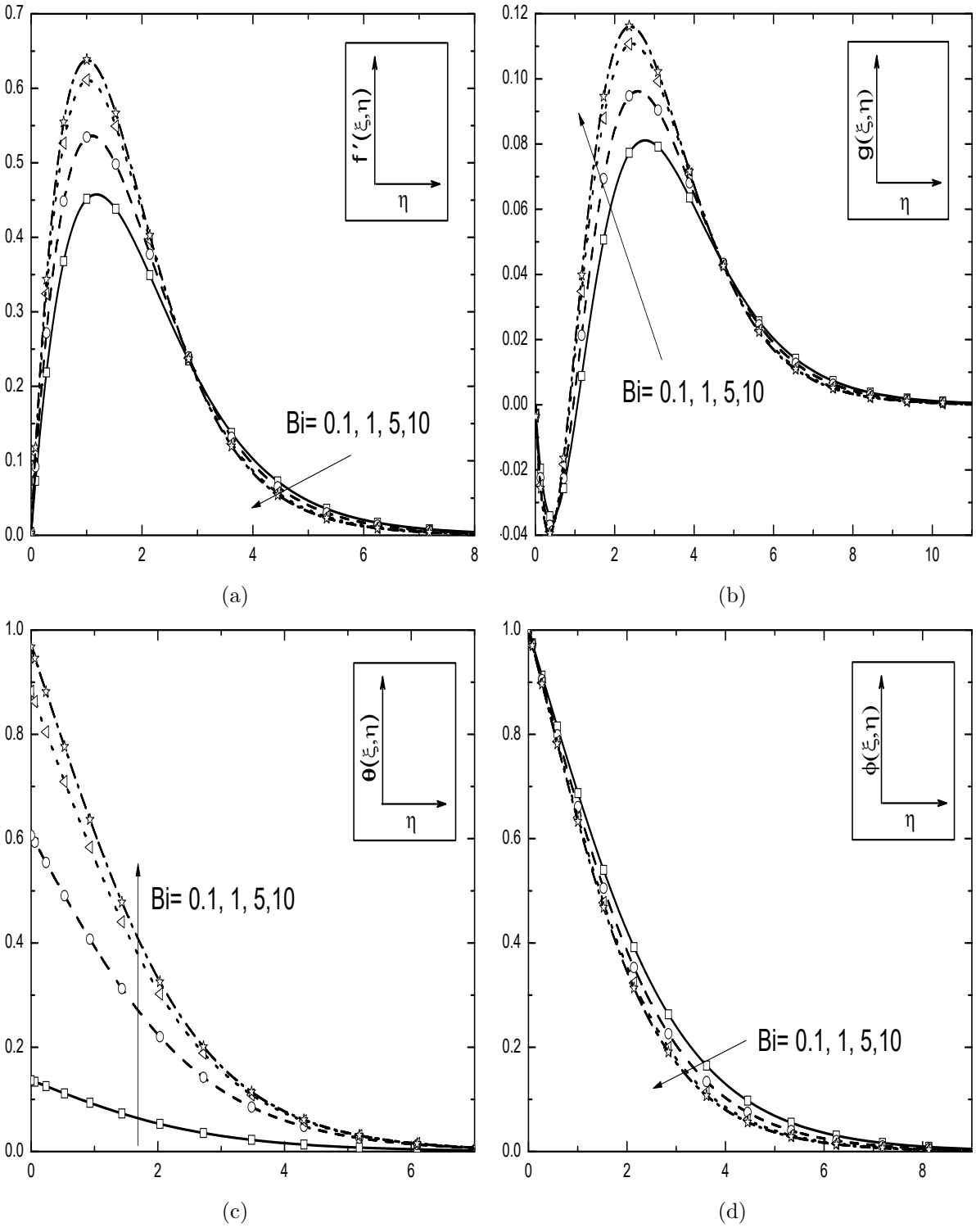

Figure 2.4: *Effect of Bi on the (a) velocity, (b) microrotation, (c) temperature and (d) concentration along* η *with the fixed values of* $\xi = 0.1$, $\alpha_1 = 1$, $\alpha_2 = 1$, $\Omega = 30^0$, $N = 0.5$ *and* $Fs = 0.5$.

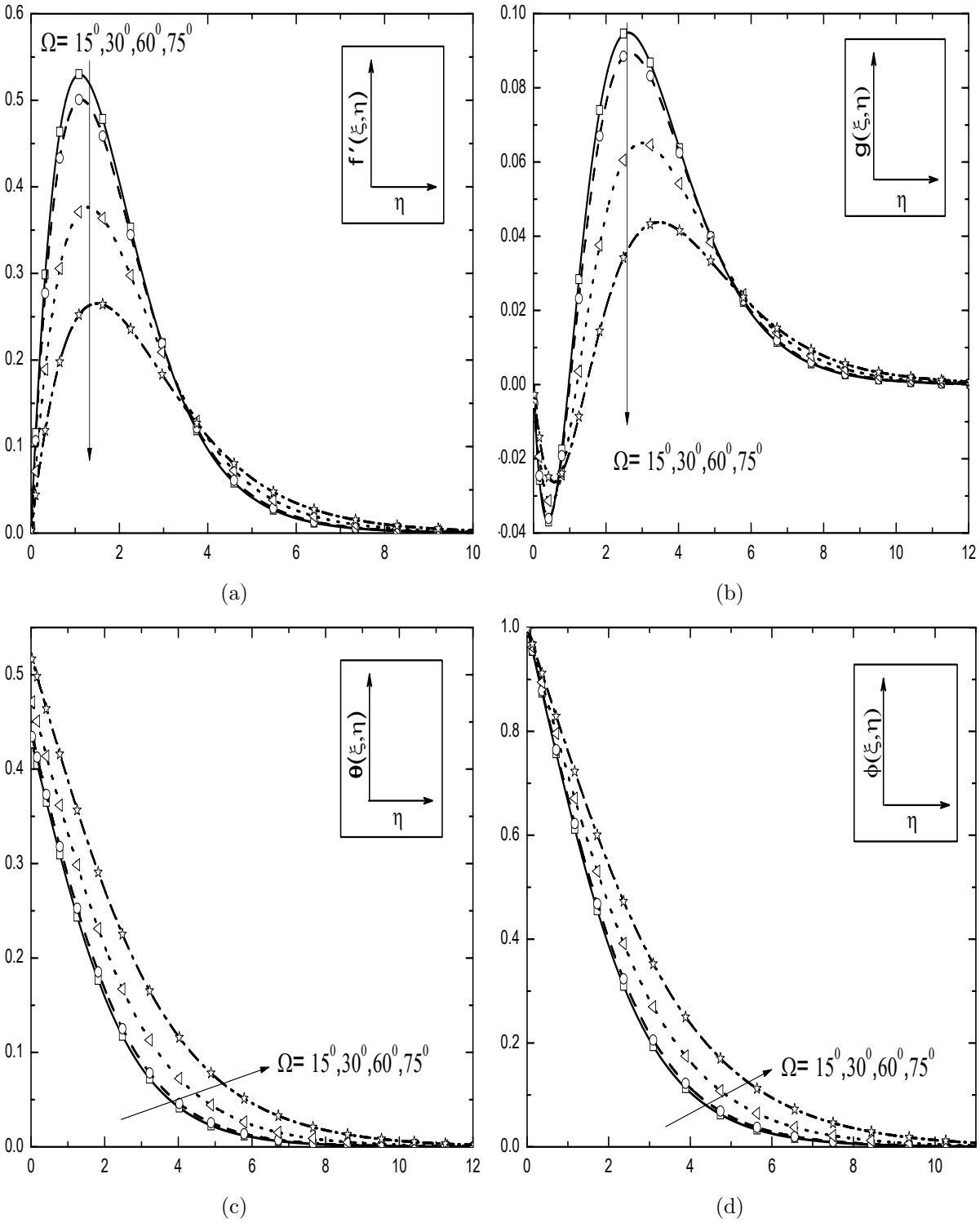

Figure 2.5: *Effect of* Ω *on the (a) velocity, (b) microrotation, (c) temperature and (d) concentration along* η *with the fixed values of* $\xi = 0.1$, $\alpha_1 = 1$, $\alpha_2 = 1$, $Bi = 0.3$, $N = 0.5$ *and* $Fs = 0.5$.

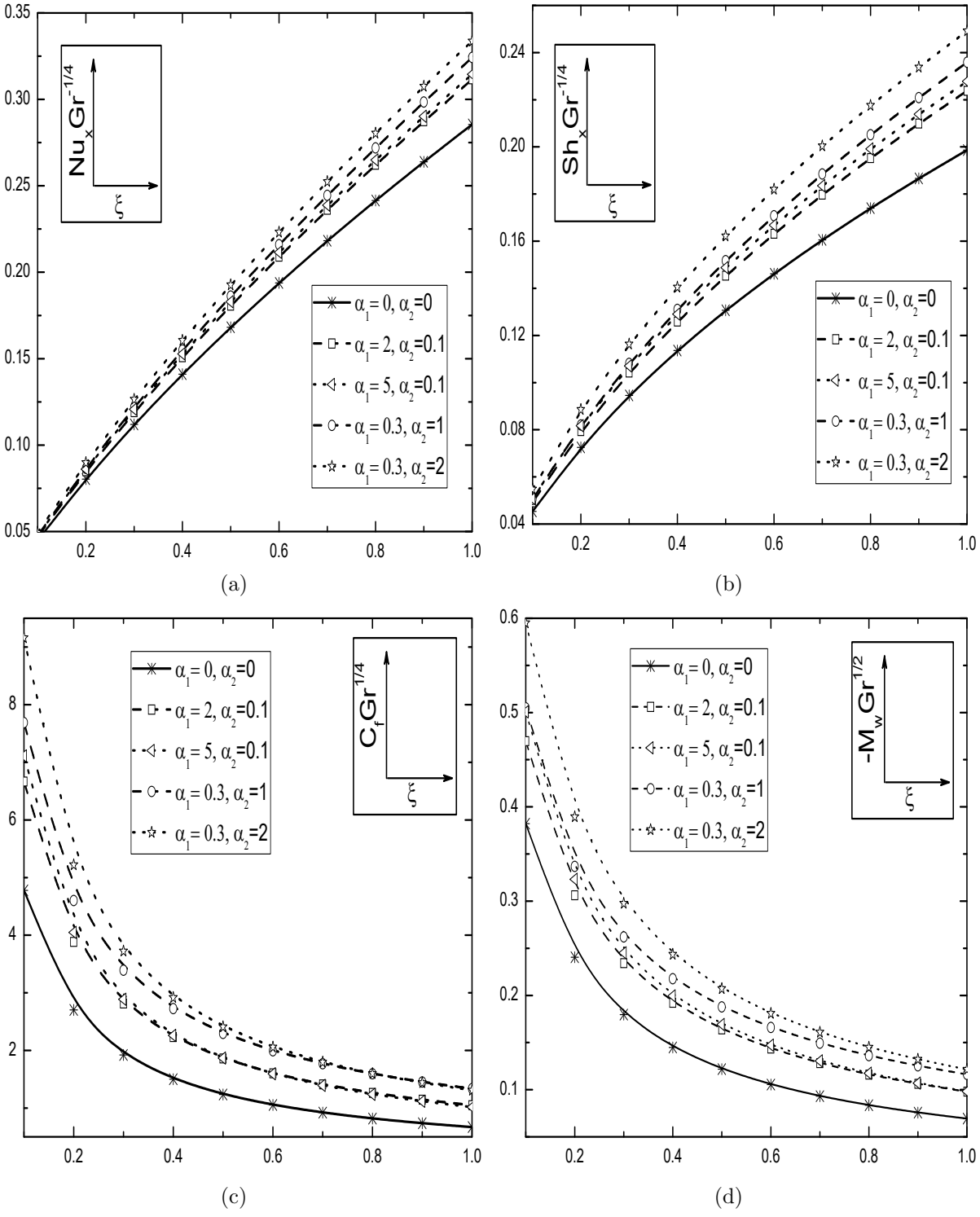

Figure 2.6: *Effects of* α_1 *and* α_2 *on the (a) heat transfer rate, (b) mass transfer rate, (c) skin friction and (d) wall couple stress along* ξ *with the fixed values of* $\Omega = 30^0$, $N = 0.5$, $Bi = 0.5$ *and* $Fs = 0.5$.

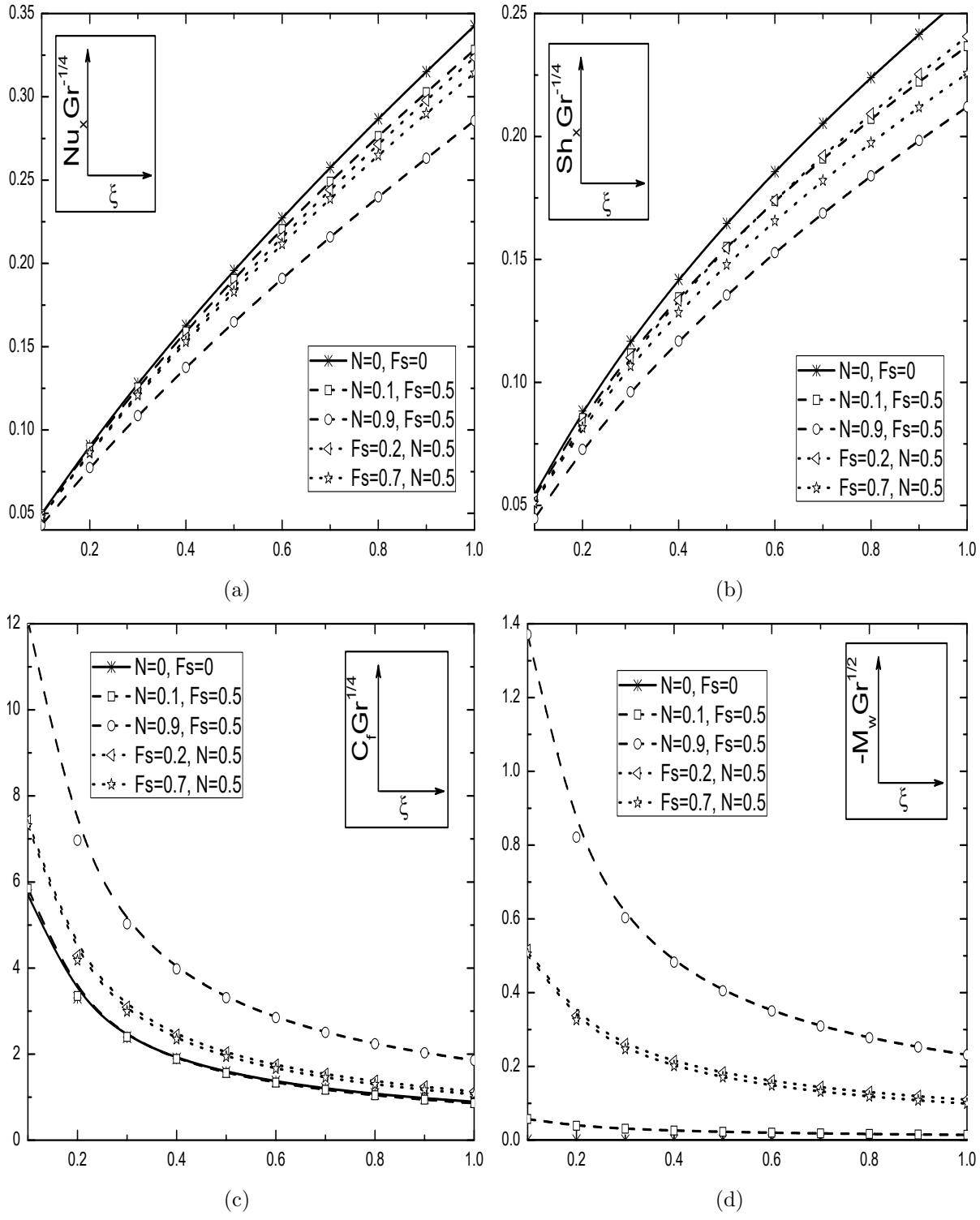

Figure 2.7: *Effects of Fs and N on the (a) heat transfer rate, (b) mass transfer rate, (c) skin friction and (d) wall couple stress along ξ with the fixed values of $\alpha_1 = 1$, $\alpha_2 = 1$, $\Omega = 30^0$ and $Bi = 0.5$.*

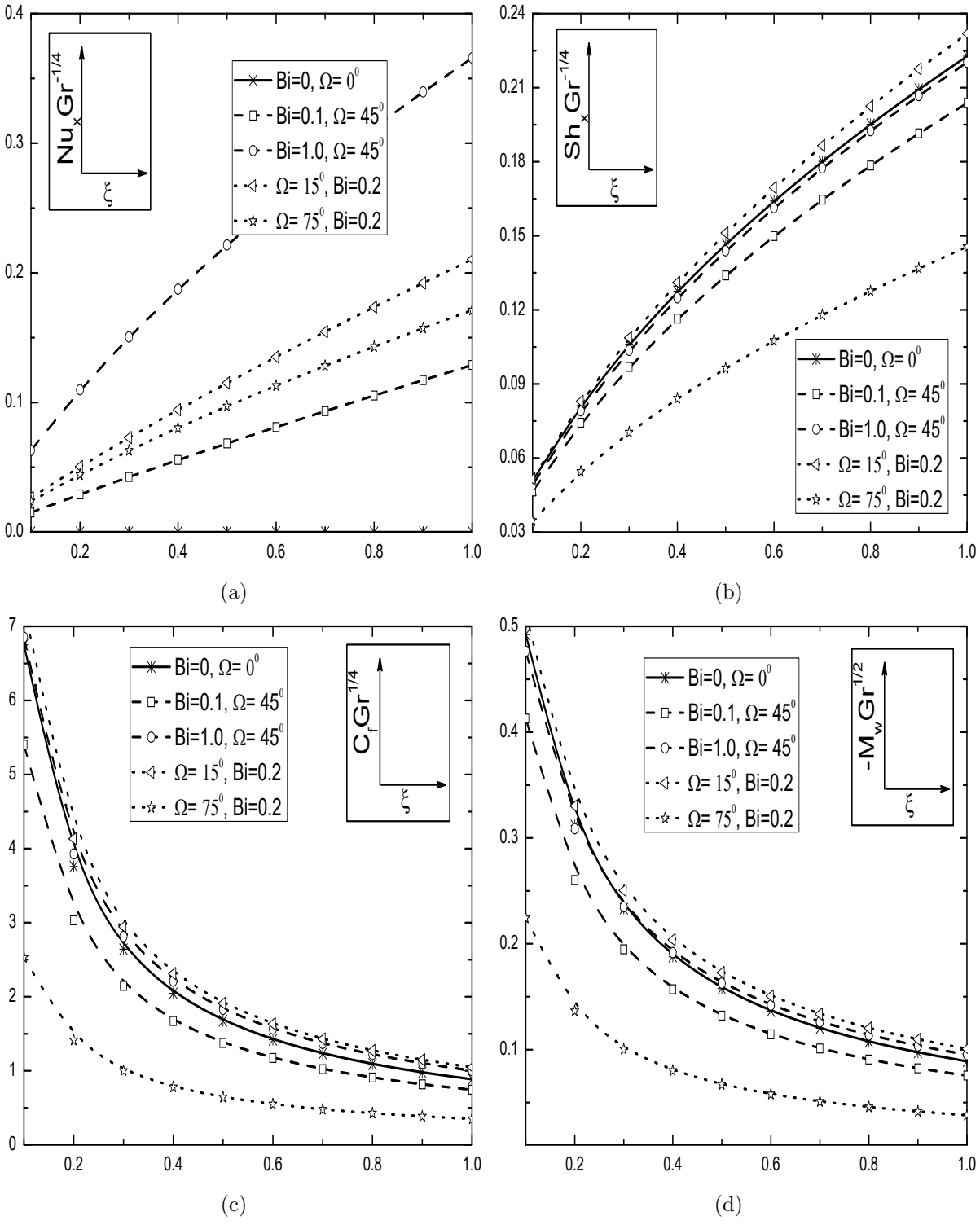

Figure 2.8: *Effects of Bi and* Ω *on the (a) heat transfer rate, (b) mass transfer rate, (c) skin friction and (d) wall couple stress along* ξ *with the fixed values of* $\alpha_1 = 1$, $\alpha_2 = 1$, $N = 0.5$, $Fs = 0.5$ *and* $Bi = 0.5$.

2.2.2 Case(b): Mixed Convection

The flow is assumed to be a mixed convective flow, which arises from both buoyancy forces and an external flow with the velocity u_∞. We introduce the following dimensionless variables

$$\begin{gathered}\xi = \frac{x}{L},\ \eta = \frac{y}{L}\left(\frac{Re}{\xi}\right)^{1/2},\ f(\xi,\eta) = \left(\frac{Re}{\xi}\right)^{1/2}\frac{\psi(\xi,\eta)}{Lu_\infty} \\ \mathrm{g}(\xi,\eta) = \frac{L\omega}{u_\infty}\left(\frac{\xi}{Re}\right)^{1/2},\ \theta(\xi,\eta) = \frac{T-T_\infty}{T_f-T_\infty},\ \phi(\xi,\eta) = \frac{C-C_\infty}{C_w-C_\infty}\end{gathered} \tag{2.49}$$

where $Re = \dfrac{u_\infty L}{\nu}$ is the global Reynold's number and u_∞ is free stream velocity.

Substituting the stream function (2.7) and the transformations (2.49) into Eqs.(2.2)-(2.5), we get the following linear momentum, angular momentum, energy and concentration equations

$$\begin{aligned}\frac{1}{\varepsilon}\left(\frac{1}{1-N}\right)f''' + \frac{1}{2\varepsilon^2}f\ f'' + \left(\frac{N}{1-N}\right)\ g' + Ri\,\xi\left[\theta(1+\alpha_1\theta) + \mathcal{B}\varphi(1+\alpha_2\phi)\right]\cos\Omega \\ + \frac{1}{Da\,Re}\xi\left(1-f'\right) + \frac{Fs}{Da}\xi\left(1-f'^2\right) = \frac{\xi}{\varepsilon^2}\left(f'\frac{\partial f'}{\partial\xi} - f''\frac{\partial f}{\partial\xi}\right)\end{aligned} \tag{2.50}$$

$$\lambda\, g'' + \frac{1}{2\varepsilon}(f'\ g + f\ g') - \left(\frac{N}{1-N}\right)\mathcal{J}\xi\left(2g + \frac{1}{\varepsilon}f''\right) = \frac{\xi}{\varepsilon}\left(f'\frac{\partial g}{\partial\xi} - \frac{\partial f}{\partial\xi}g'\right) \tag{2.51}$$

$$\frac{1}{\mathrm{Pr}}\theta'' + \frac{1}{2}f\theta' = \xi\left(f'\frac{\partial\theta}{\partial\xi} - \frac{\partial f}{\partial\xi}\theta'\right) \tag{2.52}$$

$$\frac{1}{Sc}\phi'' + \frac{1}{2}f\phi' = \xi\left(f'\frac{\partial\varphi}{\partial\xi} - \frac{\partial f}{\partial\xi}\phi'\right) \tag{2.53}$$

The boundary conditions (2.6) become

$$\begin{gathered}f'(\xi,0) = 0,\ f(\xi,0) = -2\xi\left(\frac{\partial f}{\partial\xi}\right)_{\eta=0},\ g(\xi,0) = 0,\ \theta'(\xi,0) = -Bi\xi^{1/2}\left[1-\theta(\xi,0)\right], \\ \phi(\xi,0) = 1,\ \ f'(\xi,\infty) = 1,\ \ g(\xi,\infty) = 0,\ \ \theta(\xi,\infty) = 0,\ \ \phi(\xi,\infty) = 0.\end{gathered} \tag{2.54}$$

In the above equations, $\mathcal{J} = \dfrac{L^2}{j\ Re}$ is the micro-inertia density, $Bi = \dfrac{h_f\, L}{k_f\, Re^{1/2}}$ is the Biot number and $Ri = \dfrac{Gr}{Re^2}$ is the mixed convection parameter.

The physical quantities of present interest (such as shear stress, wall couple stress heat and

mass transfer rates), are defined as

$$C_f = \frac{2}{\rho\, u_\infty^2}\left[(\mu+\kappa)\frac{\partial u}{\partial y} + \kappa\omega\right]_{y=0},\ M_w = \frac{\gamma}{\rho\, u_\infty^2 L}\left[\frac{\partial \omega}{\partial y}\right]_{y=0}$$
$$Nu_x = -\frac{x}{(T_f - T_\infty)}\left[\frac{\partial T}{\partial y}\right]_{y=0},\ Sh_x = -\frac{x}{(C_w - C_\infty)}\left[\frac{\partial C}{\partial y}\right]_{y=0} \tag{2.55}$$

The non-dimensional skin friction C_f, wall couple stress M_w, local Nusselt number Nu_x and the Sherwood number Sh_x, are given by

$$C_f Re^{1/2} = \left(\frac{2}{1-N}\right)\ \xi^{\frac{-1}{2}}\ f''(\xi,0),\ \ M_w Re = \left(\frac{\lambda}{\xi\ \mathcal{J}}\right) g'(\xi,0),$$
$$Nu_x Re^{-1/2} = -\xi^{\frac{1}{2}}\ \theta'(\xi,0),\ Sh_x Re^{-1/2} = -\xi^{\frac{1}{2}}\ \phi'(\xi,0) \tag{2.56}$$

Results and Discussion

The reduced nonlinear partial differential equations (2.50) - (2.53) along with the boundary conditions (2.54) are solved numerically using SLM together with the local similarity and non-similarity procedures, as explained in the case (a) of this chapter. In order to assess the accuracy of the present solutions, we have validated our results by comparing the surface shear stress $f''(\xi, 0)$ and the surface heat transfer rate $\theta'(\xi, 0)$ for isothermal case ($Bi \to \infty$), non-isothermal case ($Bi = 0.2$), Newtonian fluid ($N = 0$), and micropolar fluid ($N = 0.14$) with the results of Chang [25]. These comparisons are shown in Figs.2.9(a)-2.9(b) and results are found to be in good agreement with the results of Chang [25]. Also, a comparison between the present results and results of Lloyd and Sparrow [59] for various values of the mixed convection parameter Ri and the stream-wise coordinate ξ, are given in Tab. (2.3). The comparison shows that the present results are in good agreement with the similarity solutions reported by Lloyd and Sparrow [59]. In addition, a comparison is made with the results of shooting method for specific values of the other physical parameters, as appeared in the Tab. (2.4). The results are in excellent agreement pointing to the accuracy of solutions obtained by SLM.

In the present study, the numerical computations are carried out by following the fixed values of parameters: $\mathcal{B} = 1$, $Re = 200$, $Da = 0.1$, $\varepsilon = 0.5$, $\mathrm{Pr} = 0.71$, $Sc = 0.22$ and $Ri = 2$. The value of dimensionless micro-inertia density $\mathcal{J} = 1.0$ is chosen to satisfy the thermodynamic restrictions on the material parameters given by Eringen [40]. These values are used throughout the computations,

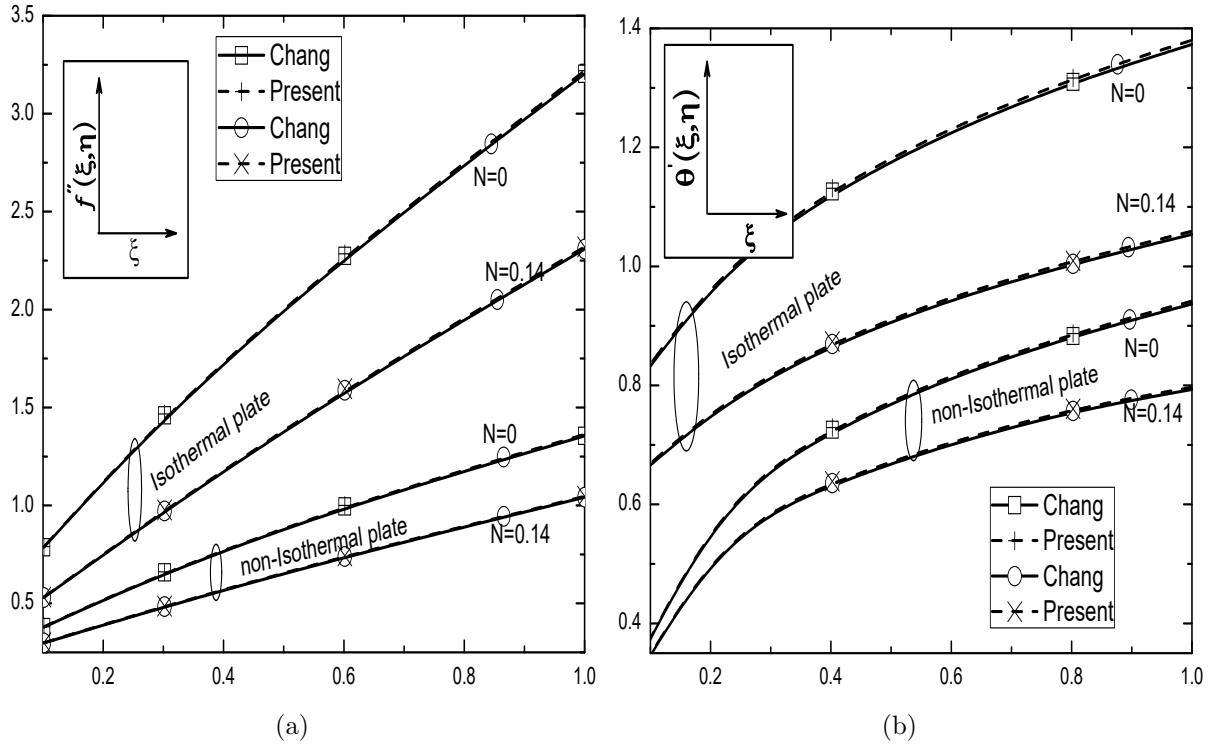

Figure 2.9: *Comparison of (a) $f''(\xi, 0)$ and (b) $\theta'(\xi, 0)$ for $Bi \to \infty$, $Bi = 2$, $N = 0$ and $N = 0.14$ along ξ with that of Chang [25].*

unless otherwise indicated.

The dimensionless velocity, microrotation, temperature and concentration profiles have been computed for different values of the pertinent parameters and presented graphically in Figs.2.10(a)-2.14(d). The effects of nonlinear density-temperature (NDT) parameter (α_1), nonlinear density-concentration (NDC) parameter (α_2), non-Darcy parameter (Fs), micropolar parameter (N), mixed convection parameter (Ri), Biot number (Bi) and inclination angle (Ω) have been discussed.

The effect of nonlinear density-temperature parameter (α_1) on the velocity, microrotation, temperature and the concentration profiles are shown in Figs.2.10(a)-2.10(d). These results indicate that the velocity distribution increases with the increase of α_1 and the value $\mathcal{B} = 1$ implies that the thermal and solutal buoyancy forces are of the same order of magnitude. Physically, $\alpha_1 > 0$ implies that $T_f > T_\infty$; hence, there will be a supply of heat to the flow region from the wall. Similarly $\alpha_1 < 0$ implies that $T_f < T_\infty$, and in such case there will be a heat transfer from the fluid to the wall. Also, the changes in velocity with positive values of α_1 is more prominent in the presence of mixed convection parameter. Further, the temperature and concentration boundary

Table 2.3: *Comparison of* $-\theta'(\xi, 0)$ *for* $N = 0$, $\mathcal{B} = 0$, $\Omega = 0$, $\alpha_1 = 0$ *and* $\alpha_2 = 0$ *with* $Da \to \infty$, $\lambda = 0$, $\varepsilon = 1$ *and* $Bi \to \infty$.

Variation of $-\theta'(\xi, 0)$ with Ri							Variation of $-\theta'(\xi, 0)$ with ξ		
$\xi \to 0$	Pr = 0.72		Pr = 10		Pr = 100		$Ri = 7.928$	Pr = 10	
Ri	[59]	Present	[59]	Present	[59]	Present	ξ	[59]	Present
0.0	0.2956	0.2956	0.7281	0.7281	1.5718	1.5720	0.00125	0.7313	0.7315
0.01	0.2979	0.2979	0.7312	0.7313	1.5754	1.5750	0.00500	0.7404	0.7398
0.04	0.3043	0.3044	0.7403	0.7404	1.5855	1.5850	0.01250	0.7574	0.7569
0.1	0.3156	0.3158	0.7572	0.7574	1.6058	1.6050	0.05000	0.8259	0.8255
0.4	0.3559	0.3561	0.8254	0.8259	1.6905	1.6910	0.12500	0.9212	0.9218
1.0	0.4053	0.4058	0.9207	0.9212	1.8265	1.8260	0.25000	1.0290	1.0288

Table 2.4: *Comparison of* $f'', -g', -\theta', -\phi'$ *using the Shooting method and SLM for various values of* N *with* $\alpha_1 = 1.2$, $\varepsilon = 1.0$, $\mathcal{B} = 0.5$, $Da \to \infty$, $\alpha_2 = 1.5$, $Bi \to \infty$, $\xi \to 0$ *and* $\Omega = 30^0$.

	SLM				Shooting Method			
N	f''	$-g'$	$-\theta'$	$-\phi'$	f''	$-g'$	$-\theta'$	$-\phi'$
0.1	1.63733	0.00222	0.46467	0.26000	1.63733	0.00222	0.46467	0.2600
0.3	1.38112	0.00851	0.44225	0.25119	1.38112	0.00851	0.44225	0.25119
0.6	0.94169	0.02846	0.39436	0.23097	0.94169	0.02846	0.39436	0.23097
0.9	0.34256	0.09345	0.29884	0.18580	0.34256	0.09345	0.29884	0.18580

layer thicknesses decrease with the increase of α_1.

Figures 2.11(a) to 2.11(d) depict the influence of nonlinear density-concentration parameter (α_2) for a fixed value of α_1 on the velocity, microrotation, temperature and concentration profiles. The initial velocity is zero at the surface of the plate and increases gradually away from the plate and reaches the free stream velocity to satisfy the outer boundary condition as plotted in Fig. 2.11(a). However, the rise in NDC parameter changes the sign of microrotation from negative to positive within the boundary layer as shown in Fig.2.11(b). In the absence, as well as, in the presence of nonlinear density-concentration parameter α_2, the magnitudes of the temperature and concentration decrease with the increase of α_2 which is presented in Figs.2.11(c)-2.11(d). Further, the impact of α_2 on the temperature and concentration distributions is more effective, as compared with that of α_1.

Figures 2.12(a)-2.12(d) display the velocity, microrotation, temperature and concentration distributions of the fluid flow for different values of the Biot number Bi. It is noteworthy from Figs.2.12(a) and 2.12(b) that, as the Biot number increases, the velocity profile increases and the microrotation changes its behaviour from decreasing to increasing values within the boundary layer. Fig.2.12(c) demonstrates that the effect of Biot number on the temperature profile and mainly shows two results. The convective boundary condition is changing into wall condition, when the Biot number tends to infinity and it is proven by Fig.2.12(c). As Bi increases from thermally thin case ($Bi < 0.1$) to thermally thick case ($Bi > 0.1$) the temperature distribution increases at the plate. The effect of Biot number on the concentration profile is displayed in Fig.2.12(d) and it reveals that the concentration reduces when the Biot number changes its value from least to large value.

Figures 2.13(a) to 2.13(d) illustrate the variation of the velocity, microrotation, temperature and concentration for different values of the angle of inclination ($0^0 \leq \Omega \leq 90^0$). Moreover, the equations for the limiting cases of the vertical and horizontal plates are recovered from the transformed equations by setting $\Omega = 0^0$ and $\Omega = 90^0$ respectively. The influence of inclination angle on the velocity profile is displayed in Fig.2.13(a). Due to the reduction in the thermal and solutal buoyancy in Eq.(2.50) with respect to changes in the inclination angle Ω, the velocity distribution reduces within the momentum boundary layer, as shown in Fig.2.13(a). In other words, an increase in the inclination angle leads to reduce the velocity distribution within the momentum boundary layer region. Also, one can observe from Fig.2.13(a) that the maximum buoyancy force for the temperature and concentration difference occurs for $\Omega = 0^0$ (vertical plate). When the position of the flat plate is changed from vertical to horizontal, it is observed that the microrotation increases near the plate and far away from the plate it shows a reverse trend as portrayed in Fig.2.13(b). It is noticed from Fig.2.13(c) and Fig.2.13(d) that the temperature and concentration enhance with an increase in the inclination angle. In particular, when the surface is vertical, a small change in temperature and concentration distributions is observed, whereas there is large change for the horizontal surface.

Changes in fluid flow profiles are depicted in Figs.2.14(a) to 2.14(d) for different values of the mixed convection parameter Ri in both aiding ($Ri > 0$) and opposing ($Ri < 0$) flows. It reveals that as the value of Ri increases, the dimensionless velocity rises. Compared with the limiting case of $Ri = 0.0$ (i.e., pure forced convection), an increase in the value of Ri gives rise to a higher velocity.

Since a greater value of Ri indicates a greater buoyancy effects in mixed convective flow leads to an acceleration of the fluid flow. From Fig.2.14(b), we see that the microrotation completely negative within the boundary layer in both aiding ($Ri > 0$) and opposing ($Ri < 0$) flows. Also, it is clear that the microrotation increases with an increase in the mixed convection parameter Ri. Fig. 2.14(c) displays the dimensionless temperature for selected values of Ri in both aiding and opposing flows. The results indicate that the dimensionless temperature decreases with an increasing value of Ri. In the limiting case of $Ri = 0$ (i.e., pure forced convection), an increase in the value of Ri gives rise to a reduced temperature. The reason for this is that a greater value of Ri indicates a greater buoyancy effects, which increases the convection cooling effect and hence reduces the temperature. The effect of mixed convection parameter Ri on the dimensionless concentration is depicted in Fig. 2.14(d) in both aiding and opposing flows. It is clear that the concentration of the fluid decreases with the increase of mixed convection parameter Ri.

Figures 2.15(a)-2.15(d) are depicted for the effects of nonlinear density-temperature (NDT) and nonlinear density-concentration (NDC) parameters on the non-dimensional skin friction, wall couple stress, local heat and mass transfer rates against the stream wise coordinate ξ. It is observed that both heat and mass transfer rates increase with α_1, when other parameters are fixed. The effect of α_2 on Nusselt and Sherwood numbers shows the same behavior as that of α_1. Also, the influence of these two parameters are very prominent on the skin friction and wall couple stress of micropolar fluid and these are magnified by α_1 and α_2.

The effects of non-Darcy parameter (Forchheimer number; Fs) and micropolar martial parameter N on the non-dimensional physical quantities of the flow are portrayed in Figs.2.16(a)-2.16(d). The results indicate that as Fs increases, the skin friction, wall couple stress, local heat and mass transfer rates also increase for a fixed value of micropolar parameter. Hence, the inertial effect in micropolar fluid saturated non-Darcy porous medium increases the physical quantities of the fluid flow. Also, it can be observed from these figures that, for a fixed value of Fs, the heat and mass transfer coefficients fall down with the rise of micropolar parameter. Therefore the presence of microscopic effects arising from the local structure and micro-motion of the fluid elements reduce the heat and mass transfer coefficients.

The effects of Biot number Bi and inclination angle Ω on the skin friction, wall couple stress, local heat and mass transfer rates are depicted in Figs.2.17(a)-2.17(d). The influence of inclination angle on the heat and mass transfer rates are noted along the stream-wise coordinate ξ, as shown

in Figs.2.17(a)-2.17(b). The results reveal that the local Nusselt number and Sherwood number reduce gradually when the plate is displaced from its vertical to horizontal position. Also, a nominal effect on the wall couple stress and considerable increment in the skin friction are noticed for high enough values of the Biot number Bi, as depicted in Figs.2.17(c)- 2.17(d).

Finally, the influence of mixed convection parameter on the physical quantities of the flow are displayed by Figs.2.18(a)-2.18(d). It is found that the skin friction, wall couple stress, local heat and mass transfer rates increase when the flow direction is changed from opposing to aiding, and the effect of mixed convection parameter is more on skin friction and wall couple stress as compared with that of the heat and mass transfer rates.

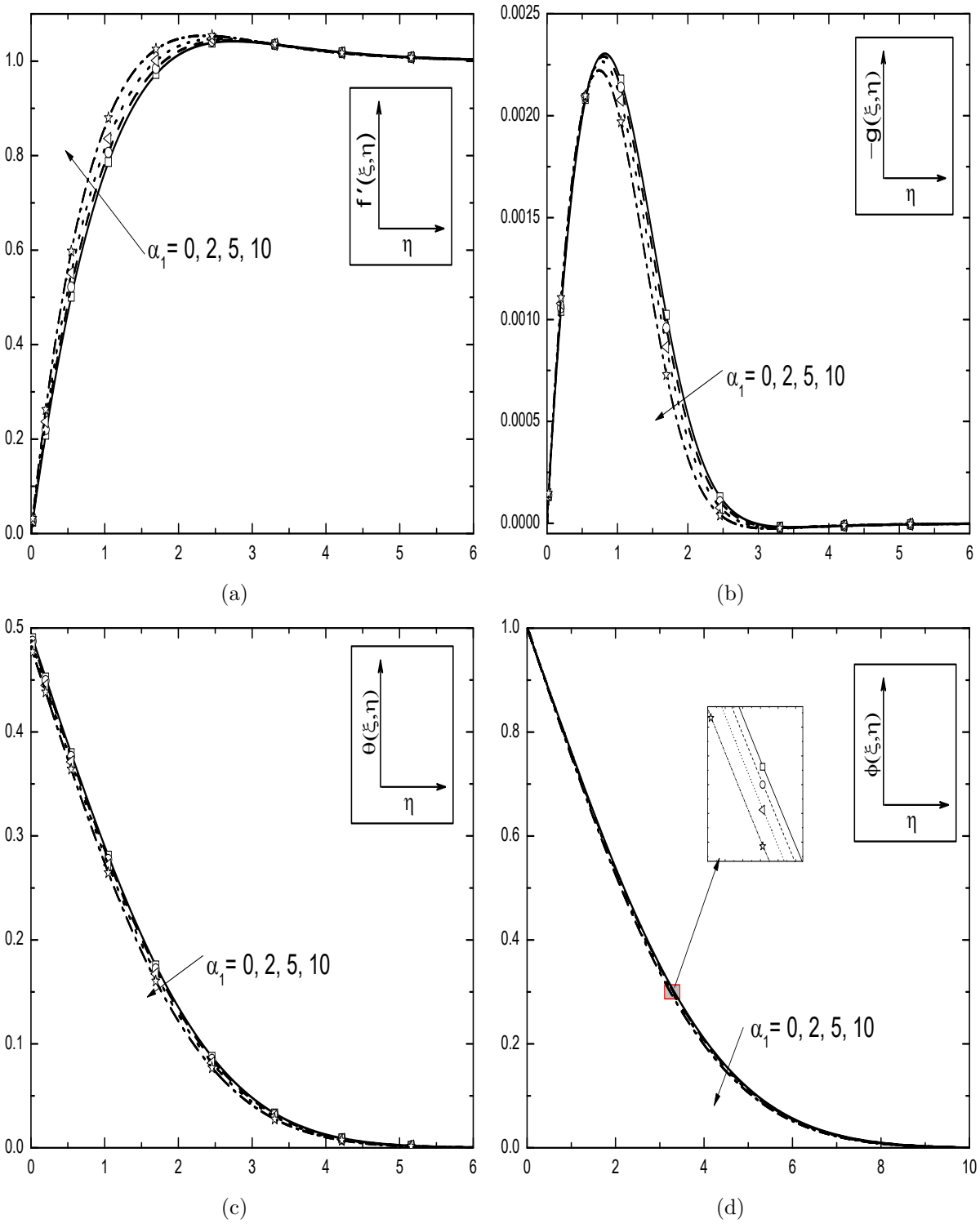

Figure 2.10: *Effect of* α_1 *on the (a) velocity, (b) microrotation, (c) temperature and (d) concentration along* η *with the fixed values of* $\xi = 0.5$, $\alpha_2 = 0.5$, $\Omega = 30^0$, $N = 0.3$, $Bi = 0.6$, $Ri = 1.0$ *and* $Fs = 0.2$.

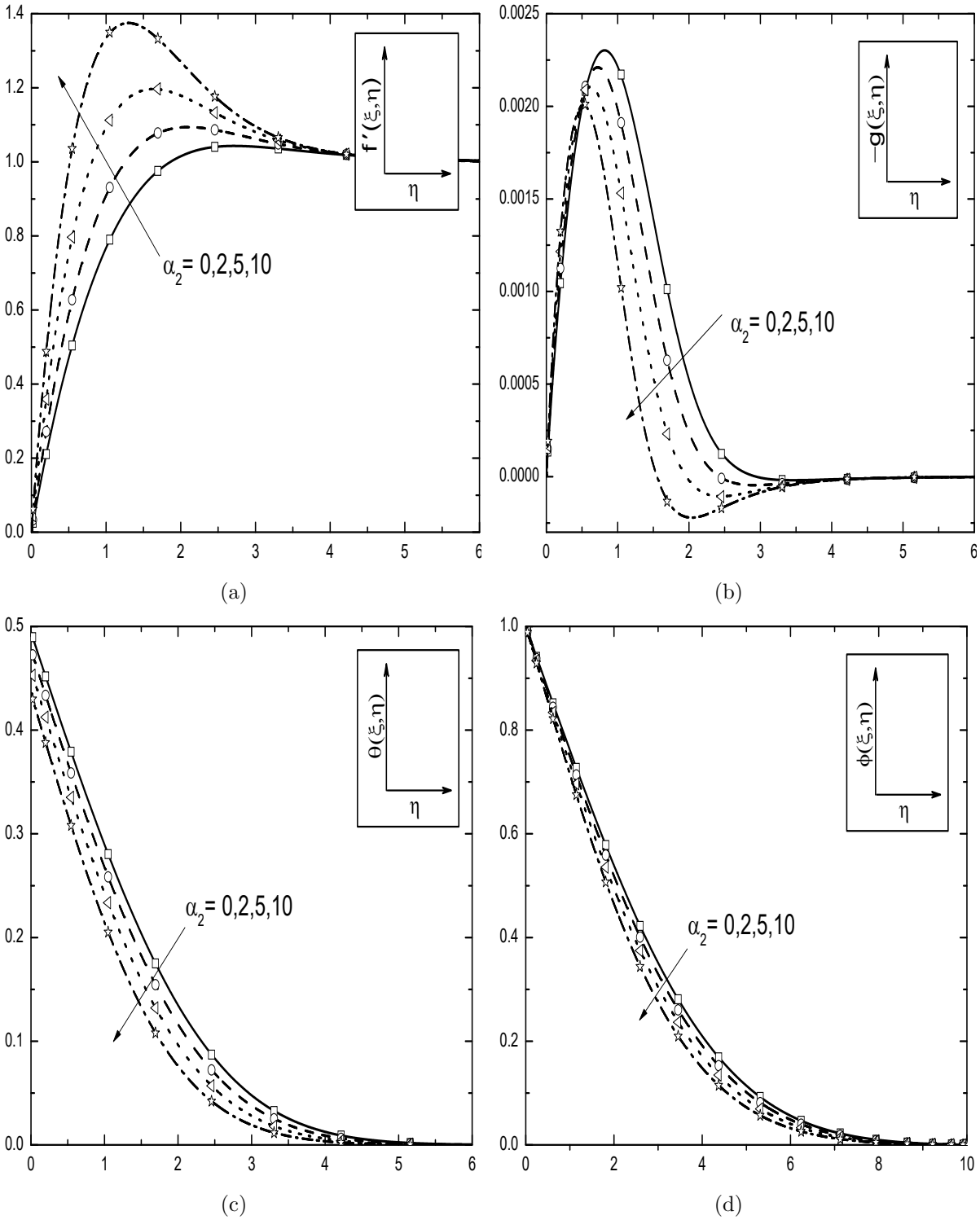

Figure 2.11: *Effect of α_2 on the (a) velocity, (b) microrotation, (c) temperature and (d) concentration along η with the fixed values of $\xi = 0.5$, $\alpha_1 = 1$, $\Omega = 30^0$, $N = 0.3$, $Bi = 0.6$, $Ri = 1.0$ and $Fs = 0.2$.*

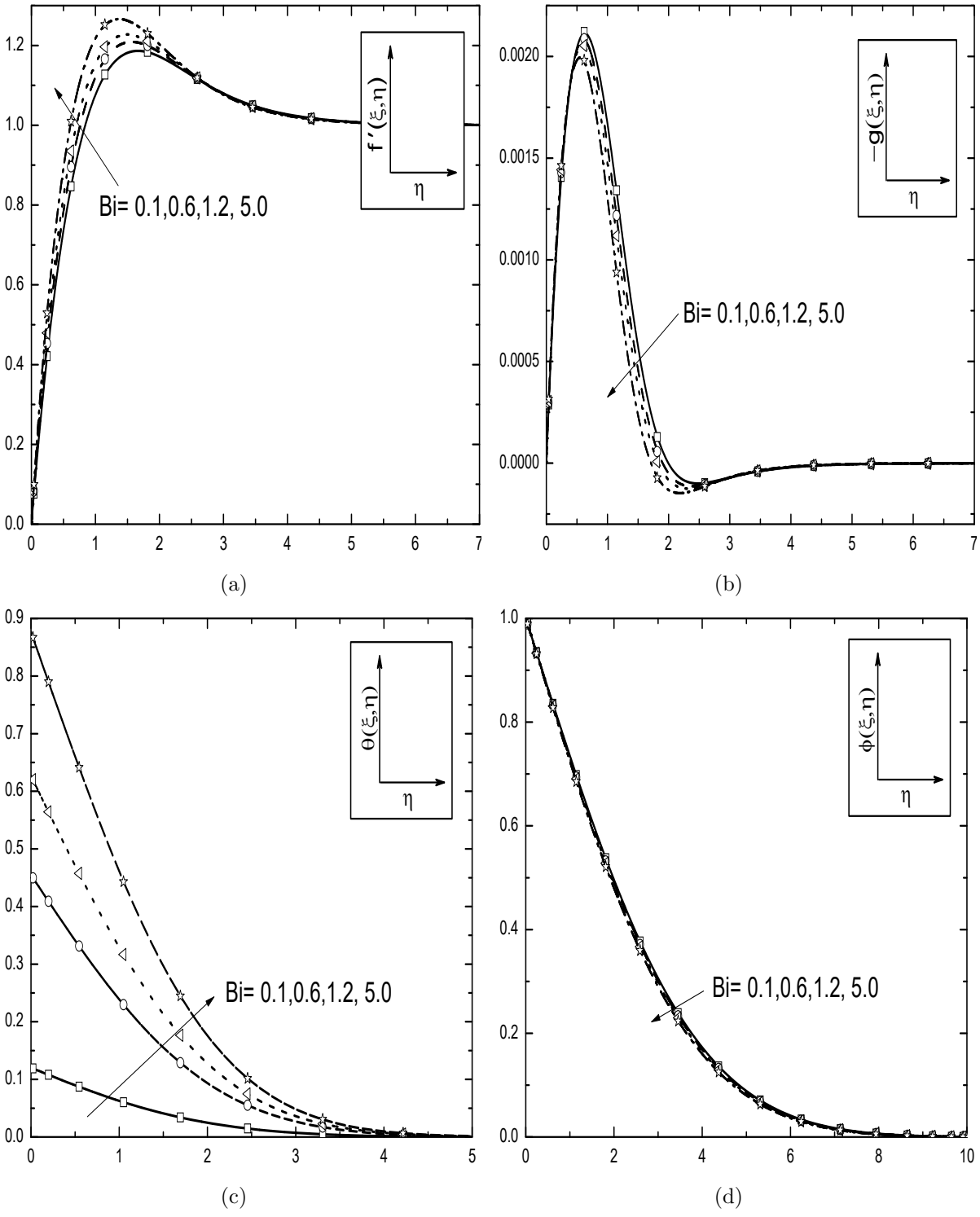

Figure 2.12: *Effect of Bi on the (a) velocity, (b) microrotation, (c) temperature and (d) concentration along* η *with the fixed values of* $\xi = 0.5$, $\alpha_1 = 1$, $\alpha_2 = 1$, $\Omega = 30^0$, $Ri = 1.0$, $N = 0.3$ *and* $Fs = 0.2$.

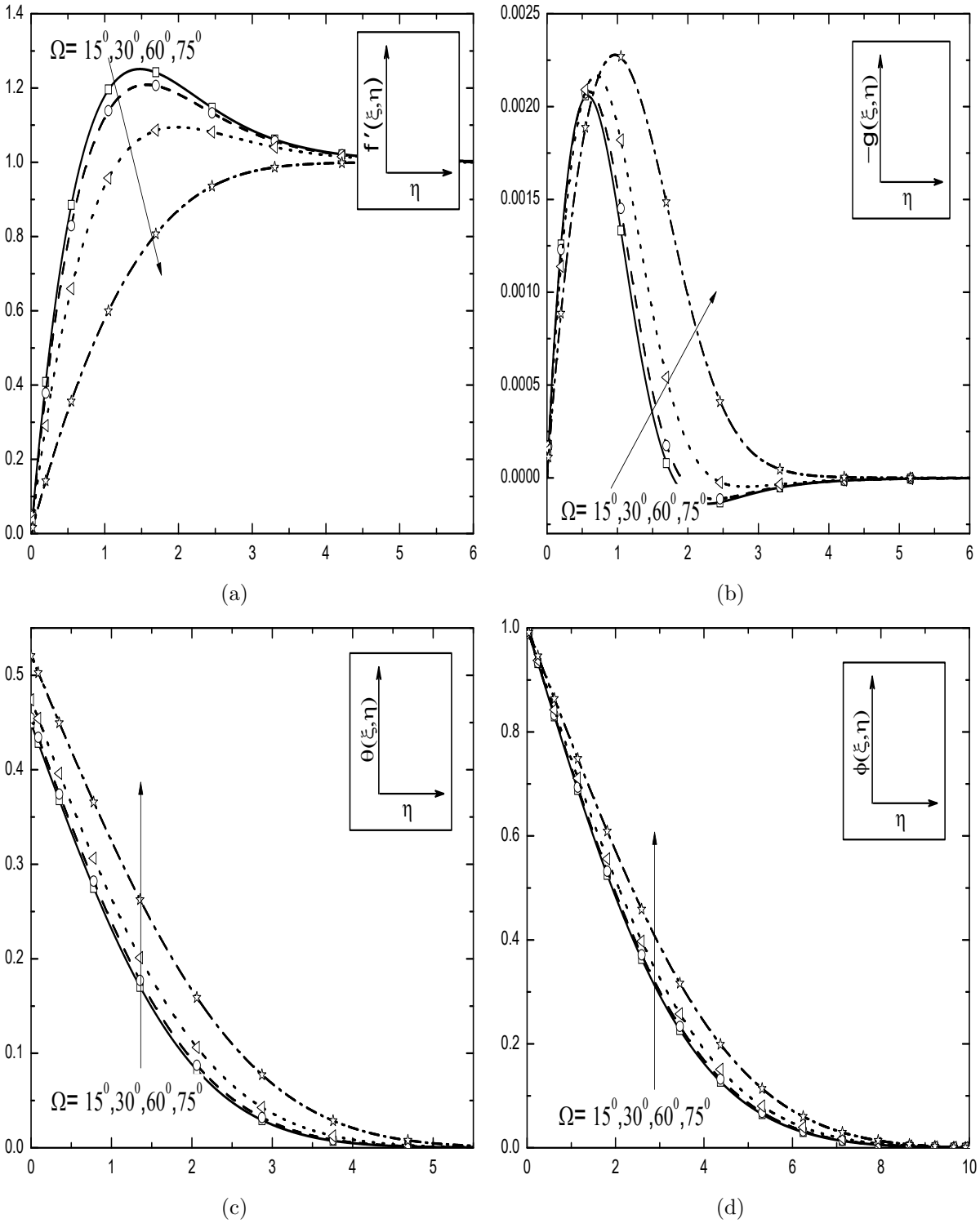

Figure 2.13: *Effect of* Ω *on the (a) velocity, (b) microrotation, (c) temperature and (d) concentration along* η *with the fixed values of* $\xi = 0.5$, $\alpha_1 = 1$, $\alpha_2 = 1$, $Ri = 1.0$, $Bi = 0.6$, $N = 0.3$ *and* $Fs = 0.2$.

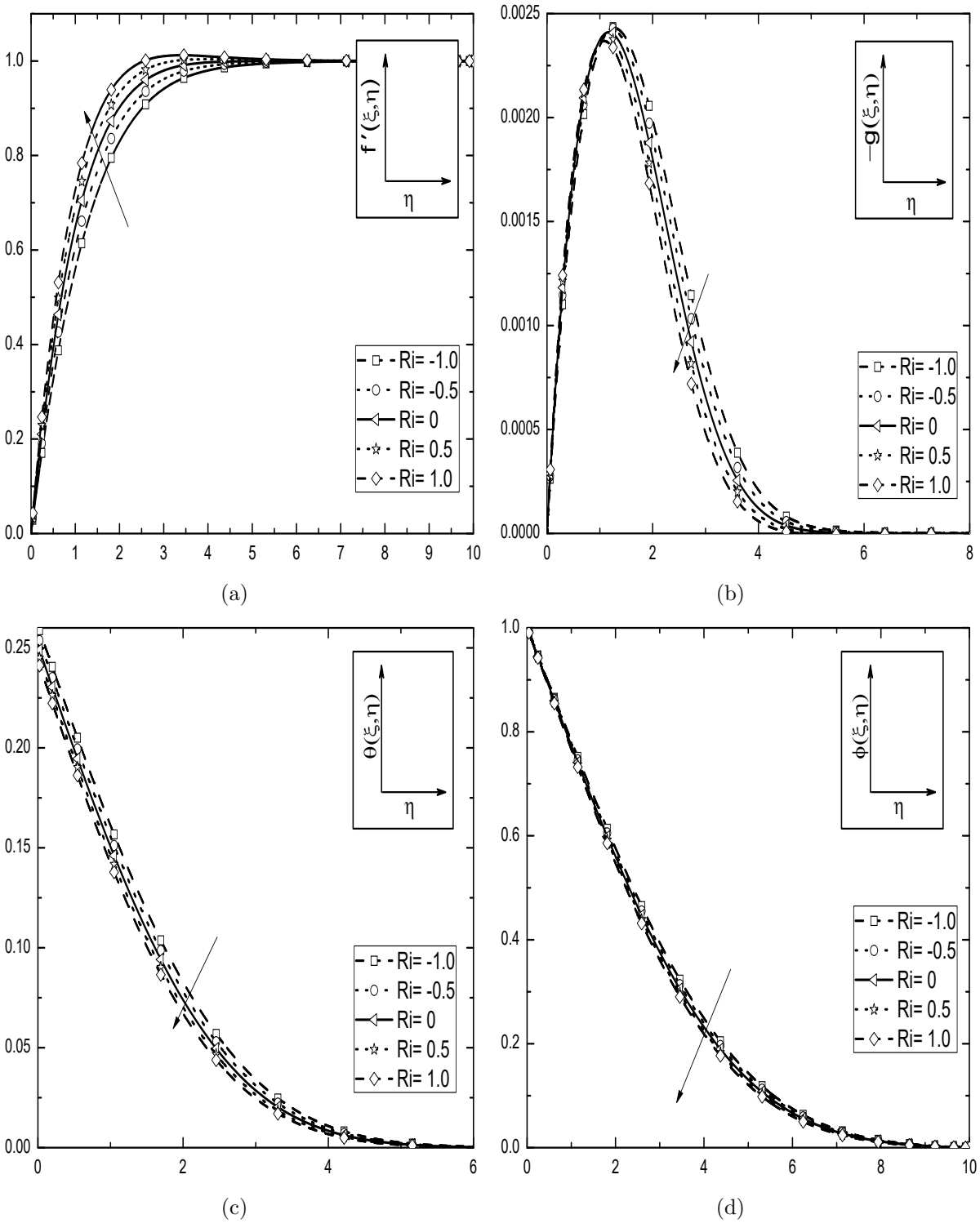

Figure 2.14: *Effect of Ri on the (a) velocity, (b) microrotation, (c) temperature and (d) concentration along* η *with the fixed values of* $\xi = 0.5$, $\alpha_1 = 1$, $\alpha_2 = 1$, $\Omega = 30^0$, $Bi = 0.3$, $N = 0.5$ *and* $Fs = 0.5$.

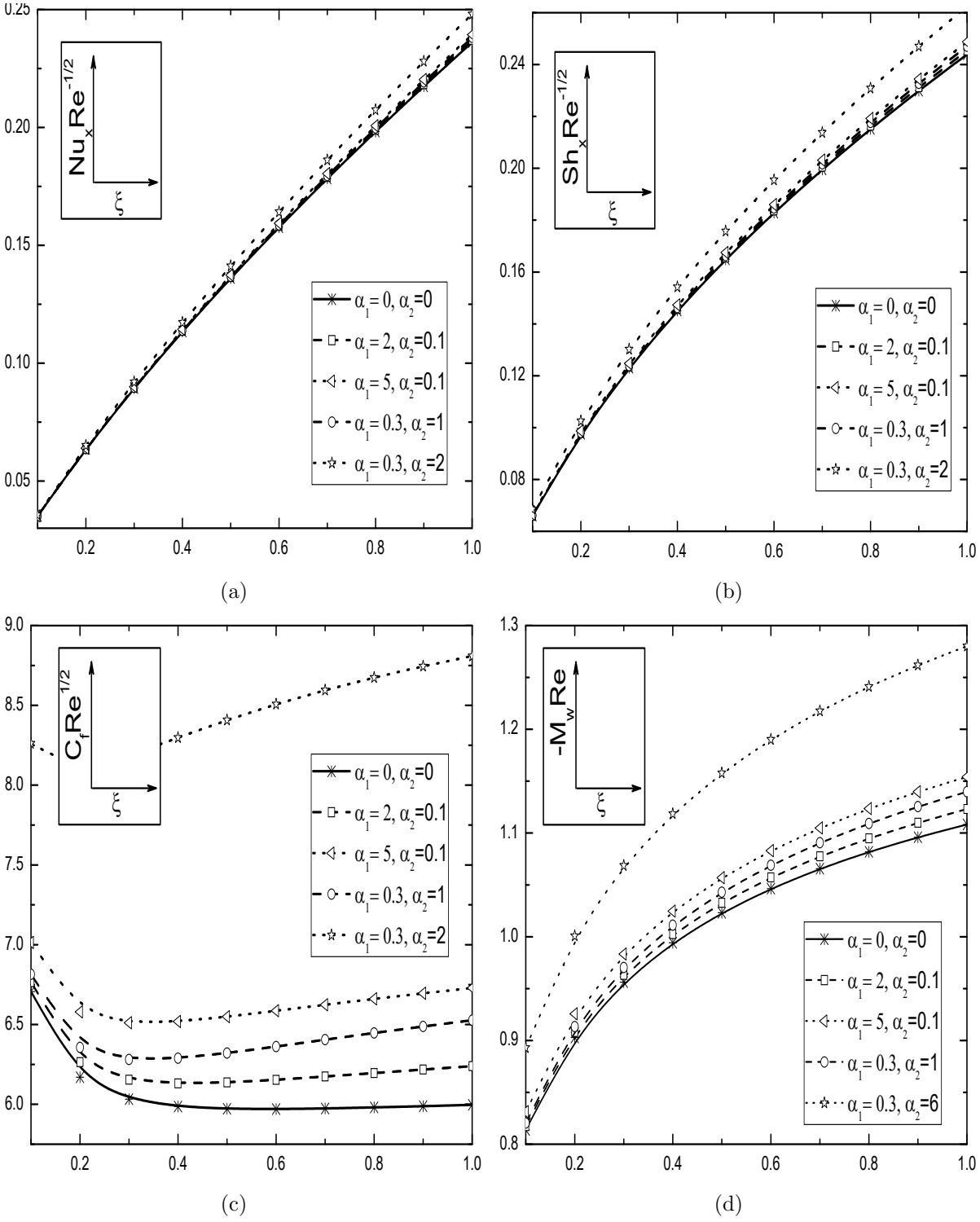

Figure 2.15: *Effects of* α_1 *and* α_2 *on the (a) heat transfer rate, (b) mass transfer rate, (c) skin friction and (d) wall couple stress along* ξ *with the fixed values of* $\Omega = 30^0$, $N = 0.5$, $Ri = 1.0$, $Bi = 0.5$ *and* $Fs = 0.5$.

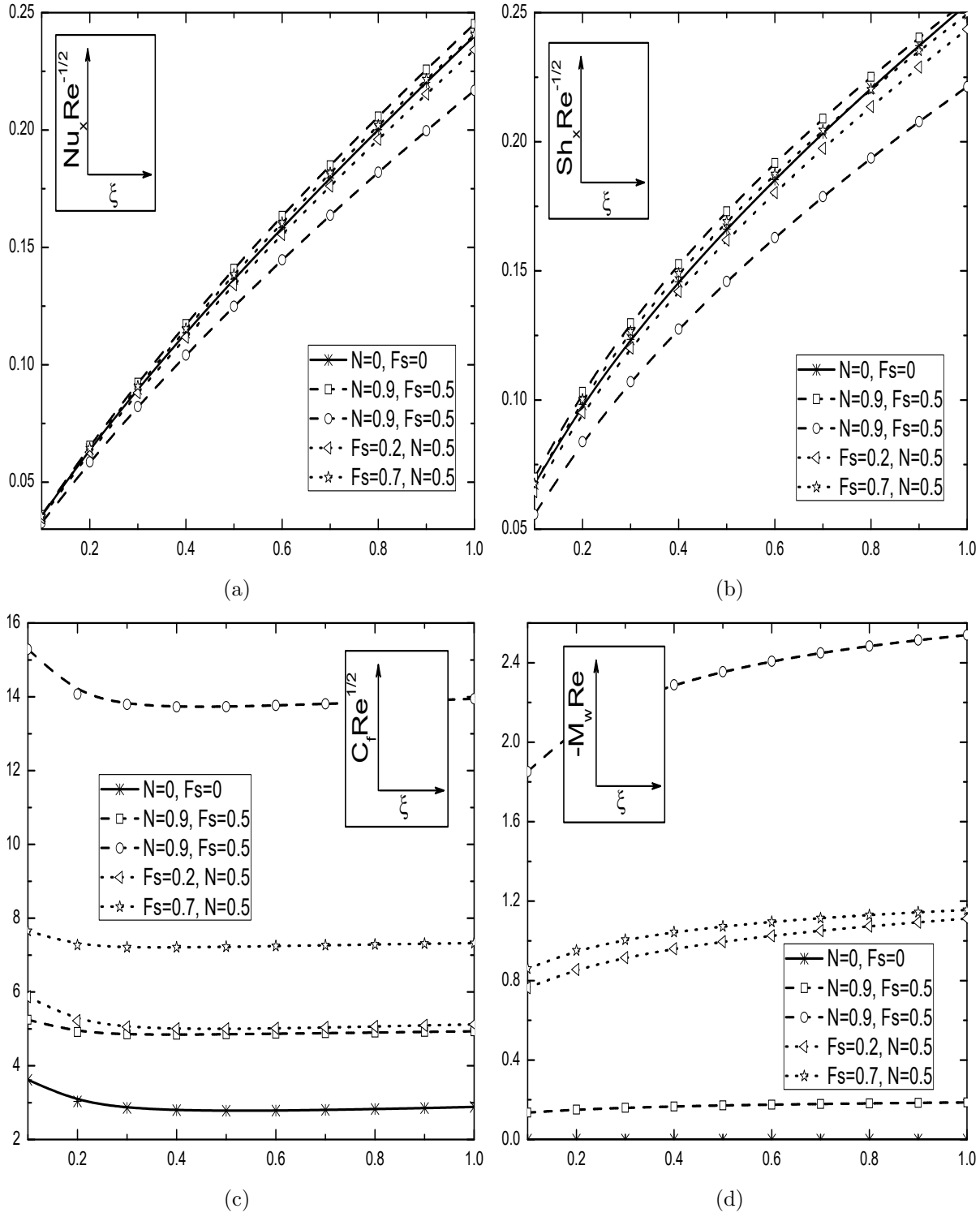

Figure 2.16: *Effects of Fs and N on the (a) heat transfer rate, (b) mass transfer rate, (c) skin friction and (d) wall couple stress along ξ with the fixed values of $\alpha_1 = 1$, $\alpha_2 = 1$, $\Omega = 30^0$, $Ri = 1$ and $Bi = 0.6$.*

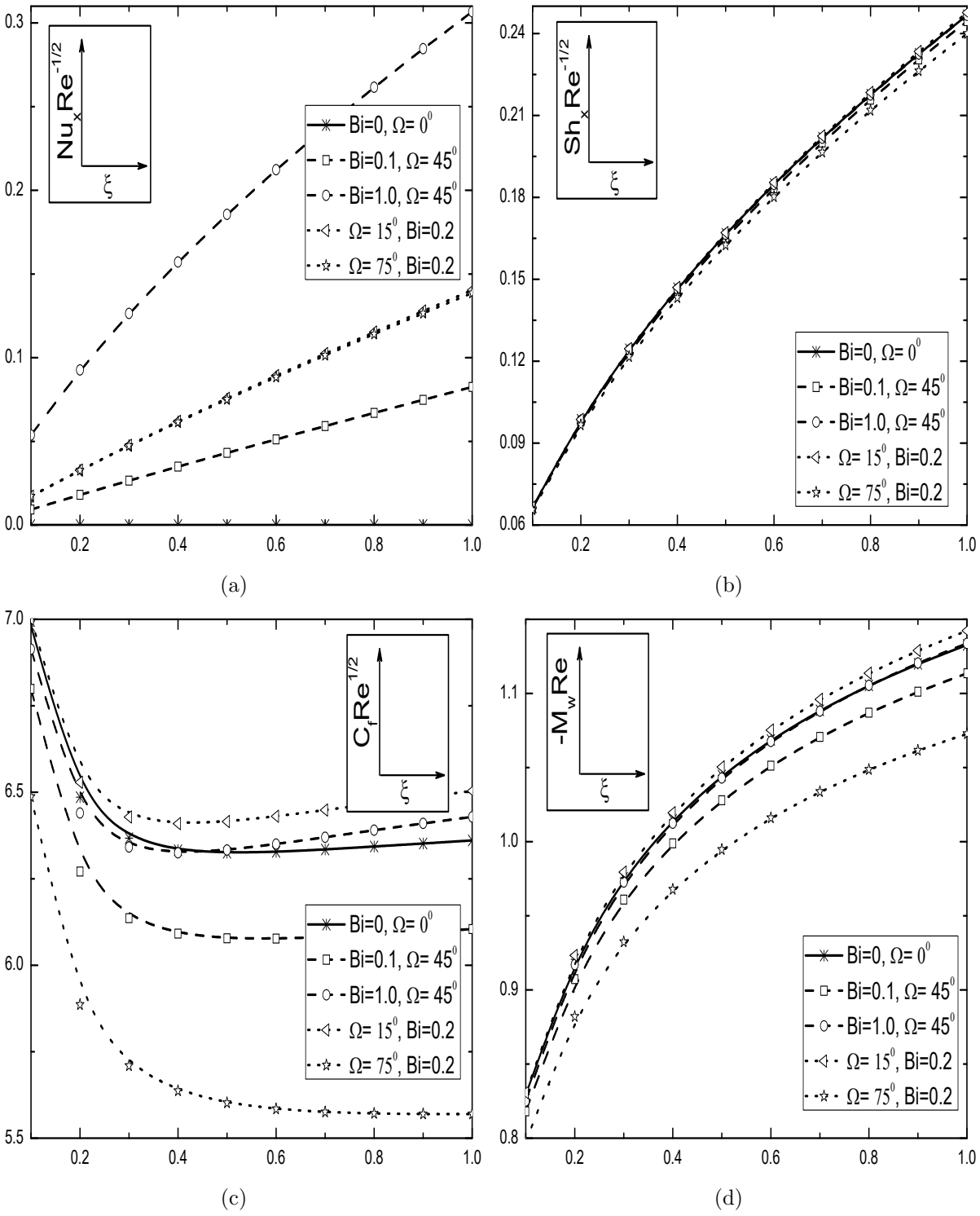

Figure 2.17: *Effects of Bi and* Ω *on the (a) heat transfer rate, (b) mass transfer rate, (c) skin friction and (d) wall couple stress along* ξ *with the fixed values of* $\alpha_1 = 1$, $\alpha_2 = 1$, $N = 0.3$, $Fs = 0.2$, $Ri = 1.0$ *and* $Bi = 0.6$.

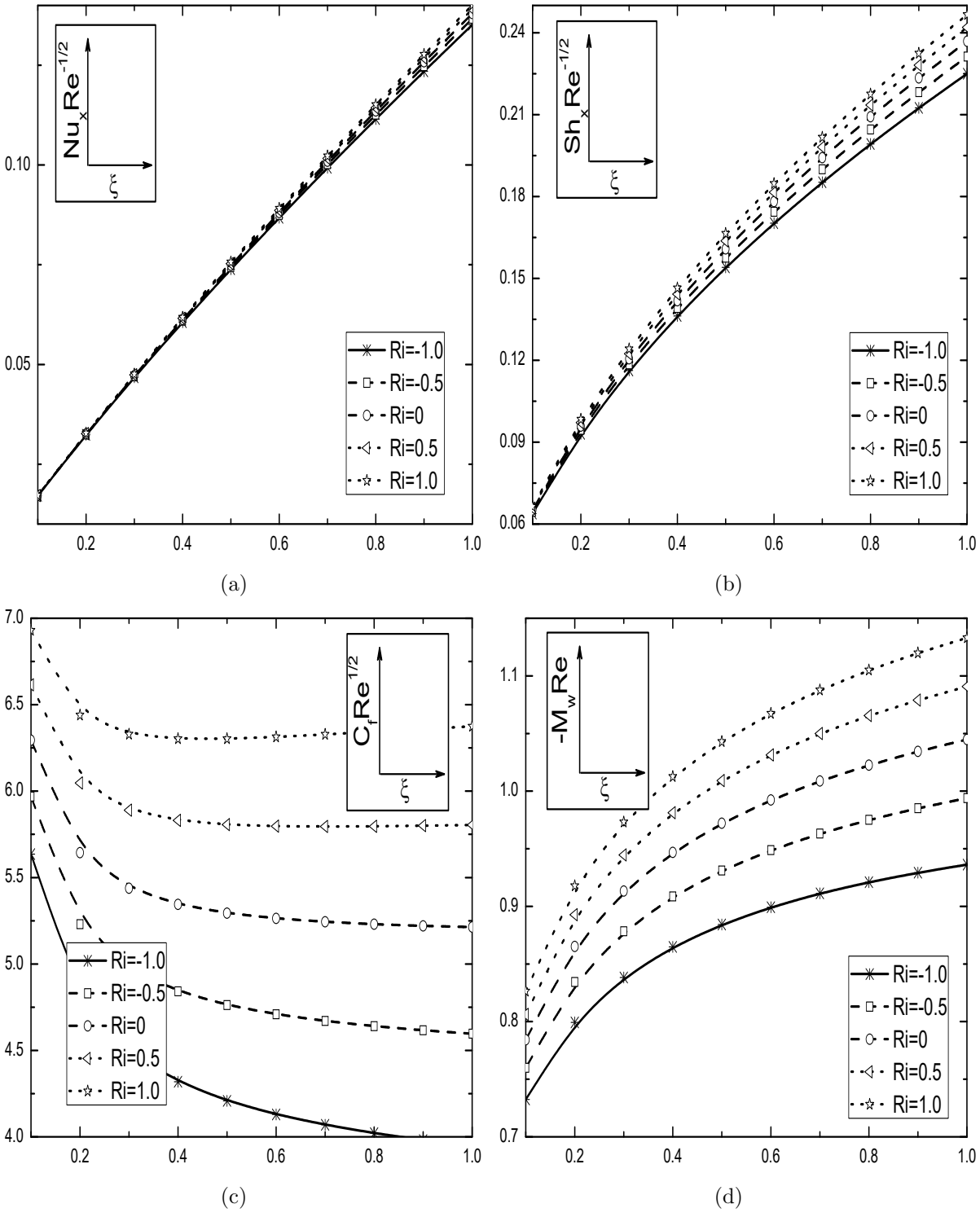

Figure 2.18: *Effect of Ri on the (a) heat transfer rate, (b) mass transfer rate, (c) skin friction and (d) wall couple stress along* ξ *with the fixed values of* $\alpha_1 = 1$, $\alpha_2 = 1$, $N = 0.5$, $Fs = 0.5$, $\Omega = 30^0$ *and* $Bi = 0.5$.

2.3 Conclusions

In this chapter, a problem of nonlinear convective flow of a micropolar fluid along an inclined plate in a non-Darcy porous medium under the convective boundary condition has been investigated in two cases: (a) natural convection and (b) mixed convection. The solution of system of non-dimensional partial differential equations along with the associated boundary conditions, is obtained by using the successive linearisation method together with the local similarity and non-similarity approaches. From this analysis, the following conclusions can be drawn for both the cases (a) and (b).

An increase in the nonlinear density-temperature (NDT) parameter tends to increase the skin friction, heat and mass transfer rates, but decrease the temperature and concentration of micropolar fluid in both free and mixed convection cases. The velocity distribution is more near the plate and far away from the plate, it shows reverse trend with an increase of NDT parameter in case (a), but in case (b) the velocity increases. Further, the effect of the NDT parameter on the microrotation is notable in every part of the boundary layer, but more significant away from the plate and also the rise in NDT parameter changes the sign of microrotation in both cases (a) and (b). The influence of NDC parameter is same as NDT parameter, but it gives more significant influence as compared with NDT parameter. An increase in the Biot number leads to increase the velocity near the plate and away from the plate it decreases in case (a). But in case (b), velocity is magnified by Biot number. The temperature, skin friction and heat transfer rates enhance with Biot number whereas the concentration reduces in both cases (a) and (b). In case (a) and case (b), an increase in the inclination angle leads to decrease the velocity, whereas it increases the temperature and concentration distributions within the boundary layer region. Further, the micropolar parameter diminishes the wall couple stress, heat and mass transfer rates, whereas it expands skin friction of micropolar fluid.

Chapter 3

Effect of Cross-Diffusion in a Micropolar Fluid Saturated Non-Darcy Porous Medium with Convective Boundary Condition [1]

3.1 Introduction

Exceptional studies are established in the analysis of heat and mass transport phenomena of free and mixed convective flow of a micropolar fluid over different geometries in porous media. Various disciplines in geophysical and engineering industries are enforced to study the microscopic nature of fluid elements such as the cooling systems, petroleum reservoirs, agricultural fields, fiber insulation, ceramic processes, grain storage devices, coal combustions, etc. A comprehensive report on convective flow of a micropolar fluid in a Darcy, as well as, in a non-Darcy porous medium can be found in the textbook by Nield and Bejan [75] and also see the citations therein.

In many circumstances, the temperature and concentration are directly coupled under the

[1] Case(a): Published in "**International Journal of Pure and Applied Mathematics**" 113 (8) (2017) 46–53, Case(b): Published in "**Computational Thermal Sciences: An International Journal**" 11(3) (2019) 205–218

condition that the cross-diffusion (namely, Soret and Dufour) effects are not negligible and these effects are more significant in areas such as geosciences, petrology, and hydrology etc. In view of these applications, Awad and Sibanda [10] analyzed the effect of cross-diffusion on micropolar fluid flow through horizontal channel. Hayat *et al.* [42] provided a semi-analytical solution to examine cross-diffusion effects on stagnation-point flow along a stretching sheet in a micropolar fluid. Several authors to mention few, Beg *et al.* [17] and Pal *et al.* [77] extended this concept to various fields of fluid dynamics.

Due to the realistic nature of convective boundary condition, the analysis of heat transfer with the convective boundary condition has prominent applications in industrial and engineering fields such as nuclear plants, gas turbines, heat exchangers, etc. In the presence of convective boundary condition, heat is supplied to the convecting fluid through a bounding surface with a finite heat capacity, which provides a convective heat transfer coefficient. Makinde *et al.* [63] addressed the impacts of cross-diffusion effects on hydromagnetic flow of a cold fluid over a vertical plate in the presence of convective boundary condition, whereas Swapna *et al.* [102] developed a theoretical model to analyze the collective impact of convective boundary condition and variable viscosity on the radiative magneto-micropolar fluid flow.

Based on the above-mentioned applications and analysis, the authors are motivated to study the influence of nonlinear convection on micropolar fluid flow along an inclined plate by including convective boundary condition and cross-diffusion effects for the first time. Using local similarity and non-similarity techniques, the governing nonlinear partial differential equations are converted into a sequence of nonlinear ordinary differential equations and then the resultant equations are solved by successive linearization method. The fluid flow characteristics are shown and analyzed through graphical representation. The results are compared with relevant results in the existing literature and found to be in good agreement.

3.2 Mathematical Formulation

Consider the steady, laminar and two-dimensional flow of an incompressible micropolar fluid over a semi-infinite inclined flat plate embedded in a non-Darcy porous medium. The plate is inclined at angle Ω to the vertical direction. The x-axis is along the vertical plate and y-axis normal to the

plate. This chapter is an extension of chapter-2 by considering the Soret and Dufour effects. Under the assumptions made in chapter-2 and using the Darcy-Forcheimer model and Dupuit-Forchheimer relationship [75], the governing equations describing the micropolar fluid are:

$$\frac{\partial u}{\partial x}+\frac{\partial v}{\partial y}=0 \tag{3.1}$$

$$\begin{aligned}\frac{\rho}{\varepsilon^2}\left(u\frac{\partial u}{\partial x}+v\frac{\partial u}{\partial y}\right)&=\frac{1}{\varepsilon}\left(\mu+\kappa\right)\frac{\partial^2 u}{\partial y^2}+\kappa\frac{\partial \omega}{\partial y}+\frac{\mu}{K_p}\left(u_\infty-u\right)+\frac{\rho\, b}{K_p}\left(u_\infty^2-u^2\right)\\&+\rho g^*\left[\beta_0\left(T-T_\infty\right)+\beta_1(T-T_\infty)^2+\beta_2\left(C-C_\infty\right)+\beta_3(C-C_\infty)^2\right]\cos\Omega\end{aligned} \tag{3.2}$$

$$\frac{\rho j}{\varepsilon}\left(u\frac{\partial \omega}{\partial x}+v\frac{\partial \omega}{\partial y}\right)=\gamma\frac{\partial^2\omega}{\partial y^2}-\kappa\left(2\omega+\frac{1}{\varepsilon}\frac{\partial u}{\partial y}\right) \tag{3.3}$$

$$u\frac{\partial T}{\partial x}+v\frac{\partial T}{\partial y}=\alpha\frac{\partial^2 T}{\partial y^2}+\frac{D\,K_T}{C_s\,C_p}\frac{\partial^2 C}{\partial y^2} \tag{3.4}$$

$$u\frac{\partial C}{\partial x}+v\frac{\partial C}{\partial y}=D\frac{\partial^2 C}{\partial y^2}+\frac{D\,K_T}{T_m}\frac{\partial^2 T}{\partial y^2} \tag{3.5}$$

where C_s is the concentration susceptibility, C_p is the specific heat capacity, K_T is the thermal diffusion ratio and T_m is the mean fluid temperature.

The corresponding boundary conditions are

$$\begin{aligned}u=0,\ v=0,\ \omega=0,\ -k_f\frac{\partial T}{\partial y}=h_f(T_f-T),\ C=C_w\ \text{ at }\ y=0\\ u=u_\infty,\ \omega=0,\ T=T_\infty,\ C=C_\infty\ \text{as}\ y\to\infty\end{aligned} \tag{3.6}$$

In this chapter also, two types (cases) of problems are considered: (a) free/natural convection and (b) mixed convection.

3.2.1 Case(a): Natural Convection

In the case of natural convection, the fluid flow is due to buoyancy forces only and hence, the velocity of the outer flow becomes zero ($i.e., u_\infty = 0$). We introduce the following non-dimensional

variables

$$\xi = \frac{x}{L},\ \eta = \frac{y}{L}\left(\frac{Gr}{\xi}\right)^{1/4},\ \psi(\xi,\eta) = \frac{\mu\, Gr^{1/4}\ \xi^{3/4}}{\rho} f(\xi,\eta)$$
$$\omega(\xi,\eta) = \frac{\mu\, Gr^{3/4}\ \xi^{1/4}}{\rho L^2}\ g(\xi,\eta),\ \theta(\xi,\eta) = \frac{T-T_\infty}{T_f-T_\infty},\ \phi(\xi,\eta) = \frac{C-C_\infty}{C_w-C_\infty} \tag{3.7}$$

Substituting the stream function (2.7) and the transformations (3.7) into Eqs.(3.1) - (3.5), we obtain the following linear momentum, angular momentum, energy and concentration equations

$$\frac{1}{\varepsilon}\left(\frac{1}{1-N}\right) f''' + \frac{3}{4\varepsilon^2} f f'' - \frac{1}{2\varepsilon^2} f'^2 + \left(\frac{N}{1-N}\right) g' - \frac{1}{Da\, Gr^{\frac{1}{2}}} \xi^{\frac{1}{2}} f' - \frac{Fs}{Da} \xi\, f'^2 + [\theta(1+\alpha_1\theta) + \mathcal{B}\phi(1+\alpha_2\phi)]\cos\Omega = \frac{\xi}{\varepsilon^2}\left(f'\frac{\partial f'}{\partial \xi} - f''\frac{\partial f}{\partial \xi}\right) \tag{3.8}$$

$$\lambda g'' + \frac{3}{4\varepsilon} f g' - \frac{1}{4\varepsilon} f' g - \left(\frac{N}{1-N}\right)\mathcal{J}\xi^{\frac{1}{2}}\left(2g + \frac{1}{\varepsilon} f''\right) = \frac{\xi}{\varepsilon}\left(f'\frac{\partial g}{\partial \xi} - \frac{\partial f}{\partial \xi} g'\right) \tag{3.9}$$

$$\frac{1}{\mathrm{Pr}}\theta'' + \frac{3}{4} f\theta' + Du\,\phi'' = \xi\left(f'\frac{\partial \theta}{\partial \xi} - \frac{\partial f}{\partial \xi}\theta'\right) \tag{3.10}$$

$$\frac{1}{Sc}\phi'' + \frac{3}{4} f\phi' + Sr\,\theta'' = \xi\left(f'\frac{\partial \phi}{\partial \xi} - \frac{\partial f}{\partial \xi}\phi'\right) \tag{3.11}$$

where $Sr = \dfrac{D\, K_T(T_f - T_\infty)}{T_m \nu (C_w - C_\infty)}$ is the Soret number and $Du = \dfrac{D K_T (C_w - C_\infty)}{C_s C_p \nu (T_f - T_\infty)}$ is the Dufour number.

The associated boundary conditions (3.6) become

$$f'(\xi,0) = 0,\ f(\xi,0) = -\frac{4}{3}\xi\left(\frac{\partial f}{\partial \xi}\right)_{\eta=0},\ g(\xi,0) = 0,\ \theta'(\xi,0) = -Bi\,\xi^{\frac{1}{4}}\left[1-\theta(\xi,0)\right],$$
$$\phi(\xi,0) = 1,\ f'(\xi,\infty) = 0,\ g(\xi,\infty) = 0,\ \theta(\xi,\infty) = 0,\ \phi(\xi,\infty) = 0. \tag{3.12}$$

The non-dimensional shear stress C_f, wall couple stress M_w, local Nusselt number Nu_x and the Sherwood number Sh_x, are given by

$$C_f Gr^{\frac{1}{4}} = \left(\frac{2}{1-N}\right)\xi^{\frac{-3}{4}} f''(\xi,0),\ M_w Gr^{\frac{1}{2}} = \left(\frac{\lambda}{\xi\ \mathcal{J}}\right) g'(\xi,0),$$
$$Nu_x\, Gr^{\frac{-1}{4}} = -\xi^{\frac{3}{4}}\ \theta'(\xi,0),\ Sh_x\, Gr^{\frac{-1}{4}} = -\xi^{\frac{3}{4}}\ \phi'(\xi,0). \tag{3.13}$$

Results and Discussion

In this chapter also, the highly coupled nonlinear partial differential equations (3.8)- (3.11) together with boundary conditions (3.12) are converted into a set of eight coupled nonlinear ordinary differential equations using local similarity and non-similarity approaches. After that, a novel successive linearization method is applied to solve the reduced system of nonlinear ordinary differential equations for those eight unknowns, as explained in the case (a) of previous chapter. In the absence of cross-diffusion effects, the problem considered in this case reduces to the case (a) of the previous chapter. Validation of the present problem in this case, can be done on comparison as it was done in the case (a) of chapter-2. Further, the numerical computations are carried out by following the fixed values of parameters: $\mathcal{J} = 5.0$, $\lambda = 5.0$, $\mathcal{B} = 1.0$, Pr $= 0.7$, $Sc = 0.22$, $Gr = 10$, $\varepsilon = 0.4$, $Da = 0.1$ and $\xi = 0.5$, and these values are unaltered in this study, unless otherwise specified.

Figures 3.1(a)-3.1(d) are plotted for different values of NDT and NDC parameters on the non-dimensional velocity (f'), microrotation (g), temperature (θ) and concentration (ϕ) with $N = 0.6$, $Fs = 0.5$, $\Omega = 45^0$, $Bi = 0.6$, $Du = 0.3$ and $Sr = 1.0$. The nonlinear convection parameters (α_1 and α_2) measure the nonlinearity in the density-temperature and density-concentration relationships. The influences of α_1 and α_2 on the velocity profile are depicted in Fig.3.1(a). With the increase in both α_1 and α_2, the velocity increases, but far away from the plate, it shows the opposite trend. It is observed from Fig.3.1(b) that the microrotation shows reverse rotation near the two boundaries with the increase in both α_1 and α_2. Figs.3.1(c) and 3.1(d) exhibit the variation in temperature and concentration with respect to α_1 and α_2 and it is clear from these figures that the thermal and solutal boundary layer thicknesses reduce with an increase in both the NDT and NDC parameters.

Figures 3.2(a) -3.2(d) depict the variations of non-dimensional velocity (f'), microrotation (g), temperature (θ) and concentration (ϕ) across the boundary layers for various values of Biot number and non-Darcy parameter with $N = 0.5$, $\Omega = 30^0$, $Du = 0.3$, $Sr = 0.5$, $\alpha_1 = 1$ and $\alpha_2 = 1$. Fig.3.2(a) displays the fluid velocity profiles for different values of Biot number and non-Darcy parameter. Initially, the fluid velocity is zero at the surface of the plate and then it rises gradually away from the plate. Finally, the fluid velocity satisfies the free stream boundary conditions. It is interesting to reveal that the fluid velocity enhances with an enhancement in the Biot number (Bi) and reduces with the non-Darcy parameter (Fs). From Fig.3.2(b), it is clear that the microrotation profile shows reverse rotation near the two boundaries. Fig.3.2(c) depicts that the temperature of

the fluid is maximum at the wall and it diminishes exponentially to zero far away from the plate. Comparatively, the internal thermal resistance of the plate is more for a large value of Biot number than the boundary layer thermal resistance. From Fig.3.2(d), it is noticed that the concentration increases with an increase in both non-Darcy parameter and Biot number.

Variations in the dimensionless velocity, microrotation, temperature, and concentration profiles with respect to the Dufour and Soret numbers, are exhibited in Figs.3.3(a) to 3.3(d) for the fixed values: $N = 0.5$, $\Omega = 30^0$, $Bi = 0.3$, $Fs = 0.5$, $\alpha_1 = 1$ and $\alpha_2 = 1$. From Fig.3.3(a), it is clear that the velocity of the micropolar fluid increases with the increase of Soret and Dufour numbers. Fig.3.3(b) reveals that the microrotation has nominal affect based on the influences of Soret and Dufour numbers. Figs.3.3(c) and 3.3(d) indicates the influences of Soret and Dufour numbers on the temperature and concentration profiles. It is noted from these figures that, as the Dufour number increases, the temperature of fluid increases whereas the concentration decreases. But, the influence of Soret number is opposite to that of Dufour number on the same temperature and concentration profiles. It is involved directly in the concentration equation and increases the concentration, whereas it decreases the temperature of micropolar fluid.

Impacts of the coupling number and inclination angle on the dimensionless velocity, microrotation, temperature and concentration profiles are shown for $Du = 0.4$, $Sr = 1.0$, $Bi = 0.3$, $Fs = 0.5$, $\alpha_1 = 1$ and $\alpha_2 = 1$ by Figs.3.4(a)-3.4(d). It is observed from Fig.3.4(a) that the velocity of micropolar fluid flow diminishes with the increase of N and it is not as much as that in a viscous fluid. Influence of coupling number on the microrotation of micropolar fluid is depicted by Fig.3.4(b) and it reveals that the microrotation changes sign from negative to positive within the boundary layer. Additionally, with respect to coupling number, microrotation increases close to the plate and it diminishes far away from the plate, whereas inclination angle gives opposite change. Further, the microrotation tends to zero as $N \longrightarrow 0$, so the linear momentum equation is uncoupled with angular momentum equation and hence the resultant equations reduce to the viscous fluid flow equations. The impacts of inclination angle on the temperature and concentration profiles are portrayed in Figs.3.4(c) and 3.4(d) separately. An increase in the angle of inclination increases the fluid temperature and concentration. This is because of reduction in the thermal and concentration buoyancy caused by an enhancement in Ω. Also, one can notice that the temperature and concentration of the micropolar fluid increases with the enhancement of coupling number as shown in Figs.3.4(c) and 3.4(d).

Figures 3.5(a) to 3.5(d) are prepared to exhibit the influences of α_1 and α_2 on the skin friction ($C_f Gr^{\frac{1}{4}}$), wall couple stress ($M_w Gr^{\frac{1}{2}}$), heat transfer rate ($Nu_x\, Gr^{\frac{-1}{4}}$) and mass transfer rate ($Sh_x\, Gr^{\frac{-1}{4}}$) against the stream-wise coordinate ξ with $N = 0.6$, $Fs = 0.5$, $Bi = 0.6$, $Du = 0.3$, $Sr = 1.0$. It is observed that from these figures that, the above said four physical quantities increase with an increase in α_1 for a fixed value of α_2. The effect of α_2 is showing the same behavior on $C_f Gr^{\frac{1}{4}}$, $M_w Gr^{\frac{1}{2}}$, $Nu_x\, Gr^{\frac{-1}{4}}$ and $Sh_x\, Gr^{\frac{-1}{4}}$, as that of α_1.

The influences of Biot number and non-Darcy parameter on the skin friction ($C_f Gr^{\frac{1}{4}}$), wall couple stress ($M_w Gr^{\frac{1}{2}}$), heat transfer rate ($Nu_x\, Gr^{\frac{-1}{4}}$) and mass transfer rate ($Sh_x\, Gr^{\frac{-1}{4}}$) are displayed through Figs.3.6(a) to 3.6(d). Here the magnitudes of these four quantities ($C_f Gr^{\frac{1}{4}}$, $M_w Gr^{\frac{1}{2}}$, $Nu_x\, Gr^{\frac{-1}{4}}$ and $Sh_x\, Gr^{\frac{-1}{4}}$) decrease by the Forchheimer number. Also for fixed $N = 0.5$, $\Omega = 30^0$, $Du = 0.3$, $Sr = 0.5$, $\alpha_1 = 1$ and $\alpha_2 = 1$, the skin-friction as well as heat transfer rate increase, whereas the mass transfer rate decreases with the increase of Biot number Bi.

Effects of Soret and Dufour numbers on the physical quantities of a micropolar fluid are discussed through Figs.3.7(a) to 3.7(d) for $N = 0.5$, $\Omega = 30^0$, $Bi = 0.3$, $Fs = 0.5$, $\alpha_1 = 1$ and $\alpha_2 = 1$. Increment of Dufour number leads to decrease in both the surface drag coefficient and microrotation gradients, whereas the Soret number shows opposite influences on these two quantities compared to that of the Dufour number and this can be noticed from Figs.3.7(a) and 3.7(b). An increase in the Dufour number decreases the temperature of the fluid and thus, increases the Nusselt number as plotted in Fig.3.7(c). In the similar manner, the Soret number enhances the Sherwood number, as projected in Fig.3.7(d). Thus, the cross-diffusion coefficients Sr and Du have an opposite influence on the Nusselt and Sherwood numbers, as portrayed in Figs.3.7(c) -3.7(d).

The influences of coupling number and inclination angle on the skin friction, wall couple stress, heat and mass transfer rates are depicted through Figs.3.8(a) to 3.8(d) for $Du = 0.4$, $Sr = 1.0$, $Bi = 0.3$, $Fs = 0.5$, $\alpha_1 = 1$ and $\alpha_2 = 1$. An increase in the coupling number leads to enhance both the skin friction and wall couple stress, whereas these two quantities decrease with the angle of inclination as plotted in Figs.3.8(a) and 3.8(b). Further, the heat and mass transfer rates of micropolar fluid are decelerated with both inclination angle and coupling number, as depicted in Fig.3.8(c) and 3.8(d) respectively.

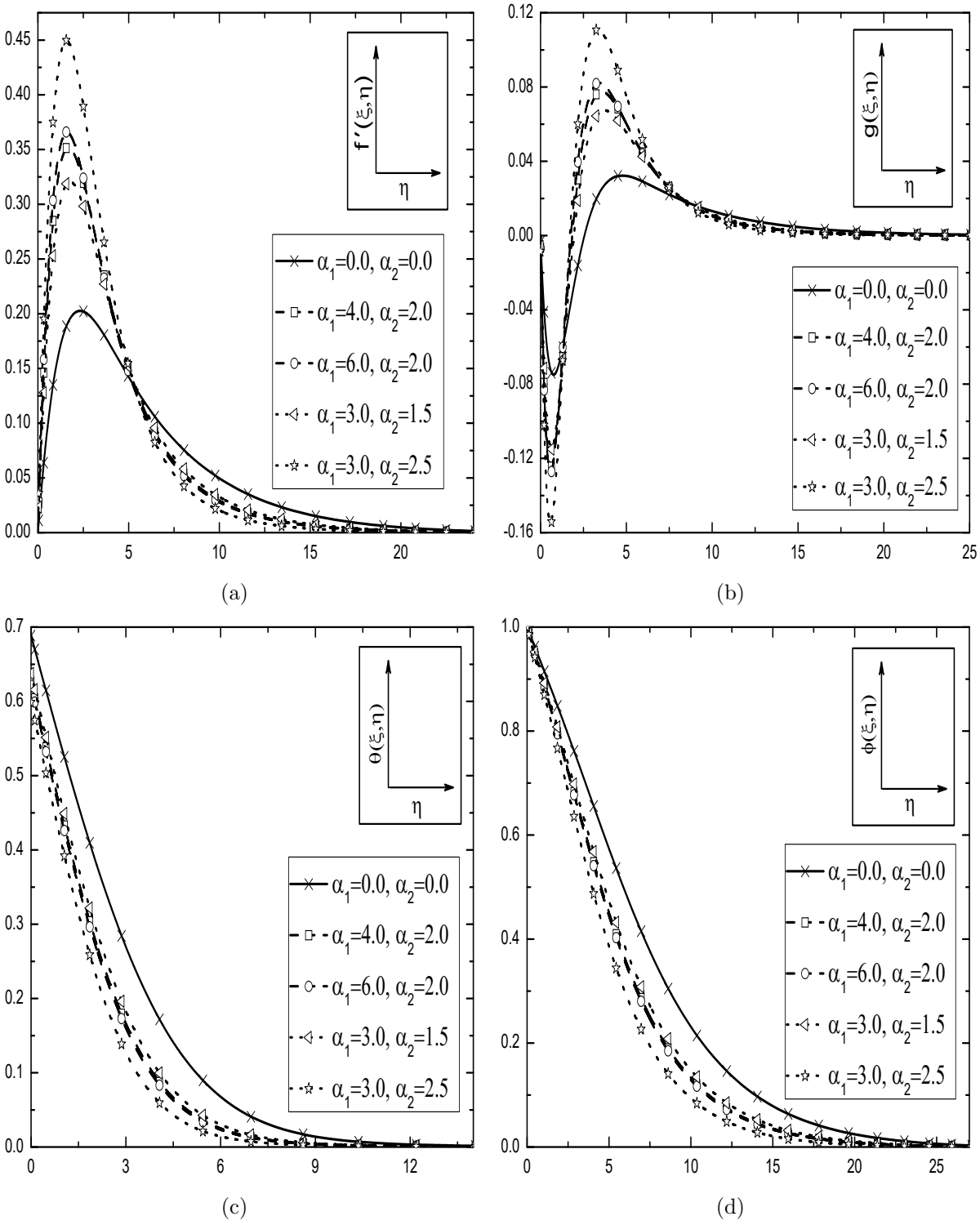

Figure 3.1: *Effects of α_1 and α_2 on the (a) velocity, (b) microrotation, (c) temperature and (d) concentration along η with the fixed values of $\xi = 0.5$, $N = 0.6$, $Fs = 0.5$, $\Omega = 45^0$, $Bi = 0.6$, $Du = 0.3$ and $Sr = 1.0$.*

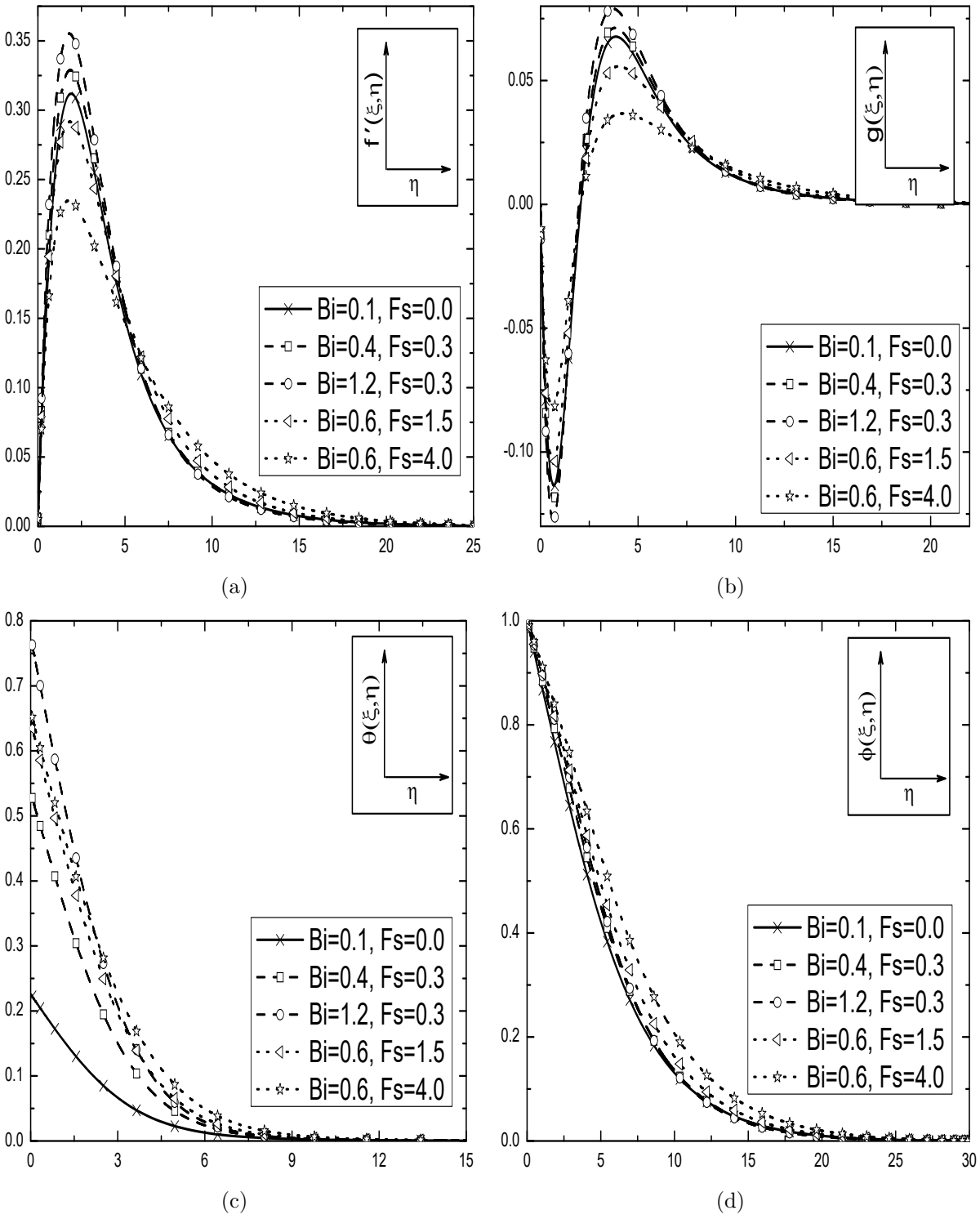

Figure 3.2: *Effects of Bi and Fs on the (a) velocity, (b) microrotation, (c) temperature and (d) concentration along η with the fixed values of $\xi = 0.5$, $N = 0.5$, $\Omega = 30^0$, $Du = 0.3$, $Sr = 0.5$, $\alpha_1 = 1$ and $\alpha_2 = 1$.*

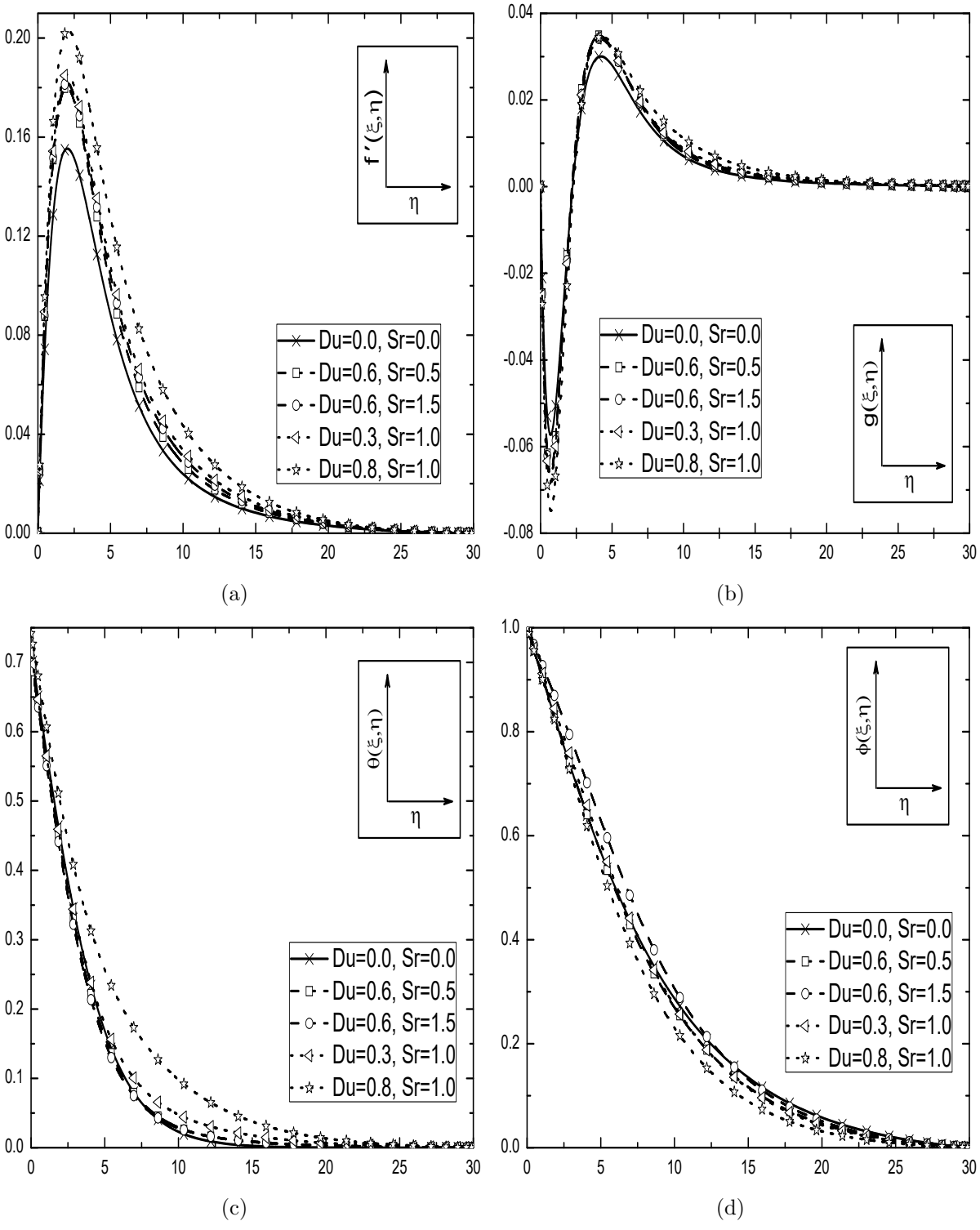

Figure 3.3: *Effects of Du and Sr on the (a) velocity, (b) microrotation, (c) temperature and (d) concentration along* η *with the fixed values of* $N = 0.5$, $\Omega = 30^0$, $Bi = 0.3$, $Fs = 0.5$, $\alpha_1 = 1$ *and* $\alpha_2 = 1$.

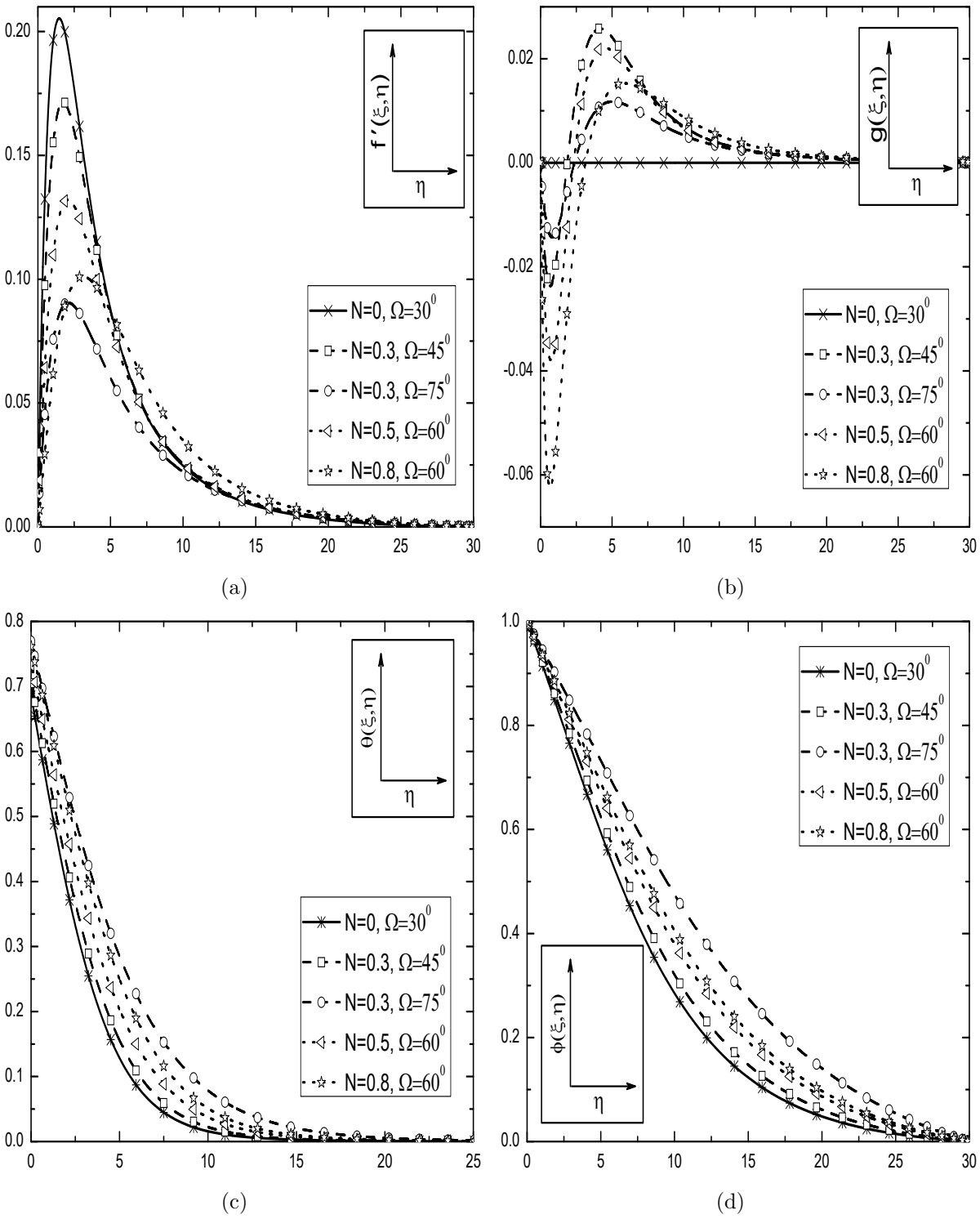

Figure 3.4: *Effects of N and Ω on the (a) velocity, (b) microrotation, (c) temperature and (d) concentration along η with the fixed values of $Du = 0.4$, $Sr = 1.0$, $Bi = 0.3$, $Fs = 0.5$, $\alpha_1 = 1$ and $\alpha_2 = 1$.*

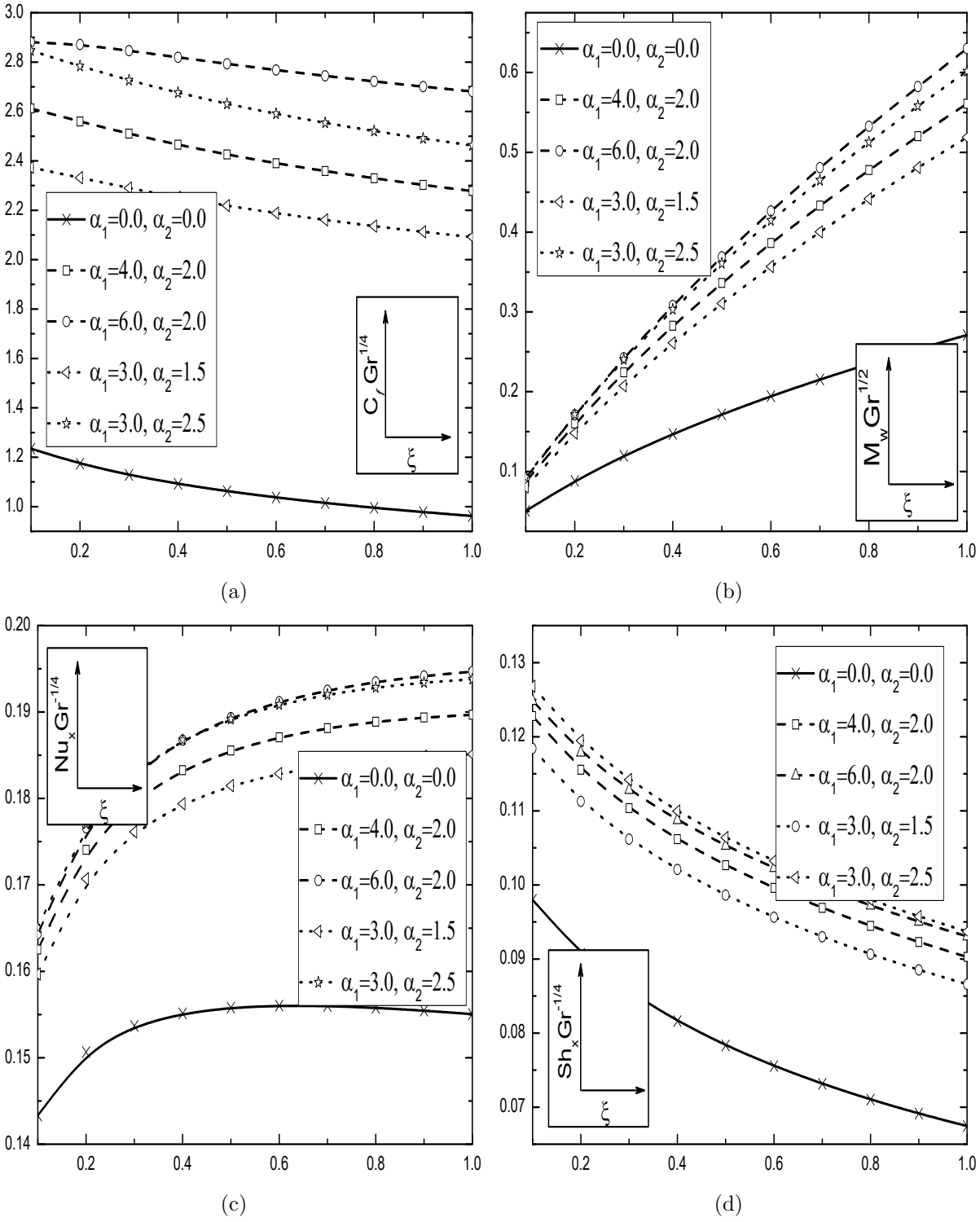

Figure 3.5: *Effects of* α_1 *and* α_2 *on the (a) skin friction, (c) wall couple stress, (c) Nusselt number and (d) Sherwood number along the stream-wise coordinate* ξ *with the fixed values of* $N = 0.6$, $Fs = 0.5$, $Bi = 0.6$, $Du = 0.3$ *and* $Sr = 1.0$.

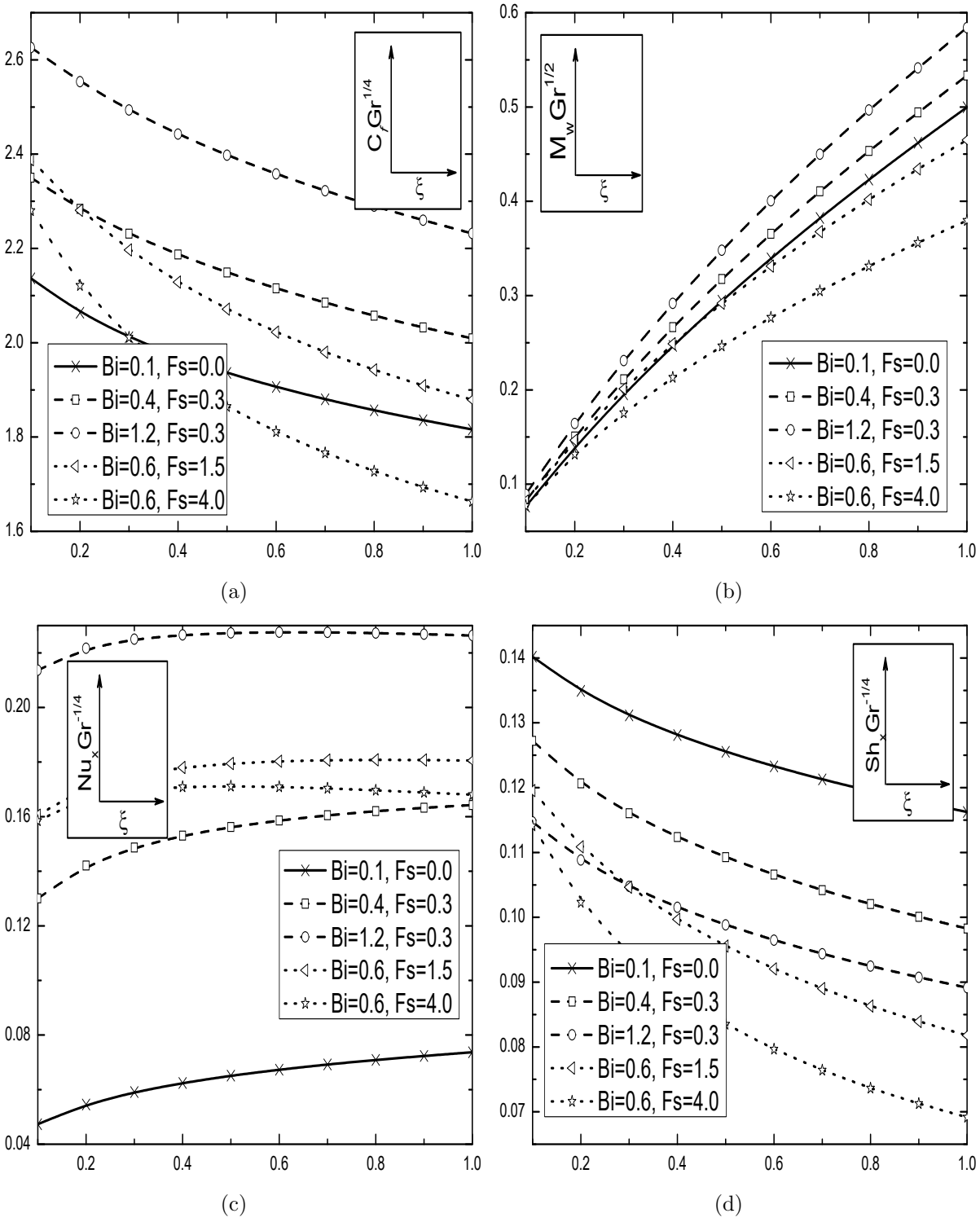

Figure 3.6: *Effects of Bi and Fs on the (a) skin friction, (c) wall couple stress, (c) Nusselt number and (d) Sherwood number along the stream-wise coordinate ξ with the fixed values of $N = 0.5$, $\Omega = 30^0$, $Du = 0.3$, $Sr = 0.5$, $\alpha_1 = 1$ and $\alpha_2 = 1$.*

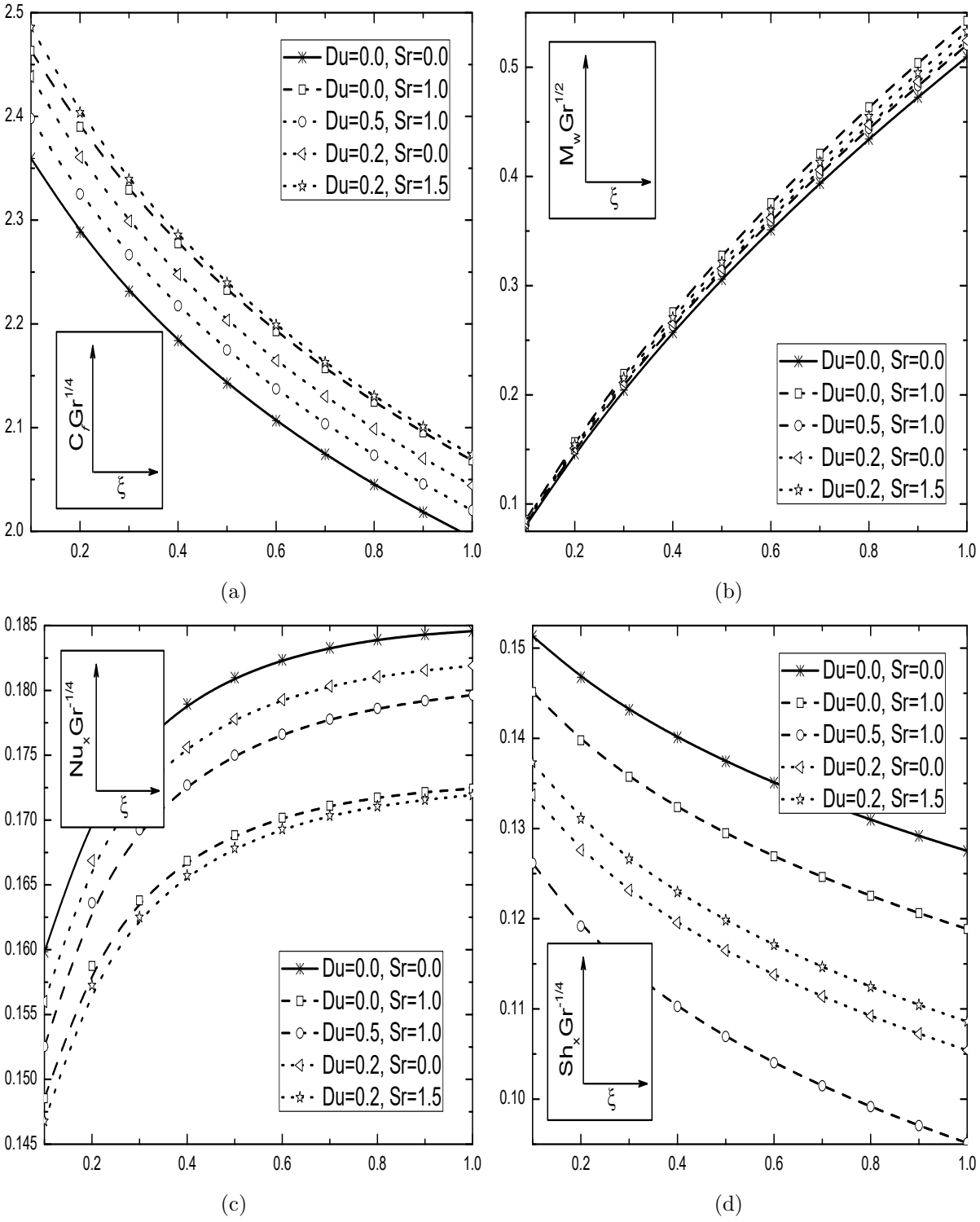

Figure 3.7: *Effects of Du and Sr on the (a) skin friction, (c) wall couple stress, (c) Nusselt number and (d) Sherwood number along the stream-wise coordinate ξ with the fixed values of $N = 0.5$, $\Omega = 30^0$, $Bi = 0.3$, $Fs = 0.5$, $\alpha_1 = 1$ and $\alpha_2 = 1$.*

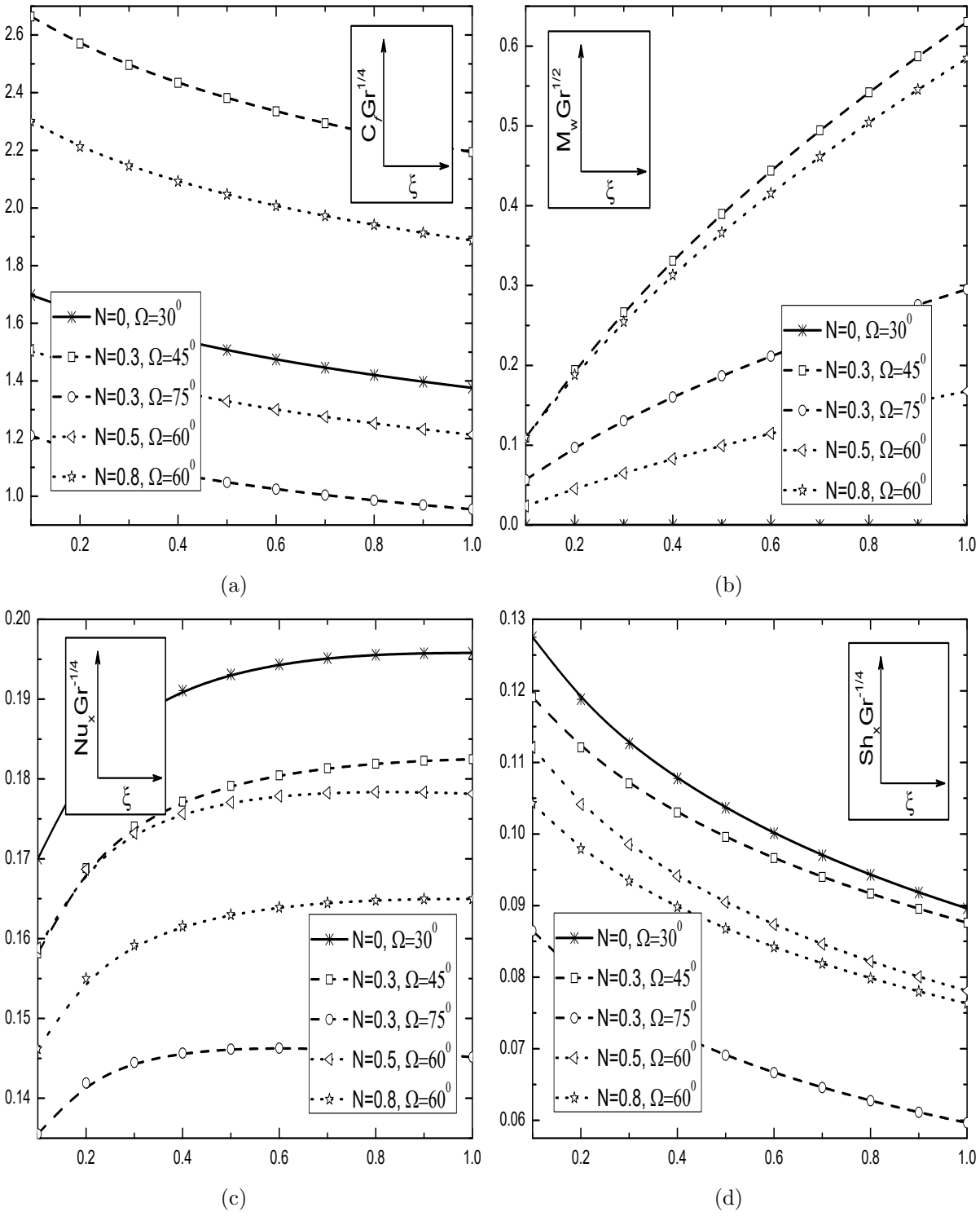

Figure 3.8: *Effects of N and Ω on the (a) skin friction, (c) wall couple stress, (c) Nusselt number and (d) Sherwood number along the stream-wise coordinate ξ with the fixed values of $Du = 0.4$, $Sr = 1.0$, $Bi = 0.3$, $Fs = 0.5$, $\alpha_1 = 1$ and $\alpha_2 = 1$.*

3.2.2 Case(b): Mixed Convection

Assume that the flow to be a mixed convective flow, which arises from an external flow with the velocity u_∞ and buoyancy forces. We introduce the following dimensionless variables

$$\xi = \frac{x}{L},\ \eta = \left(\frac{y}{L}\right)\left(\frac{Re}{\xi}\right)^{1/2},\ \psi(\xi,\eta) = \left(\frac{\xi}{Re}\right)^{1/2} L\, u_\infty\, f(\xi,\eta)$$
$$\omega(\xi,\eta) = \left(\frac{Re}{\xi}\right)^{1/2}\left(\frac{u_\infty}{L}\right) g(\xi,\eta),\ \theta(\xi,\eta) = \frac{T-T_\infty}{T_f - T_\infty},\ \phi(\xi,\eta) = \frac{C-C_\infty}{C_w - C_\infty} \tag{3.14}$$

Substituting the stream function (2.7) and the transformations (3.14) into Eqs.(3.1)-(3.5), we obtain the following linear momentum, angular momentum, energy and concentration equations

$$\frac{1}{\varepsilon}\left(\frac{1}{1-N}\right) f''' + \frac{1}{2\varepsilon^2} f f'' + \left(\frac{N}{1-N}\right) g' + \frac{1}{Da\, Re}\,\xi\,(1-f') + \frac{Fs}{Da}\xi\,(1-f'^2) + Ri\,\xi\,[\theta(1+\alpha_1\theta) + \mathcal{B}\phi(1+\alpha_2\phi)]\cos\Omega = \frac{\xi}{\varepsilon^2}\left(f'\frac{\partial f'}{\partial \xi} - f''\frac{\partial f}{\partial \xi}\right) \tag{3.15}$$

$$\lambda g'' + \frac{1}{2\varepsilon}(fg' - f'g) - \left(\frac{N}{1-N}\right)\mathcal{J}\xi\left(2g + \frac{1}{\varepsilon}f''\right) = \frac{\xi}{\varepsilon}\left(f'\frac{\partial g}{\partial \xi} - \frac{\partial f}{\partial \xi}g'\right) \tag{3.16}$$

$$\frac{1}{\mathrm{Pr}}\theta'' + \frac{1}{2} f\theta' + Du\,\phi'' = \xi\left(f'\frac{\partial \theta}{\partial \xi} - \frac{\partial f}{\partial \xi}\theta'\right) \tag{3.17}$$

$$\frac{1}{Sc}\phi'' + \frac{1}{2} f\phi' + Sr\,\theta'' = \xi\left(f'\frac{\partial \phi}{\partial \xi} - \frac{\partial f}{\partial \xi}\phi'\right) \tag{3.18}$$

Boundary conditions (3.6) in terms of f, g, θ, ϕ become

$$f(\xi,0) = -2\,\xi\left(\frac{\partial f}{\partial \xi}\right)_{\eta=0},\ f'(\xi,0) = 0,\ g(\xi,0) = 0,\ \theta'(\xi,0) = -Bi\,\xi^{\frac{1}{2}}\,[1-\theta(\xi,0)],$$
$$\phi(\xi,0) = 1,\ f'(\xi,\infty) = 1,\ g(\xi,\infty) = 0,\ \theta(\xi,\infty) = 0,\ \phi(\xi,\infty) = 0. \tag{3.19}$$

The non-dimensional shear stress C_f, wall couple stress M_w, local Nusselt number Nu_x and the Sherwood number Sh_x, are given by

$$C_f Re^{1/2} = \left(\frac{2}{1-N}\right)\ \xi^{\frac{-1}{2}}\ f''(\xi,0),\ \ M_w Re = \left(\frac{\lambda}{\xi\ \mathcal{J}}\right) g'(\xi,0),$$
$$Nu_x Re^{-1/2} = -\xi^{\frac{1}{2}}\ \theta'(\xi,0),\ Sh_x Re^{-1/2} = -\xi^{\frac{1}{2}}\ \phi'(\xi,0) \tag{3.20}$$

Results and Discussion

The highly coupled nonlinear partial differential equations (3.15)-(3.18) together with the boundary conditions (3.19) are solved numerically using the successive linearization method along with local similarity and non-similarity approaches, as explained in the previous chapter. In the absence of cross-diffusion effects, this case reduces to the case (b) problem of the chapter-2. Validation of this case of the present problem can be done on comparison, as it was done in the case (b) of chapter-2. Further, the numerical computations are carried out by following the fixed values of parameters: $Ri = 2$, $\mathcal{J} = 0.01$, $\lambda = 0.5$, $\mathcal{B} = 1.0$, Pr $= 0.71$, $Sc = 0.22$, $Re = 200$, $\varepsilon = 0.5$, $Da = 0.1$ and $\xi = 0.5$. These values are continued same throughout this study, unless otherwise specified.

The effects of nonlinear convection parameters (α_1 and α_2), Biot number (Bi), non-Darcy parameter (Fs), coupling number (N), angle of inclination (Ω), Soret and Dufour numbers (Sr and Du) on the fluid flow profiles and other physical quantities of the present interest are shown graphically and displayed in Figs.3.9(a)-3.16(d).

The effects of NDT and NDC parameters (α_1 and α_2) on the velocity, microrotation, temperature and concentration profiles are shown in Figs.3.9(a)-3.9(d). The results demonstrate that the velocity distribution increases with the increase of NDT parameter and also for NDC parameter. The initial velocity is zero at the surface of the plate and then it increases gradually away from the plate. Finally, the velocity becomes unity to satisfy the boundary conditions as portrayed in Fig.3.9(a). However, rise in NDT and NDC parameters change the sign of microrotation from negative to positive inside the boundary layer as displayed in Fig.3.9(b). In the absence, as well as, in the presence of NDT and NDC parameters, the magnitudes of the temperature and concentration decrease with the increase of both α_1 and α_2 as plotted in Figs.3.9(c)-3.9(d). By the experience of these two nonlinear variations (α_1 and α_2), one can conclude that the influence of α_2 is more prominent on the fluid flow profiles as compared with that of α_1.

The influences of the non-Darcy parameter (Fs) and coupling number (N) on the dimensionless velocity, microrotation, temperature and concentration are plotted in Figs.3.10(a)-3.10(d) with the fixed values of other parameters. It is found from Fig.3.10(a) that, the velocity decreases for the higher values of both N and Fs. Since $N \to 0$ corresponds to the viscous fluid, the velocity in the case of a micropolar fluid is less compared to that of viscous fluid case. From Fig.3.10(b), it is observed that the microrotation profiles have nominal variation at the wall and increase just

away from the wall with increasing values of N. Because, an increase in the value of N implies a higher vortex viscosity of fluid which promotes the microrotation of the micropolar fluid. But, the non-Darcy parameter gives opposite influence to the velocity when compared to the influence of coupling number. The temperature and concentration of the fluid enhance with the increase of both non-Darcy parameter and coupling number as portrayed in Figs.3.10(c) and 3.10(d).

Figures 3.11(a)-3.11(d), plotted for $N = 0.3$, $Du = 0.5$, $Sr = 2.5$, $\alpha_1 = 1.0$, $\alpha_2 = 1.0$ and $Fs = 0.2$, refer the variation of angle of inclination and Biot number on the non-dimensional velocity (f'), microrotation (g), temperature (θ) and concentration (ϕ) across the boundary layers. It is noticed from Fig.3.11(a) that, an increase in Bi leads to enhance the fluid velocity within the momentum boundary layer. In Fig.3.11(b), microrotation shows reverse rotation near to the boundaries with the increase of Bi. But, the influence of angle of inclination is reversed to the influence of Biot number on the velocity and microrotation profiles. As Biot number increases, the convective heating rises and non-isothermal surface becomes the isothermal surface as displayed Fig.3.11(c). That is, $\theta(0) = 1$ as $Bi \to \infty$ and this condition is known as isothermal condition at the wall. Usually, for higher values of the Biot number, the internal thermal resistance of the plate is high and the boundary layer thermal resistance is low. In this case, the fluid temperature is maximum at the surface of plate and decreases exponentially to zero far away from the plate. Further, the temperature increases with the increase of angle of inclination as depicted in Fig.3.11(c). Figure 3.11(d) shows the effects of Biot number and angle of inclination on concentration. It reveals that concentration increases with respect to both Biot number and inclination angle.

Changes in the non-dimensional velocity, microrotation, temperature, and concentration are displayed through Figs. 3.12(a)-3.12(d) for different values of cross-Diffusion parameters (Du and Sr) along η with $\xi = 0.5$, $N = 0.3$, $\Omega = 30^0$, $\alpha_1 = 1.0$, $\alpha_2 = 1.0$, $Bi = 0.5$ and $Fs = 0.2$. With an increase of Dufour number, there is a considerable enhancement in the velocity profile whereas the nominal effect is noticed for microrotation. Also, the influence of Soret number is the same on these two (velocity and microrotation) profiles as shown in Figs. 3.12(a)-3.12(b). Figs. 3.12(c)-3.12(d) depict the effects of Soret and Dufour numbers on the temperature and concentration along the free stream coordinate η. The temperature increases with the Dufour number Du but, it decreases with the Soret number Sr. On the other hand, concentration increases with the Soret number Sr, but it decreases with the Dufour number Du.

Figures 3.13(a)-3.13(d) show the surface drag ($C_f Re^{1/2}$), gradient of microrotation ($M_w Re$),

heat and mass transfer rates ($Nu_x Re^{-1/2}$ and $Sh_x Re^{-1/2}$) for various values α_1 and α_2. One can observe from Figs.3.13(a)-3.13(d) that, an increase in α_1 leads to decrease the Nusselt number, whereas it increase the Sherwood number, wall couple stress and skin friction. Also, from Figs.3.13(a)-3.13(d), it is noticed that influence of α_2 is same on these physical quantities but more effective compared to α_1.

Influences of Biot number and non-Darcy parameter on the local heat transfer rate, local mass transfer rate, skin friction and wall couple stress are plotted through Figs.3.14(a) and 3.14(d). An increase in the Biot number enhances the Nusselt number and skin friction in both Darcy porous medium (i.e., for $Fs = 0$) and non-Darcy porous medium (i.e., for $Fs \neq 0$) along the stream wise coordinate ξ. Further, the effect of Biot number in non-Darcy porous medium is more significant compared to the results in the Darcy porous medium as displayed in Figs.3.14(a) and 3.14(c). The reverse effect is observed from Figs.3.14(b) and 3.14(d) on the mass transfer rate and wall couple stress.

Variations of local heat transfer rate, local mass transfer rate, skin friction and wall couple stress for different values of N and Ω are plotted through Figs.3.15(a) and 3.15(d). The case of mixed convection has a significant impact with the angle of inclination Ω for the physical geometry. Here, the results are discussed for a special case of the micropolar fluid parameter with $N = 0$ and $N \neq 0$. From Figs.3.15(a) and 3.15(b), it is observed that both heat and mass transfer rates decrease when the position of inclined plate is changed from the vertical to horizontal, and this will be same in a viscous fluid and micropolar fluid. A rise in inclination angle diminishes the buoyancy force and hence it reduces the wall couple stress and skin friction coefficients, whereas these coefficients increase with the increase of coupling number and the same result is shown in Figs.3.15(c)-3.15(d).

The impacts of Soret and Dufour numbers on the skin friction, wall couple stress, heat and mass transfer rates are displayed in 3.16(a)-3.16(d). Higher values of Dufour number (Du) lead to reduce the heat transfer rate and enhance the mass transfer rate, whereas these show reverse trend with the increase of Soret number (Sr). Thus, the cross-diffusion coefficients (Sr and Du) have opposite influence on Nusselt and Sherwood numbers as portrayed in Figs.3.16(a)-3.16(b). However, Figs.3.16(c)-3.16(d) indicate a notable effect on the wall couple stress and skin friction with high enough values of Dufour number, while the influence of Soret number is nominal on the same physical quantities.

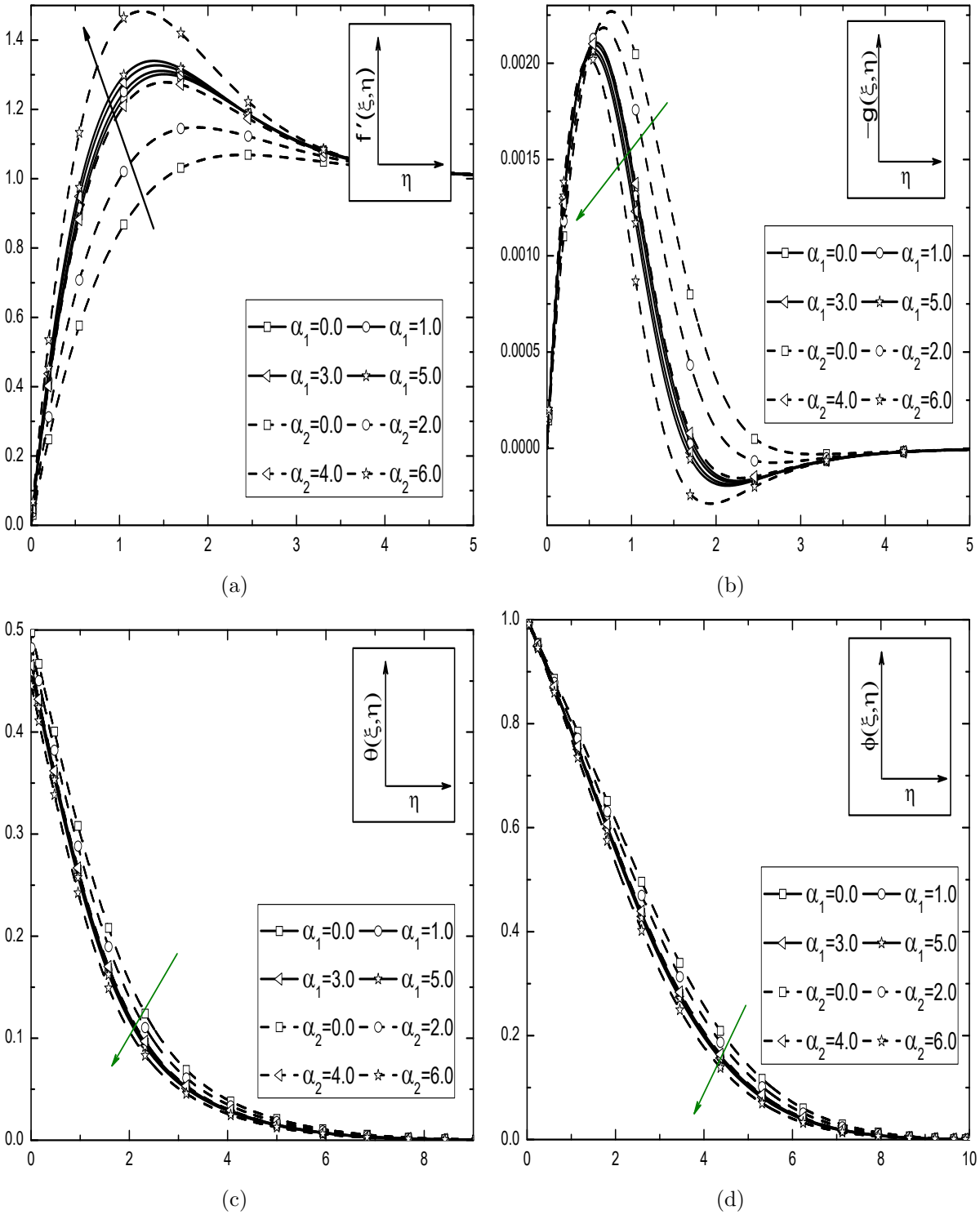

Figure 3.9: *Effects of* α_1 *and* α_2 *on the (a) velocity, (b) microrotation, (c) temperature and (d) concentration along* η *with fixed* $\xi = 0.5$, $\Omega = 30^0$, $N = 0.3$, $Du = 0.5$, $Sr = 2.5$, $Bi = 0.5$ *and* $Fs = 0.2$.

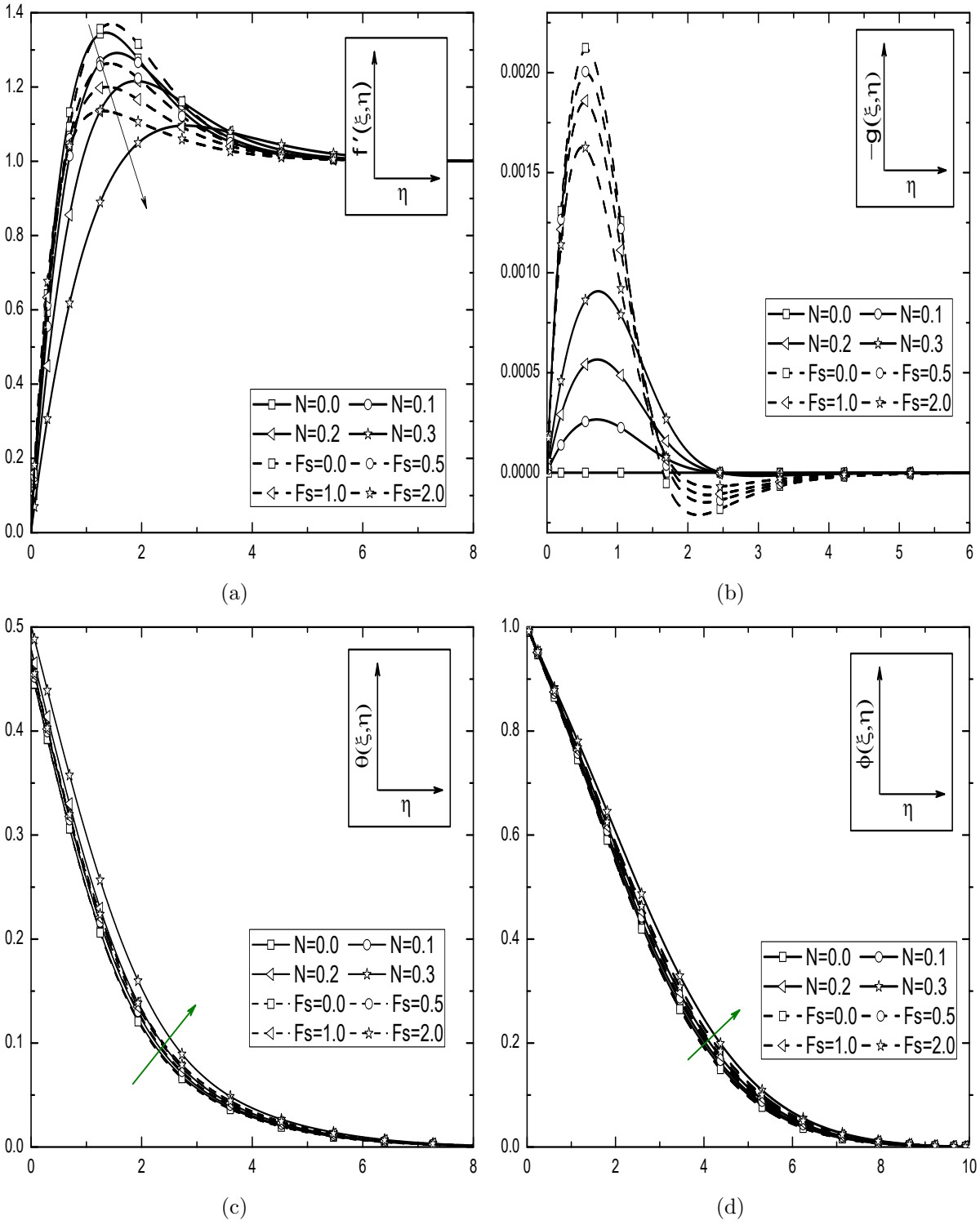

Figure 3.10: *Effects of N and Fs on the (a) velocity, (b) microrotation, (c) temperature and (d) concentration along η with the fixed values of $\xi = 0.5$, $\Omega = 30^0$, $\alpha_1 = 1.0$, $\alpha_2 = 1.0$, $Du = 0.5$, $Sr = 2.5$ and $Bi = 0.5$.*

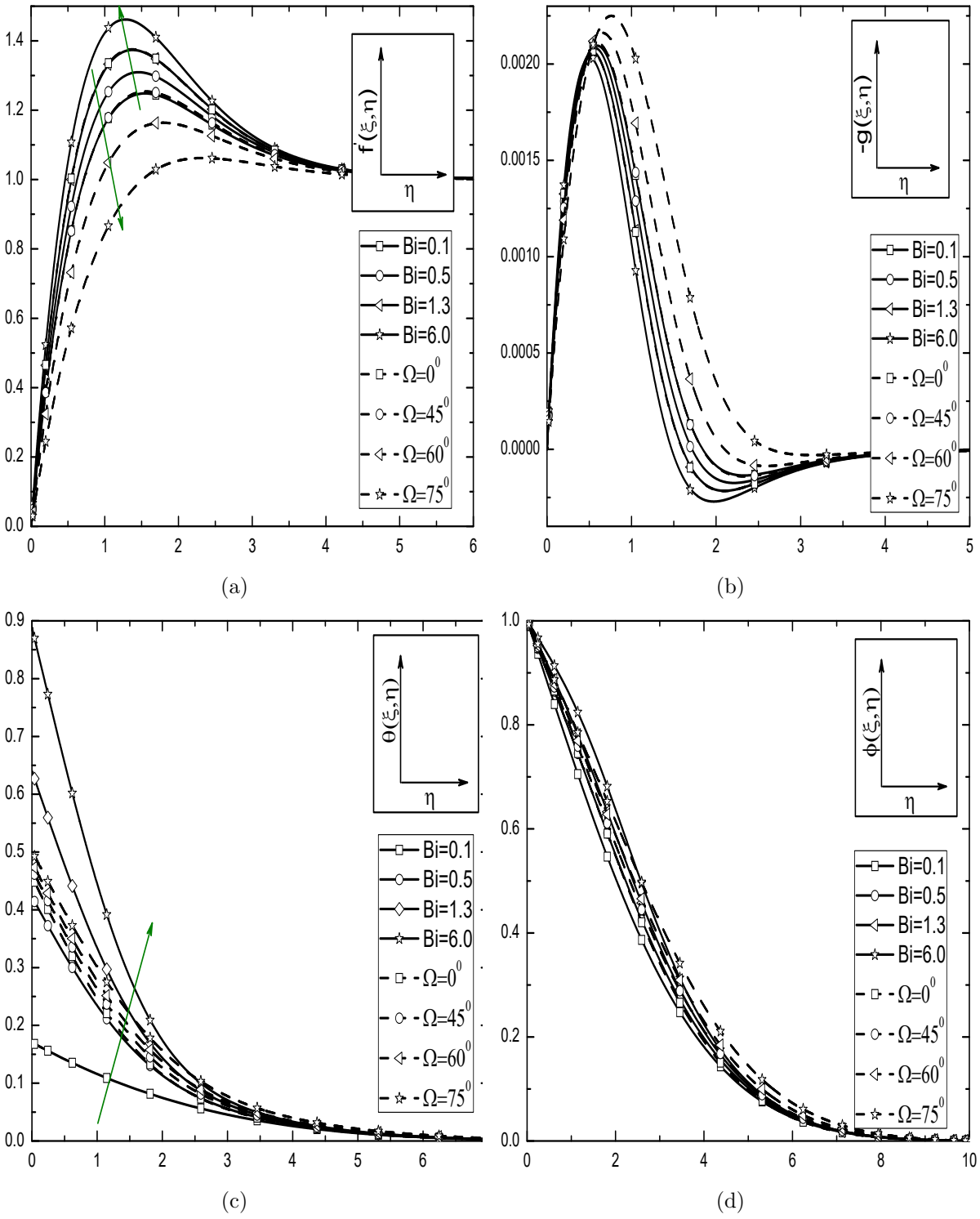

Figure 3.11: *Effects of Bi and* Ω *on the (a) velocity, (b) microrotation, (c) temperature and (d) concentration along* η *with the fixed values of* $\xi = 0.5$, $N = 0.3$, $Du = 0.5$, $Sr = 2.5$, $\alpha_1 = 1.0$, $\alpha_2 = 1.0$ *and* $Fs = 0.2$.

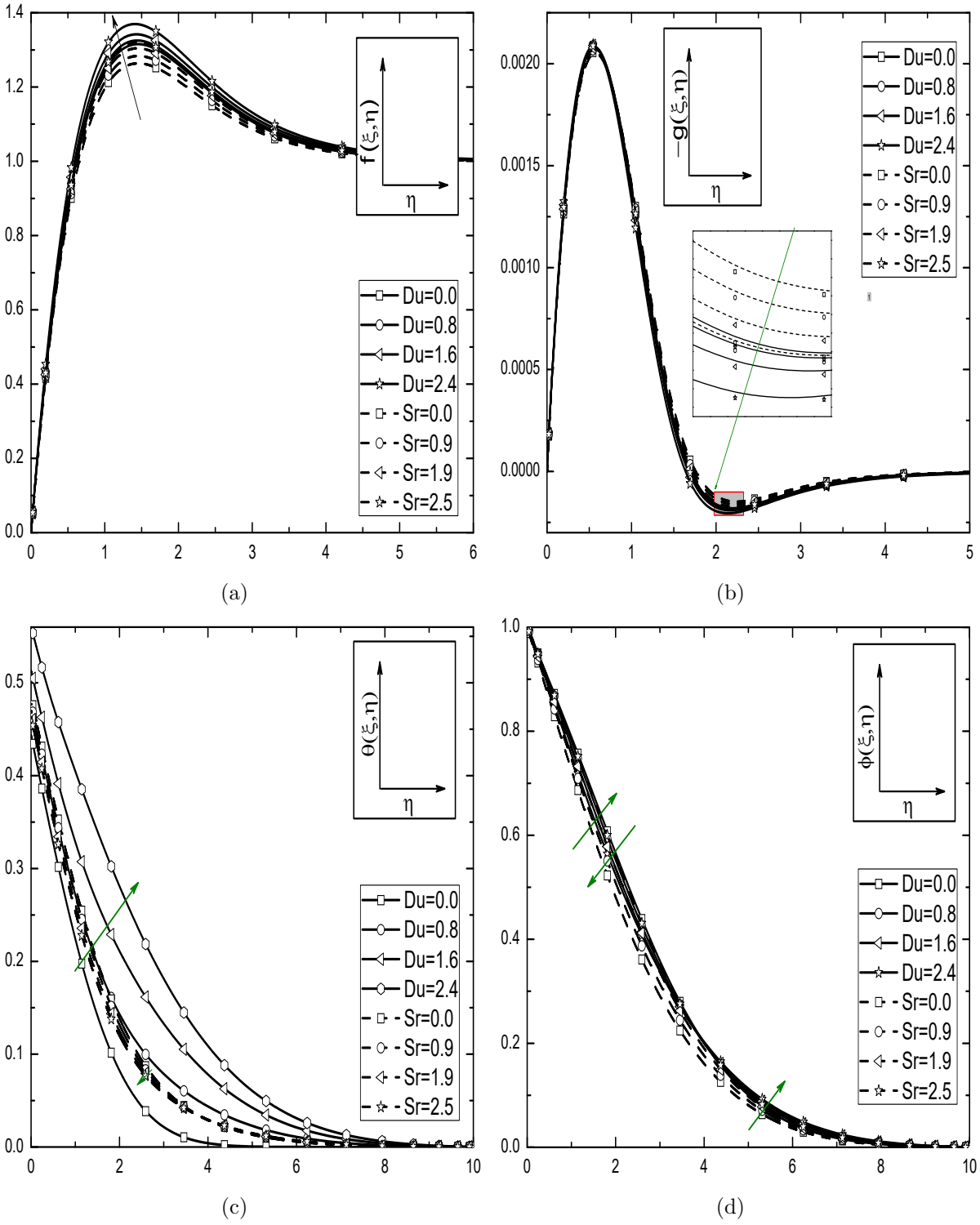

Figure 3.12: *Effects of Du and Sr on the (a) velocity, (b) microrotation, (c) temperature and (d) concentration along* η *with the fixed values of* $\xi = 0.5$, $N = 0.3$, $\Omega = 30^0$, $\alpha_1 = 1.0$, $\alpha_2 = 1.0$, $Bi = 0.5$ *and* $Fs = 0.2$.

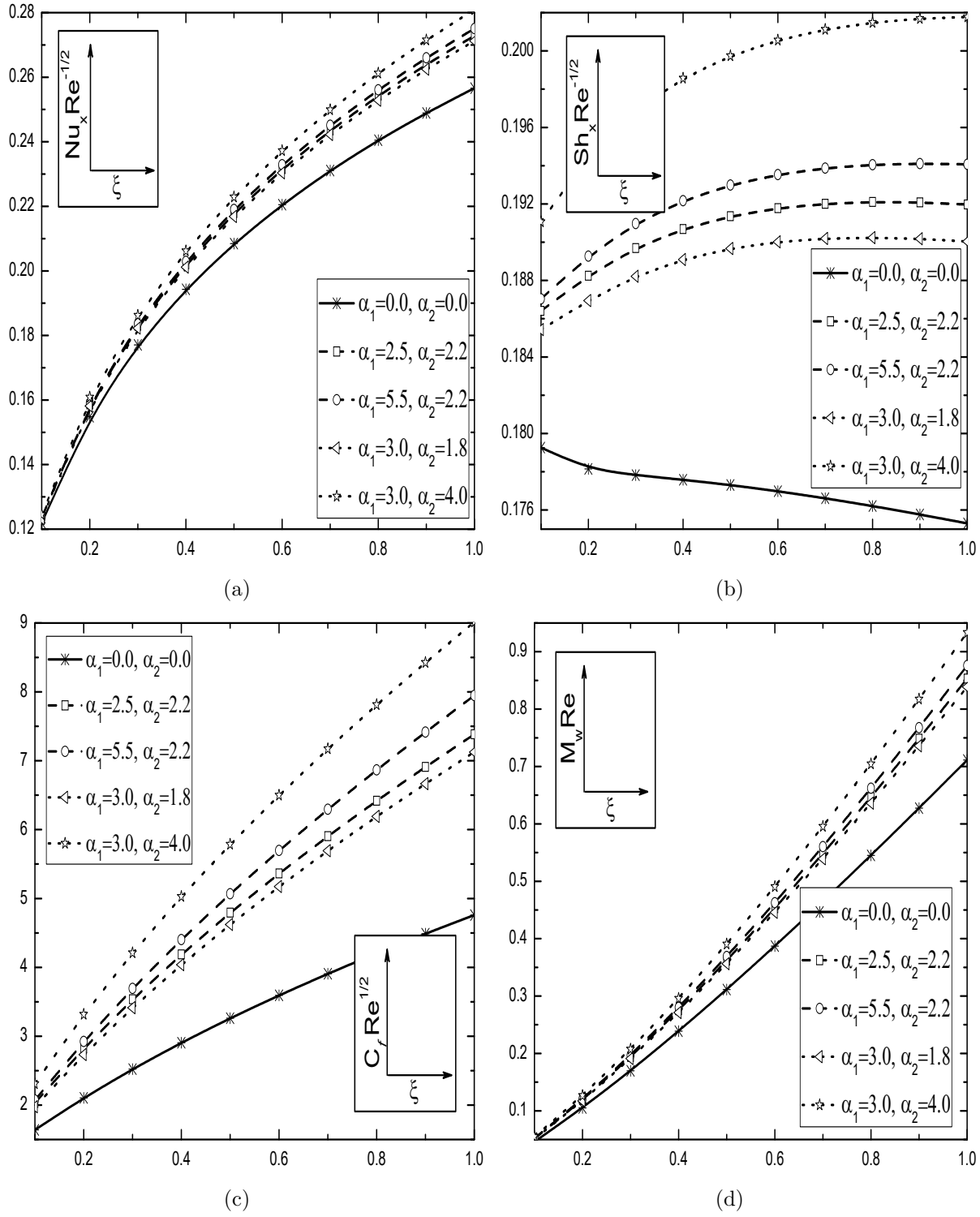

Figure 3.13: *Effects of* α_1 *and* α_2 *on the (a) heat transfer rate, (b) mass transfer rate, (c) skin friction and (d) wall couple stress along the stream-wise coordinate* ξ *with the fixed values of* $N = 0.3$, $\alpha_1 = 1.0$, $\alpha_2 = 1.0$, $\Omega = 30^0$, $Du = 0.5$, $Sr = 2.5$, $Bi = 0.5$ *and* $Fs = 0.2$.

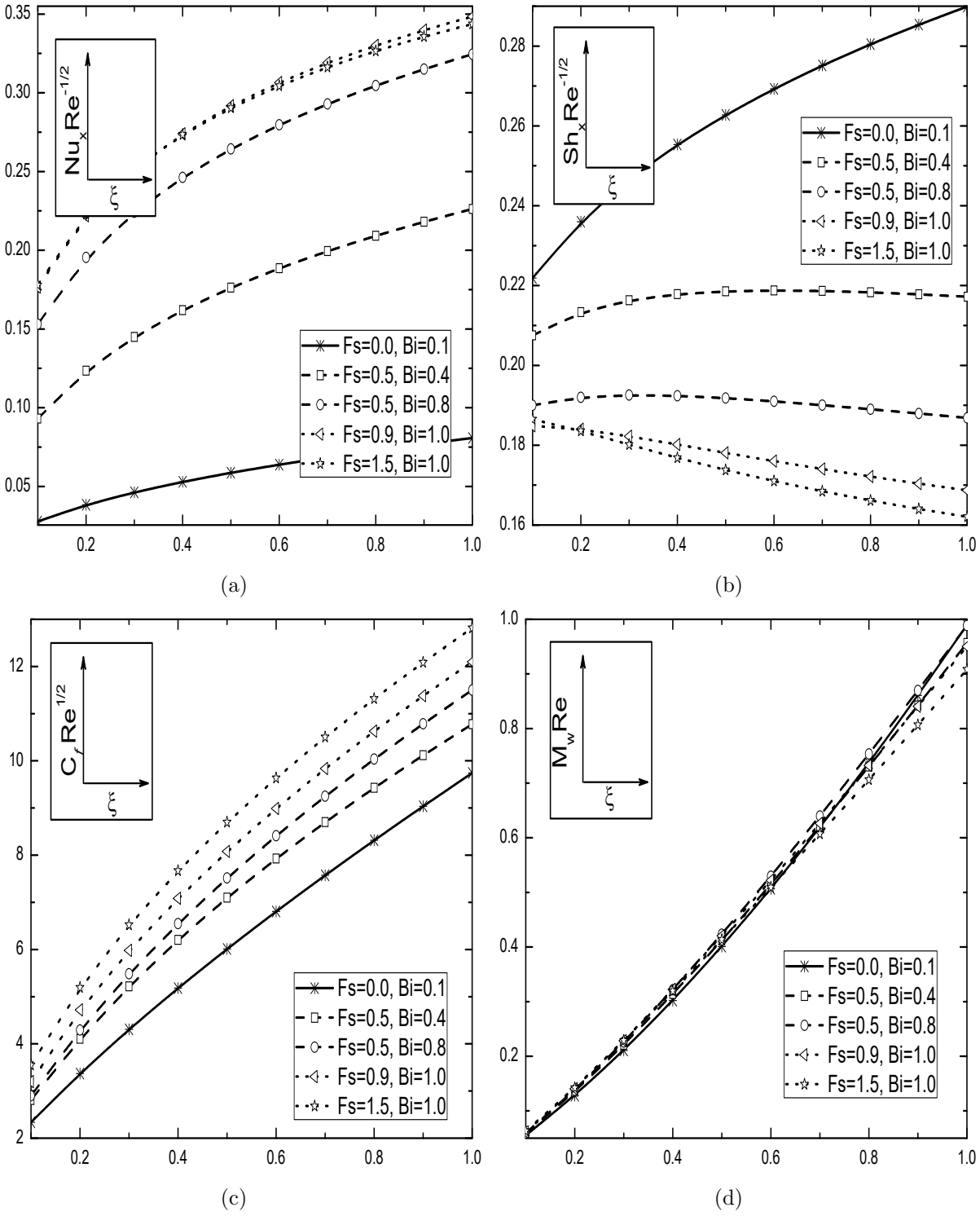

Figure 3.14: *Effects of Bi and Fs on the (a) heat transfer rate, (b) mass transfer rate, (c) skin friction and (d) wall couple stress along the stream-wise coordinate ξ with the fixed values of $\Omega = 30^0$, $N = 0.3$, $Du = 0.5$, $Sr = 2.5$, $\alpha_1 = 1.0$ and $\alpha_2 = 1.0$.*

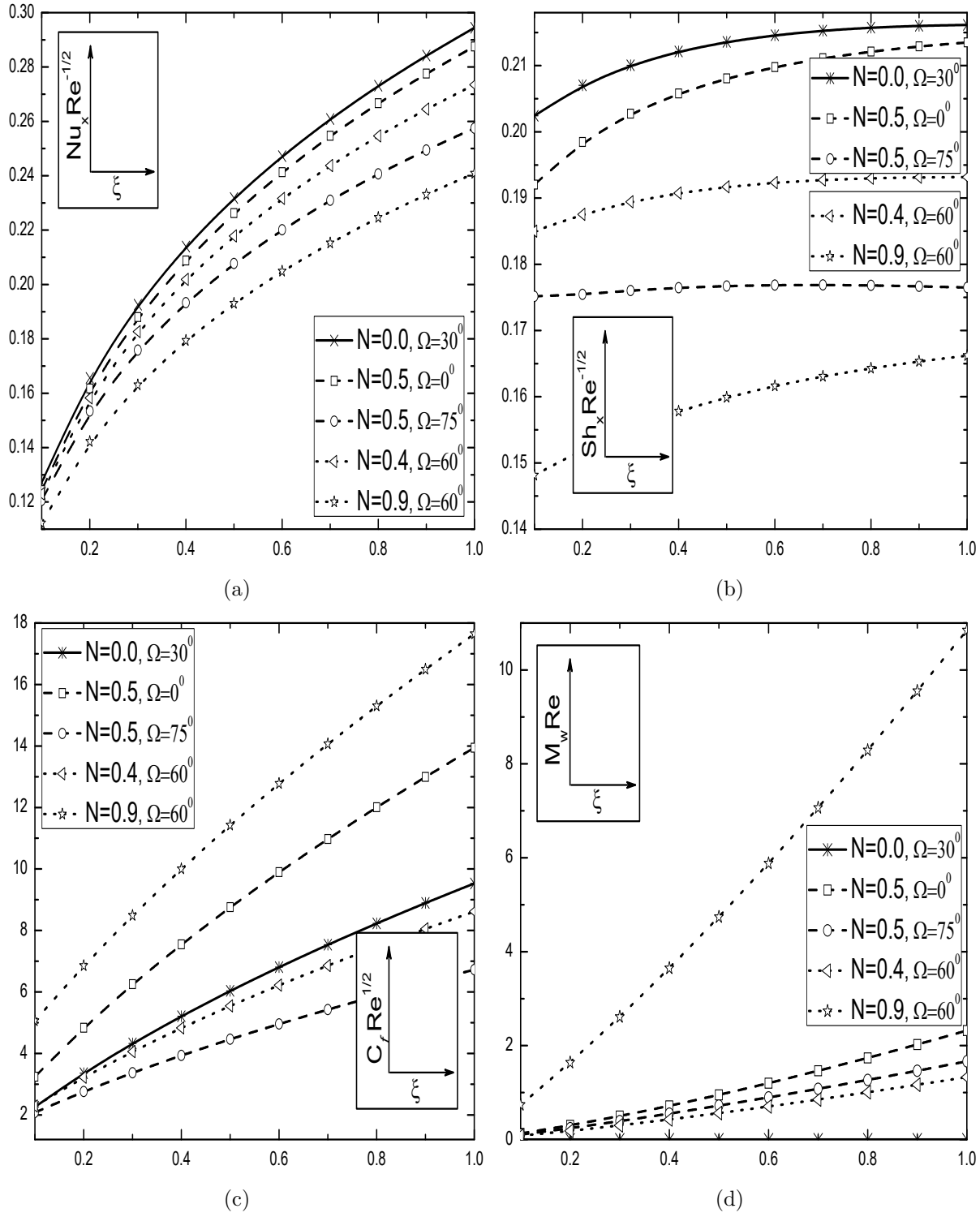

Figure 3.15: *Effects of* N *and* Ω *on the (a) heat transfer rate, (b) mass transfer rate, (c) skin friction and (d) wall couple stress along the stream-wise coordinate* ξ *with the fixed values of* $Bi = 0.6$, $Fs = 0.2$, $Du = 0.5$, $Sr = 2.5$, $\alpha_1 = 1.0$ *and* $\alpha_2 = 1.0$.

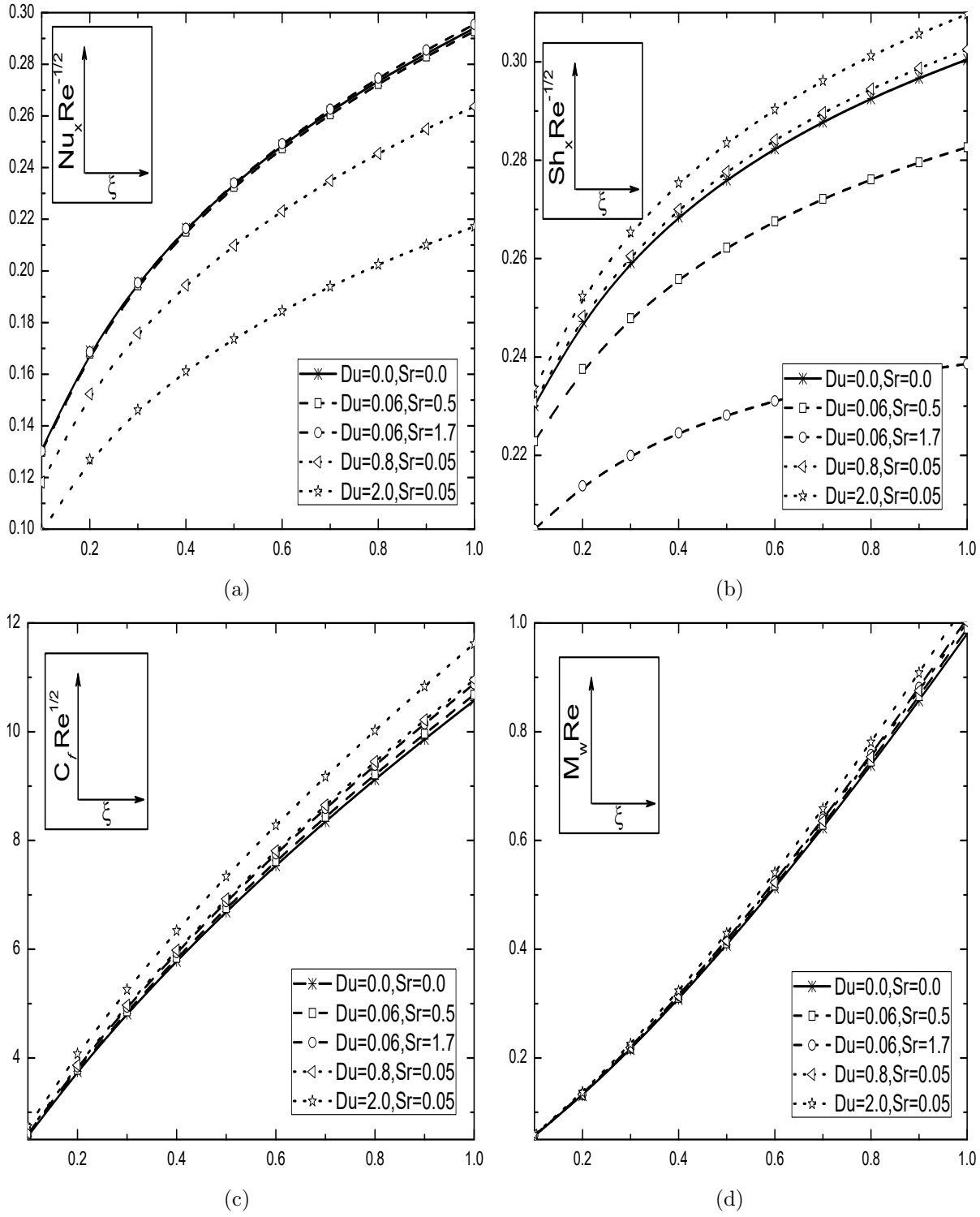

Figure 3.16: *Effects of Du and Sr on the (a) heat transfer rate, (b) mass transfer rate, (c) skin friction and (d) wall couple stress along the stream-wise coordinate* ξ *with the fixed values of* $\Omega = 30^0$, $N = 0.3$, $Bi = 0.6$, $Fs = 0.2$, $\alpha_1 = 1.0$ *and* $\alpha_2 = 1.0$.

3.3 Conclusions

The natural and mixed convective flows over an inclined plate embedded in a porous medium saturated by a micropolar fluid with Soret an Dufour effects, are analyzed in this chapter. From this computational analysis, the following conclusions are drawn for both case (a) and case (b):

As in the previous chapter, the behavior of nonlinear convection parameters is found to be similar on various profiles. An increase in the Biot number decreases the mass transfer rate and microrotation, whereas it increases the heat transfer rate, skin friction coefficient, velocity, temperature and concentrations in both case (a) and case (b). The Soret number reduces the temperature and local Nusselt number, whereas it increases the concentration, skin friction and velocity in case (a). However, the local Nusselt number and concentration show an opposite trend in case (b). In case (a) and case (b), the velocity, temperature and heat transfer rates increase, whereas the concentration and mass transfer rates decrease with the influence of Dufour number. An increase in Fs decreases the surface drag, local Nusselt number and local Sherwood number, but it increases the temperature and concentration in case (a). These profiles and physical quantities show a reverse trend in case (b).

Chapter 4

Double Dispersion Effects on Nonlinear Convective Flow along an Inclined Plate in a Micropolar Fluid Saturated Non-Darcy Porous Medium

[1]

4.1 Introduction

The theory of micropolar fluid saturated porous medium is very rich in literature with various aspects of the problem having been investigated. To name a few, Helmy *et al.* [44] and Kim [57] investigated the flow of a micropolar fluid over a flat plate in a Darcy porous medium whereas Abo *et al.* [1], Srinivasacharya and RamReddy [96], and Rawat *et al.* [86] analysed the flow of a micropolar fluid saturated non-Darcy porous medium under different circumferences.

From the literature it seems that the thermal and solutal dispersions play an important role

[1]Case(a): Published in "**Heat Transfer - Asian Research**" 48 (2019) 414–434, Case(b): Published in "**Engineering Science and Technology, an International Journal**" 21(5) (2018) 984–995.

in a non-Darcy porous medium due to the presence of inertial effects (see Nield and Bejan [75]). Hence, the effects of thermal and solutal dispersion on the convective heat and mass transfer flows of non-Newtonian fluids through porous media, are considered by several researchers. To name a few, Murti *et al.* [71] analyzed the effects of chemical reaction and double dispersion on a radiative-convective flow of non-Newtonian fluid in a non-Darcy porous medium. A note on the double dispersion effects in a non-Darcy porous medium saturated by a nanofluid has been given by Awad *et al.* [12]. Benazir and Sivaraj [20] conducted numerical study to examine the double dispersion effects over a cone in a chemically reacting Casson fluid saturated non-Darcy porous medium.

The convective boundary condition has been attracted great interest for the analysis of heat transfer in fluid flow problems and it is usually simulated via Biot number. Aman *et al.* [7] investigated the magneto-hydrodynamic flow of a micropolar fluid along a convectively heating vertical plate. Recently, Shehzad *et al.* [90] considered the convective thermal boundary condition in the analysis of heat transfer in a micropolar fluid flow along the stretching surface.

The effects of double dispersion and Biot number on the convective flow of a micropolar fluid over an inclined plate embedded in a non-Darcy porous medium, are discussed in this chapter. According to the author's knowledge, the present study has not been addressed in the literature. As in the previous chapters, here also the governing equations and their associated boundary conditions are solved numerically using the successive linearization method together with the local similarity and non-similarity approaches. The results are compared with the relevant results in the existing literature and are found to be in good agreement. Also, the influences of various physical parameters on the micropolar fluid flow with heat and mass transfer characteristics are examined and displayed through graphs.

4.2 Mathematical Formulation

A steady, laminar, two-dimensional and convective flow of an incompressible micropolar fluid over an inclined plate in a non-Darcy porous medium, is considered. As projected in Fig.(2.1), the plate is inclined about the vertical direction with an angle Ω. This chapter is an extension of chapter-2 by considering the double dispersion (thermal and solutal dispersions) effects. By employing the nonlinear Boussinesq approximation and with the assumptions made in chapter-2, the governing

equations for micropolar fluid saturated non-Darcy porous medium are given by

$$\frac{\partial u}{\partial x}+\frac{\partial v}{\partial y}=0 \tag{4.1}$$

$$\begin{aligned}\frac{\rho}{\varepsilon^2}\left(u\frac{\partial u}{\partial x}+v\frac{\partial u}{\partial y}\right)&=\frac{1}{\varepsilon}\left(\mu+\kappa\right)\frac{\partial^2 u}{\partial y^2}+\kappa\frac{\partial \omega}{\partial y}+\frac{\mu}{K_P}(u_\infty-u)+\frac{\rho\, b}{K_P}(u_\infty^2-u^2)\\&+\rho g^*\left[\beta_0\left(T-T_\infty\right)+\beta_1(T-T_\infty)^2+\beta_2\left(C-C_\infty\right)+\beta_3(C-C_\infty)^2\right]\cos\Omega\end{aligned} \tag{4.2}$$

$$\frac{\rho j}{\varepsilon}\left(u\frac{\partial \omega}{\partial x}+v\frac{\partial \omega}{\partial y}\right)=\gamma\frac{\partial^2 \omega}{\partial y^2}-\kappa\left(2\omega+\frac{1}{\varepsilon}\frac{\partial u}{\partial y}\right) \tag{4.3}$$

$$u\frac{\partial T}{\partial x}+v\frac{\partial T}{\partial y}=\frac{\partial}{\partial y}\left[\alpha_e\frac{\partial T}{\partial y}\right] \tag{4.4}$$

$$u\frac{\partial C}{\partial x}+v\frac{\partial C}{\partial y}=\frac{\partial}{\partial y}\left[D_e\frac{\partial C}{\partial y}\right] \tag{4.5}$$

along with the boundary conditions

$$\begin{aligned}u=0,\ v=0,\ \omega=0,\ -k_f\frac{\partial T}{\partial y}=h_f(T_f-T),\ C=C_w\ \text{ at }\ y=0\\ u=u_\infty,\ \omega=0,\ T=T_\infty,\ C=C_\infty\ \text{as}\ y\to\infty\end{aligned} \tag{4.6}$$

where α is the molecular thermal diffusivity, D is the molecular solutal diffusivity, χ is the thermal dispersion coefficient, d is the pore diameter and ζ is the solutal dispersion coefficient. Further, the effective thermal and solutal diffusivities are defined as, $\alpha_e=\alpha+\chi\, d\, u$ and $D_e=D+\zeta\, d\, u$ (Ref. Telles and Trevisan [104], Murthy [67]) respectively.

In this chapter also, two types (cases) of problems are considered: (a) free/natural convection and (b) mixed convection.

4.2.1 Case(a): Natural Convection

The flow is assumed to be a natural convective flow which is caused by only buoyancy forces and without any external agent. Hence, the velocity of the external flow becomes zero ($i.e., u_\infty=0$).

Now, we introduce the following non-dimensional variables

$$\begin{aligned}\xi = \frac{x}{L},\ \eta = \frac{y}{L}\left(\frac{Gr}{\xi}\right)^{1/4},\ \psi(\xi,\eta) = \frac{\mu\, Gr^{1/4}\ \xi^{3/4}}{\rho}\, f(\xi,\eta)\\ \omega(\xi,\eta) = \frac{\mu\, Gr^{3/4}\ \xi^{1/4}}{\rho L^2}\ g(\xi,\eta),\ \theta(\xi,\eta) = \frac{T-T_\infty}{T_f-T_\infty},\ \phi(\xi,\eta) = \frac{C-C_\infty}{C_w-C_\infty}\end{aligned} \tag{4.7}$$

Substituting the stream function (2.7) and the transformations (4.7) in Eqs.(4.1) - (4.5), we get the following non-dimensional equations

$$\begin{aligned}\frac{1}{\varepsilon}\left(\frac{1}{1-N}\right) f''' + \frac{3}{4\varepsilon^2} f f'' - \frac{1}{2\varepsilon^2} f'^2 + \left(\frac{N}{1-N}\right) g' - \frac{Fs}{Da}\xi\, f'^2 - \frac{\xi^{\frac{1}{2}}}{Da\, Gr^{\frac{1}{2}}} f'\\ + \left[\theta(1+\alpha_1\theta) + \mathcal{B}\phi(1+\alpha_2\phi)\right]\cos\Omega = \frac{\xi}{\varepsilon^2}\left(f'\frac{\partial f'}{\partial \xi} - f''\frac{\partial f}{\partial \xi}\right)\end{aligned} \tag{4.8}$$

$$\lambda g'' - \frac{1}{4\varepsilon} f'\, g + \frac{3}{4\varepsilon} f\, g' - \left(\frac{N}{1-N}\right)\mathcal{J}\xi^{\frac{1}{2}}\left(\frac{1}{\varepsilon} f'' + 2\, g\right) = \frac{\xi}{\varepsilon}\left(f'\,\frac{\partial g}{\partial \xi} - \frac{\partial f}{\partial \xi}\, g'\right) \tag{4.9}$$

$$\frac{1}{\mathrm{Pr}}\theta'' + D_s\,\xi^{\frac{1}{2}}\left(f'\,\theta'\right)' + \frac{3}{4}\, f\,\theta' = \xi\left(f'\frac{\partial \theta}{\partial \xi} - \frac{\partial f}{\partial \xi}\theta'\right) \tag{4.10}$$

$$\frac{1}{Sc}\phi'' + D_c\,\xi^{\frac{1}{2}}\left(f'\,\phi'\right)' + \frac{3}{4} f\phi' = \xi\left(f'\frac{\partial \phi}{\partial \xi} - \frac{\partial f}{\partial \xi}\phi'\right) \tag{4.11}$$

along with the non-dimensional form boundary conditions

$$\begin{aligned}f'(\xi,0) = 0,\ f(\xi,0) + \frac{4}{3}\xi\left(\frac{\partial f}{\partial \xi}\right)_{\eta=0} = 0,\ g(\xi,0) = 0,\ \theta'(\xi,0) = -Bi\xi^{\frac{1}{4}}\left[1-\theta(\xi,0)\right],\\ \phi(\xi,0) = 1,\ f'(\xi,\infty) = 0,\ g(\xi,\infty) = 0,\ \theta(\xi,\infty) = 0,\ \phi(\xi,\infty) = 0.\end{aligned} \tag{4.12}$$

where $D_s = \dfrac{\chi\, d\, Gr^{\frac{1}{2}}}{L}$ is the thermal dispersion parameter and $D_c = \dfrac{\zeta\, d\, Gr^{\frac{1}{2}}}{L}$ is the solutal dispersion parameter.

The physical quantities of present interest (such as shear stress, wall couple stress, heat and mass transfer rates), are defined as

$$\begin{aligned}C_f = \frac{2}{\rho\, u_*^2}\left[(\mu+\kappa)\frac{\partial u}{\partial y} + \kappa\omega\right]_{y=0},\ M_w = \frac{\gamma}{\rho\, u_*^2 L}\left[\frac{\partial \omega}{\partial y}\right]_{y=0}\\ Nu_x = -\frac{x}{k_f(T_f-T_\infty)}\left[k_e\frac{\partial T}{\partial y}\right]_{y=0},\ Sh_x = -\frac{x}{D(C_w-C_\infty)}\left[D_e\frac{\partial C}{\partial y}\right]_{y=0}\end{aligned} \tag{4.13}$$

where k_e is the effective thermal conductivity of the medium which is the sum of the molecular thermal conductivity k_f and the dispersion thermal conductivity k_d. Further, D_e is the effective solutal diffusivity of the medium which is the sum of the molecular diffusivity D and the dispersion solutal diffusivity D_d. Here, the dispersion thermal conductivity and the dispersion solutal diffusivity are defined as $k_d = \rho\,\chi\,C_p\,d\,u$ and $D_d = \zeta\,d\,u$ (Telles and Trevisan [104], Murthy [67]) respectively.

The non-dimensional skin friction C_f, wall couple stress M_w, local Nusselt number Nu_x and the Sherwood number Sh_x, are given by

$$C_f Gr^{\frac{1}{4}} = \left(\frac{2}{1-N}\right)\xi^{\frac{-3}{4}} f''(\xi,0),\;\; M_w Gr^{\frac{1}{2}} = \left(\frac{\lambda}{\xi\;\mathcal{J}}\right) g'(\xi,0),$$
$$\frac{Nu_x}{Gr^{1/4}} = -\xi^{\frac{3}{4}}\;\left[1 + D_s\,\mathrm{Pr}\,\xi^{\frac{1}{2}}\,f'(\xi,0)\right]\theta'(\xi,0),\;\; \frac{Sh_x}{Gr^{1/4}} = -\xi^{\frac{3}{4}}\;\left[1 + D_c\;Sc\;\xi^{\frac{1}{2}}\;f'(\xi,0)\right]\phi'(\xi,0) \tag{4.14}$$

Results and Discussion

The reduced governing Eqs.(4.8)-(4.11) along with the boundary conditions (4.12) are solved numerically using successive linearization method together with local similarity and non-similarity approaches as explained in the case (a) of chapter-2. In the absence of double dispersion effects, this case reduces to the case (a) problem of the chapter-2. Validation of the present problem, in this case, can be done on comparison as it was done in the case (a) of chapter-2. Further, the numerical computations are carried out by following the fixed values of parameters: $\mathcal{J} = 0.01$, $\lambda = 0.5$, $\mathcal{B} = 1.0$, $\mathrm{Pr} = 0.71$, $Sc = 0.22$, $Ri = 2$, $\varepsilon = 0.5$, $Da = 0.1$ and $\xi = 0.5$. These values are continued same throughout this study, unless otherwise specified. The changes in fluid flow profiles f', g, θ and ϕ are projected in Figs.(4.1)-(4.3) for different values of α_1, α_2, Fs, D_s, D_c, Bi, $\mathcal{B}$, N and Ω.

Variations of fluid flow profiles (such as f', g, θ and ϕ) for $\alpha_1(1.5, 3.5)$, α_2 $(0.5, 2.5)$ and $Fs(0.0, 0.5)$ with $D_c = 0.3$, $\mathcal{B} = 1.0$, $D_s = 0.5$, $Bi = 0.3$, $N = 0.6$, $\xi = 0.5$ and $\Omega = 60^0$, are displayed in Figs.4.1(a)-4.1(d). As NDT parameter (α_1) increases, the direction of fluid velocity is changed from increasing to decreasing nearer to the free stream value as shown in Fig.4.1(a). Physically, $\alpha_1 > 0$ implies that $T_f > T_\infty$; hence, the surface of the wall will induce some amount of heat to the fluid flow region. It is observed from Fig.4.1(b) that the impact of α_1 on the angular momentum

is notable in every part of the boundary layer, but more significant away from the plate. Also, Figs.4.1(a) and 4.1(b) depict the influence of NDC parameter (α_2) on the boundary layer profiles of velocity and angular momentum. Usually, the velocity of the fluid flow increases sequentially far from the plate, so that it reaches a maximum position within the boundary layer and after that it drops to fulfill the free stream value as displayed in Fig.4.1(a). Moreover, Figs.4.1(a) and 4.1(b) indicate that a rise in α_1 or α_2 changes the sign of angular momentum within the boundary layer from negative to positive and also, the trend of angular momentum is changed from increasing to decreasing away from the plate. Thus, the momentum and angular momentum boundary layer thicknesses are increased nearer to the surface of the inclined plate for both α_1 and α_2. The boundary layer thicknesses of temperature and concentration diminish with the rise of α_1 or α_2, which is clearly observed from Figs.4.1(c) and 4.1(d). The nonlinear differences between the wall and ambient medium temperature and concentration improve with the large values of α_1 and α_2. Because of this, a tremendous addition in f' and g, and a little change in θ and ϕ are noticed. However, the variations in velocity and angular velocity of the micropolar fluid are more in the Darcy flow when compared with the non-Darcy flow results as displayed in Figs.4.1(a)-4.1(b). Further, Figs.4.1(c)-4.1(d) indicate a reverse trend to temperature and concentration with respect to Fs influence. That is, the temperature and concentration of micropolar fluid increase with Fs and the variations in these two profiles are very less in the absence of Fs in comparison with its presence. Further, by the experience of these two NDT and NDC parameters, one can conclude that the impact of nonlinear convection parameters on heat and mass transfer seems to be more in the Darcy porous medium when compared to those in the non-Darcy porous medium.

Figures 4.2(a) to 4.2(d) are prepared to exhibit the significances of double dispersion parameters D_s (0.2, 0.8), D_c (0.1, 0.9) and the Biot number Bi (0.5, 6) on f', g, θ and ϕ for the fixed values of $\alpha_1 = 3$, $\alpha_2 = 3$, $Fs = 0.5$, $\mathcal{B} = 1.0$, $N = 0.6$, $\xi = 0.5$ and $\Omega = 60^0$. From Figs.4.2(a)-4.2(b), it is noteworthy that for individual enhancement of double dispersion parameters, both the velocity and angular velocity of the micropolar fluid are increased and these changes are found to be more in the case of thermal dispersion when compared to that of the solutal dispersion. It is because the supplementation of thermal dispersion in the energy equation will favor to the conduction over convection. Figure 4.2(a) reveals that the velocity of the flow field attains peak position (i.e., maximum state) in the neighborhood of the plate with the increase of conductive-convection parameter Bi and this may be due to the reduction in thermal resistance of the inclined plate.

Additionally, one can observe that, as the Biot number increases, the microrotation changes the direction (from increasing to decreasing) within the boundary layer as plotted in Fig.4.2(b).

Figure 4.2(c) signifies the impact of Biot number on the temperature distribution and also, it shows some special cases for non-isothermal and wall conditions. The convective boundary condition is reduced to wall condition when $Bi \to \infty$ (Ref., Aziz [13]) and it is again proven in Fig.4.2(c). Usually, for a large value of Biot number, the internal thermal resistance of the plate is high and the boundary layer thermal resistance is low. Further, when $Bi = 0$ (i.e., without Biot number) the left side of the plate with hot fluid is totally insulated and the internal thermal resistance of the plate is extremely high, then there is no convective heat transfer to the cold fluid on the right side of the plate takes place. As Bi increase from $Bi < 0.1$ (thermally thin case) to $Bi > 0.1$ (thermally thick case), the temperature distribution accelerates on the surface of the plate. On the other hand, there is a considerable decrement in the temperature profile for D_s and it is nominal for D_c. Fig.4.2(d) reveals that the concentration profile diminishes with the increasing value of Bi. Concerning dispersion parameters, the changes in concentration profiles are observed to be reverse when compared to those changes in temperature profiles. Moreover, the results of thermal and solutal dispersion coefficients are unproductive on the boundary layer profiles for a large value of Biot number.

The influences of inclination of angle Ω $(20^0, 70^0)$ and coupling number N $(0.1, 0.6)$ on f', g, θ and ϕ are portrayed through Figs.4.3(a)-4.3(d) in both aiding ($\mathcal{B} = 0.5$) and opposing ($\mathcal{B} = -0.5$) buoyancy cases. Changes in Ω (form 0^0 to 90^0) lead to decrease the thermal and solutal buoyancy in momentum equation (4.2), and it ceases the velocity distribution inside the boundary layer region as displayed in Fig.4.3(a). Also, it can be observed from Fig.4.3(a) that the maximum buoyancy occurs for the vertical plate and the velocity profile magnifies with coupling number. An increase in N leads to enhance the angular momentum, whereas this gradient has a opposite influence with Ω. Notwithstanding, the direction of the angular momentum is changed within the boundary layer for these two parameters N and Ω as shown in Fig.4.3(b) and similar results can be found in the work of Rahaman *et al.* [81]. It is observed from Figs.4.3(c) and 4.3(d) that the temperature and concentration increase with the enhancement of both coupling number and angle of inclination. Moreover, the changes in velocity, angular momentum and concentration profiles are high in opposing buoyancy for both Ω and N as compared with the aiding buoyancy changes, but temperature profile has different change with respect to both N and Ω.

The significance of the nonlinear convective parameters $\alpha_1(1.5, 3.5)$ and $\alpha_2(0.5, 2.5)$ on the local Nusselt number, local Sherwood number, skin friction and wall couple stress against the stream-wise coordinate ξ, are discussed in the fourth set of Figs.4.4(a)-4.4(d) with $D_s = 0.5$, $D_c = 0.3$, $Bi = 0.3$, $\mathcal{B} = 1.0$, $N = 0.6$, $\xi = 0.5$ and $\Omega = 60^0$. This analysis is undertaken for both Darcy (i.e., for $Fs = 0.0$) and non-Darcy (i.e., for $Fs = 0.5$) cases. The rises in α_1 and α_2 enhance all the pertinent characteristics of the flow field for the fixed values of other parameters. However, the impact of α_1 and α_2 is less in the non-Darcy porous medium as compared to the Darcy porous medium results. This is due to the nonlinear enhancement of thermal and solutal density differences. But, along the stream-wise coordinate ξ, the nature of heat transfer rate is contrary to the mass transfer rate, skin friction and wall couple stress.

Figures 4.5(a)-4.5(d) indicate the impact of the double dispersion parameters D_s $(0.2, 0.8)$, D_c $(0.1, 0.9)$ and Biot number Bi $(0.5, 6.0)$ on the physical quantities of the flow for the fixed values: $\alpha_1 = 3$, $\alpha_2 = 3$, $Fs = 0.5$, $\mathcal{B} = 1.0$, $N = 0.6$, $\xi = 0.5$ and $\Omega = 60^0$. When the inertial effects are prevalent, the thermal and solutal dispersion effects becomes more important. These effects are significant in forced and mixed convective flows as well as in natural convective flows. The results point out that the mass transfer rate, skin friction and wall couple stress increase significantly with the rise in both Biot number and solutal dispersion parameter, whereas these quantities shows reverse trend with thermal dispersion parameter. On the other hand, the local Nusselt number decreases with the Biot number, whereas it increases for both thermal and solutal dispersion parameters.

Influences of coupling number N $(0.1, 0.6)$ and inclination angle Ω $(20^0, 70^0)$ on the heat transfer rate, mass transfer rate, skin friction and wall couple stress are shown by Figs.4.6(a)-4.6(d) in the case of aiding ($\mathcal{B} = 0.5$) and opposing ($\mathcal{B} = -0.5$) buoyancy forces with $D_s = 0.5$, $D_c = 0.3$, $Bi = 0.3$, $\alpha_1 = 3$, $\alpha_2 = 3$, $Fs = 0.5$ and $\xi = 0.5$. As Ω increases, there is a decrement in $g^* cos\Omega$ component in the direction of displacement of the plate, and this decreases the buoyancy force in that direction. Hence, the reduction in the thermal and solutal buoyancy will lead to diminish heat and mass transfer rates. Also, when the coupling number increases heat and mass transfer rates decrease. One can notice that, a rise in the coupling number causes an expansion in the wall couple stress and skin friction, whereas these physical quantities shows an opposite trend with Ω. The Nusselt number and Sherwood number have opposite variations in both aiding and opposing buoyancy cases, but the skin friction and wall couple stress are increased in these two cases.

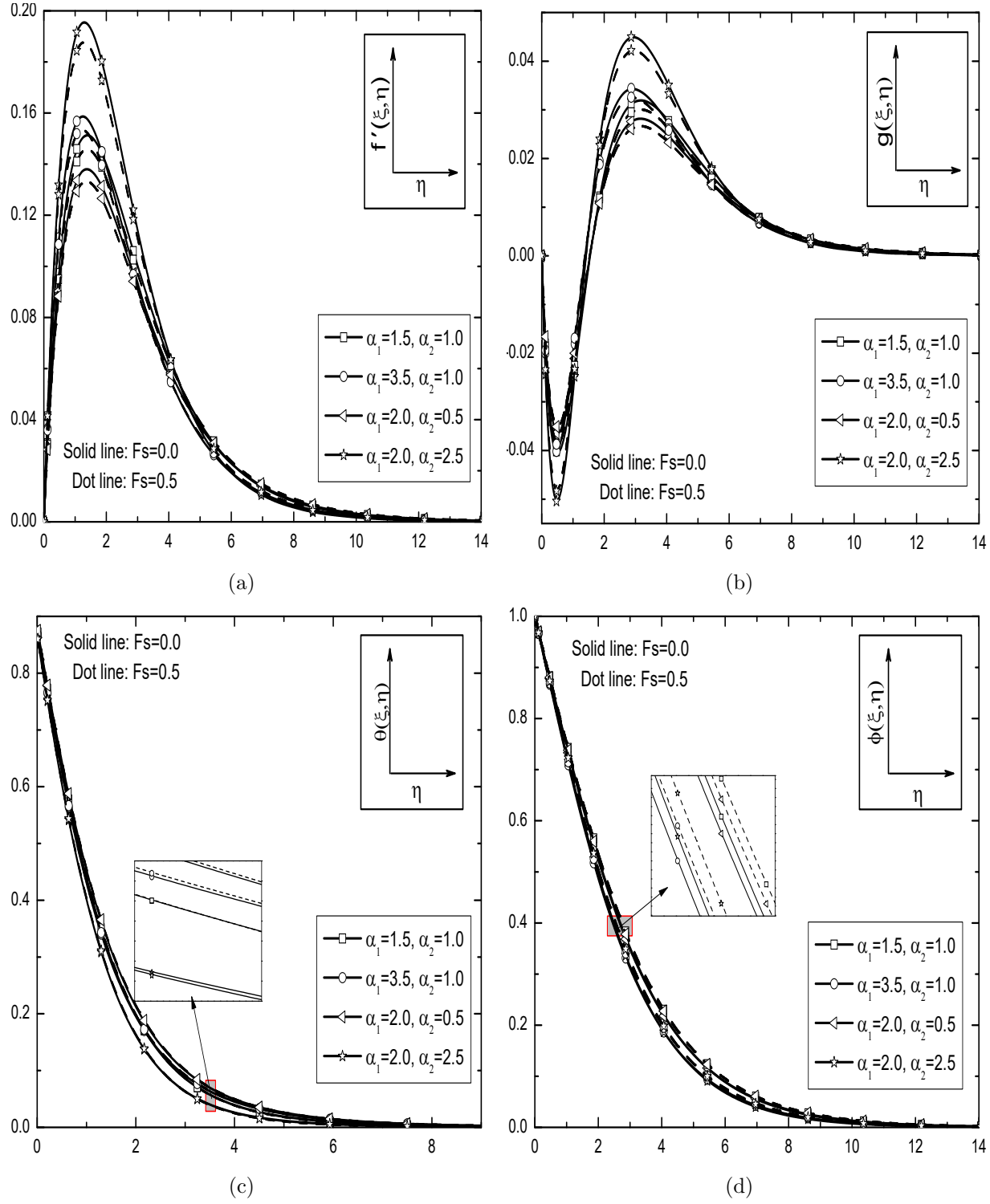

Figure 4.1: *Effects of α_1 and α_2 for different values of Fs on the (a) velocity, (b) angular momentum, (c) temperature and (d) concentration* with fixed values of $\mathcal{B} = 1.0$, $N = 0.6$, $Bi = 0.3$, $D_s = 0.5$, $D_c = 0.3$, $\Omega = 60^0$ and $\xi = 0.5$.

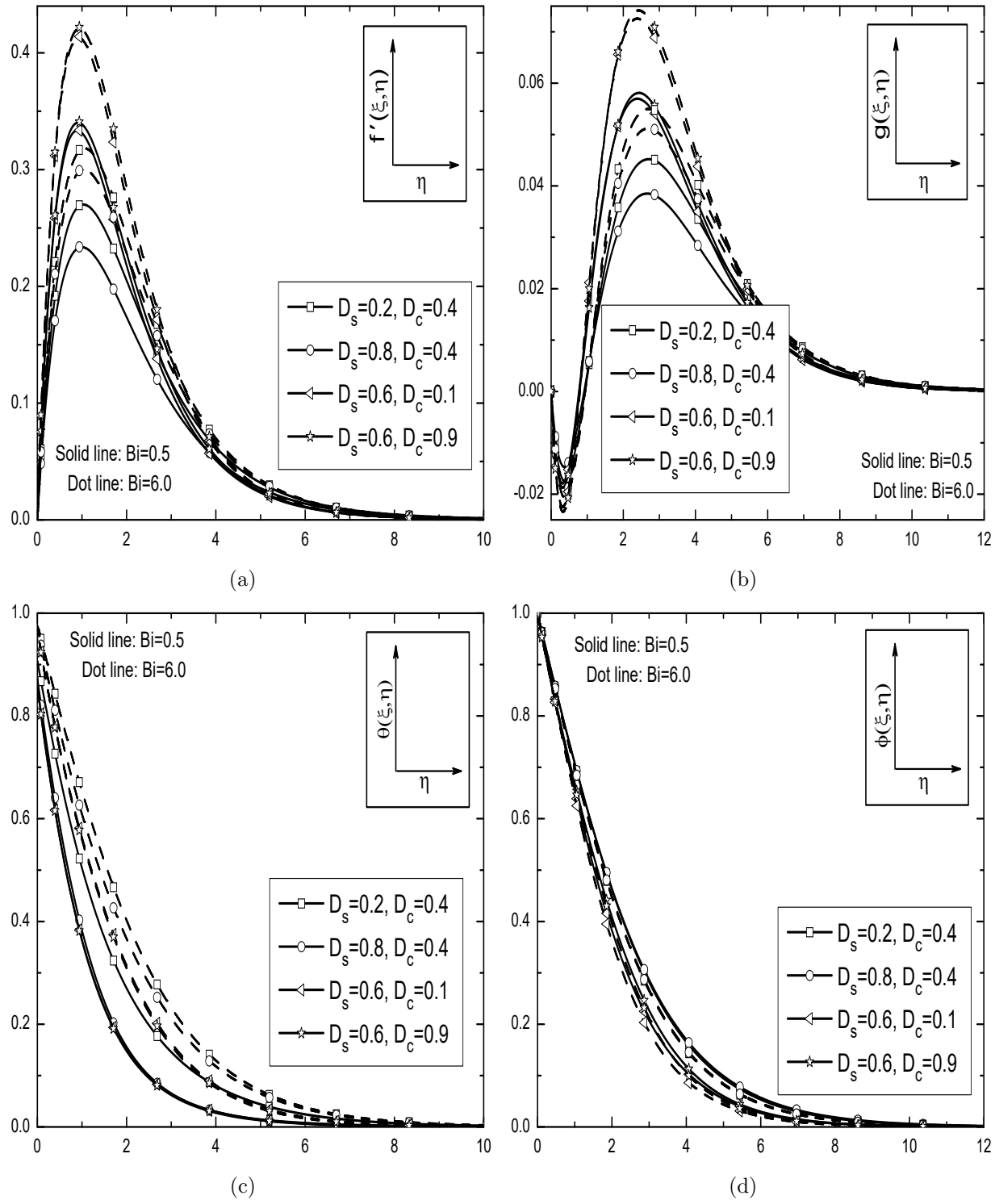

Figure 4.2: *Effects of D_s and D_c for different values of Bi on the (a) velocity, (b) angular momentum, (c) temperature and (d) concentration* with fixed values of $\mathcal{B} = 1.0$, $Fs = 0.5$, $N = 0.6$, $\alpha_1 = 3$, $\alpha_2 = 3$, $\Omega = 60^0$ and $\xi = 0.5$.

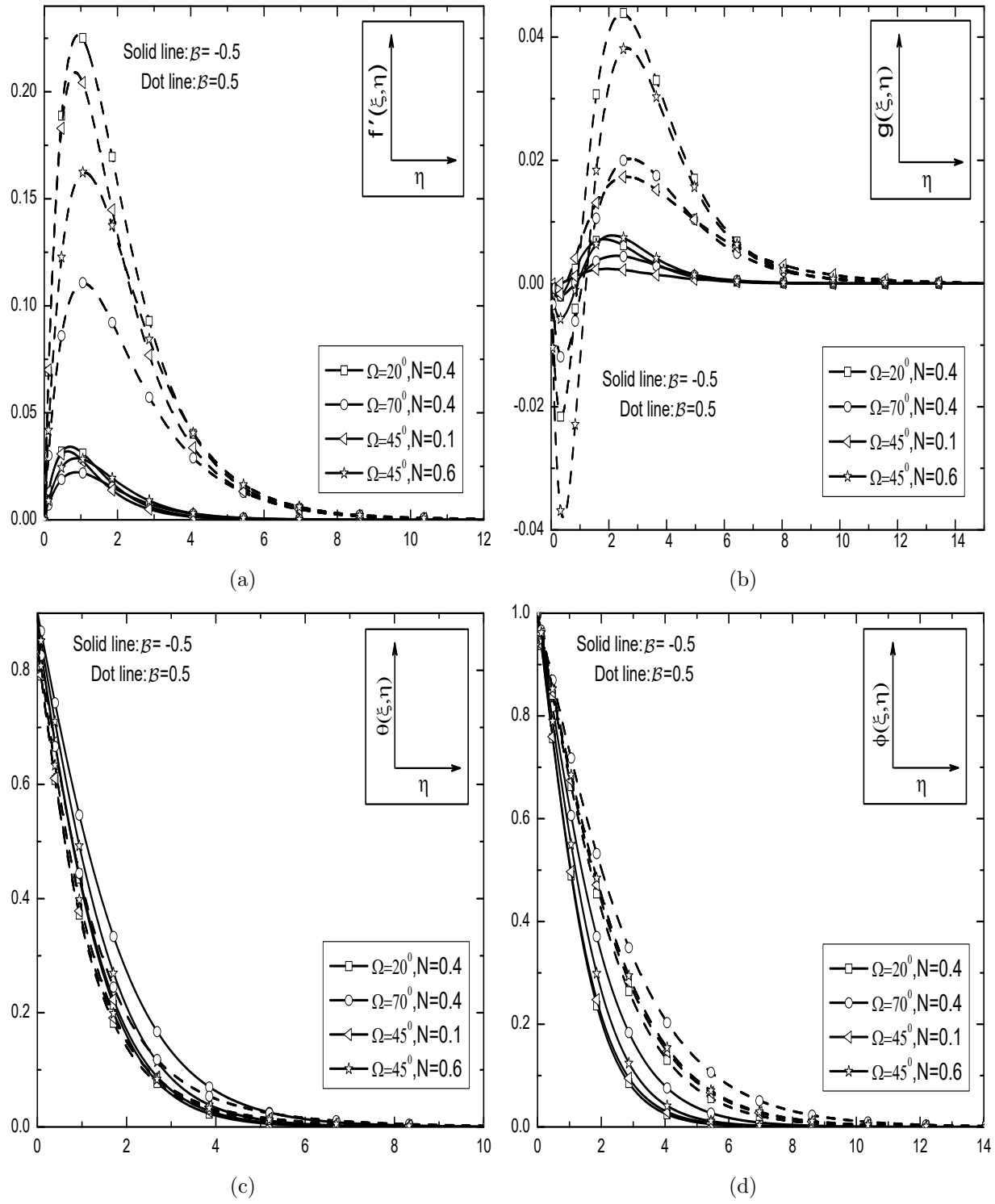

Figure 4.3: *Effects of* N *and* Ω *for different values of* $\mathcal{B}$ *on the (a) velocity, (b) angular momentum, (c) temperature and (d) concentration with fixed values of* $Fs = 0.5$, $\alpha_1 = 3$, $\alpha_2 = 3$, $Bi = 0.3$, $D_s = 0.5$, $D_c = 0.3$ *and* $\xi = 0.5$.

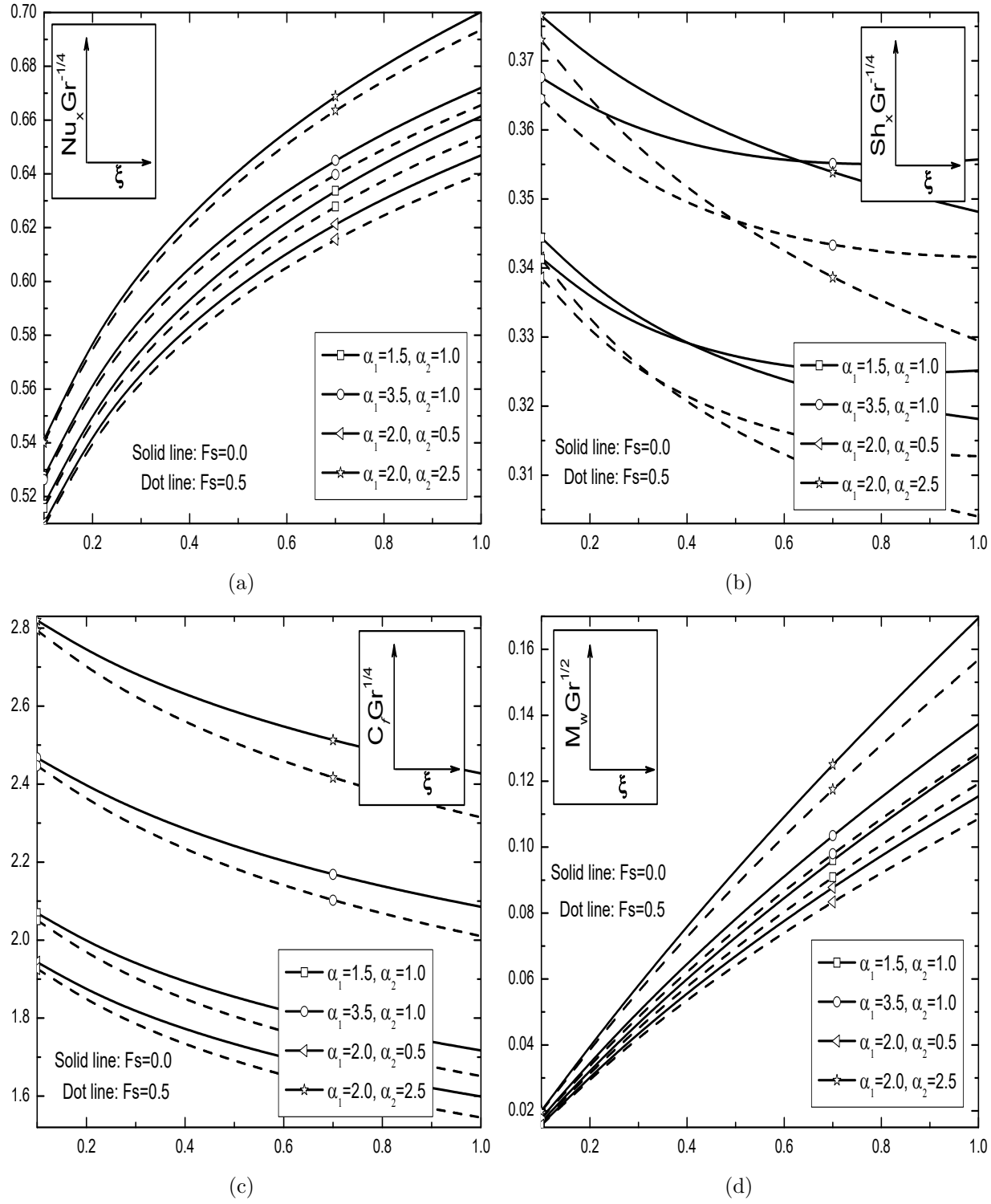

Figure 4.4: *Effects of α_1 and α_2 for different values of Fs on the (a) heat transfer rate, (b) mass transfer rate, (c) skin friction and (d) wall couple stress along stream wise coordinate ξ with fixed values of $D_s = 0.5$, $\mathcal{B} = 1.0$, $Bi = 0.3$, $N = 0.3$, $D_c = 0.3$ and $\Omega = 30^0$.*

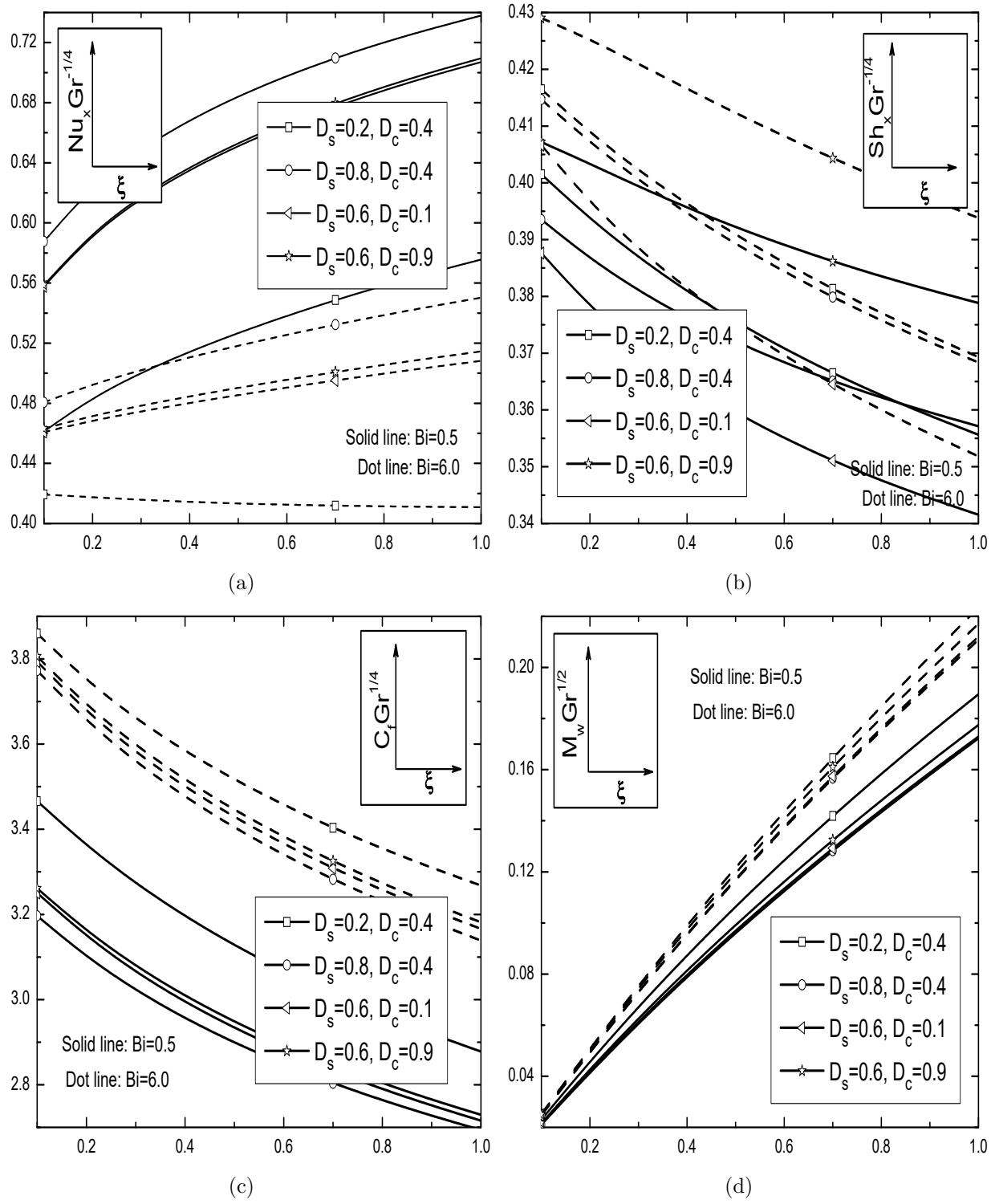

Figure 4.5: *Effects of D_s and D_c for different values of Bi on the (a) heat transfer rate, (b) mass transfer rate, (c) skin friction and (d) wall couple stress along stream wise coordinate ξ with fixed values of $N = 0.3$, $\alpha_1 = 3$, $\mathcal{B} = 1.0$, $Fs = 0.5$, $\alpha_2 = 3$ and $\Omega = 30^0$.*

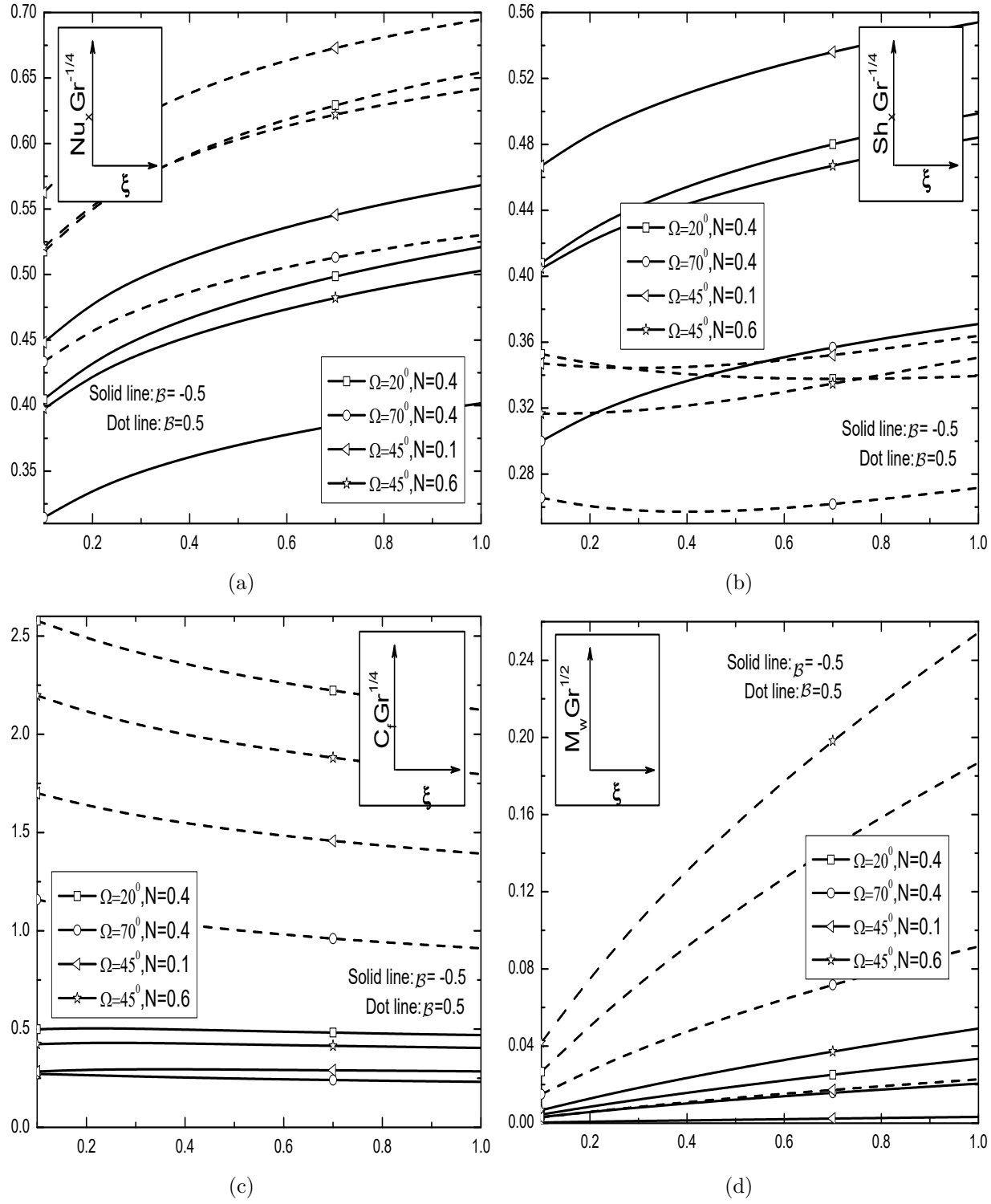

Figure 4.6: *Effects of N and Ω for different values of $\mathcal{B}$ on the (a) heat transfer rate, (b) mass transfer rate, (c) skin friction and (d) wall couple stress along stream wise coordinate ξ with fixed values of $\alpha_1 = 3$, $Fs = 0.5$, $\alpha_2 = 3$, $Bi = 0.3$, $D_s = 0.5$ and $D_c = 0.3$*

4.2.2 Case(b): Mixed Convection

Consider the flow to be a mixed convective flow, which arises from an external flow with the velocity u_∞ and buoyancy forces. We introduce the following dimensionless variables

$$\begin{gathered}\xi = \frac{x}{L},\ \eta = \frac{y}{L}\left(\frac{Re}{\xi}\right)^{1/2},\ \psi(\xi,\eta) = \left(\frac{\xi}{Re}\right)^{1/2} L\, u_\infty\, f(\xi,\eta),\\ \omega(\xi,\eta) = \left(\frac{Re}{\xi}\right)^{1/2}\frac{u_\infty}{L}\, g(\xi,\eta),\ \theta(\xi,\eta) = \frac{T-T_\infty}{T_f-T_\infty},\ \phi(\xi,\eta) = \frac{C-C_\infty}{C_w-C_\infty}.\end{gathered} \tag{4.15}$$

Substituting the stream function (2.7) and the transformations (4.15) into Eqs.(4.1) - (4.5), the resultant dimensionless flow equations can be presented as

$$\begin{aligned}\frac{1}{\varepsilon}\left(\frac{1}{1-N}\right) f''' + \left(\frac{N}{1-N}\right) g' + \frac{1}{2\varepsilon^2} f f'' + \frac{Fs}{Da}\xi\,(1-f'^2) + \frac{1}{Da\,Re}\,\xi\,(1-f')\\ + Ri\,\xi\,[\theta(1+\alpha_1\theta) + \mathcal{B}\phi(1+\alpha_2\phi)]\cos\Omega = \frac{\xi}{\varepsilon^2}\left(f'\frac{\partial f'}{\partial\xi} - f''\frac{\partial f}{\partial\xi}\right),\end{aligned} \tag{4.16}$$

$$\lambda g'' - \left(\frac{N}{1-N}\right)\mathcal{J}\xi\left(2\,g + \frac{1}{\varepsilon}f''\right) + \frac{1}{2\varepsilon}(f\,g' + f'\,g) = \frac{\xi}{\varepsilon}\left(f'\frac{\partial g}{\partial\xi} - \frac{\partial f}{\partial\xi}g'\right), \tag{4.17}$$

$$\frac{1}{\mathrm{Pr}}\theta'' + D_s\left(f'\,\theta'\right)' + \frac{1}{2}f\theta' = \xi\left(f'\frac{\partial\theta}{\partial\xi} - \frac{\partial f}{\partial\xi}\theta'\right), \tag{4.18}$$

$$\frac{1}{Sc}\phi'' + D_c\left(f'\,\phi'\right)' + \frac{1}{2}f\phi' = \xi\left(f'\frac{\partial\phi}{\partial\xi} - \frac{\partial f}{\partial\xi}\phi'\right). \tag{4.19}$$

Boundary conditions (4.6) in terms of f, g, θ and ϕ can be written as

$$\begin{gathered}f(\xi,0) = -2\,\xi\left(\frac{\partial f}{\partial\xi}\right)_{\eta=0},\ f'(\xi,0) = 0,\ g(\xi,0) = 0,\ \theta'(\xi,0) = -Bi\,\xi^{\frac{1}{2}}\,[1-\theta(\xi,0)],\\ \phi(\xi,0) = 1,\ f'(\xi,\infty) = 1,\ g(\xi,\infty) = 0,\ \theta(\xi,\infty) = 0,\ \phi(\xi,\infty) = 0.\end{gathered} \tag{4.20}$$

In the above non-dimensional equations, thermal dispersion parameter is taken as $D_s = \dfrac{\chi d u_\infty}{\nu}$ and the solutal dispersion parameter is taken as $D_c = \dfrac{\zeta d u_\infty}{\nu}$.

The physical quantities of present interest (such as shear stress, wall couple stress, heat and

mass transfer rates), are defined as

$$C_f = \frac{2}{\rho\, u_\infty^2}\left[(\mu+\kappa)\frac{\partial u}{\partial y} + \kappa\omega\right]_{y=0},\ M_w = \frac{\gamma}{\rho\, u_\infty^2 L}\left[\frac{\partial \omega}{\partial y}\right]_{y=0}$$
$$Nu_x = -\frac{x}{k_f(T_f - T_\infty)}\left[k_e\frac{\partial T}{\partial y}\right]_{y=0},\ Sh_x = -\frac{x}{D(C_w - C_\infty)}\left[D_e\frac{\partial C}{\partial y}\right]_{y=0} \tag{4.21}$$

The non-dimensional skin friction C_f, wall couple stress M_w, local Nusselt number Nu_x and the Sherwood number Sh_x, are given by

$$C_f Re^{1/2} = \left(\frac{2}{1-N}\right)\ \xi^{\frac{-1}{2}}\ f''(\xi,0), \qquad M_w Re = \left(\frac{\lambda}{\xi\ \mathcal{J}}\right) g'(\xi,0),$$
$$\frac{Nu_x}{Re^{\frac{1}{2}}} = -\xi^{\frac{1}{2}}\ \left[1 + D_s\ \mathrm{Pr}\ f'(\xi,0)\right]\ \theta'(\xi,0),\ \ \frac{Sh_x}{Re^{\frac{1}{2}}} = -\xi^{\frac{1}{2}}\ \left[1 + D_c\, Sc\, f'(\xi,0)\right]\ \phi'(\xi,0) \tag{4.22}$$

Results and Discussion

As in the previous case, the nonlinear partial differential equations (4.16) - (4.19) subject to the boundary conditions (4.20) are solved numerically using the successive linearization method together with local similarity and non-similarity approaches. In the absence of double dispersion effects, this case reduces to the case (b) problem of chapter-2. Validation of the present problem in this case can be done on comparison, as it was done in the case (b) of chapter-2.

We have computed the solutions for the dimensionless velocity (f'), microrotation (g), temperature (θ), concentration (ϕ), drag coefficient ($C_f Re^{1/2}$), gradient of microrotation ($-M_w Re$), heat and mass transfer rates ($Nu_x\, Re^{-1/2}$ and $Sh_x\, Re^{-1/2}$), as shown graphically in Figs.4.7(a)-4.12(d). The effects of nonlinear convection parameters (α_1, α_2), double dispersion parameters (D_s, D_c), Biot number (Bi) and angle of inclination (Ω) have been discussed. To study the effects of α_1, α_2, D_s, D_c, Bi and Ω, the computations were carried out by taking $Da = 0.1$, $\mathcal{J} = 0.01$, $\mathrm{Pr} = 0.71$, $N = 0.3$, $Re = 200$, $\varepsilon = 0.5$, $\lambda = 0.5$, $Sc = 0.22$, $Fs = 0.5$ and $\mathcal{B} = 1.0$. These values are continued same throughout this study, unless otherwise specified.

Influences of nonlinear convection parameters on the fluid flow profiles are displayed through the first set of figures for both aiding and opposing flow cases with $N = 0.3$, $Bi = 0.5$, $D_s = 0.5$, $D_c = 0.3$, $\Omega = 30^0$ and $\xi = 0.5$. Figs.4.7(a)-4.7(b) represents the profiles of velocity and microrotation for nonlinear convection parameters and it is observed that the velocity enhances while microrotation

reduces for the larger values of both α_1 and α_2 in aiding flow case. In opposing flow case, the trend of these parameters is reverse to the aiding flow results. Impacts of α_1 and α_2 on the temperature and concentration of micropolar fluid are depicted in Figs.4.7(c) and 4.7(d). It is found that both temperature and concentration and their associated thicknesses of boundary layer fall down for the rise of α_1 and α_2 in the case of aiding flow, whereas these boundary layer profiles increase in the case opposing flow.

The behaviors of velocity, microrotation, temperature, and concentration of micropolar fluid with respect to the Biot number and angle of inclination are depicted in Figs 4.8(a)-4.8(d) with the fixed values: $N = 0.3$, $\alpha_1 = 1$, $\alpha_2 = 1$, $D_s = 0.5$, $D_c = 0.3$ and $\xi = 0.5$. From Fig.4.8(a), it is noted that velocity enhances with the increase of Biot number in the case of aiding flow, whereas it diminishes in the case of opposing flow. A reduction in microrotation is observed for larger values of Biot number as shown in Fig.4.8(b). It is also important to note that velocity is more for vertical plate compared to the horizontal plate in aiding flow case, and in the case of opposing flow this variation is opposite. In both aiding and opposing flow cases, the temperature and concentration are magnified by the Biot number and degraded with the angle of inclination as depicted in Figs.4.8(c) and 4.8(d).

Figures 4.9(a)-4.9(b) are prepared to discuss the effect of thermal dispersion on temperature profile and solutal dispersion on concentration profile with $N = 0.3$, $Bi = 0.5$, $\alpha_1 = 1$, $\alpha_2 = 1$, $\Omega = 30^0$ and $\xi = 0.5$ for both aiding and opposing flow cases respectively. When the inertial effects are prevalent, the thermal and solutal dispersion effects become more significant. Further, these effects are important in forced and mixed convective flows as well as in natural convective flows. Figure 4.9(a) shows the effect of thermal dispersion parameter on the temperature profile for both aiding and opposing flow cases. It is observed that temperature decreases with the increase of thermal dispersion parameter in both aiding and opposing flow cases. The concentration of micropolar fluid increases by the solutal dispersion parameter as shown in Fig.4.9(b) in both the cases of aiding and opposing flows.

The influences of NDT (α_1) and NDC (α_2) parameters on the surface drag ($C_f Re^{1/2}$), gradient of microrotation ($-M_w Re$), heat transfer rate ($Nu_x\, Re^{-1/2}$) and mass transfer rate ($Sh_x\, Re^{-1/2}$), are displayed in Figs.4.10(a)-4.10(d) with the fixed values: $Bi = 0.5$, $\Omega = 30^0$, $D_s = 0.5$, $D_c = 0.3$, $N = 0.3$, $Ri = -0.5$ (for opposing flow) and $Ri = 2.0$ (for aiding flow). It is always very essential to estimate the magnitudes of heat and mass transfer rates, since the quality of the final product

depends on the heat and mass transfer rates from the surface. In this context, it is worth to mention that the non-dimensional heat transfer rate ($Nu_x\, Re^{-1/2}$) and mass transfer rate ($Sh_x\, Re^{-1/2}$) increase with the enhancement of Ri as shown in Fig.4.10(a) and Fig.4.10(b). Hence the mixed convection parameter has an important role in controlling the temperature and concentration. The effect of mixed convection parameter Ri on the skin friction coefficient ($C_f Re^{1/2}$) and the wall couple stress ($-M_w Re$) is portrayed in Fig.4.10(c) and Fig.4.10(d) respectively. It is observed that the skin friction coefficient ($C_f Re^{1/2}$) increases as Ri increases. It is because, an increase in the buoyancy in mixed convective flow leads to accelerate the fluid flow, which increases the skin friction coefficient. Also, it is found that the wall couple stress decreases with the increase of mixed convection parameter Ri. This observation is consistent with the velocity, microrotation, temperature and concentration distributions.

Figure 4.10(a) reveals that the local Nusselt number ($Nu_x\, Re^{-1/2}$) decrease as α_1 increases in the opposing flow case, whereas the reverse trend is observed in the case of aiding flow. Physically, $\alpha_1 > 0$ implies that $T_f > T_\infty$; hence, there will be a supply of heat to the flow region from the wall. Similarly $\alpha_1 < 0$ implies that $T_f < T_\infty$, and in such case, there will be a transfer of heat from the fluid to the wall. Also, Fig.4.10(a) reveals the influence of α_2 on the heat transfer rate and the impact of α_2, which is same but more significant as compared with α_1. The effects of nonlinear convection parameters on the mass transfer rate ($Sh_x\, Re^{-1/2}$), wall couple stress ($-M_w Re$), and skin friction ($C_f Re^{1/2}$) are identical with the heat transfer rate ($Nu_x\, Re^{-1/2}$) results as shown in Figs.4.10(b)-4.10(d). However, along the stream-wise coordinate ξ, the Nusselt number and wall couple stress increase, whereas the opposite trend can be observed in Sherwood number and skin friction. By the experience of these two NDT and NDC parameters, one can that the influence of NDC parameter is more prominent compared with that of NDT parameter in both aiding and opposing flows. This is due to the presence of Biot number which controls the influence of NDT parameter.

Variations in heat transfer rate ($Nu_x\, Re^{-1/2}$), mass transfer rate ($Sh_x\, Re^{-1/2}$), skin friction ($C_f Re^{1/2}$) and wall couple stress ($-M_w Re$) for different values of the Biot number $Bi(0, 0.05, 0.5, 1.0)$ and inclination of angle $\Omega(45^0, 75^0)$, are displayed in Figs.4.11(a)-4.11(d) with $\alpha_1 = 5$, $\alpha_2 = 6$, $D_s = 0.5$, $D_c = 0.3$, $Ri = -0.5$ (for opposing flow) and $Ri = 2.0$ (for aiding flow). Fig.4.11(a) indicates the effect of Bi on the heat transfer rate ($Nu_x\, Re^{-1/2}$) and it is magnified with the enhancement of Bi in both the cases of aiding and opposing flows at the surface of an inclined plate.

A small reduction can be noticed for mass transfer rate ($Sh_x\, Re^{-1/2}$) with the increment of Bi in opposing flow case, whereas reverse change can be found for aiding case as depicted in Fig.4.11(b).

The convective boundary condition is the generalization of isothermal boundary condition and it effectively furnishes a mechanism for comparing the conduction resistance within a solid body to the convection resistance external to that body (offered by the surrounding fluid) for heat transfer. The wall condition, $\theta(0) = 1$ is a limiting result of the convective boundary condition when h_f tends to infinity (stated by Aziz [13]), and it is proven by temperature profile. Usually, for high Biot number, the internal thermal resistance of the plate is high and the boundary layer thermal resistance is low. Further, when $Bi = 0$ (i.e., without Biot number) the left side of the plate with hot fluid is totally insulated, then the internal thermal resistance of the plate is extremely high and no convective heat transfer to the cold fluid on the right side of the plate takes place, which is clearly observed from the Fig.4.11(a). These results are similar to the work of Beg *et al.* [18] in the case of assisting flow. Finally, it is observed that the skin friction and wall couple stress increase with the enhancement of Bi as shown in Fig.4.11(c) and Fig.4.11(d) respectively.

The mixed convective flow has a significant impact with the inclination angle, and so the heat transfer rate ($Nu_x\, Re^{-1/2}$), in aiding flow, decreases with the increase of angle of inclination and in the case of opposing flow it has opposite trend as shown in Fig.4.11(a). Also, from Fig.4.11(b), a similar effect is pointed out to the Sherwood number ($Sh_x\, Re^{-1/2}$) with reference to the angle of inclination. Clearly, Figs.4.11(a) and 4.11(b) reveal that, an increase in angle of inclination decreases the buoyancy force and it retards the flow. Also, a reduction in the heat and mass transfer rates is noticed. The maximum values of the dimensionless heat and mass transfer rates are observed when the plate is in vertical position; in which, the buoyancy force is at its maximum. Therefore, the heat and mass transfer rates are at a lower level for $\Omega \neq 0^0$. From Figs.4.11(c) and 4.11(d), it is observed that an increase in the angle of inclination lower the buoyancy force and hence increases both the skin friction ($C_f Re^{1/2}$) and wall couple stress ($-M_w Re$) in opposing flow case, whereas it has a reverse trend in aiding flow case. The inclination of horizontal plate to the vertical plate reduces the drag force which favors the flow through the medium. Further, the results of Bi contradict the results of Ω on these coefficients.

The variations in the thermal and solutal dispersion parameters ($D_s = 2, 6$ and $D_s = 1, 5$) on $Nu_x\, Re^{-1/2}$, $Sh_x\, Re^{-1/2}$, $C_f Re^{1/2}$ and $-M_w Re$ are displayed in Figs.4.12(a)-4.12(d) for $Ri(-0.5, 2.0)$ and $\alpha_1 = 5$, $\alpha_2 = 6$, $Bi = 0.5$ and $\Omega = 30^0$. It is observed that the heat transfer rate ($Nu_x\, Re^{-1/2}$)

increases with D_s whereas it decreases for D_c in both opposing and aiding flow cases. Introducing the thermal dispersion in the energy equation, in general, it favors conduction over convection. In other words, supplementing dispersion effects to the energy equation give more dominance to thermal conduction. Further, a nominal influence is noticed for the solutal dispersion parameter on mass transfer rate for both the cases of Ri, as depicted in Fig.4.12(a). The variations of Sherwood number ($Sh_x\, Re^{-1/2}$) as a function of ξ are shown in Fig.4.12(b) for D_s and D_c with the fixed values of other parameters. It is observed from Fig.4.12(b) that the mass transfer rate decreases in aiding flow case, whereas a reverse phenomenon is observed for opposing flow case with the increase of D_s. A rise in mass transfer rate is noticed in both aiding and opposing flow cases with the increase of solutal dispersion parameter D_c, as plotted in Fig.4.12(b). Also, a nominal influence of thermal dispersion on the mass transfer rate is observed in both aiding and opposing flow cases. Figs.4.12(c)-4.12(d) reveal the impact of dispersion coefficients on skin friction and wall couple stress along stream-wise coordinate. These graphs demonstrate that the thermal dispersion parameter D_s gives a opposite influence to the drag coefficient and wall couple stress for different values of the mixed convection parameter (i.e., $Ri = -0.5$ and $Ri = 2.0$). An increase in the solutal dispersion parameter D_c increases the skin friction and wall couple stress for opposing flow and decrease in aiding flow, as portrayed in Figs.4.12(c)-4.12(d).

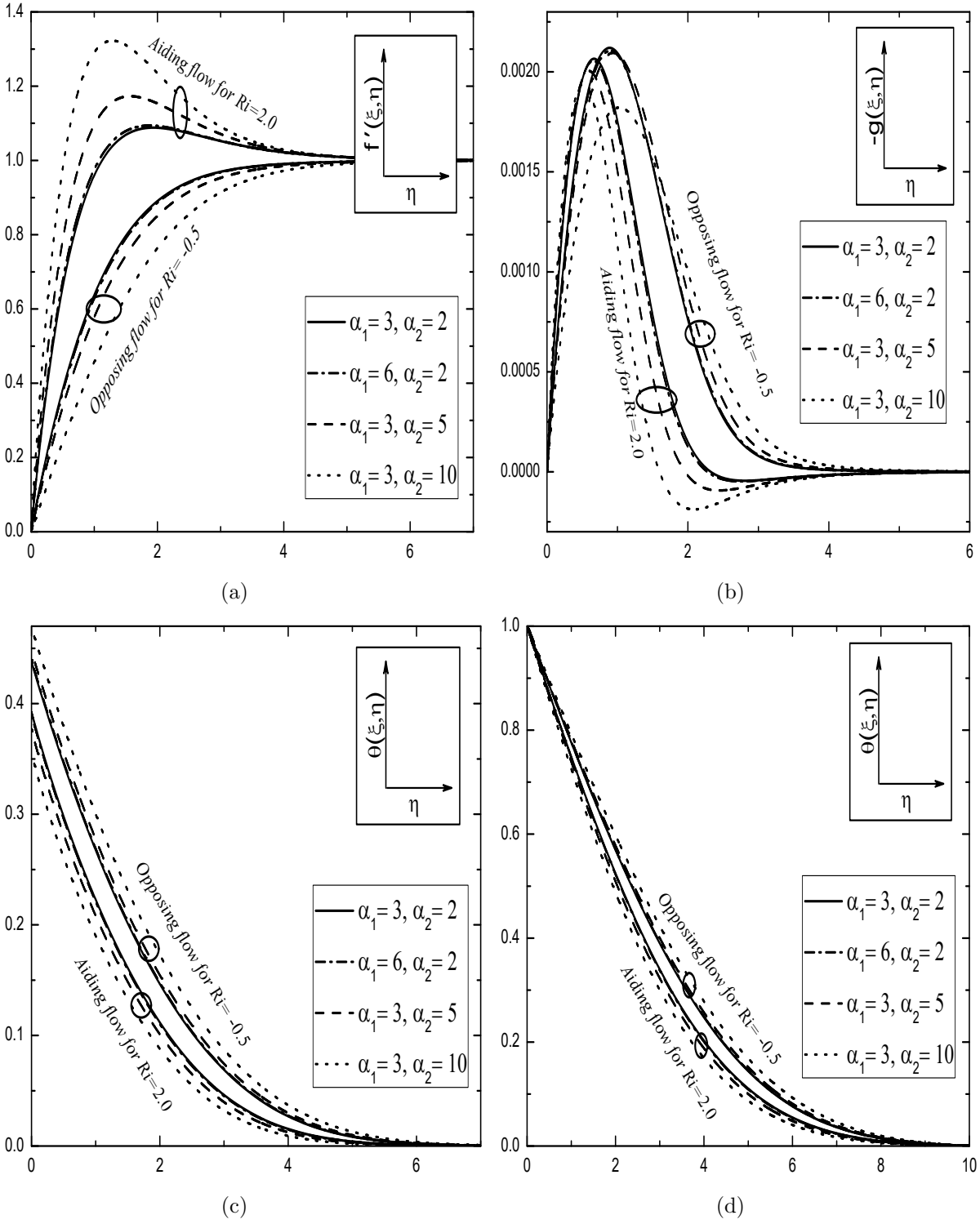

Figure 4.7: *Effects of* α_1 *and* α_2 *for different values of Ri on the (a) velocity, (b) micro-rotation, (c) temperature and (d) concentration with the fixed values of* $\mathcal{B} = 1.0$, $N = 0.3$, $Bi = 0.5$, $D_s = 0.5$, $D_c = 0.3$, $\Omega = 30^0$ *and* $\xi = 0.5$.

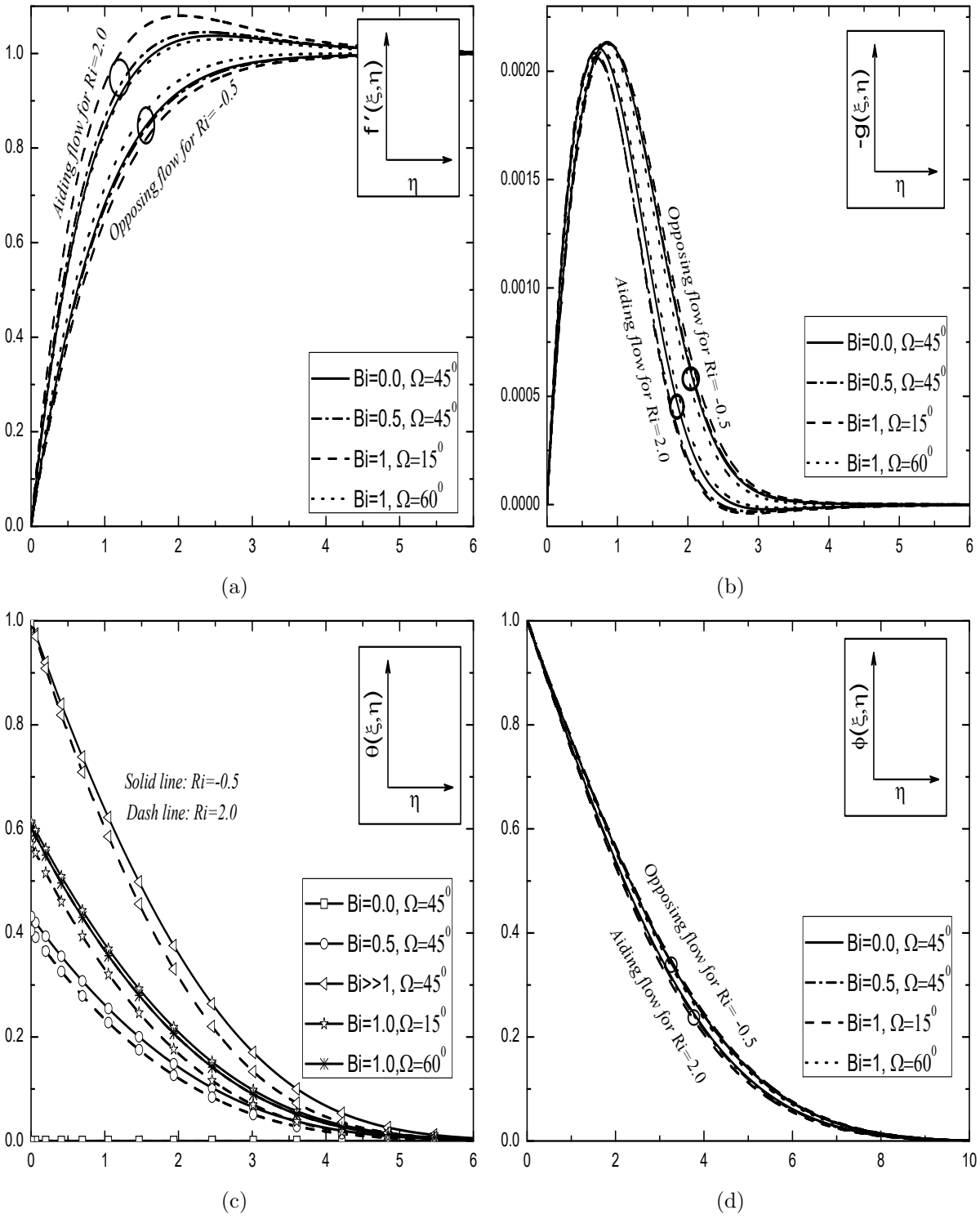

Figure 4.8: *Effects of* Ω *and Bi for different values of Ri on the (a) velocity, (b) microrotation, (c) temperature and (d) concentration with the fixed values of* $N = 0.3$, $\alpha_1 = 1$, $\alpha_2 = 1$, $D_s = 0.5$, $D_c = 0.3$ *and* $\xi = 0.5$.

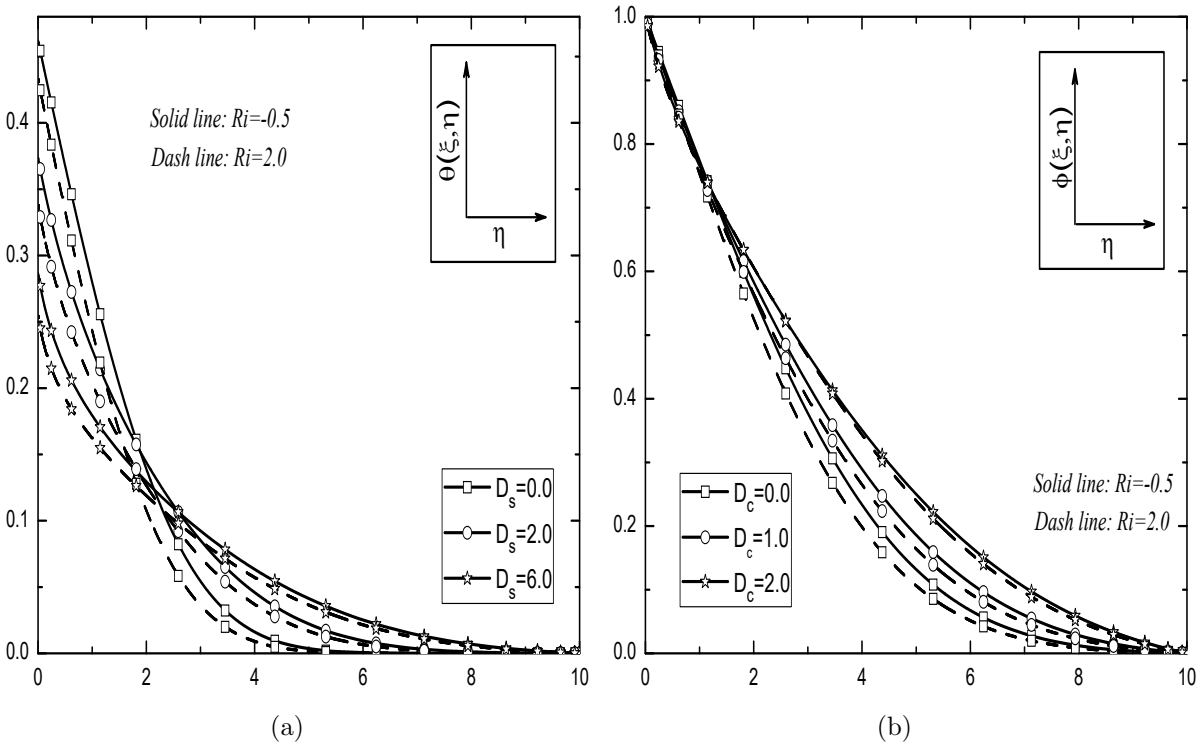

(a) (b)

Figure 4.9: *Effect of D_s on the (a) temperature, and effect of D_c on the (b) concentration for different values of Ri with the fixed values of $N = 0.3$, $Bi = 0.5$, $\alpha_1 = 1$, $\alpha_2 = 1$, $\Omega = 30^0$ and $\xi = 0.5$.*

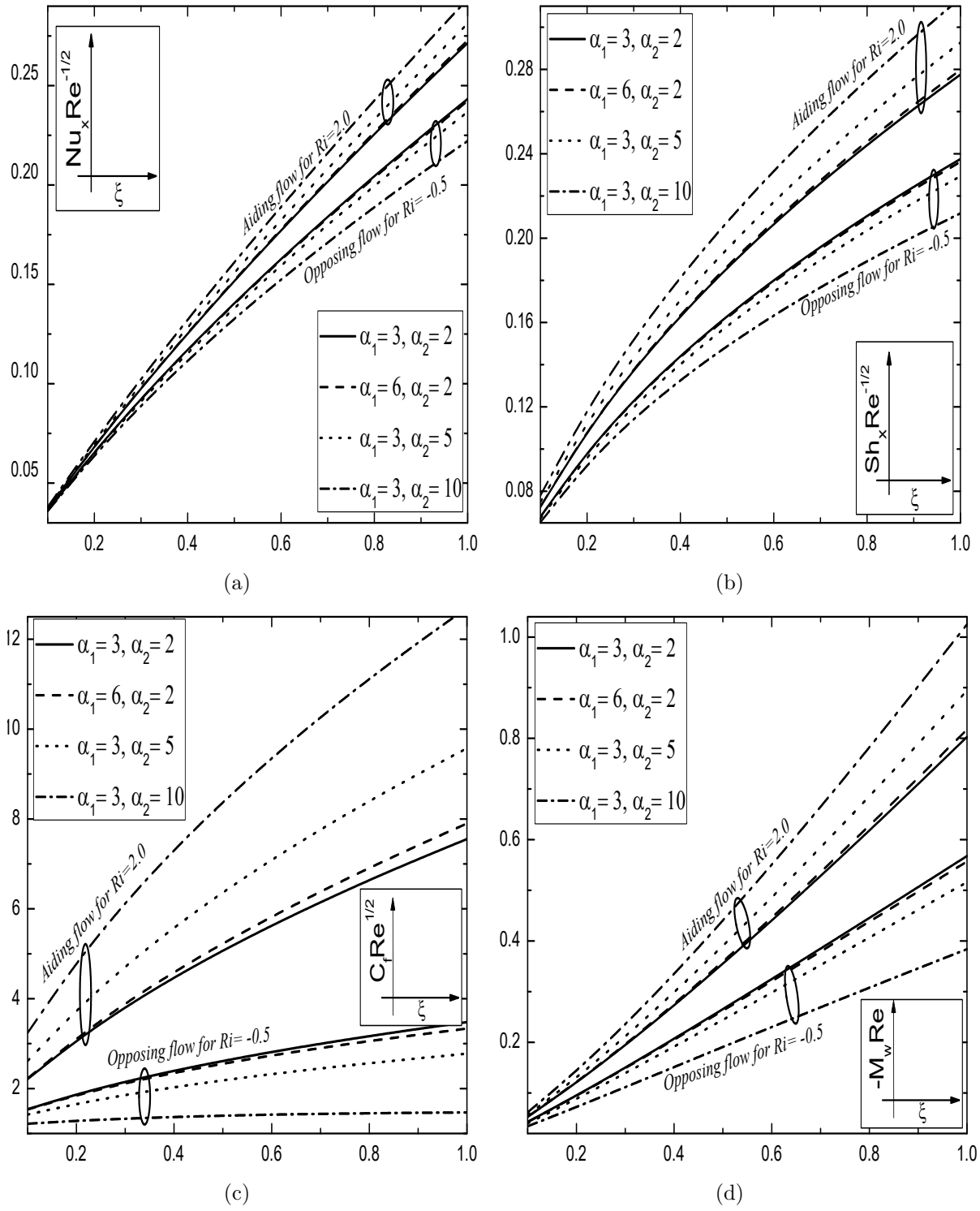

Figure 4.10: *Effects of α_1 and α_2 for different values of Ri on the (a) heat transfer rate, (b) mass transfer rate, (c) skin friction and (d) wall couple stress with the fixed values of $N = 0.3$, $Bi = 0.5$, $D_s = 0.5$, $D_c = 0.3$, $\Omega = 30^0$ and $\xi = 0.5$.*

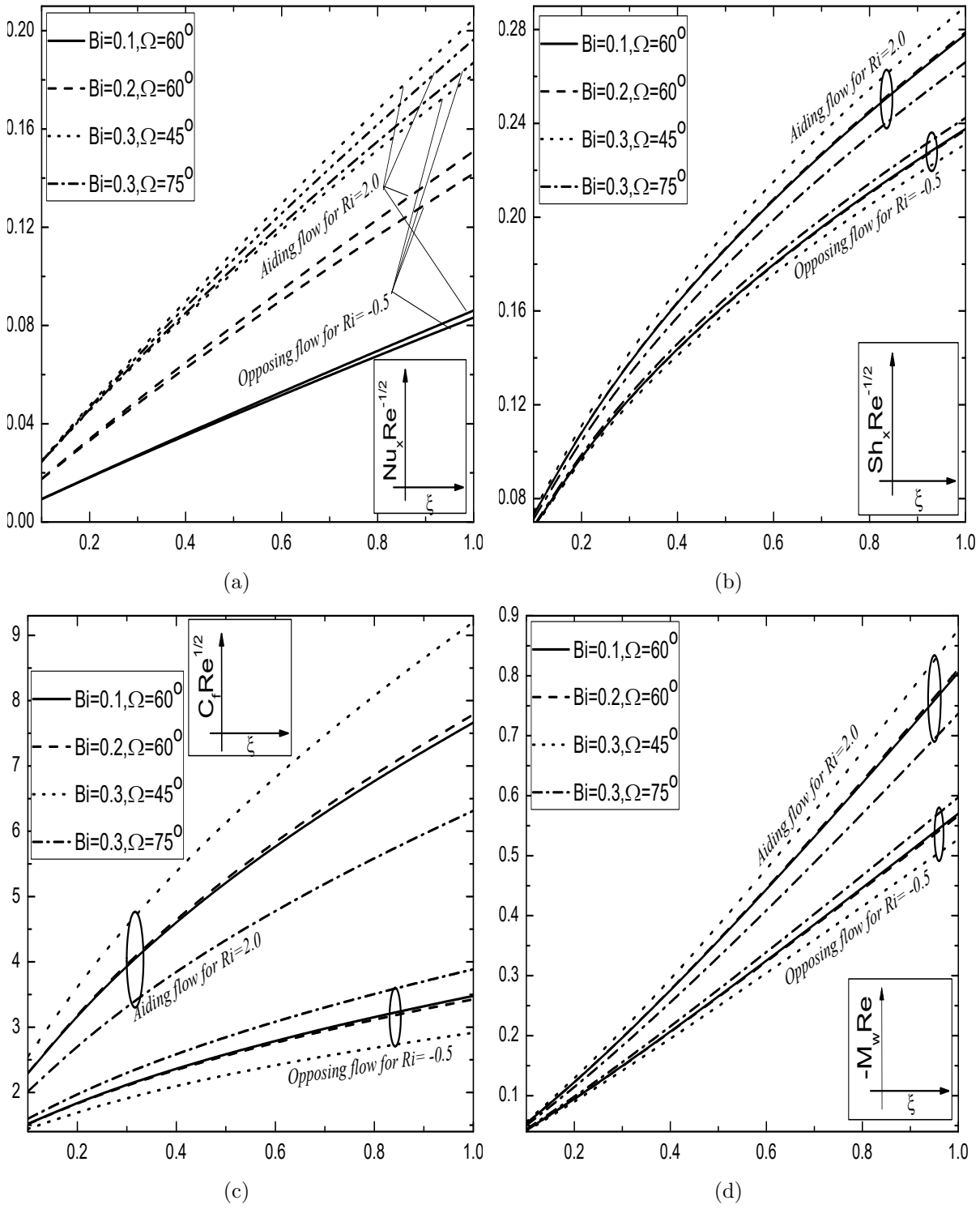

Figure 4.11: *Effects of* Ω *and Bi for different values of Ri on the (a) heat transfer rate, (b) mass transfer rate, (c) skin friction and (d) wall couple stress with the fixed values of* $N = 0.3$, $\alpha_1 = 5$, $\alpha_2 = 6$, $D_s = 0.5$, $D_c = 0.3$ *and* $\xi = 0.5$.

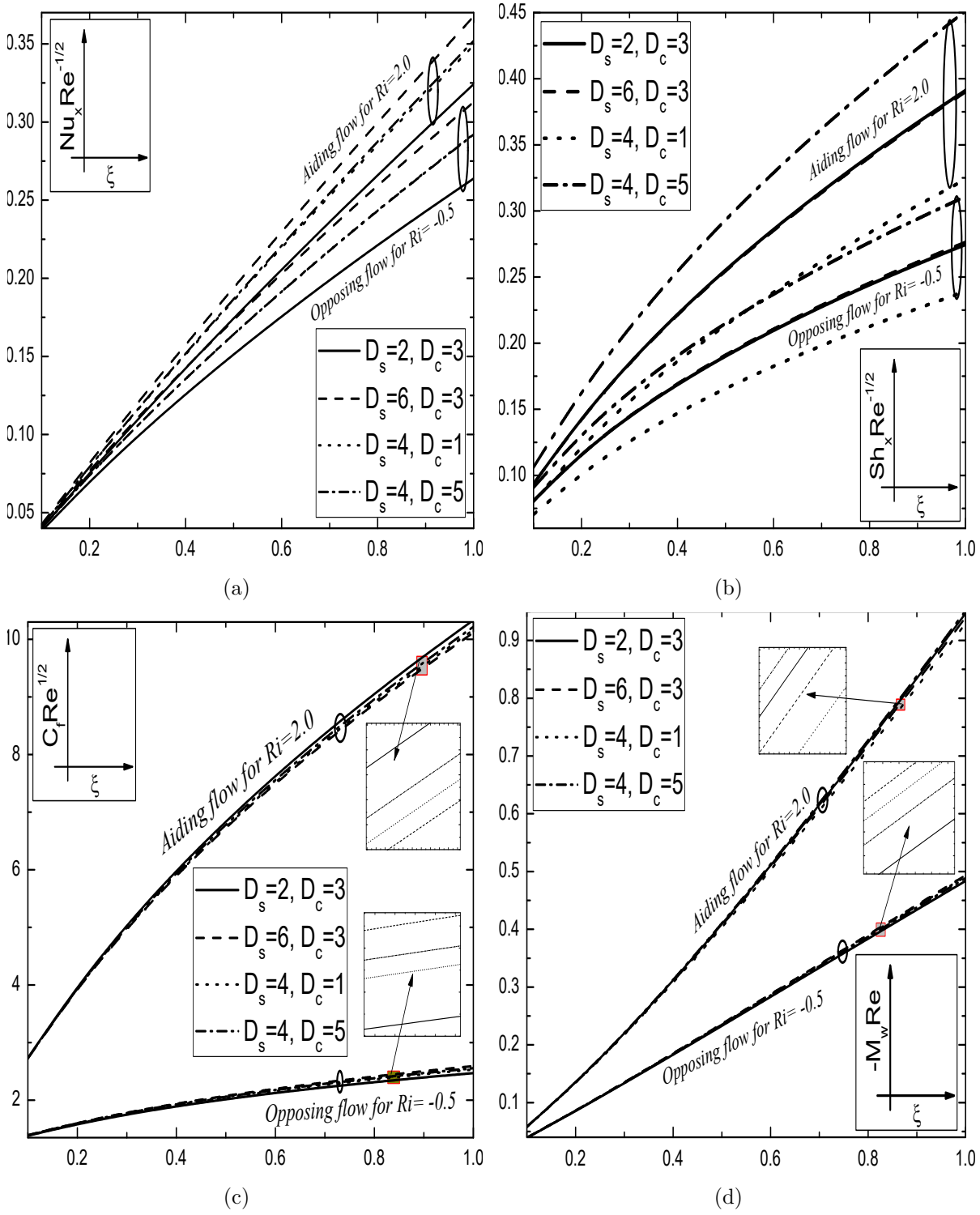

Figure 4.12: *Effects of D_s and D_c for different values of Ri on the (a) heat transfer rate, (b) mass transfer rate, (c) skin friction and (d) wall couple stress with the fixed values of $N = 0.3$, $\alpha_1 = 5$, $\alpha_2 = 6$, $D_s = 0.5$, $D_c = 0.3$ and $\xi = 0.5$.*

4.3 Conclusions

The effect of double dispersion on the nonlinear convective flow of a micropolar fluid along an inclined plate embedded in a non-Darcy porous medium, is analyzed in this chapter. The resulting equations are solved numerically by employing the successive linearization method together with the local similarity and non-similarity approaches. The main findings of this chapter are summarized as follows:

The major conclusion is that the influence of NDC parameter α_2 is more prominent on all the physical quantities of the present model compared with that of NDT parameter α_1 in both free and mixed convective flows. This may be due to the presence of Biot number as it controls the influence of NDT parameter. Additionally, the effects of NDT and NDC parameters on the heat and mass transfer are observed to be more in the Darcy porous medium when compared to those in the non-Darcy porous medium. In case (b), Sherwood number and drag coefficients are diminished with the enhancement of nonlinear convection parameters along the stream-wise coordinate, while the opposite pattern can be seen in the case of heat transfer rate and micro-rotation gradient. A variation of Biot number leads to enhance all pertinent characteristics except the Nusselt number and concentration profile. On the other side, the results of double dispersion parameters are unproductive for a large value of the Biot number. However, the thicknesses of linear momentum, angular momentum, and solutal boundary layers are enhanced by enhancement in the buoyancy ratio, whereas the thickness of the thermal boundary layer diminishes for both aiding and opposing buoyancy cases. Further, the dispersion coefficients have the strong influence on the respective convective heat and mass transfers. This effect is more prominent in the case of nonlinear Boussinesq approximation when compared to linear Boussinesq approximation for both case (a) and case (b).

Part III

NONLINEAR CONVECTION IN POWER-LAW FLUIDS

Chapter 5

Nonlinear Convective Flow of a Power-law Fluid past an Inclined Plate with Convective Boundary Condition [1]

5.1 Introduction

The study of thermal and solutal transport phenomena of a Ostwald-de Waele power-law fluid flow in porous media has gained extensive attention on account of its wide pertinence in energy and geophysical industries. For example, we can mention thermal insulation, filtration processes, geophysical flows, petroleum resource, polymer processing, and so forth. Amin [38] discussed the influence of viscous dissipation and magnetic effects on a power-law fluid flow past horizontal and vertical flat plates embedded in a porous medium. Cheng [31] investigated free convective flow of a stratified power-law fluid over a vertical wavy surface in a porous medium. Impact of convective boundary condition in the heat transfer analysis of a power-law fluid flow along a stretching sheet, is examined by Shahzad and Ramzan [89]. Chamkha *et al.* [22] investigated the laminar flow of a

[1]Case(a): Published in "**Nonlinear Engineering**" 8(1) (2019) 94–106, Case(b): Published in "**International Journal of Applied and Computational Mathematics**" 4(51) (2018) 1–18.

power-law fluid in a non-Darcy porous medium filled with nanoparticles. Recently, Ahmed *et al.* [4] applied uniform magnetic field and considered the convective boundary condition in the analysis of a radiative power-law fluid flow over a stretching sheet.

Nowadays, most of the researchers are interested to analyze the convection from an inclined surface in both the numerical and experimental works. It is because the convective heat and mass transfers over an inclined surface are frequently encountered in natural and engineering devices such as solar water heaters, electrical systems, iron removal, brine clarification, etc. It has been shown that the inclination of the horizontal plate to the vertical direction reduces the drag force which favors the flow through the medium. Due to this importance, Alam *et al.* [6] analyzed the influences of thermal radiation and thermophoresis over a permeable inclined plate in a viscous fluid, whereas the flow over an inclined plate has been considered by Sui *et al.* [101] to study the mixed convective heat transfer of a power-law fluid.

Based on the previous studies, it is relevant to discuss the free and mixed convective flows of a power-law fluid along an inclined plate embedded in a non-Darcy porous medium with Biot number effect. In addition, the nonlinear Boussinesq approximation is considered in the formulation of fluid flow equations. As in the previous chapter, here also, the successive linearization method together with the local similarity and non-similarity approaches are employed to solve the system of reduced non-linear partial differential equations. The effects of pertinent parameters on the physical quantities are studied and the results are displayed through graphs. This kind of investigation is useful in the mechanism of combustion, solar collectors which are performed at high-level temperatures.

5.2 Mathematical Formulation

A two-dimensional, steady and laminar convective flow of a power-law fluid along an inclined plate embedded in a non-Darcy porous medium, is considered in this chapter. The semi-infinite plate is inclined about vertical direction with an acute angle Ω as shown in Fig.2.1. The plate is either heated or cooled from left by convection from a fluid of temperature T_f with $T_f > T_\infty$ corresponding to a heated surface and $T_f < T_\infty$ corresponding to a cooled surface, respectively. It is assumed that the fluid and the porous medium may have constant physical properties except for the density variation in the buoyancy term. The fluid flow is moderate and the permeability of the medium

is low, so that the Darcy-Forchheimer model is employed to simulate the resistance of the porous medium. It is further assumed that the concentration at the wall is C_w and the concentration of the ambient fluid is taken as C_∞.

It has been observed that the behavior of non-Newtonian fluids in the porous matrix is quite different from that of Newtonian fluids in porous media. Shenoy [92] has been reviewed the studies of non-Newtonian fluids flow in porous media, with attention concentrated on power-law fluids. The governing equations for the flow along with heat and mass transfer of a power-law fluid saturated non-Darcy porous medium (Shenoy [92], Murthy and Singh [69] and Chen [28]), are given by

$$\frac{\partial u}{\partial x} + \frac{\partial v}{\partial y} = 0 \tag{5.1}$$

$$u^n + \frac{b\sqrt{K_p}}{\nu} u^2 = -\frac{K_p}{\mu}\left(\frac{\partial p}{\partial x} + \rho g^* \cos\Omega\right) \tag{5.2}$$

$$v^n + \frac{b\sqrt{K_p}}{\nu} v^2 = -\frac{K_p}{\mu}\left(\frac{\partial p}{\partial y}\right) \tag{5.3}$$

$$u\frac{\partial T}{\partial x} + v\frac{\partial T}{\partial y} = \alpha\left(\frac{\partial^2 T}{\partial x^2} + \frac{\partial^2 T}{\partial y^2}\right) \tag{5.4}$$

$$u\frac{\partial C}{\partial x} + v\frac{\partial C}{\partial y} = D\left(\frac{\partial^2 C}{\partial x^2} + \frac{\partial^2 C}{\partial y^2}\right) \tag{5.5}$$

As the fundametal study, several researchers analyzed the solutions of Eqs.(5.1)-(5.5) by considering the following linear Boussinesq approximation, in which density is expressed as a linear function of the temperature and concentration. i.e.,

$$\rho = \rho_\infty \left[1 - \beta_0 \left(T - T_\infty\right) - \beta_2 \left(C - C_\infty\right)\right] \tag{5.6}$$

But, the presence of temperature variation, radiation, inertia or presence of different densities and heat released by viscous dissipation, induce significant changes in density variations, and hence the density, temperature and concentration relationship become nonlinear. Due to this, the results of fluid flow problem with linear Boussinesq approximation are inaccurate. To explain this situation, Partha [79] investigated the nonlinear convection in a non-Darcy porous medium using the following nonlinear relationship called temperature-concentration-dependent density relation (also known as

nonlinear Boussinesq approximation)

$$\rho = \rho_\infty \left[1 - \beta_0 \left(T - T_\infty\right) - \beta_1 (T - T_\infty)^2 - \beta_2 \left(C - C_\infty\right) - \beta_3 (C - C_\infty)^2\right] \tag{5.7}$$

along with the associated boundary conditions

$$\begin{aligned} v = 0, \;\; -k_f \frac{\partial T}{\partial y} = h_f (T_f - T), \;\; C = C_w \quad \text{at} \quad y = 0 \\ u = u_\infty, \;\; T = T_\infty, \;\; C = C_\infty \quad \text{as} \quad y \to \infty \end{aligned} \tag{5.8}$$

where u and v are the Darcy velocity components in x and y directions respectively, ρ is the density, p is the pressure, K_p is the permeability, k_f is the thermal conductivity, C is the concentration, D is the solutal diffusivity, ν is the kinematic viscosity, h_f is the convective heat transfer coefficient, α is the thermal diffusivity, b is the empirical constant, Ω is the angle of inclination, g^* is the acceleration due to gravity and T is the temperature. Here β_0 and β_1 are the first and second order thermal expansion coefficients respectively, whereas β_2 and β_3 are the first and second order solutal expansion coefficients respectively. Further, the suffix w and ∞ indicate the conditions at the wall and at the outer edge of the boundary layer respectively.

Experimental and numerical studies on the convective heat transfer in porous media show that thermal boundary layers exist adjacent to the heated or cooled bodies. When the thermal boundary layer is thin (i.e., $x \gg y \sim \delta_T$, δ_T is the boundary layer thickness), boundary layer approximations analogous to classical boundary layer theory can be applied (Nield and Bejan [75]). Near the boundary, the normal component of seepage velocity is small compared with its other component and the derivatives of any quantity in the normal direction are large compared with the derivatives of the quantity in the direction of the wall. Now, making use of the boundary layer assumptions, nonlinear Boussinesq approximations and eliminating pressure gradient from the momentum equation, the governing equations (5.2)-(5.5) reduce to

$$\frac{\partial u^n}{\partial y} + \frac{b\sqrt{K_p}}{\nu} \frac{\partial u^2}{\partial y} = \frac{K_p g^*}{\nu} \left\{ \left[\beta_0 + 2\beta_1 (T - T_\infty)\right] \frac{\partial T}{\partial y} + \left[\beta_2 + 2\beta_3 (C - C_\infty)\right] \frac{\partial C}{\partial y} \right\} \cos\Omega \tag{5.9}$$

$$u \frac{\partial T}{\partial x} + v \frac{\partial T}{\partial y} = \alpha \frac{\partial^2 T}{\partial y^2} \tag{5.10}$$

$$u \frac{\partial C}{\partial x} + v \frac{\partial C}{\partial y} = D \frac{\partial^2 C}{\partial y^2} \tag{5.11}$$

In this chapter also, two types (cases) of problems are considered: (a) free/natural convection and (b) mixed convection.

5.2.1 Case(a): Natural Convection

The flow is assumed to be a natural convective flow caused by only buoyancy forces and without any external agent. Hence the velocity of an external flow becomes zero ($i.e., u_\infty = 0$).

We introduce the following non-dimensional variables (Huang *et al.* [45], Kairi and Murthy [50]):

$$\begin{gathered} \xi = \frac{x}{L}, \;\; \eta = \frac{y}{L}\, Ra^{\frac{1}{2}}\, \xi^{\frac{-1}{2}}, \;\; \psi(\xi,\eta) = \alpha\, \xi^{\frac{1}{2}}\, Ra^{\frac{1}{2}}\, f(\xi,\eta) \\ T(\xi,\eta) = T_\infty + (T_f - T_\infty)\; \theta(\xi,\eta), \;\; C(\xi,\eta) = C_\infty + (C_w - C_\infty)\; \phi(\xi,\eta) \end{gathered} \tag{5.12}$$

where ξ is the stream-wise coordinate, $Ra = \dfrac{L}{\alpha}\left[\dfrac{\rho_\infty K_p g^* \beta_0 (T_f - T_\infty)}{\mu^*}\right]^{1/n}$ is the global Rayleigh number, L is the characteristics length, f is the dimensionless stream function, θ is the dimensionless temperature and ϕ is the dimensionless concentration.

Substituting the stream function (2.7) and the transformations (5.12) into Eqs.(5.9) - (5.11), we obtain the following momentum, energy and concentration equations

$$n\, \left(f'\right)^{n-1} f'' + 2\, Gr^*\, f' f'' = \left[(1 + 2\,\alpha_1\,\theta)\theta' + \mathcal{B}(1 + 2\,\alpha_2\,\phi)\phi'\right] \cos\Omega \tag{5.13}$$

$$\theta'' + \frac{1}{2} f\theta' = \xi\left(f' \frac{\partial\theta}{\partial\xi} - \frac{\partial f}{\partial\xi}\theta'\right) \tag{5.14}$$

$$\frac{1}{Le}\phi'' + \frac{1}{2} f\phi' = \xi\left(f' \frac{\partial\phi}{\partial\xi} - \frac{\partial f}{\partial\xi}\phi'\right) \tag{5.15}$$

Dimensionless form of boundary conditions (5.8) become

$$\begin{gathered} f(\xi,0) = -2\,\xi\left(\frac{\partial f}{\partial\xi}\right)_{\eta=0}, \;\; \theta'(\xi,0) = -Bi\, \xi^{\frac{1}{2}}\, [1 - \theta(\xi,0)]\,, \phi(\xi,0) = 1, \\ f'(\xi,\infty) = 0, \;\; \theta(\xi,\infty) = 0, \;\; \phi(\xi,\infty) = 0. \end{gathered} \tag{5.16}$$

where $Gr^* = b\left[\dfrac{{\rho_\infty}^2 {K_p}^2 [g^* \beta_0 (T_f - T_\infty)]^{2-n}}{{\mu^*}^2}\right]^{1/n}$ is the modified Grashof number, $Sc = \dfrac{\nu}{D}$ is the

Schmidt number, $\mathcal{B} = \dfrac{\beta_2(C_w - C_\infty)}{\beta_0(T_f - T_\infty)}$ is the Buoyancy ratio, $\alpha_1 = \dfrac{\beta_1(T_f - T_\infty)}{\beta_0}$ is the nonlinear density-temperature (NDT) parameter, $\alpha_2 = \dfrac{\beta_3(C_w - C_\infty)}{\beta_2}$ is the nonlinear density-concentration (NDC) parameter, $Le = \dfrac{\alpha}{D}$ is the diffusivity ratio, $\Pr = \dfrac{\nu}{\alpha}$ is the Prandtl number and $Bi = \dfrac{h_f\, L}{k_f\ Ra^{1/2}}$ is the Biot number.

The non-dimensional Nusselt number $Nu_x = \dfrac{-x}{(T_f - T_\infty)}\left[\dfrac{\partial T}{\partial y}\right]_{y=0}$ and the Sherwood number $Sh_x = \dfrac{-x}{(C_w - C_\infty)}\left[\dfrac{\partial C}{\partial y}\right]_{y=0}$ are given by

$$Nu_x\, Ra^{\frac{-1}{2}} = -\xi^{\frac{1}{2}}\,\theta'(\xi,\,0),\ \ Sh_x\, Ra^{\frac{-1}{2}} = -\xi^{\frac{1}{2}}\,\phi'(\xi,\,0). \tag{5.17}$$

Results and Discussion

Similar to the previous chapters, the highly coupled nonlinear partial differential equations (5.13)-(5.15) together with the boundary conditions (5.16) are converted into a set of six coupled ordinary differential equations using local similarity and non-similarity approaches. After that, a novel successive linearization method is applied to solve the set of reduced ordinary differential equations for those six unknowns as explained in the chapter-2 for case(a) problem. In order to assess the validity and accuracy of the present numerical results, the results have been compared with those of previous works (Singh and Tiwari [93], and Cheng [30]) in the absence of nonlinear convection parameters. It is found that they are in good agreement, as shown in Tables (5.1) and (5.2). Therefore, the developed code can be used with great confidence to study the problem considered in this case.

The numerical computations are carried out by following the fixed values of parameters: $Le = 1$, $Gr^* = 0.5$, $\mathcal{B} = 0.5$ and $\xi = 0.5$. These values are continued same throughout this study, unless otherwise specified. The physical significance of the pertinent parameters such as ξ, α_1, α_2, Ω and Bi is determined through Figs.5.1(a) to 5.5(c) for different flow profiles. Also, the physical quantities of the present interest such as Nusselt and Sherwood numbers are plotted in Figs.5.6(a) to 5.7(b) for different values of n.

Variations in the non-dimensional velocity (f'), temperature (θ) and concentration (ϕ) across

Table 5.1: *Comparison of* $-f'(0,\,0)$ *and* $-\theta'(0,\,0)$ *for various values of* Gr^* *when* $\mathcal{B} = 0$, $\alpha_1 = 0$, $\alpha_2 = 0$, $n = 1$, $Bi \to \infty$ *and* $\Omega = 0$.

	$-f'(0,\,0)$		$-\theta'(0,\,0)$	
Gr^*	Singh & Tewari [93]	Present	Singh & Tewari [93]	Present
0.4	0.766	0.7656	0.400	0.4001
1	0.618	0.6180	0.366	0.3656
4	0.390	0.3904	0.298	0.2978
6	0.333	0.3333	0.277	0.2767
10	0.270	0.2701	0.251	0.2506

Table 5.2: *Comparison of* $-\theta'(0,\,0)$ *and* $-\phi'(0,\,0)$ *for different values of* $\mathcal{B}$ *and* Le *when* $Gr^* = 0$, $\alpha_1 = 0$, $\alpha_2 = 0$, $n = 1$, $Bi \to \infty$ *and* $\Omega = 0$.

		$-\theta'(0,\,0)$		$-\phi'(0,\,0)$	
$\mathcal{B}$	Le	Cheng [30]	Present	Cheng [30]	Present
4	1	0.9923	0.9923	0.9923	0.9923
4	4	0.7976	0.7976	2.0550	2.0549
4	10	0.6811	0.6810	3.2899	3.2898
4	100	0.5209	0.5208	10.521	10.521
1	4	0.5585	0.5585	1.3575	1.3575
2	4	0.6494	0.6495	1.6243	1.6244
3	4	0.7278	0.7278	1.8525	1.8524

the boundary layers are plotted in Figs.5.1(a) to 5.1(c) for different values of ξ along the free stream coordinate η. In a non-similar problem, the flow quantities change along the stream-wise direction (in the present problem along x-axis). Therefore, it is needed to have a x-dependent non-dimensional parameter (ξ) which acts as a non-dimensional x-axis. This parameter determines the stream-wise position where the flow quantities are calculated. When $\xi \to 0$, the flow governing equations are independent of stream-wise location and hence, it shows that the existence of similarity representation for the present problem. With an increase in the stream-wise coordinate ξ, the velocity component increases, whereas the temperature and concentrations decrease. Further, the wall temperature always tends to 1 as $\xi \to \infty$. Hence, the changes in these profiles clearly prove that the present problem is non-similar. It means that the solutions are not unique for different values of ξ.

Figures 5.2(a) to 5.2(c) depict the variations of momentum, thermal and solutal boundary layer

profiles in the presence and absence of α_1 for various values of n. As expected from Fig.5.2(a), an increase in the power-law index n (from $n < 1$ to $n > 1$) leads to enhance the velocity, due to the effect of shear-thinning in power-law fluids. In addition, the non-Newtonian fluid with a higher power-law index has a lesser thermal and concentration boundary-layer thickness, as shown in Figs.5.2(b) and 5.2(c). Fig.5.2(a) reveals that the velocity increases with the increase of α_1, whereas it shows reverse trend away from the plate. Physically, $\alpha_1 > 0$ implies that $T_f > T_\infty$; hence, there will be a supply of heat to the flow region from the wall and it accelerates the flow at the wall. An increase in α_1 leads to reduce the temperature and concentration boundary layer profiles in all three types of power-law fluids and the same results are displayed in Figs.5.2(b) and 5.2(c). Moreover the strength of α_1 gradually decreases when power-law index is turned from $n < 1$ to $n > 1$.

The effects of nonlinear density-concentration parameter on the dimensionless velocity, temperature and concentration profiles, are shown in Figs.5.3(a) to 5.3(c). The influence of nonlinear density-concentration parameter α_2 (here, α_1 is fixed) on the velocity reported similar behavior to that of α_1. Thus, the hydrodynamic boundary layer thickness increases near to the surface for different values of α_2. The effects of nonlinear density-concentration parameter on the temperature and concentration of the power-law fluid flow, are plotted in Figs.5.3(b) and 5.3(c) respectively. It is noticed from these figures that the temperature and concentration profiles decrease with the increase of α_2. However, the boundary layer thicknesses of the temperature and concentration are more in the absence of α_1 and α_2 in comparison with its presence. This is due to the enhancement of thermal and solutal gradients by nonlinear terms in the momentum equation.

The significance of Biot number (Bi) on the boundary layer profiles is portrayed in Figs.5.4(a) to 5.4(c) for different values of n. Figure 5.4(a) displays the variation of the velocity profile with or without Biot number. It is interesting to note that without Biot number (i.e. $Bi = 0$) the velocity is low. As the Biot number increases, the velocity in the neighborhood of the inclined plate increases significantly. Figs.5.4(b) and 5.4(c) represent the effects of Biot number on the temperature and concentration profiles of the flow. It is evident that, as Biot number enhances from $Bi < 1$ (thermally thin case) to $Bi > 1$ (thermally thick case), the temperature of the flow increases whereas the concentration decreases. The convective boundary condition is the generalization of isothermal boundary condition and it effectively furnishes a mechanism for comparing the conduction resistance within a solid body to the convection resistance external to that body (offered by the surrounding

fluid) for heat transfer. The isothermal boundary condition is a limiting case of the convective boundary condition when h_f tends to infinity and it is proven by Fig.5.4(b). Usually, for high Biot number, the internal thermal resistance of the plate is high and the boundary layer thermal resistance is low. Further, when $Bi = 0$ (i.e., without Biot number) the left side of the plate with hot fluid is totally insulated, the internal thermal resistance of the plate is extremely high and no convective heat transfer to the cold fluid on the right side of the plate takes place. In this case, the fluid temperature is maximum at the surface of plate and decreases exponentially to zero far away from the plate, which is clearly observed from the Fig.5.4(b). However, the temperature distribution is less in dilatant fluid and Newtonian fluid as compared to the pseudo-plastic fluid. A similar observation was made by Khan and Gorla [55].

The influence of inclination angle (Ω) ranging from 0^0 to 90^0, on the boundary layer profiles are displayed in Figs.5.5(a) to 5.5(c). The physical reason for the depletion in velocity profile with respect to inclination angle is that the thermal and concentration buoyancy $\rho g^* \cos\Omega$ (as considered in Eq.(5.9)) falls down when the angle Ω changes from 0^0 to 90^0, as displayed in Fig.5.5(a). It is observed from Figs.5.5(b) and 5.5(c) that the dimensionless temperature and concentrations enhance with an increase in the inclination angle. Moreover, one can observe that the maximum buoyancy force for the same temperature and concentration differences occur for $\Omega = 0^0$ (vertical plate) and there is no buoyancy force for the case $\Omega = 90^0$ (horizontal plate). In this case, the results of thermal and solutal distributions are identically equal to the works of Chamkha *et al.* [23] and Chen [27].

Here, the fluid flow profiles (namely, velocity, temperature and concentration) are drawn for the three distinct values of the power-law index. From the above said discussions, it is observed that the rise in power-law index increases the velocity of a power-law fluid and also increase the horizontal boundary layer thickness. That is, the thicknesses is much smaller for shear thinning (pseudo plastic) fluids than that of shear thickening (dilatant) fluids. In the case of a shear thinning fluid ($n < 1$), the shear rates near the walls are higher than those for a Newtonian fluid. Further, an increase in the powerlaw index decreases both temperature and concentrations of the fluid and it lead to thinning of both thermal and solutal boundary layer thickness.

The heat and mass transfer rates are analyzed against the stream-wise coordinate ξ for α_1 and α_2 through Figs.5.6(a) and 5.6(b) together with the power-law index n. Both the Nusselt and Sherwood numbers increase with respect to the power-law index in the presence and/or absence of

nonlinear convection parameters. Along the stream-wise coordinate ξ, both heat and mass transfer rates are increased and the influence of α_2 is prominent as compared to α_1.

Effects of Biot number and inclination angle on the physical quantities of the fluid flow are displayed in Figs.5.7(a) to 5.7(b) for different values of n. It is worth to mention that, as the Biot number increases from $Bi < 1$ (thermally thin case) to $Bi > 1$ (thermally thick case), evidently, both heat and mass rates increase as shown in Figs.5.7(a) and 5.7(b). Further, the dimensionless heat transfer rate and mass transfer rate decrease with an increase in inclination angle Ω. Therefore, an increase in the buoyancy leads to decrease the temperature and concentration which will enhance the heat and mass transfer rates. Thus, the heat and mass transfer rates are more for the case of vertical surface ($\Omega = 0^0$) as compared to the horizontal surface ($\Omega = 90^0$).

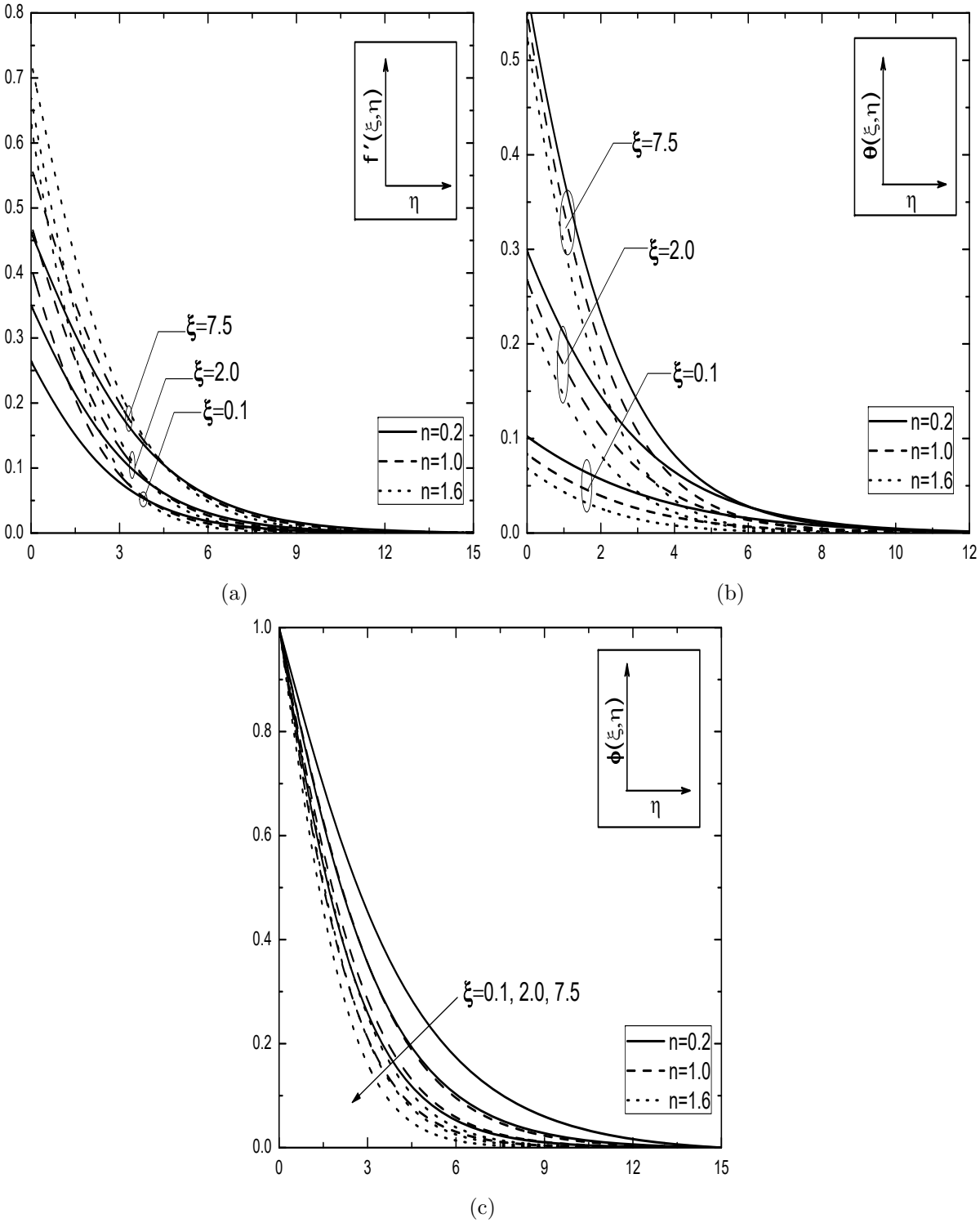

Figure 5.1: *Effect of ξ for different values of n on the (a) velocity, (b) temperature and (c) concentration with the fixed values of $\alpha_1 = 1$, $\alpha_2 = 1$, $Bi = 0.2$ and $\Omega = 30^0$.*

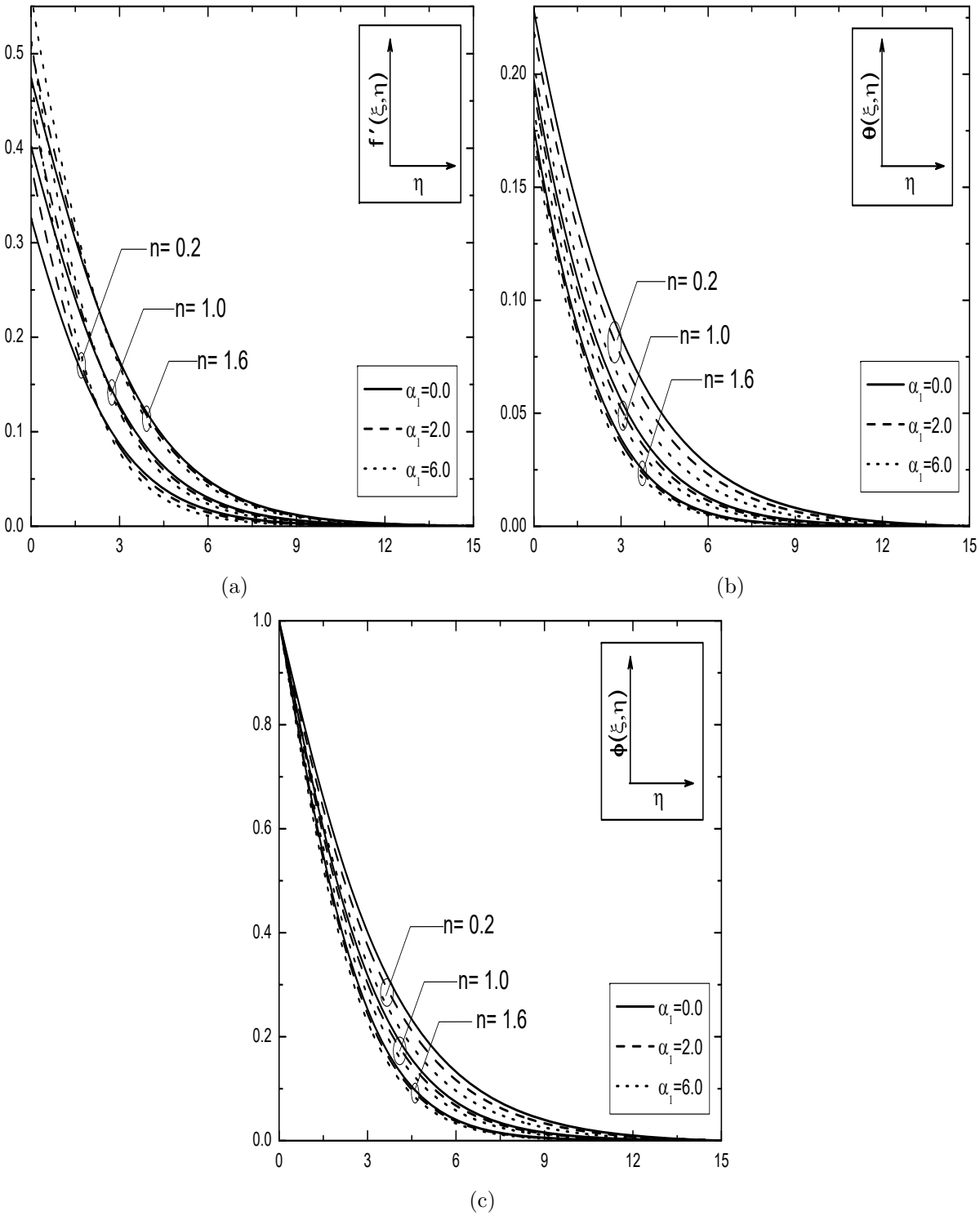

Figure 5.2: *Effect of α_1 for different of values n on the (a) velocity, (b) temperature and (c) concentration with the fixed values of $Bi = 0.5$, $\alpha_2 = 1$, $\Omega = 30^0$ and $\xi = 0.5$.*

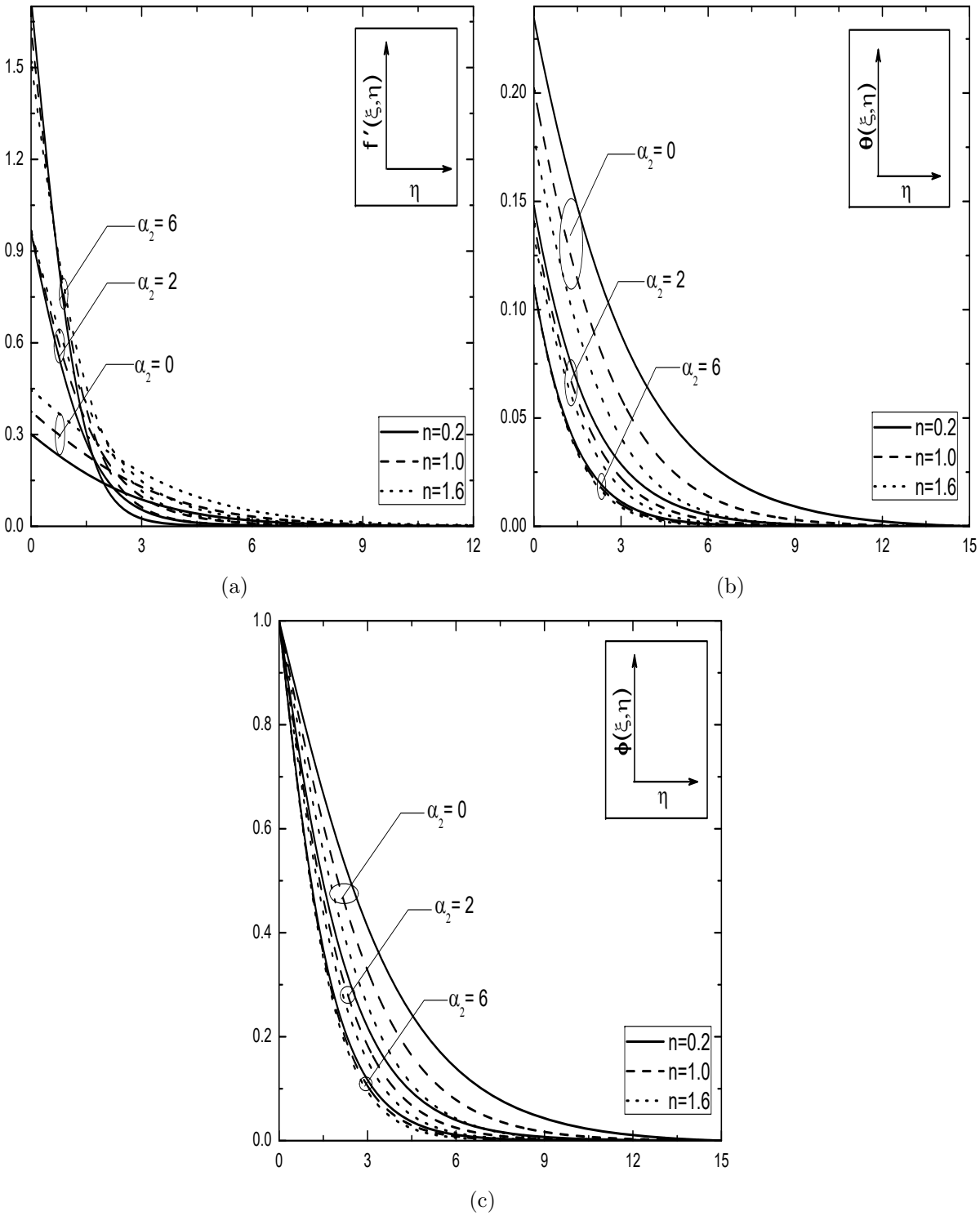

Figure 5.3: *Effect of α_2 for different values of n on the (a) velocity, (b) temperature and (c) concentration with the fixed values of $Bi = 0.5$, $\alpha_1 = 1$, $\Omega = 30^0$ and $\xi = 0.5$.*

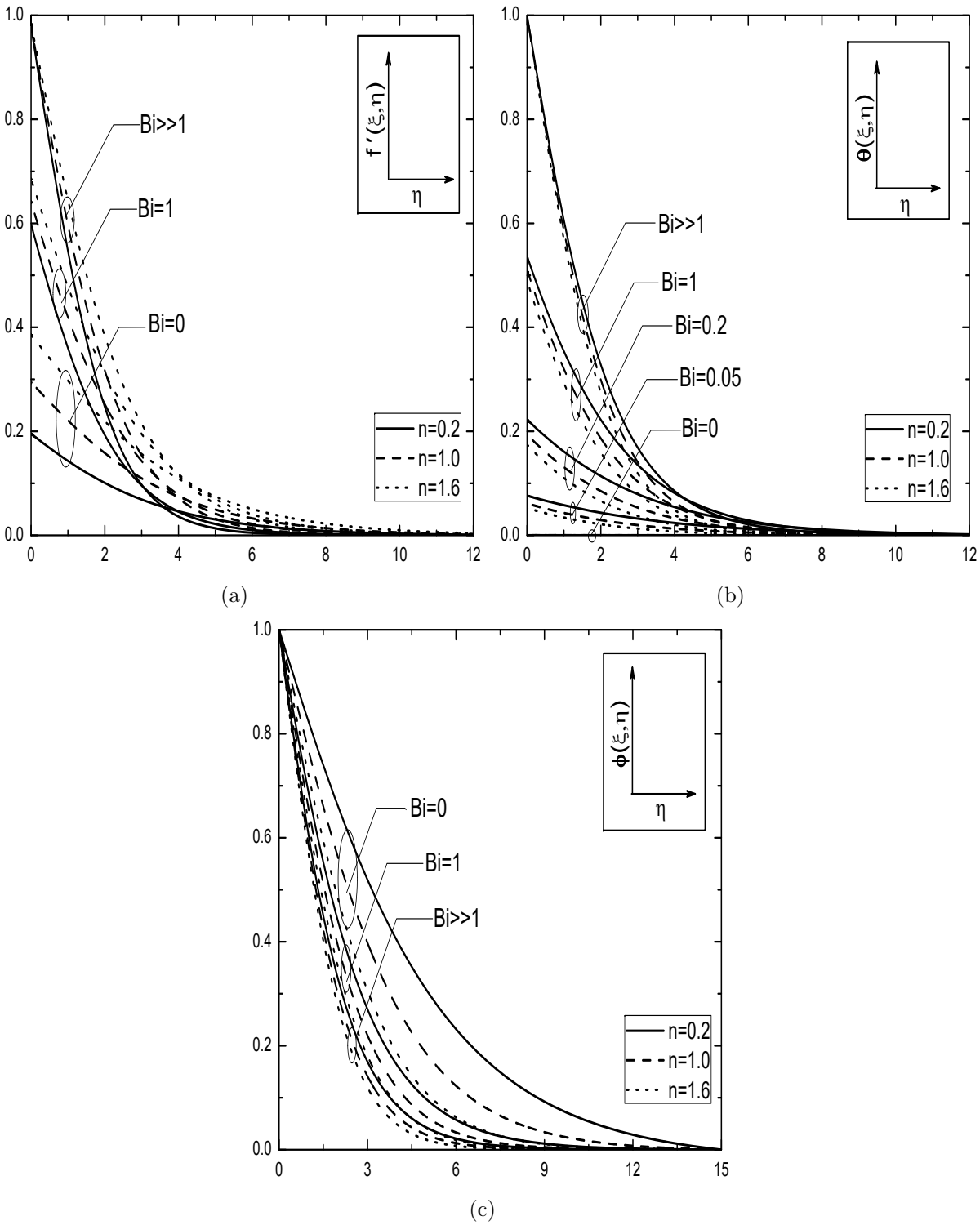

Figure 5.4: *Effect of Bi for different values of n on the (a) velocity, (b) temperature and (c) concentration with the fixed values of* $\alpha_1 = 1$, $\alpha_2 = 1$, $\Omega = 30^0$ *and* $\xi = 0.5$.

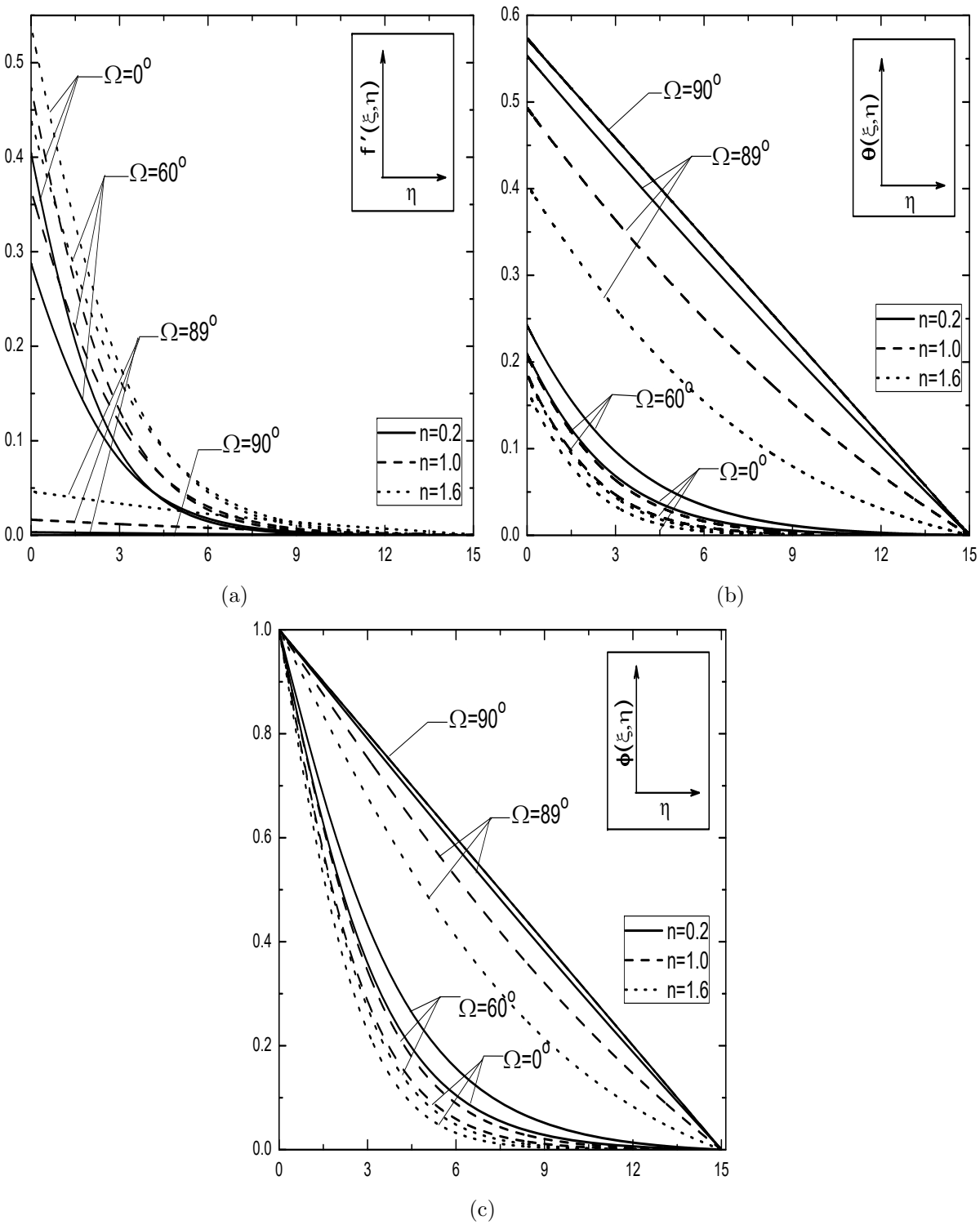

Figure 5.5: *Effect of* Ω *for different values of* n *on the (a) velocity, (b) temperature and (c) concentration with the fixed values of* $\alpha_1 = 1$, $\alpha_2 = 1$, $Bi = 0.1$ *and* $\xi = 0.5$.

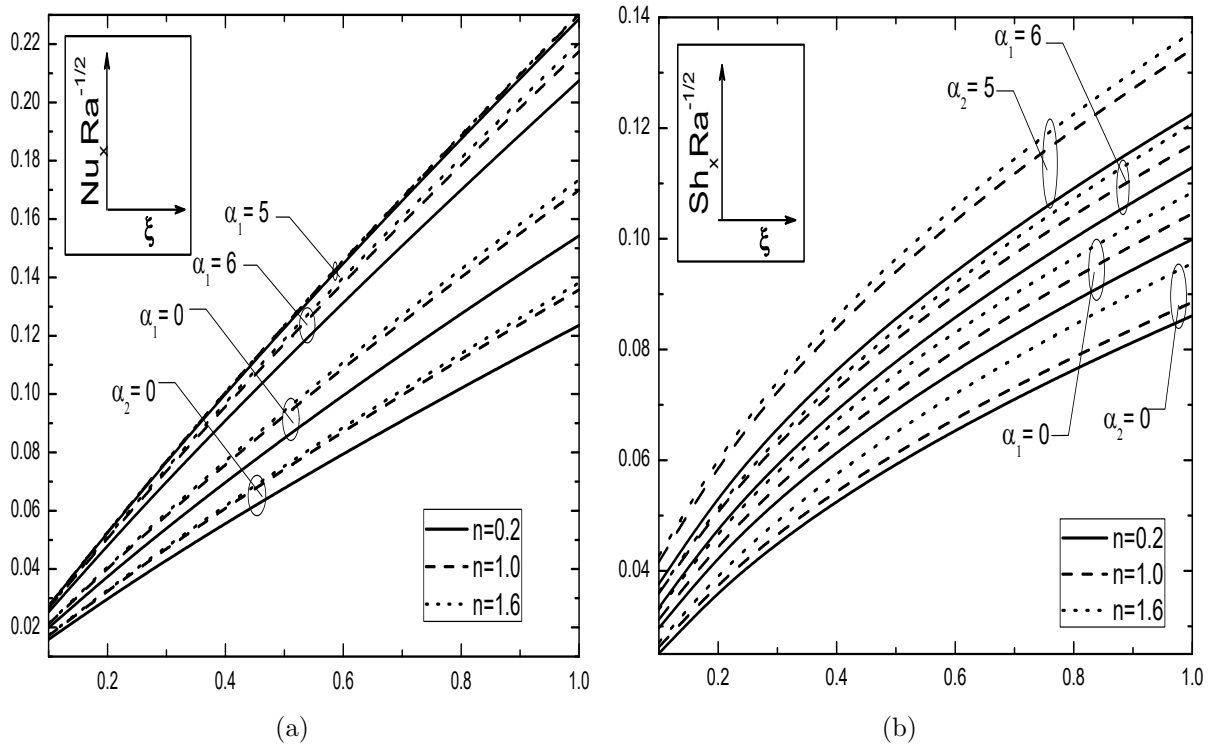

Figure 5.6: *Effects of α_1 and α_2 for different values of n on the (a) Nusselt number and (b) Sherwood number against ξ with the fixed values of $Bi = 0.5$ and $\Omega = 30^0$.*

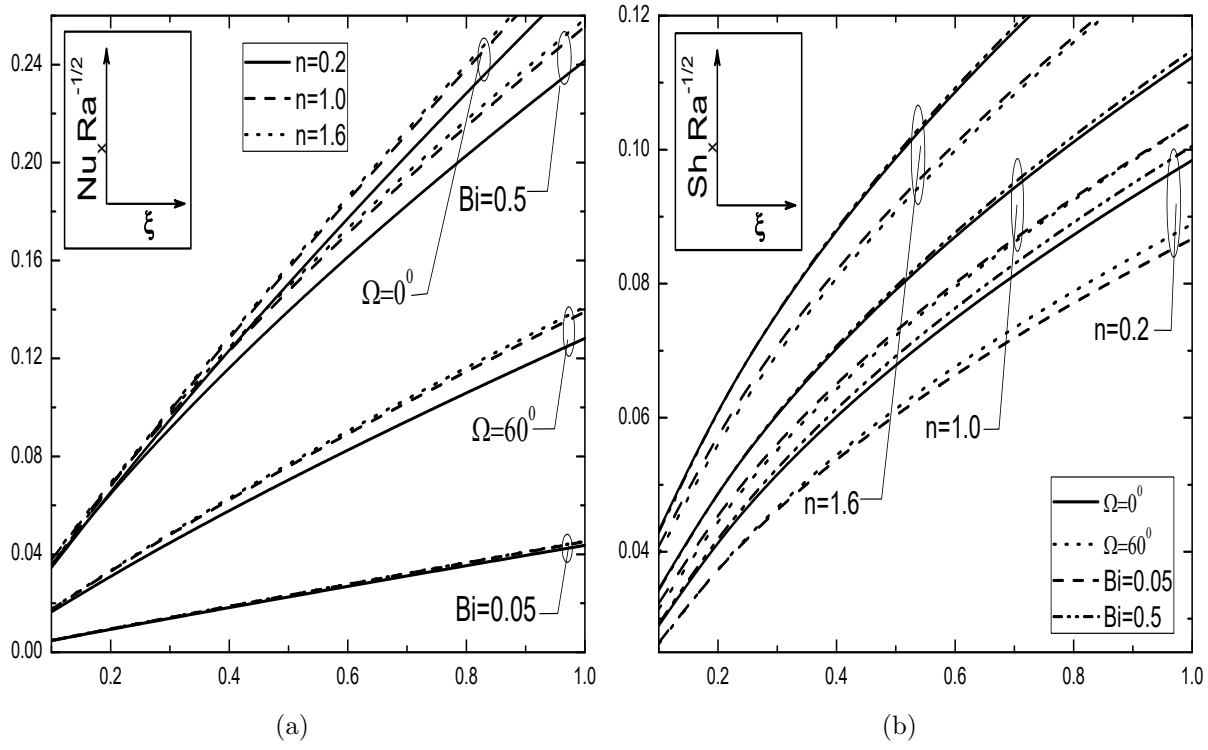

Figure 5.7: *Effects of Bi and Ω for different values of n on the (a) Nusselt number and (b) Sherwood number against ξ with the fixed values of $\alpha_1 = 1$ and $\alpha_2 = 1$.*

5.2.2 Case(b): Mixed Convection

Consider the flow to be a mixed convective flow which arises from an external force with the velocity u_∞ and buoyancy forces. We introduce the dimensionless variables as follows

$$\begin{gathered}\xi = \frac{x}{L},\ \ \eta = \frac{y}{L}\, Pe^{\frac{1}{2}}\, \xi^{\frac{-1}{2}},\ \ \psi(\xi,\eta) = \alpha\, \xi^{\frac{1}{2}}\, Pe^{\frac{1}{2}}\, f(\xi,\eta) \\ T(\xi,\eta) = T_\infty + (T_f - T_\infty)\ \theta(\xi,\eta),\ \ \ C(\xi,\eta) = C_\infty + (C_w - C_\infty)\ \phi(\xi,\eta)\end{gathered} \tag{5.18}$$

where $Pe = \dfrac{u_\infty\, L}{\alpha}$ is the global Peclet's number.

Substituting the stream function (2.7) and the transformations (5.18) into Eqs.(5.1) - (5.11), the resultant dimensionless momentum, energy and concentration equations can be presented as

$$n\ \left(f'\right)^{n-1} f'' + 2\, Fs\, f' f'' = (Ri)^n \left[(1 + 2\,\alpha_1\,\theta)\theta' + \mathcal{B}(1 + 2\,\alpha_2\,\phi)\phi'\right] \cos\Omega \tag{5.19}$$

$$\theta'' + \frac{1}{2} f\theta' = \xi \left(f' \frac{\partial \theta}{\partial \xi} - \frac{\partial f}{\partial \xi}\theta' \right) \tag{5.20}$$

$$\frac{1}{Le}\phi'' + \frac{1}{2} f\phi' = \xi \left(f' \frac{\partial \phi}{\partial \xi} - \frac{\partial f}{\partial \xi}\phi' \right) \tag{5.21}$$

The associate boundary conditions (5.8) in terms of f, θ, and ϕ can be written as

$$\begin{gathered}f(\xi,0) = -2\,\xi \left(\frac{\partial f}{\partial \xi} \right)_{\eta=0},\ \theta'(\xi,0) = -Bi\, \xi^{\frac{1}{2}} \left[1 - \theta(\xi,0)\right], \phi(\xi,0) = 1, \\ f'(\xi,\infty) = 1,\ \theta(\xi,\infty) = 0,\ \phi(\xi,\infty) = 0.\end{gathered} \tag{5.22}$$

In usual definitions, $Pe_d = \dfrac{u_\infty d}{\alpha}$ is the pore diameter-dependent Peclet number, $Ri = \dfrac{Ra}{Pe}$ is the mixed convection parameter, $Fs = \left(\dfrac{b\sqrt{K_p}}{\nu} \right) \left(\dfrac{\alpha\, Pe_d}{d} \right)^{2-n}$ is the non-Darcy parameter (Forchheimer number) and $Bi = \dfrac{h_f L}{k_f\ Pe^{1/2}}$ is the Biot number.

The non-dimensional Nusselt number $Nu_x = \dfrac{-x}{(T_f - T_\infty)} \left[\dfrac{\partial T}{\partial y} \right]_{y=0}$ and the Sherwood number $Sh_x = \dfrac{-x}{(C_w - C_\infty)} \left[\dfrac{\partial C}{\partial y} \right]_{y=0}$ are given by

$$Nu_x\, Pe^{\frac{-1}{2}} = -\xi^{\frac{1}{2}} \theta'(\xi,\, 0),\ \ \ Sh_x\, Pe^{\frac{-1}{2}} = -\xi^{\frac{1}{2}} \phi'(\xi,\, 0). \tag{5.23}$$

Results and Discussion

As explained in the previous chapter (i,e. chapter 2), here also, the the successive linearization method together with the local similarity and non-similarity procedure is employed to solve the non-homogeneous and nonlinear coupled partial differential equations (5.19)-(5.21) along with the boundary conditions (5.22). The validation of the present results is cross verified with previously established results (Chaoyang *et al.* [26], Murthy [67]) in the absence of nonlinear convection parameters, as shown in Tab.(5.3) and Tab.(5.4). From these two tables, we have noticed that the error between present and previously published numerical results is negligible, so that the numerical practice which we made by SLM is an appropriate scheme for the present analysis.

The numerical computations are carried out by following the fixed values: $\mathcal{B} = 0.5$, $Fs = 1.2$, $\mathrm{Pr} = 1$, $Le = 1$, $Ri = 2$ and $\xi = 0.5$. These values are unaltered throughout this study, unless otherwise specified. The impacts of the pertinent parameters such as nonlinear convection parameters (α_1, α_2), angle of inclination (Ω) and Biot number (Bi) are determined through Figs.5.8(a)-5.12(c) for the fluid flow. Also, the physical quantities of the flow, namely local Nusselt and Sherwood numbers (i.e, $Nu_x\, Pe^{\frac{-1}{2}}$ and $Sh_x\, Pe^{\frac{-1}{2}}$) are depicted in Figs.5.13(a)-5.14(b).

The occurrence of non-similar solutions in the present analysis is shown in the Figs.5.8(a)-5.8(c). On boosting the value of stream-wise coordinate $\xi(0.1, 0.5, 1.0)$, the momentum boundary layer thickness increases, whereas the thermal and solutal boundary layer thickness decrease. Further, the wall temperature always tends to 1 as $\xi \to \infty$ and also, the changes in these profiles clearly prove that the present results are non-similar. It means that the solutions are not unique for different values of ξ.

The figures displayed in Figs.5.9(a)-5.9(c) exhibit the dependence of NDT parameter $\alpha_1(0, 2, 6)$ and power-law index $n\,(0.5, 1.0, 1.5)$ on the boundary layer profiles. It reveals that the variation of the power-law index is considerable and it enhances the momentum boundary layer thickness, whereas it diminishes the thermal and solutal boundary layer thickness. With respect to the variation of α_1, the dimensionless velocity increases more at the surface of the inclined plate and it reaches unity for η_{max} value. The same result is shown in Fig.5.9(a). From Fig.5.9(b)-5.9(c), one can notice that the rise of α_1 leads to reduce the temperature and solutal boundary layer thicknesses. Also, the temperature and concentration gradients are more in the absence of α_1 as compared to its presence. Responses of boundary layer profiles for NDC parameter ($\alpha_2 = 0, 3, 7$)

Table 5.3: *Comparison of* $-\theta'(0,\,0)$ *for various values of Ri when* $Fs = 0$, $\mathcal{B} = 0$, $\xi \to 0$, $\alpha_1 = 0$, $\alpha_2 = 0$, $Bi \to \infty$ *and* $\Omega = 0$.

	$n = 0.5$		$n = 1.0$		$n = 1.5$	
Ri	Chaoyang *et al.* [26]	Present	Chaoyang *et al.* [26]	Present	Chaoyang *et al.* [26]	Present
0	0.5641	0.5642	0.5641	0.5642	0.5641	0.5642
0.5	0.8209	0.8217	0.6473	0.6474	0.6034	0.6034
1.0	0.9303	0.9296	0.7205	0.7206	0.6634	0.6634
4.0	1.3010	1.3007	1.0250	1.0558	1.0180	1.0176
8.0	1.6100	1.6097	1.3540	1.3801	1.3800	1.4357
15.0	2.0010	2.0005	1.8120	1.8123	1.8620	1.8606

Table 5.4: *Comparison of* $f'(0,\,0)$, $-\theta'(0,\,0)$ *and* $-\phi'(0,\,0)$ *for different values of* $\mathcal{B}$, *Le*, *Ri when* $Fs = 1.0$, $\xi \to 0$, $\alpha_1 = 0$, $\alpha_2 = 0$, $n = 1$, $Bi \to \infty$ *and* $\Omega = 0$.

				$Le = 1$		$Le = 10$			
		$f'(0,\,0)$		$-\theta'(0,\,0)$ & $-\phi'(0,\,0)$		$-\theta'(0,\,0)$		$-\phi'(0,\,0)$	
	Ri	Murthy [67]	Present	Murthy [67]	Present	Murthy [67]	Present	Murthy [67]	Present
$\mathcal{B} = -0.5$	0	1.0	1.0	0.5645	0.5642	0.5642	0.5642	1.7841	1.7841
	1	1.1583	1.1583	0.5922	0.5922	0.6054	0.6054	1.9329	1.9329
	5	1.6794	1.6794	0.6793	0.6793	0.7244	0.7244	2.3534	2.3534
	10	2.1926	2.1926	0.7580	0.7580	0.8247	0.8247	2.7009	2.7009
	20	3.0	3.0	0.8706	0.8706	0.9617	0.9617	3.1686	3.1686
$\mathcal{B} = 1.0$	0	1.0	1.0	0.5642	0.5642	0.5642	0.5642	1.7841	1.7841
	1	1.5616	1.5616	0.6603	0.6603	0.6377	0.6377	2.1381	2.1381
	5	3.0	3.0	0.8706	0.8706	0.8083	0.8083	2.8864	2.8865
	10	4.217	4.2167	1.0203	1.0203	0.9358	0.9358	3.4061	3.4061
	20	6.0	6.0	1.2097	1.2097	1.1012	1.1012	4.0548	4.0548

are portrayed for the three different values of the power-law index in Figs.5.10(a)-5.10(c). The results of this set of figures repeat the same kind of behavior like α_1 in all three profiles, but the influence of α_2 is more on these three boundary layer profiles and also in all three kinds of fluids (pseudo-plastic, Newtonian and dilatant fluid) compared to the influence of α_1.

Figures 5.11(a)-5.11(c) show the impacts of the Biot number ($Bi = 0.05, 1.0, 20$) on the non-dimensional velocity, temperature, and concentration for the pseudo-plastic, Newtonian, and dilatant fluids. A rise in Biot number changes the magnitude of the velocity in the increasing direction, as depicted in Fig.5.11(a). The utility of convective boundary condition is possible in two ways; first, as an isothermal condition and another one as a non-isothermal condition. It is because of the isothermal condition is a limiting result of the convective boundary condition when h_f tends to infinity (stated by Aziz [13]) and this is proven again by Fig.5.11(b). It means that there is a drastic change in temperature distribution at the surface of the plate when the Biot number approaches to a large value. The effect of Biot number on the concentration profile is displayed in Fig.5.11(c) and it reveals that the concentration profile decreases when the Biot number increases from zero to a large value. For a fixed value of Biot number, the enhancement of the power-law index leads to increase the velocity distribution, whereas it decreases the temperature and concentration distributions within the boundary layers. As Biot number enhances from $Bi < 1$ to $Bi > 1$, the temperature increases whereas the concentration decreases as shown in Figs.5.11(b) and 5.11(c) respectively.

An inclined plate is displaced from vertical to horizontal position with reference to the angle of inclination ($\Omega = 0^0, 40^0, 80^0$) and the resulting variations in boundary layer profiles are portrayed in Figs.5.12(a)-5.12(c). The physical reason for the depletion of velocity profile with respect to the angle of inclination is that the thermal and concentration buoyancy fall down when the angle of inclination changed from $\Omega = 0^0$ to 90^0 as shown in Fig.5.12(a). Moreover, from Fig.5.12(a), one can observe that the maximum buoyancy force occurs for the temperature and concentration differences along the vertical plate only. It is observed from Figs.5.12(b) and 5.12(c) that the concentration and temperature enhance with the rising values of inclination angle.

The variations in the physical quantities (specifically, $Nu_x\, Pe^{\frac{-1}{2}}$ and $Sh_x\, Pe^{\frac{-1}{2}}$) of the present analysis are portrayed through the graphs Figs.5.13(a)-5.14(b) for the fixed values: $\alpha_1 = 0, 6$, $\alpha_2 = 0, 5$, $Bi = 0.05, 1.0$, and $\Omega = 0^0, 60^0$. The magnitude of the heat transfer rate ($Nu_x\, Pe^{\frac{-1}{2}}$) slightly increases when α_1 is increased from zero to a nonzero value and the same kind of changes

occurred for α_2, but the influence of α_2 is more when compared to α_1 effect as plotted in Fig.5.13(a) for all n. On the other side, for a fixed value of these two parameters, the heat transfer rate is more for dilatant fluid compared to Newtonian and pseudo-plastic fluids. Fig.5.13(b) drawn for Sherwood number ($Sh_x\, Pe^{\frac{-1}{2}}$) also shows same results as $Nu_x\, Pe^{\frac{-1}{2}}$. Figs.5.14(a)-5.14(b) demonstrate that the $Nu_x\, Pe^{\frac{-1}{2}}$ and $Sh_x\, Pe^{\frac{-1}{2}}$ show the opposite trend when the plate is displaced from vertical to horizontal position with reference to the angle Ω. But, in the case of Bi, variations in these two quantities are same and increased. However, for a fixed value of either Bi or Ω, both $Nu_x\, Pe^{\frac{-1}{2}}$ and $Sh_x\, Pe^{\frac{-1}{2}}$ fall down when the power-law index moves from $n < 1$ to $n > 1$.

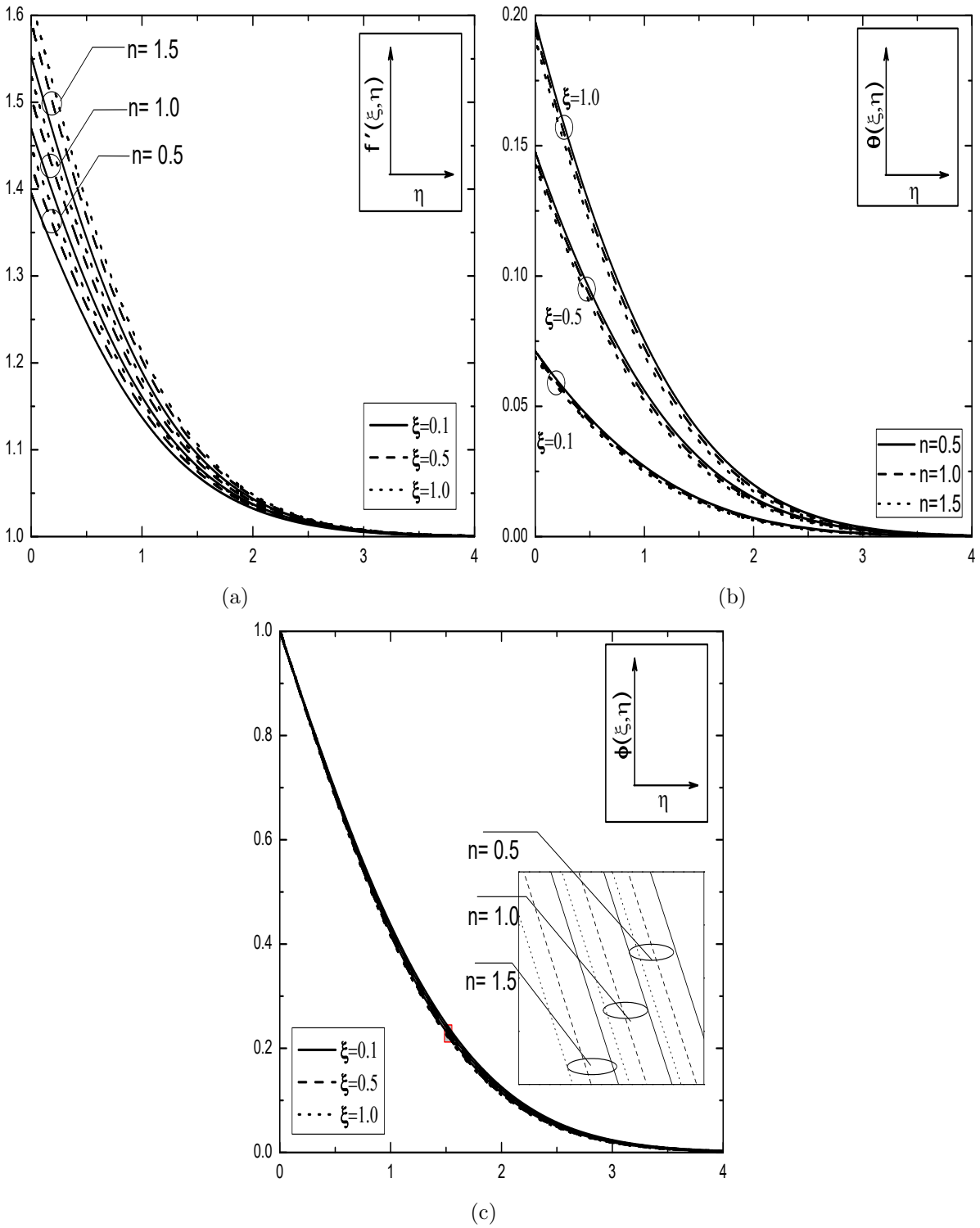

Figure 5.8: *Effect of ξ for different values of n on the (a) velocity, (b) temperature and (c) concentration with the fixed values of $\alpha_1 = 1$, $\alpha_2 = 1$, $Bi = 0.2$ and $\Omega = 30^0$.*

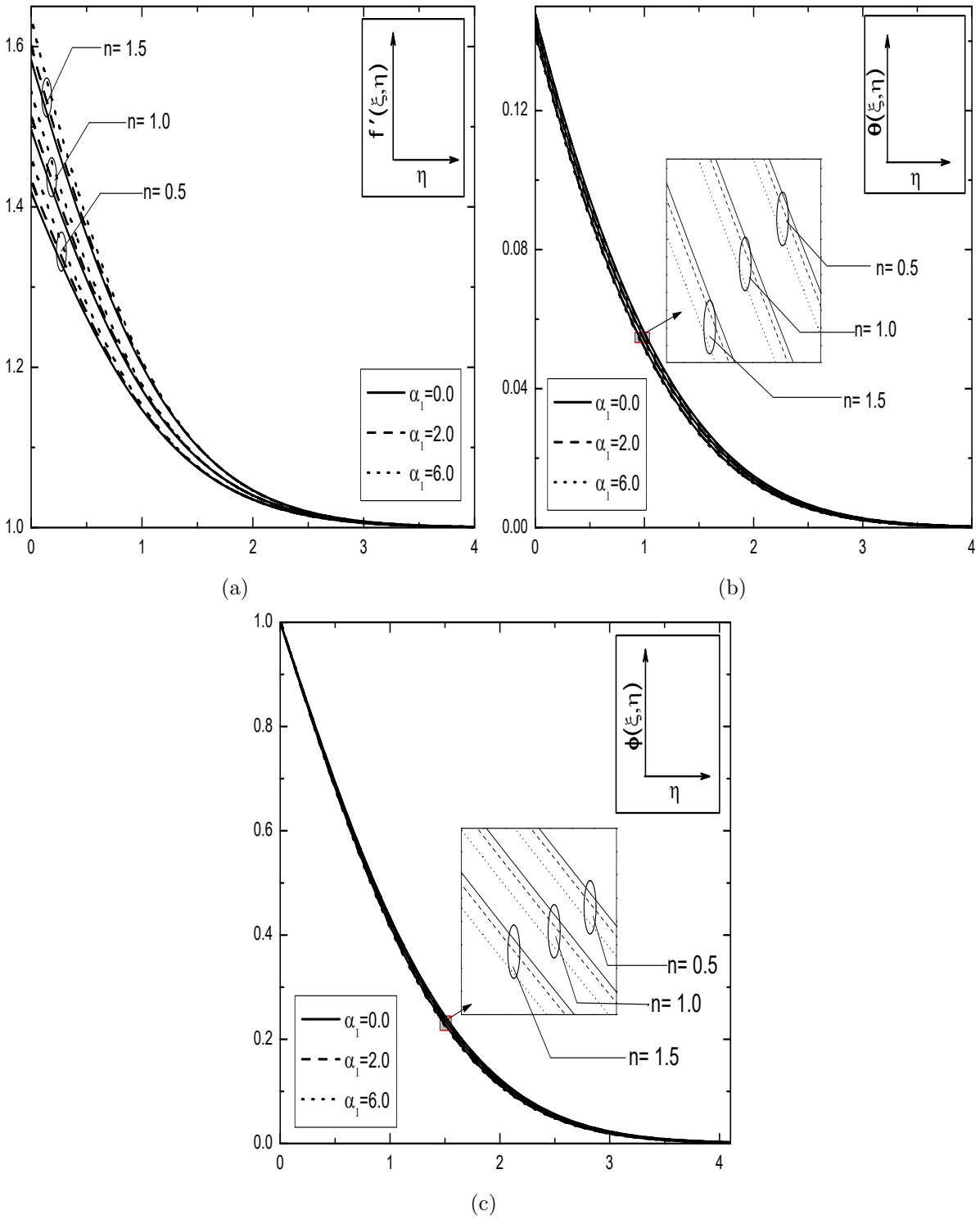

Figure 5.9: *Effect of α_1 for different values of n on the (a) velocity, (b) temperature and (c) concentration with the fixed values of $Bi = 0.2$, $\alpha_2 = 1$, $\Omega = 30^0$ and $\xi = 0.5$.*

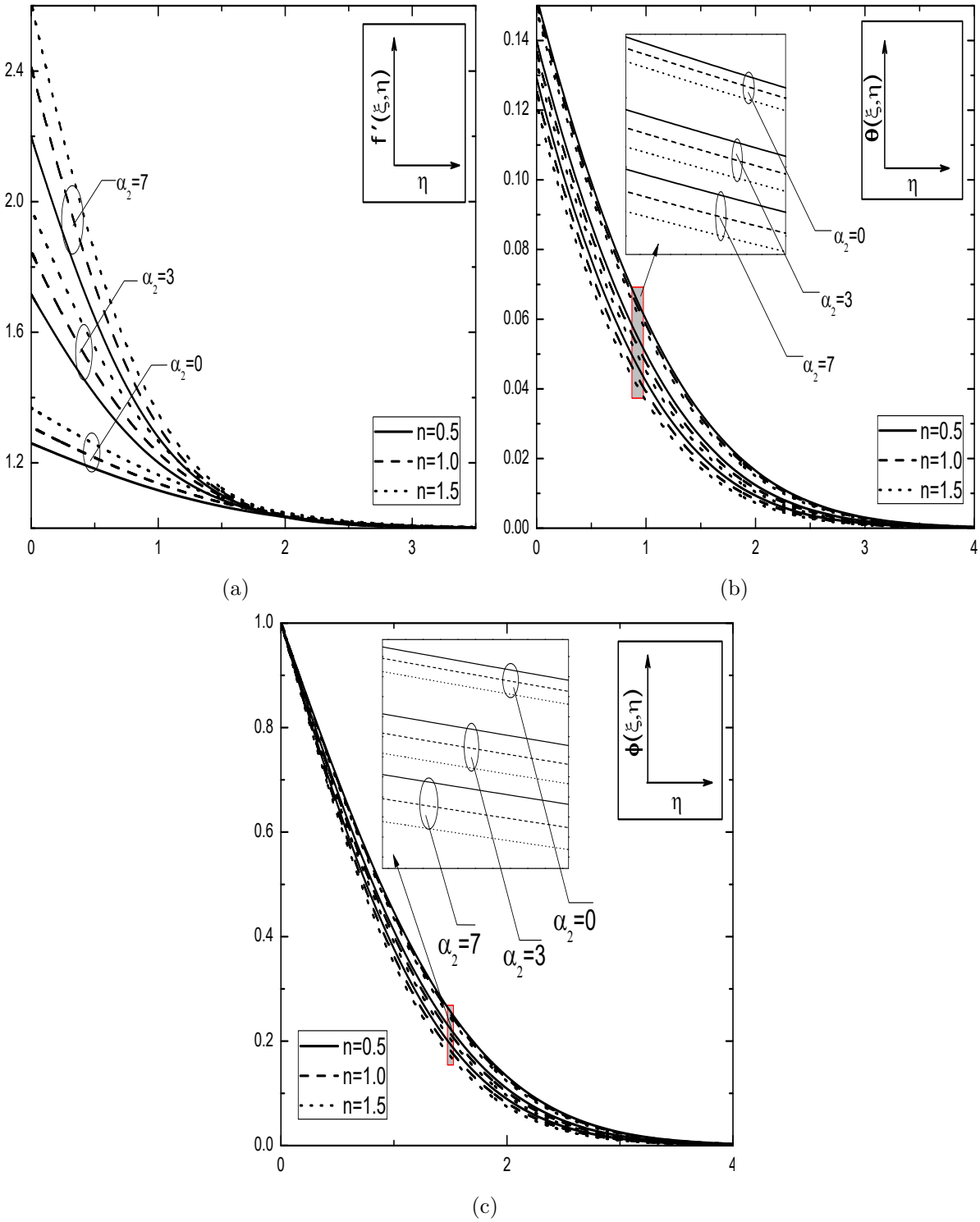

Figure 5.10: *Effect of α_2 for different values of n on the (a) velocity, (b) temperature and (c) concentration with the fixed values of $Bi = 0.2$, $\alpha_1 = 1$, $\Omega = 30^0$ and $\xi = 0.5$.*

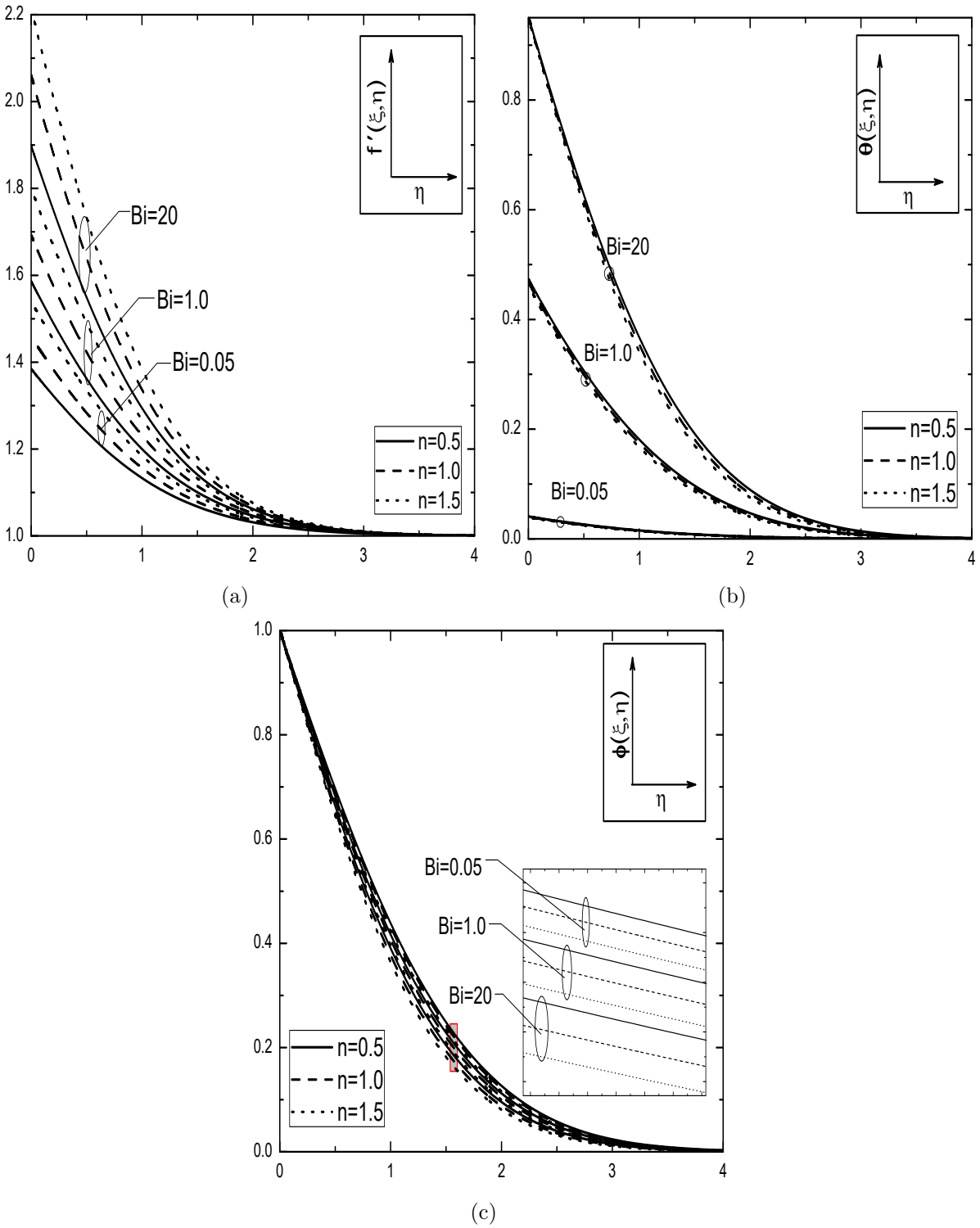

Figure 5.11: *Effect of Bi for different values of n on the (a) velocity, (b) temperature and (c) concentration with the fixed values of* $\alpha_1 = 1$, $\alpha_2 = 1$, $\Omega = 30^0$ *and* $\xi = 0.5$.

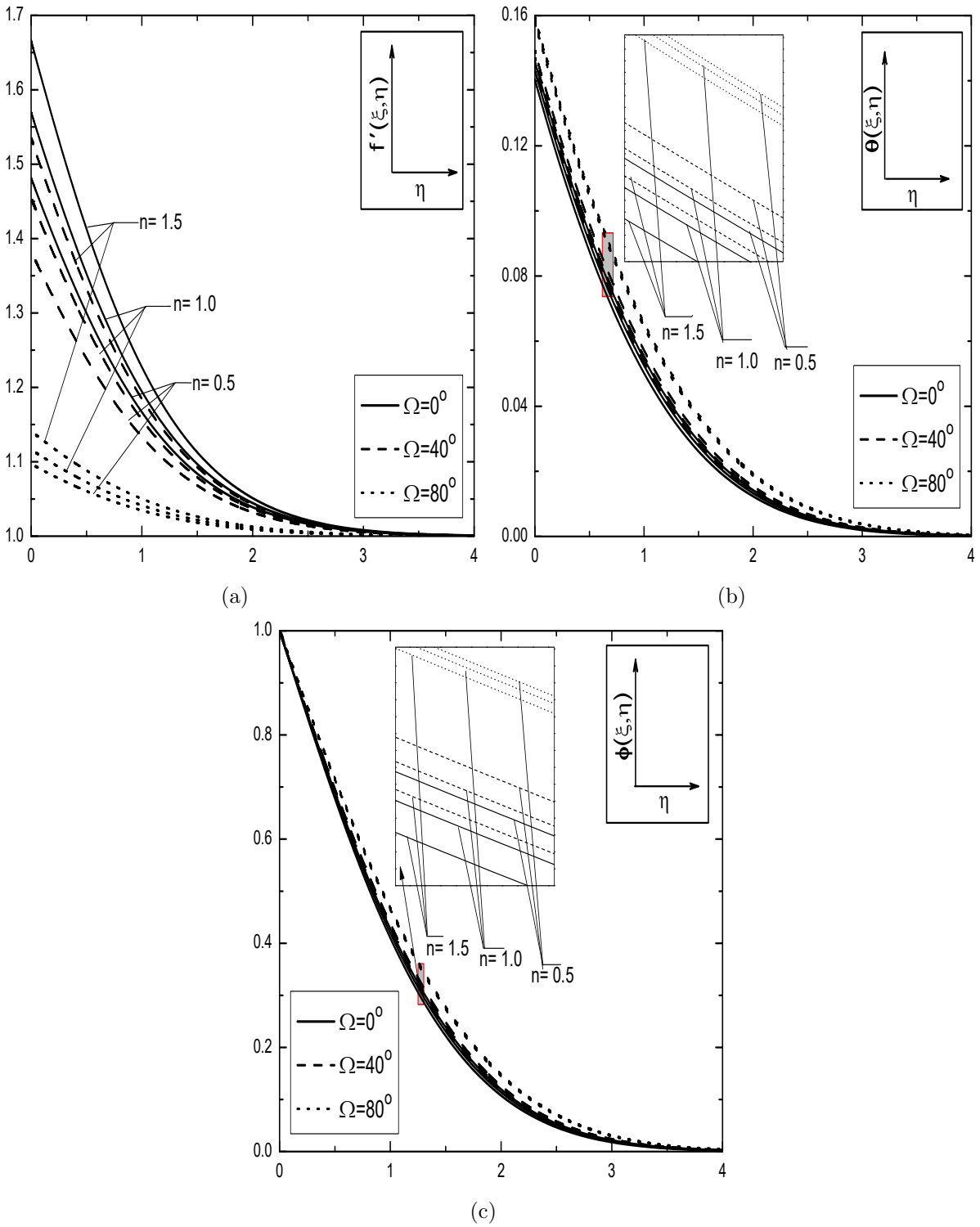

Figure 5.12: *Effect of* Ω *for different values of* n *on the (a) velocity, (b) temperature and (c) concentration with the fixed values of* $\alpha_1 = 1$, $\alpha_2 = 1$, $Bi = 0.2$ *and* $\xi = 0.5$.

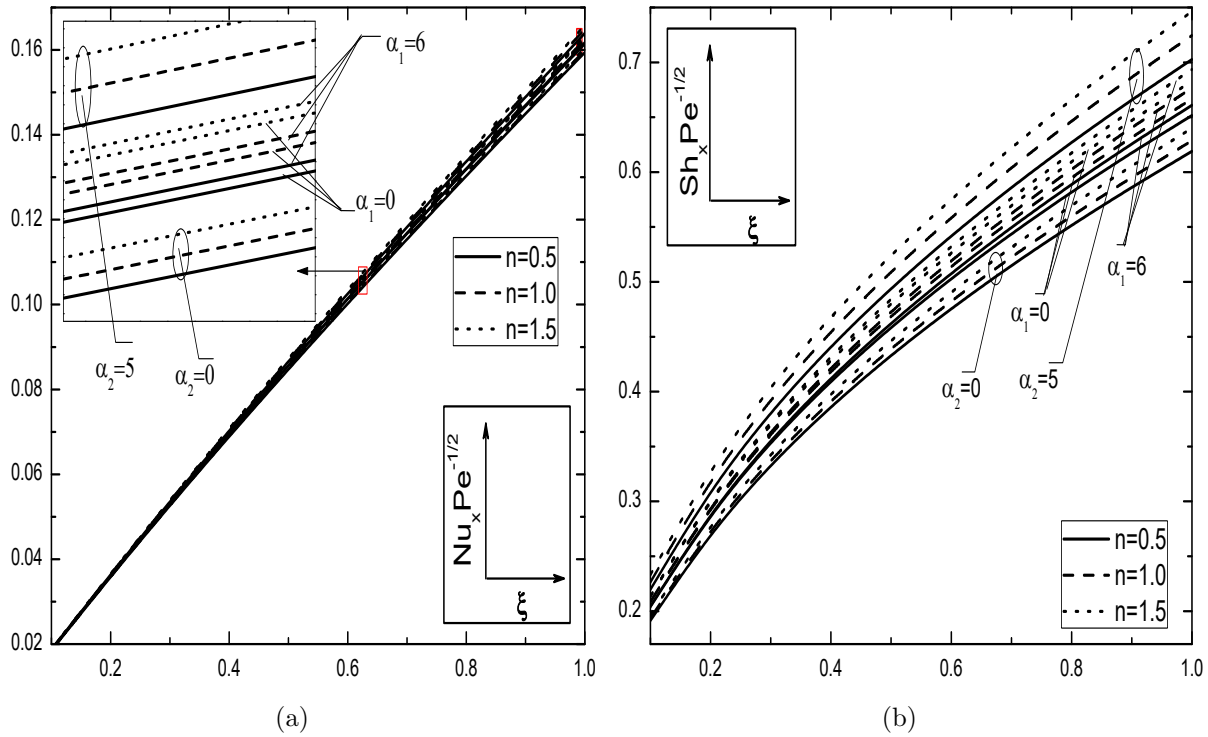

Figure 5.13: *Effects of α_1 and α_2 for different values of n on the (a) heat transfer rate and (b) mass transfer rate against ξ with the fixed values of $Bi = 0.5$ and $\Omega = 30^0$.*

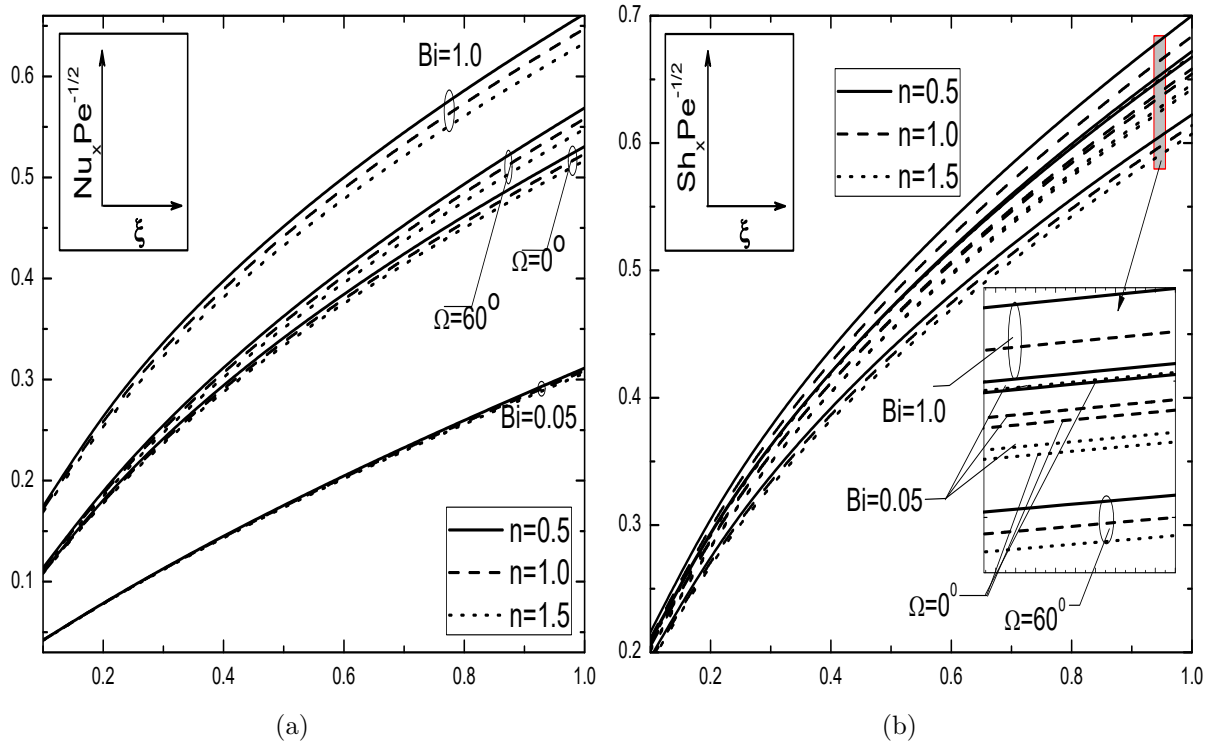

Figure 5.14: *Effects of Bi and Ω for different values of n on the (a) heat transfer rate and (b) mass transfer rate against ξ with the fixed values of $\alpha_1 = 1$ and $\alpha_2 = 1$.*

5.3 Conclusions

In the present chapter, the nonlinear Boussinesq approximation is considered in the analysis of heat and mass transfer phenomena of a Ostwald-de Waele power-law fluid flow over a convectively heated inclined plate in a non-Darcy porous medium. The impact of pertinent parameters on the velocity, temperature, concentration together with the heat and mass transfer rates have been analyzed. From this study, the conclusions drawn in both cases (a) and (b) can be summarized as follows:

The influences of α_1 and α_2 are prominent on all the physical characteristics of the present, compared therewith its absence, and these two effects are more influenced for pseudo-plastic fluids in both case (a) and case (b). In both case (a) and case (b), the variation of the Biot number leads to enhance all the pertinent characteristics and it effectively furnishes a mechanism for comparing the conduction resistance within a solid body to the convection resistance external to that body (offered by the surrounding fluid) for heat transfer. Further, it is found that the velocity and mass transfer rate diminish, whereas the thermal and solutal boundary layer thicknesses enhance with the increase of angle of inclination. On the other hand, heat transfer rate increases with the angle of inclination in case (a), but it decreases in case (b).

Chapter 6

Effects of Biot Number and Cross-Diffusion on Nonlinear Convective Flow of a Power-law Fluid in a Non-Darcy Porous Medium [1]

6.1 Introduction

The effect of cross-diffusion plays a vital role in the analysis related to heat and mass transfer of moving fluid and has unavoidable importance. In view of the above, the analysis of convective flow along a horizontal/vertical plate in a power-law fluid saturated non-Darcy porous medium with cross-diffusion effects, has been contemplated by many researchers. In most of the previous studies, these effects are considered as a second-order phenomenon and furthermore called Soret-Dufour effects. The importance of Soret and Dufour effects on mixed convective flow a power-law fluid along an isothermal vertical plate embedded in a porous medium with suction/injection effects, is discussed by Mahdy [61]. The importance of convective transport along a vertical plate in a stratified power-law fluid saturated non-Darcy porous medium in the presence of Soret and Dufour

[1]Case(a): Published in "**Journal of Nanofluids**" 7(4) (2018) 766–775, Case(b): Published in "**Advanced Science, Engineering and Medicine**" 10 (2018) 1–8.

effects, is examined by Srinivasacharya *et al.* [99].

From the literature survey, it is observed that the study of free and mixed convective flows of a power-law fluid over an inclined plate with cross-diffusion effects has not been investigated so far. Therefore, a problem of nonlinear convective flow of a power-law fluid along inclined plate embedded in a non-Darcy porous medium under the influence of cross-diffusion and convective boundary condition, is considered in this chapter. Further, the reduced system of non-dimensional partial differential equations is solved numerically by employing successive linearization method along with the local similarity and non-similarity approaches. The effects of Soret number, Dufour number, Biot number, nonlinear convection parameters and angle of inclination on the velocity, temperature, and concentration profiles are presented graphically for all three kinds fluids (pseudo-plastic, Newtonian and dilatant fluids). Moreover, the non-dimensional Nusselt and Sherwood numbers against the stream-wise coordinate for various values of the pertinent parameters are also analyzed through graphs.

6.2 Mathematical Formulation

An incompressible power-law fluid flow over an inclined plate in a non-Darcy porous medium, is considered in this chapter. Further, the flow is assumed to be laminar and in steady state. Choose the two-dimensional coordinate system such that the x-axis is taken along the plate and y-axis is measured normal to it. The geometry of the problem is shown in Fig.(2.1). If the direct coupling between the temperature and concentration gradients exists in the problem and when these gradients are very large, then the problem becomes more significant from practical point of view. Hence, an extension of chapter-5 is considered in the present chapter by including the cross-diffusion effects.

By invoking the assumptions made in chapter-5 along with the nonlinear Boussinesq approximation, the governing equations that describe the physical situation of present problem, can be written as

$$\frac{\partial u}{\partial x}+\frac{\partial v}{\partial y}=0 \tag{6.1}$$

$$\frac{\partial u^n}{\partial y}+\frac{b\sqrt{K_p}}{\nu}\frac{\partial u^2}{\partial y}=\frac{K_p g^*}{\nu}\left\{\left[\beta_0+2\beta_1(T-T_\infty)\right]\frac{\partial T}{\partial y}+\left[\beta_2+2\beta_3(C-C_\infty)\right]\frac{\partial C}{\partial y}\right\}\cos\Omega \tag{6.2}$$

$$u\frac{\partial T}{\partial x}+v\frac{\partial T}{\partial y}=\alpha\frac{\partial^2 T}{\partial y^2}+\frac{D\,K_T}{C_s\,C_p}\frac{\partial^2 C}{\partial y^2} \tag{6.3}$$

$$u\frac{\partial C}{\partial x}+v\frac{\partial C}{\partial y}=D\frac{\partial^2 C}{\partial y^2}+\frac{D\,K_T}{T_m}\frac{\partial^2 T}{\partial y^2} \tag{6.4}$$

The corresponding boundary conditions are

$$\begin{aligned} v=0,\;\; -k_f\frac{\partial T}{\partial y}=h_f(T_f-T),\;\; C=C_w \quad \text{at} \quad y=0 \\ u=0,\;\; T=T_\infty,\;\; C=C_\infty \quad \text{as} \quad y\to\infty \end{aligned} \tag{6.5}$$

where C_s is the concentration susceptibility, C_p is the specific heat capacity, K_T is the thermal diffusion ratio and T_m is the mean fluid temperature.

In this chapter also, two types (cases) of problems are considered: (a) free/natural convection and (b) mixed convection.

6.2.1 Case(a): Natural Convection

The flow is assumed to be a natural convective flow, caused by only buoyancy forces and without any external agent. Hence, the velocity of the external flow becomes zero ($i.e., u_\infty = 0$). Next, we introduce the following non-dimensional transformations

$$\begin{aligned} \xi=\frac{x}{L},\;\; \eta=\frac{y}{L}\,Ra^{\frac{1}{2}}\,\xi^{\frac{-1}{2}},\;\; \psi(\xi,\eta)=\alpha\,\xi^{\frac{1}{2}}\,Ra^{\frac{1}{2}}\,f(\xi,\eta) \\ T(\xi,\eta)=T_\infty+(T_f-T_\infty)\;\theta(\xi,\eta),\quad C(\xi,\eta)=C_\infty+(C_w-C_\infty)\;\phi(\xi,\eta) \end{aligned} \tag{6.6}$$

where $Ra=\dfrac{L}{\alpha}\left[\dfrac{\rho_\infty K_p g^* \beta_0 (T_f-T_\infty)}{\mu^*}\right]^{1/n}$ is the global Rayleigh number.

Substituting the stream function (2.7) and the transformations (6.6) into Eqs.(6.1) - (6.4), we obtain the following momentum, energy and concentration equations as

$$n\;\left(f'\right)^{n-1}f''+2\,Gr^*f'f''=\left[(1+2\,\alpha_1\theta)\theta'+\mathcal{B}(1+2\,\alpha_2\phi)\phi'\right]\cos\Omega \tag{6.7}$$

$$\theta''+\frac{1}{2}f\theta'+\;Du\,\phi''=\xi\left(f'\frac{\partial\theta}{\partial\xi}-\frac{\partial f}{\partial\xi}\theta'\right) \tag{6.8}$$

$$\frac{1}{Le}\phi''+\frac{1}{2}f\phi'+\;Sr\,\theta''=\xi\left(f'\frac{\partial\phi}{\partial\xi}-\frac{\partial f}{\partial\xi}\phi'\right) \tag{6.9}$$

Boundary conditions (6.5) in terms of f, θ and ϕ can be written as

$$f(\xi,0) = -2\,\xi\left(\frac{\partial f}{\partial \xi}\right)_{\eta=0},\ \theta'(\xi,0) = -Bi\,\xi^{\frac{1}{2}}\left[1-\theta(\xi,0)\right], \phi(\xi,0) = 1,$$
$$f'(\xi,\infty) = 0,\ \theta(\xi,\infty) = 0,\ \phi(\xi,\infty) = 0. \tag{6.10}$$

In usual definitions, $Sr = \dfrac{D\,K_T(T_f - T_\infty)}{T_m \nu (C_w - C_\infty)}$ is the Soret number, $Du = \dfrac{DK_T(C_w - C_\infty)}{C_s C_p \nu (T_f - T_\infty)}$ is the Dufour number and Biot number is taken as $Bi = \dfrac{h_f L}{k_f\ Ra^{1/2}}$.

The non-dimensional Nusselt number $Nu_x = \dfrac{-x}{(T_f - T_\infty)}\left[\dfrac{\partial T}{\partial y}\right]_{y=0}$ and the Sherwood number $Sh_x = \dfrac{-x}{(C_w - C_\infty)}\left[\dfrac{\partial C}{\partial y}\right]_{y=0}$ are given by

$$Nu_x\, Ra^{\frac{-1}{2}} = -\xi^{\frac{1}{2}}\,\theta'(\xi,0),\ Sh_x\, Ra^{\frac{-1}{2}} = -\xi^{\frac{1}{2}}\,\phi'(\xi,0). \tag{6.11}$$

Results and Discussion

With the help of explanations given in previous chapters, the system of Eqs.(6.7)-(6.9) subject to the boundary conditions (6.10) have been solved numerically using the successive linearization method along with the local similarity and local non-similarity procedures. In the absence of cross-diffusion effects, this case reduces to the case (a) problem of the chapter-5. Validation of the present problem in this case, can be done on comparison as it was done in the case (a) of chapter-5. Further, the numerical computations are carried out by following the fixed values of parameters: $Gr^* = 0.5$, $\mathcal{B} = 1$, $Le = 1$ and $\xi = 0.2$. These values remain unchanged throughout this study, unless otherwise specified. The impacts of pertinent parameters, such as the nonlinear convection parameters (α_1, α_2), cross-diffusion parameters (Du, Sr), angle of inclination (Ω) and the Biot number (Bi), are determined through Figs.6.1(a)-6.3(c) within the boundary layer profiles. Additionally, the physical quantities of the flow, namely Nusselt and Sherwood numbers (i.e, $Nu_x\, Ra^{\frac{-1}{2}}$ and $Sh_x\, Ra^{\frac{-1}{2}}$) are anticipated in Figs.6.4(a)-6.6(b).

Variations of fluid flow profiles (such as f', θ and ϕ) for $\alpha_1(0,\ 6)$, α_2 $(0,\ 5)$ and n $(0.5,\ 1.0,\ 1.5)$ with $Du = 0.5$, $Sr = 1.0$, $Bi = 0.5$, $\xi = 0.5$ and $\Omega = 30^0$, are depicted in the first set of

Figs.6.1(a)-6.1(c). The dimensionless velocity increase more at the surface of the inclined plate and it reaches free stream value for η_{max} value with the increase of α_1, the similar result can be noticed in Fig.6.1(a). Additionally, Fig.6.1(a) portrays the behaviour of velocity profile for α_2 to the three distinct values of the power-law index. The results of velocity for α_2 repeat the same kind of behavior as like α_1 in all three fluids. The thermal and solutal boundary layer thicknesses diminish with the rise of α_1 or α_2, and the same results are displayed in Figs.6.1(b) and 6.1(c). The difference between wall and ambient medium increases for larger values of α_1 and α_2. Due to this, higher velocity (see., Fig.6.1(a)), smaller temperature (see., Fig.6.1(b)) and smaller concentrations (see., in Fig.6.1(c)) are obtained. Further, the influence of α_2 is more prominent on these three boundary layer profiles and in all three kinds of fluids (among pseudo-plastic, Newtonian and dilatant fluids) compared to α_1 influence.

The second set of Figs.6.2(a)-6.2(c) exhibits the significance of cross-diffusion parameters Du (0, 0.5) and Sr (0, 1.5) on the non-dimensional velocity (f'), temperature (θ) and concentration (ϕ) in all three kinds of fluids (among pseudo-plastic, Newtonian and dilatant fluids) for $\alpha_1 = 4$, $\alpha_2 = 4$, $Bi = 0.5$, $\xi = 0.5$ and $\Omega = 30^0$. From Fig.6.2(a), it is observed that, for an individual improvement of cross-diffusion parameters (i.e when Du varies Sr is fixed and if Sr varies Du should be fixed), thickness of the momentum boundary layer increases. Diffusion-thermo (Du) and thermal-diffusion (Sr) effects on the temperature and concentration can be seen in Figs.6.2(b)-6.2(c). The Dufour number characterizes the concentration difference ratio compared to the temperature, and the Soret number is the opposite. Hence, an increasing Dufour number stands for a larger concentration difference and leads to increase temperature, while the similar kind of change is observed in concentration with respect to Soret number as shown in Figs.6.2(b)-6.2(c).

The influences of $\Omega(0^0, 60^0)$ and $Bi(0.05, 0.5)$ on the boundary layer profiles (such as, f', θ and ϕ) are plotted through the third set of Figs.6.3(a)-6.3(c) for the fixed values: $Du = 0.3$, $Sr = 1.0$, $\alpha_1 = 4$, $\alpha_2 = 4$ and $\xi = 0.5$ in three instances of $n = 0.5, 1.0, 1.5$. The velocity distribution reduces for the increase of Ω within the boundary layer as shown in Fig.6.3(a). Additionally, the most extreme buoyancy force occurs at the vertical plate. Also, it is observed from Figs.6.2(b) that the velocity of the flow field attains a maximum state in the neighborhood of the plate with the rise of Bi and this may be due to the reduction in the thermal resistance of the inclined plate. From Figs.6.3(b) and 6.3(c), one can notice that the temperature and concentration enhance with the increase of Ω. Fig.6.3(b) implies the impact of Bi on the temperature distribution and shows two

results mainly. First, the convective boundary condition becomes to isothermal condition when $Bi \to \infty$ (i.e for a larger value of Bi), as shown Fig.6.3(a). Secondly, the temperature distribution is accelerates on the surface of the plate when Bi increases from the thermally thin case ($Bi < 0.1$) to the thermally thick case ($Bi > 0.1$). Further, Fig.6.3(c) reveals that the influence of Biot number is nominal on the concentration profile.

The above mentioned figures also uncover the effect of power-law index n on f', θ and ϕ in the presence or absence of pertinent parameters α_1, α_2, Du, Sr, Bi and Ω, individually. From Figs.6.1(a), 6.2(a), and 6.3(a), it is observed that the dimensionless velocity decreases at the surface of the plate, whereas it increases in the outer part of the boundary layer for the rise of n, i.e. the fluid becomes more shear thickening (dilatant) at the plate and more shear thinning (pseudo-plastic) away from the inclined plate. It is fascinating to note that the velocity profiles crossed each other near the wall as depicted in the Figs.6.1(a), 6.2(a) and 6.3(a). The impact of the power-law index n on the temperature (portrayed by the Figs. 6.1(b), 6.2(b) and 6.3(b)) and concentration (portrayed by the Figs. 6.1(c), 6.2(c) and 6.3(c)) profiles are prepared for the same governing parameters. An increase in n leads to decrease the temperature and concentration profiles and also, it reduces the thermal and concentration boundary layer thicknesses.

The influences of $\alpha_1(0, 6)$ and $\alpha_2(0, 5)$ on the Nusselt number ($Nu_x\, Ra^{\frac{-1}{2}}$) and Sherwood number ($Sh_x\, Ra^{\frac{-1}{2}}$) against the stream wise coordinate ξ, are plotted through the fourth set of Figs.6.4(a)-6.4(b) with the fixed values: $Du = 0.3$, $Sr = 1.0$, $Bi = 0.5$ and $\Omega = 30^0$ for the three kinds of fluids. The rise in α_1 or α_2 improve all the pertinent characteristics of the pseudo-plastic fluid flow for a fixed value of α_2 or α_1 individually. Also, heat and mass transfer rates have the same change in the Newtonian and dilatant fluid flows. Moreover, the behaviour of $Nu_x\, Ra^{\frac{-1}{2}}$ is opposite to $Sh_x\, Ra^{\frac{-1}{2}}$. Further, for a non zero value of either α_1 or α_2, both the heat and mass transfer rates fall down when power-law index moves from $n < 1$ to $n > 1$, whereas both the heat and mass transfer rates are considerably enhance in the absence of either α_1 or α_2 for the change of power-law index.

The effects of $Du(0, 0.5)$ and $Sr(0, 1.5)$ on the heat and mass transfer rates are displayed in the fifth set of Figs.6.5(a)-6.5(b) for $\alpha_1 = 1$, $\alpha_2 = 1$, $Bi = 0.5$ and $\Omega = 30^0$. Higher values of the Dufour number leads to reduce $Nu_x\, Ra^{\frac{-1}{2}}$ and enhance $Sh_x\, Ra^{\frac{-1}{2}}$, while with the expansion of Sr, these heat and mass transfer rates show reverse trend. Thus, Soret and Dufour numbers have opposite influence on the heat and mass transfer rates, as depicted in Figs.6.5(a)-6.5(b). However,

the influence of power-law index n is nominal for the heat transfer rate and considerable for the mass transfer rate as shown in Figs.6.5(a)-6.5(b).

The sixth set of Figs.6.6(a)-6.6(b) describes the impact of $Bi(0.1, 10)$ and $\Omega(0^0, 60^0)$ on $Nu_x\, Ra^{\frac{-1}{2}}$ and $Sh_x\, Ra^{\frac{-1}{2}}$ for the three fluid cases with $Du = 0.03$, $Sr = 2.0$, $\alpha_1 = 3$, $\alpha_2 = 3$, $Fs = 0.5$ and $\xi = 0.5$. With an increment in Ω, there is a considerable decrement in g^* component and this degrades the buoyancy force. Hence, the reduction in the buoyancy will lead to diminish the heat and mass transfer rates when the inclined plate is displaced from vertical to horizontal direction. One can notice that an enhancement in the Biot number leads to increase $Nu_x\, Ra^{\frac{-1}{2}}$, while it reduces the mass transfer rate $Sh_x\, Ra^{\frac{-1}{2}}$. Further, the power-law index results an improvement in $Nu_x\, Ra^{\frac{-1}{2}}$ and $Sh_x\, Ra^{\frac{-1}{2}}$ for the inclined plate, whereas it shows opposite change in the case of vertical plate.

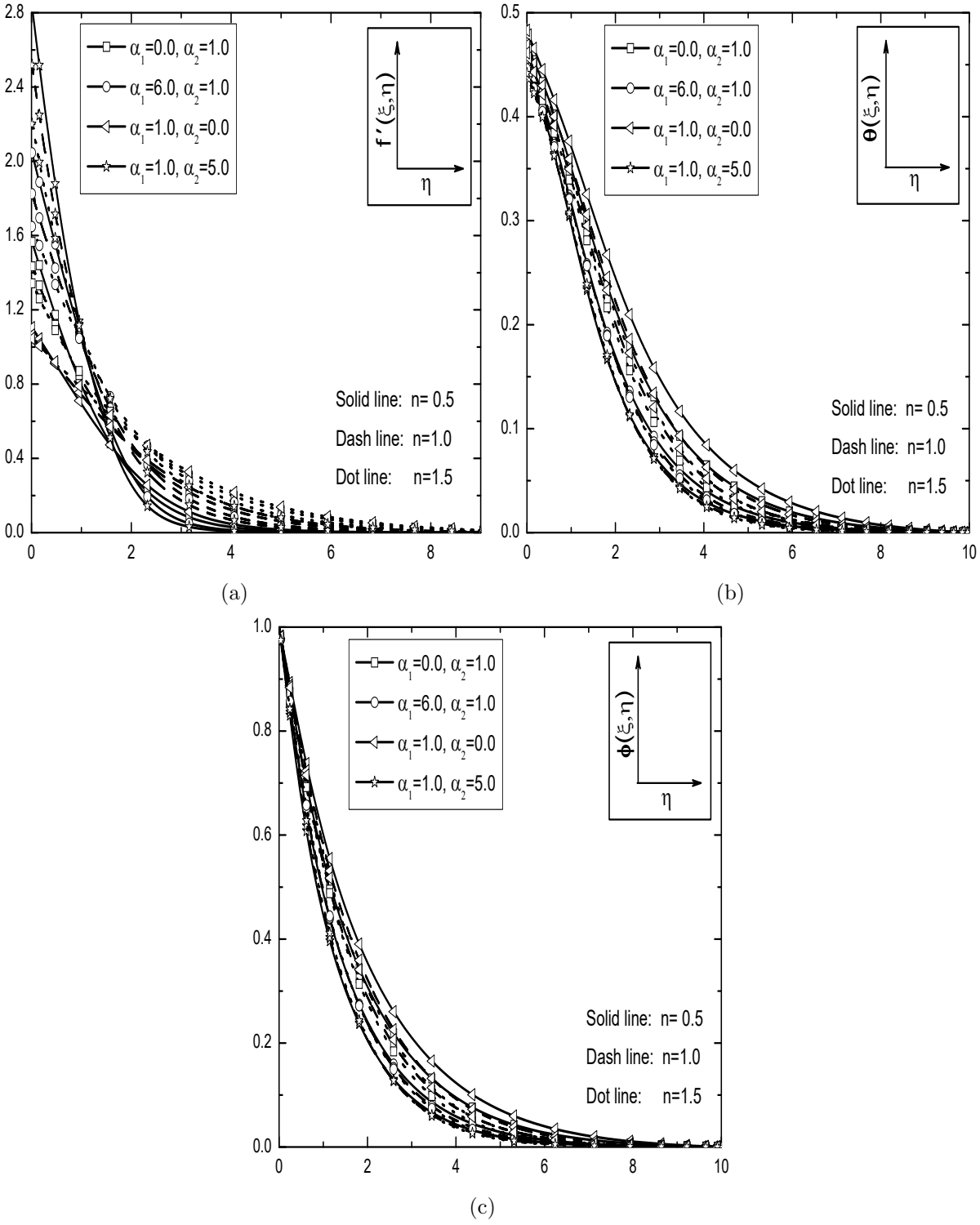

Figure 6.1: *Effects of* α_1 *and* α_2 *for different values of* n *on the (a) velocity, (b) temperature and (c) concentration with the fixed values of* $Bi = 0.5$, $Du = 0.5$, $Sr = 1.0$, $\Omega = 30^0$ *and* $\xi = 0.5$.

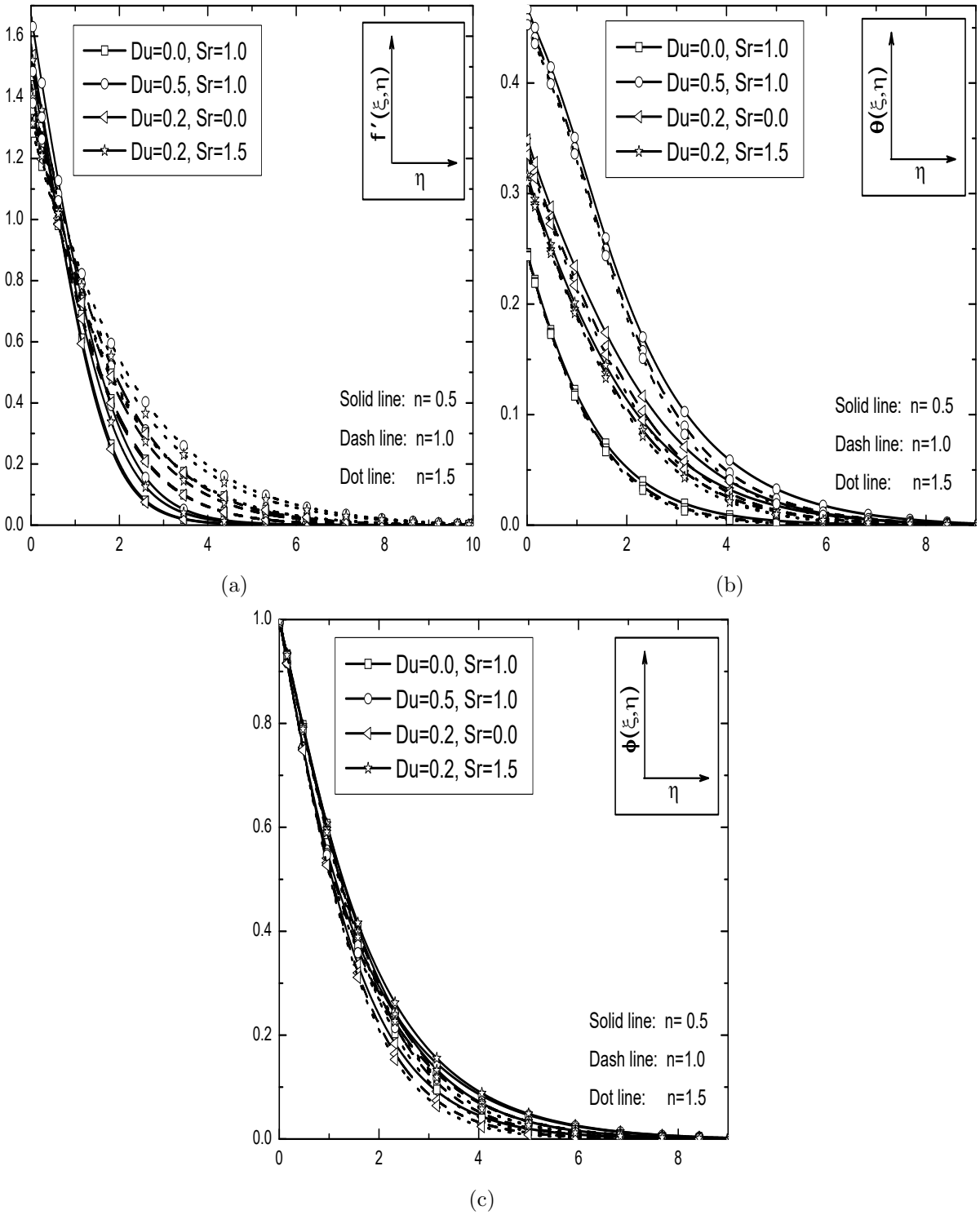

Figure 6.2: *Effects of Du and Sr for different values of n on the (a) velocity, (b) temperature and (c) concentration with the fixed values of* $Bi = 0.5$, $\alpha_1 = 4$, $\alpha_2 = 4$, $\Omega = 30^0$ *and* $\xi = 0.5$.

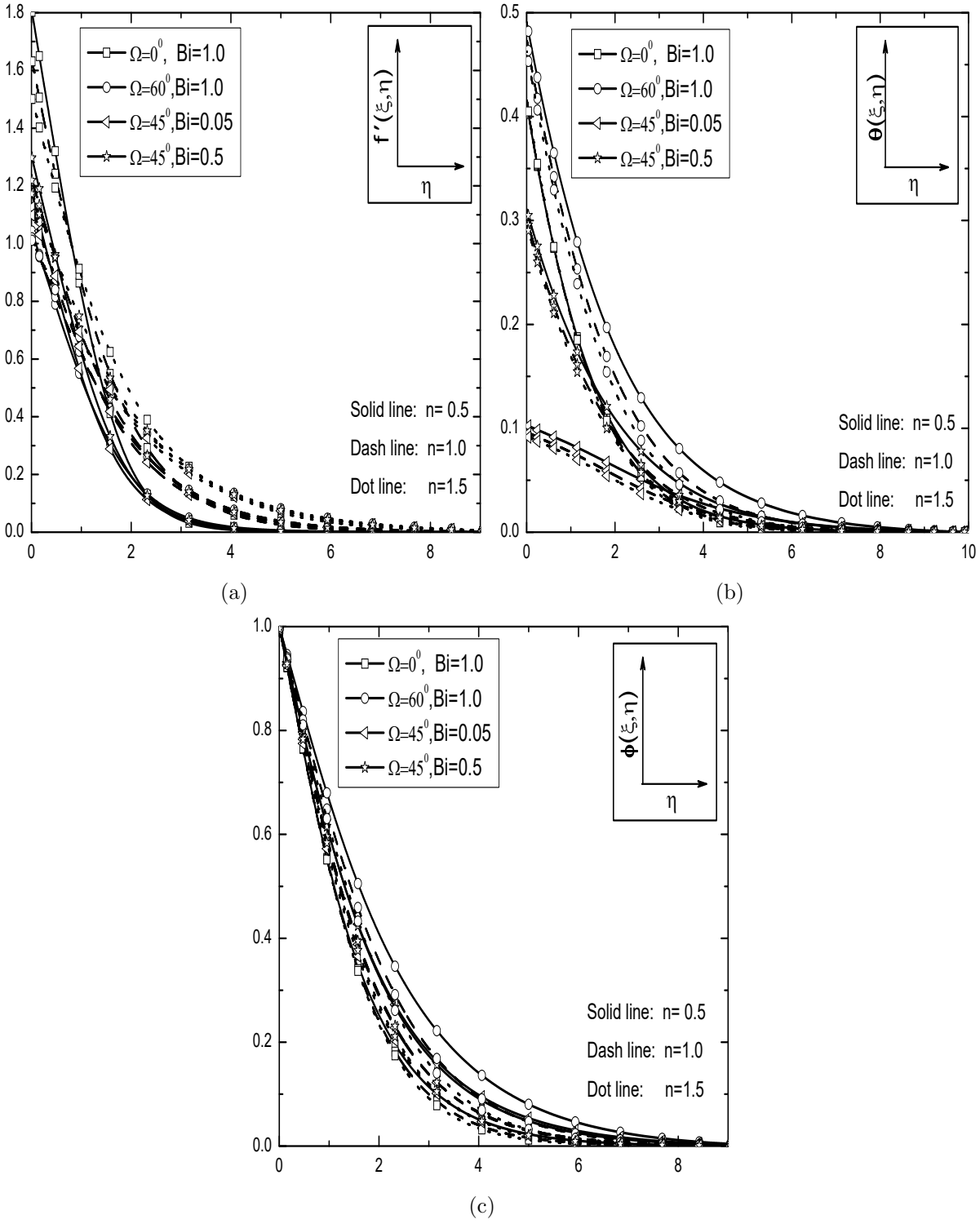

Figure 6.3: *Effects of* Ω *and* Bi *for different values of* n *on the (a) velocity, (b) temperature and (c) concentration with the fixed values of* $\alpha_1 = 4$, $\alpha_2 = 4$, $Du = 0.3$, $Sr = 1.0$ *and* $\xi = 0.5$.

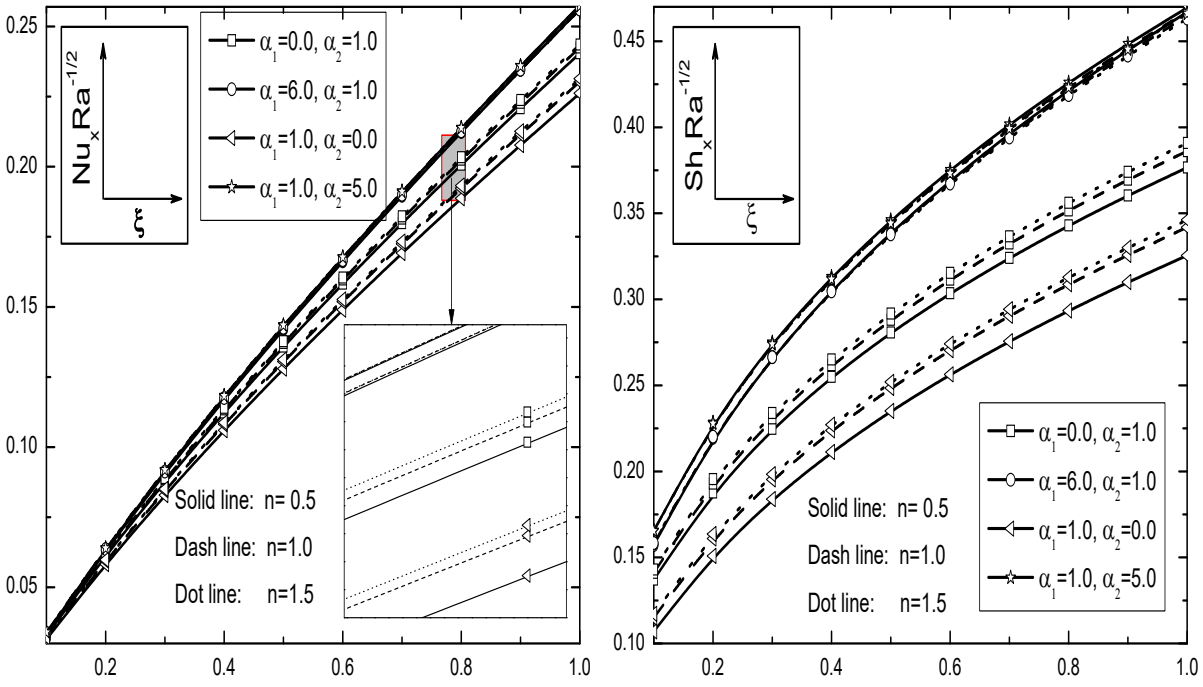

(a) (b)

Figure 6.4: *Effects of* α_1 *and* α_2 *for different values of* n *on the (a) heat transfer rate and (b) mass transfer rate against* ξ *with the fixed values of* $Bi = 0.5$, $Du = 0.3$, $Sr = 1.0$ *and* $\Omega = 30^0$.

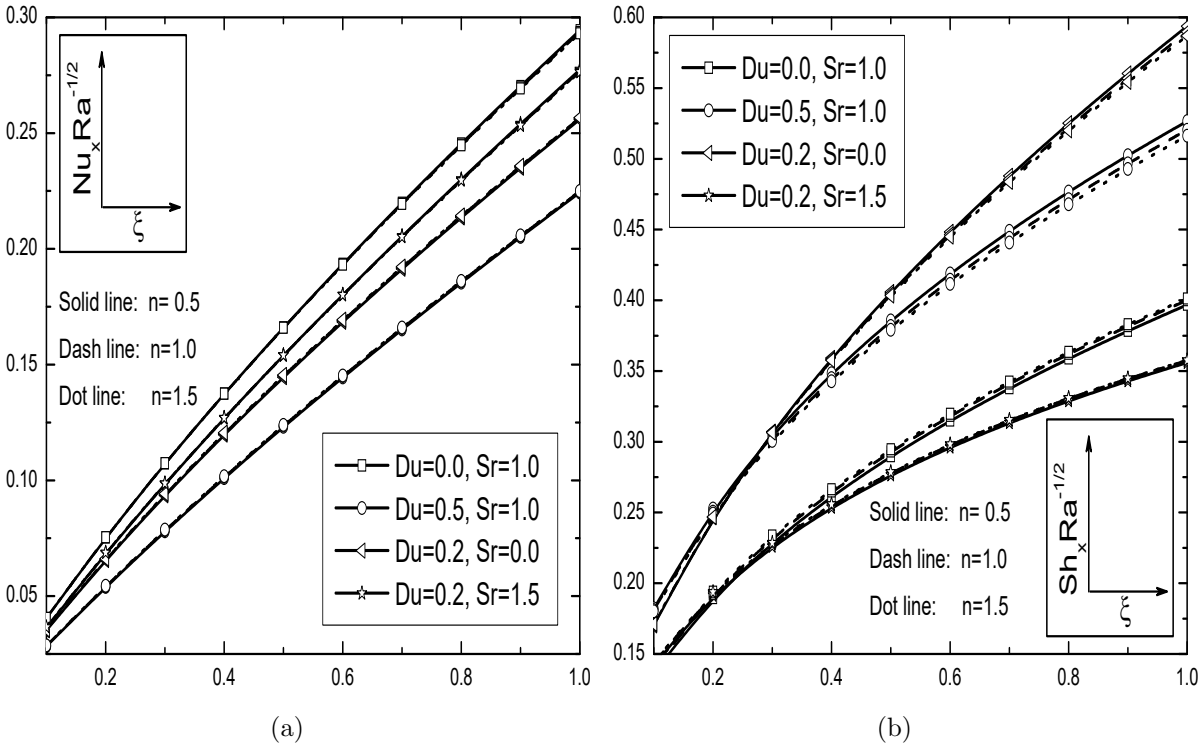

Figure 6.5: *Effects of Du and Sr for different values of n on the (a) heat transfer rate and (b) mass transfer rate against ξ with the fixed values of $Bi = 0.5$,$\alpha_1 = 4$, $\alpha_2 = 4$ and $\Omega = 30^0$.*

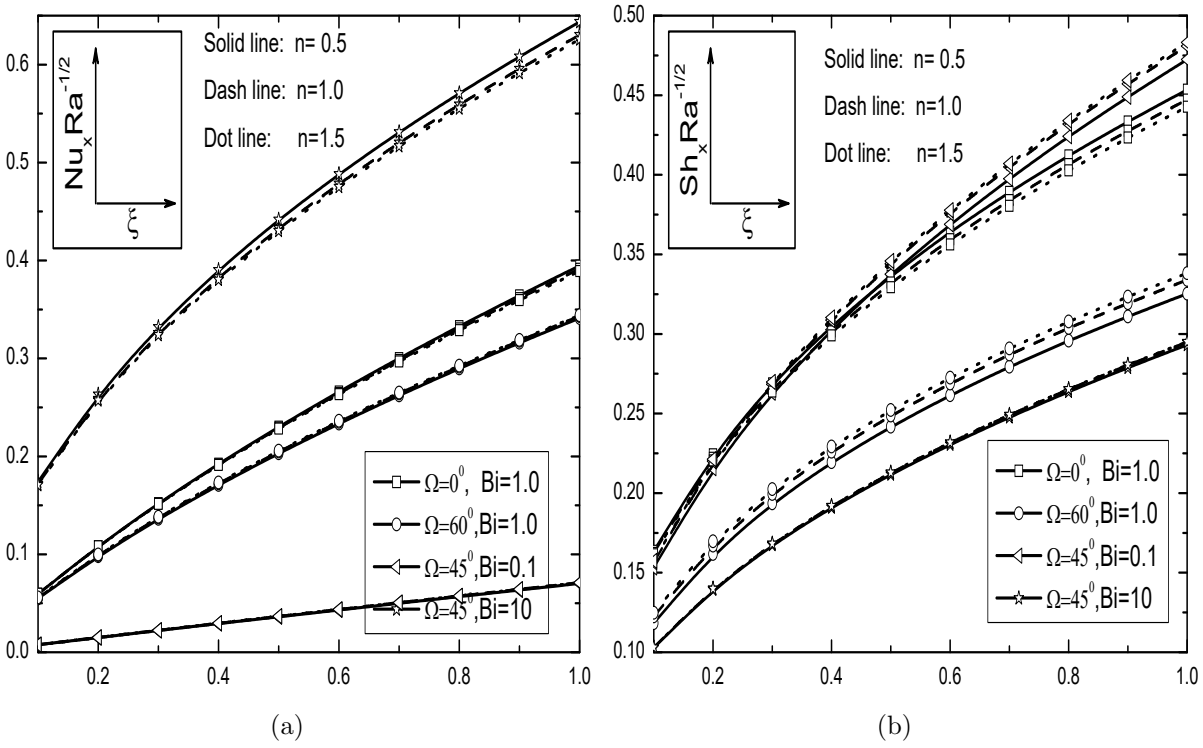

Figure 6.6: *Effects of Ω and Bi for different values of n on the (a) heat transfer rate and (b) mass transfer rate against ξ with the fixed values of $\alpha_1 = 4$, $\alpha_2 = 4$, $Du = 0.3$ and $Sr = 1.0$.*

6.2.2 Case(b): Mixed Convection

Consider the flow to be a mixed convective flow, arises from buoyancy forces and an external flow with the velocity u_∞. Now, we introduce the following dimensionless variables

$$\begin{gathered}\xi = \frac{x}{L},\ \ \eta = \frac{y}{L}\, Pe^{\frac{1}{2}}\, \xi^{\frac{-1}{2}},\ \ \psi(\xi,\eta) = \alpha\, \xi^{\frac{1}{2}}\, Pe^{\frac{1}{2}}\, f(\xi,\eta) \\ T(\xi,\eta) = T_\infty + (T_f - T_\infty)\ \theta(\xi,\eta),\ \ \ C(\xi,\eta) = C_\infty + (C_w - C_\infty)\ \phi(\xi,\eta)\end{gathered} \tag{6.12}$$

where $Pe = \dfrac{u_\infty\, L}{\alpha}$ is the global Peclet's number and u_∞ is the free stream velocity.

Substituting stream function (2.7) and the transformation (6.12) into Eqs.(6.1) - (6.4), we obtain the following momentum, energy and concentration equations

$$n\ \left(f'\right)^{n-1} f'' + 2Fs f' f'' = (Ri)^n \left[(1 + 2\,\alpha_1\theta)\theta' + \mathcal{B}(1 + 2\,\alpha_2\phi)\phi'\right] \cos\Omega \tag{6.13}$$

$$\theta'' + \frac{1}{2} f\theta' +\ Du\, \phi'' = \xi \left(f' \frac{\partial \theta}{\partial \xi} - \frac{\partial f}{\partial \xi}\theta' \right) \tag{6.14}$$

$$\frac{1}{Le}\phi'' + \frac{1}{2} f\phi' +\ Sr\, \theta'' = \xi \left(f' \frac{\partial \phi}{\partial \xi} - \frac{\partial f}{\partial \xi}\phi' \right) \tag{6.15}$$

Boundary conditions (6.5) in terms of f, θ, and ϕ can be written as

$$\begin{gathered}f(\xi,0) = -2\,\xi \left(\frac{\partial f}{\partial \xi}\right)_{\eta=0},\ \ \theta'(\xi,0) = -Bi\, \xi^{\frac{1}{2}}\, [1 - \theta(\xi,0)]\,, \phi(\xi,0) = 1, \\ f'(\xi,\infty) = 1,\ \theta(\xi,\infty) = 0,\ \phi(\xi,\infty) = 0.\end{gathered} \tag{6.16}$$

where the Biot number is taken as $Bi = \frac{h_f L}{k_f\ Pe^{1/2}}$.

The non-dimensional Nusselt number $Nu_x = \dfrac{-x}{(T_f - T_\infty)} \left[\dfrac{\partial T}{\partial y}\right]_{y=0}$ and the Sherwood number $Sh_x = \dfrac{-x}{(C_w - C_\infty)} \left[\dfrac{\partial C}{\partial y}\right]_{y=0}$ are given by

$$Nu_x Pe^{\frac{-1}{2}} = -\xi^{\frac{1}{2}}\theta'(\xi,\, 0),\ \ \ Sh_x Pe^{\frac{-1}{2}} = -\xi^{\frac{1}{2}}\phi'(\xi,\, 0). \tag{6.17}$$

Results and Discussion

Similar to the previous chapters, the numerical solution for the highly coupled nonlinear partial differential equations (6.13)- (6.15) together with the boundary conditions (6.16) are obtained by using successive linearization along with the local similarity and non-similarity approaches. In the absence of cross-diffusion effects, this case reduces to the case (b) problem of the previous chapter. Validation of the present problem in this case, can be done on comparison as it was done in the case (b) of chapter-5.

The numerical computations are carried out for the fixed values of parameters: $\mathcal{B} = 1$, $Fs = 1$, $\Pr = 1$, $Le = 1$, $Ri = 2$ and $\xi = 0.5$. These values are continued same throughout this study, unless otherwise specified. The impacts of the pertinent parameters are determined through Figs.6.7(a)-6.9(c) for the boundary layer profiles. Additionally, the physical quantities of the flow, Nusselt and Sherwood numbers (i.e, $Nu_x\, Pe^{\frac{-1}{2}}$ and $Sh_x\, Pe^{\frac{-1}{2}}$) are anticipated in Figs.6.10(a)-6.12(b) for the same values.

Variations in the fluid flow profiles (such as f', θ and ϕ) for $\alpha_1(0, 6)$, α_2 (0.5, 2.5) and n (0.5, 1.0, 1.5) with the fixed values: $Du = 0.03$, $Sr = 2.0$, $Bi = 0.5$, $\xi = 0.5$ and $\Omega = 30^0$, are displayed in the first set of Figs.6.7(a)-6.7(c). It uncovers that the variation of the power-law index is extensive and diminishes the momentum boundary layer thickness, whereas it enhances the thermal and solutal boundary layer thickness. The dimensionless velocity increases more at the surface of the inclined plate and it reaches to free stream value for η_{max} value with the increase of α_1 and this result is shown in Fig.6.7(a). Additionally, Figs.6.7(a) portrays the impact of α_2 on the behavior of velocity. The results of this figure repeat the same kind of behavior as α_1 in all three kinds of fluids. The thermal and solutal boundary layer thicknesses diminish with the rise of α_1 or α_2, and this effect is displayed in Figs.6.7(b) and 6.7(c).

The second set of Figs.6.8(a)-6.8(c) exhibits the significance of Dufour number $Du(0, 0.5)$ and Soret number $Sr(0, 1.5)$ on the profiles f', θ and ϕ in all the three kinds of fluids (pseudo-plastic, Newtonian and dilatant fluids) with $\alpha_1 = 1$, $\alpha_2 = 1$, $Bi = 0.5$, $\xi = 0.5$ and $\Omega = 30^0$. An individual improvement of cross-diffusion parameters leads to increase the thickness of the momentum boundary layer, as shown in Fig.6.8(a). When there is direct coupling between the temperature and concentration gradients, the mass flux can be generated not only by concentration gradients but also by temperature gradients. On the other hand, heat fluxes can also be created by concen-

tration gradients. Due to this, an addition in Du leads to enhance the temperature gradient and decreases the solutal boundary layer thickness, while the results of Sr are reverse to the results of Du on these two boundary layer profiles. That is, an increase in Sr leads to enhance concentration and reduces the temperature as shown in Figs.6.8(b) and 6.8(c). However, in the absence or presence of cross-diffusion parameters, the temperature and concentration gradients increases with the power-law index n.

The influences of $\Omega(0^0, 60^0)$ and $Bi(0.1, 20)$ on the different profiles are projected in the third set of Figs.6.9(a)-6.9(c) for the fixed values: $Du = 0.03$, $Sr = 2.0$, $\alpha_1 = 1$, $\alpha_2 = 1$ and $\xi = 0.5$ in three instances of power-law fluids, separately. An expansion in Ω reduces the velocity distribution inside the boundary layer region as portrayed in Fig.6.9(a). Also, that the velocity of the flow field attains maximum state in the neighborhood of the plate with the rise of Bi and this may be due to the reduction in the thermal resistance of the inclined plate. From Figs.6.9(b) and 6.9(c), one can notice that the temperature and concentration enhance with the rise of Ω. The temperature distribution accelerates on the surface of the plate when Bi increases from thermally thin case ($Bi < 0.1$) to the thermally thick case ($Bi > 0.1$), as shown in Fig.6.9(b). Further, Fig.6.9(c) reveals that the concentration profile increases within the boundary layer with the increase of Biot number.

The impact of $\alpha_1(0, 6)$ and $\alpha_2(0, 5)$ on the Nusselt number ($Nu_x Pe^{-1/2}$) and Sherwood number ($Sh_x Pe^{-1/2}$) against the stream wise coordinate ξ, are discussed through the fourth set of Figs.6.10(a)-6.10(b) with $Du = 0.03$, $Sr = 2.0$, $Bi = 1.0$ and $\Omega = 30^0$ for the three kinds of fluids. The rise in α_1 or α_2 improves all the pertinent characteristics of the pseudo-plastic fluid flow for a fixed value of α_2 or α_1 respectively. Also, these quantities have the same change in the Newtonian and dilatant fluid flows. Further, along the stream-wise coordinate ξ, the nature of $Nu_x Pe^{-1/2}$ is in opposite way to $Sh_x Pe^{-1/2}$. However, for a fixed value of either α_1 or α_2, both the heat and mass transfer rates fall down when the power-law index moves from $n < 1$ to $n > 1$.

The effects of $Du(0, 0.5)$ and $Sr = (0, 1.5)$ numbers on the heat and mass transfer rates are displayed in the fifth set of Figs.6.11(a)-6.11(b) for $\alpha_1 = 1$, $\alpha_2 = 1$, $Bi = 1$ and $\Omega = 60^0$. Higher values of Du leads to diminishes $Nu_x Pe^{-1/2}$ and enhances $Sh_x Pe^{-1/2}$, while with the expansion of Sr, these demonstrate reverse trend. Thus, the Soret and Dufour numbers have opposite effects on the Nusselt and Sherwood numbers, as shown in Figs.6.11(a)-6.11(b). However, these two transfer rates are more in the pseudo-plastic fluids when compared with the Newtonian and dilatant fluids.

The sixth set of Figs.6.12(a)-6.12(b) displays the impact of $Bi = (0.1, 20)$ and $\Omega = (0^0, 60^0)$ on $Nu_x Pe^{-1/2}$ and $Sh_x Pe^{-1/2}$ for the three fluid cases with $Du = 0.03$,$Sr = 2.0$, $\alpha_1 = 1$, $\alpha_2 = 1$, $Fs = 0.5$ and $\xi = 0.5$. As Ω increases, there is a reduction in g^* component in the direction of displacement of the plate by angle Ω and this degrades the buoyancy force in that direction. Hence, the reduction in the buoyancy leads to diminish heat and mass transfer rates when the inclined plate changes from vertical to horizontal position. One can notice that an enhancement in the Biot number causes an increase in $Nu_x Pe^{-1/2}$, whereas it decreases $Sh_x Pe^{-1/2}$. Further, the power-law index results in an improvement in $Sh_x Pe^{-1/2}$ for an isothermal condition, whereas $Sh_x Pe^{-1/2}$ has the opposite trend in the case of non-isothermal condition.

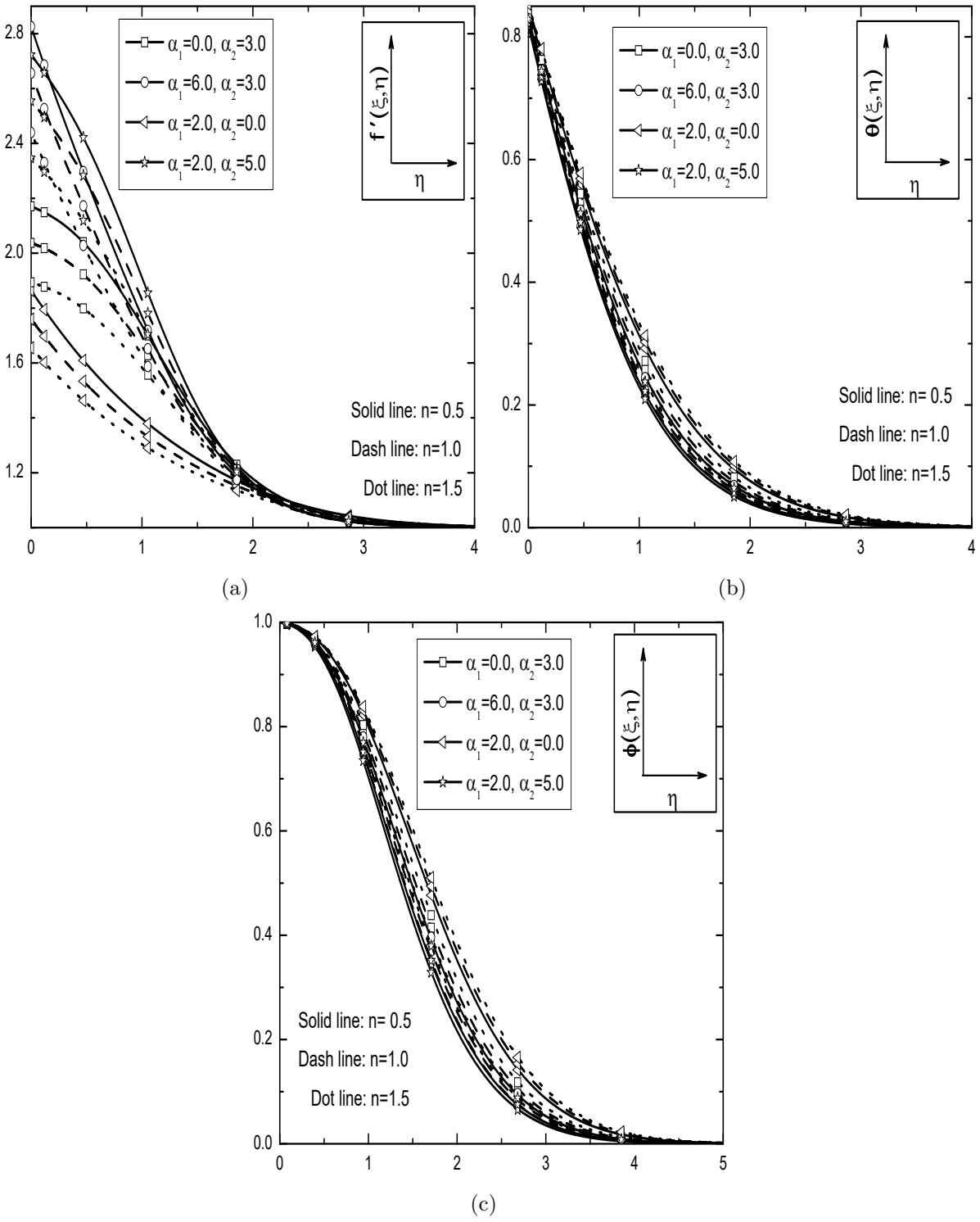

Figure 6.7: *Effects of* α_1 *and* α_2 *for different values of* n *on the (a) velocity, (b) temperature and (c) concentration with the fixed values of* $Bi = 0.5$, $Du = 0.03$, $Sr = 2.0$, $\Omega = 30^0$ *and* $\xi = 0.5$.

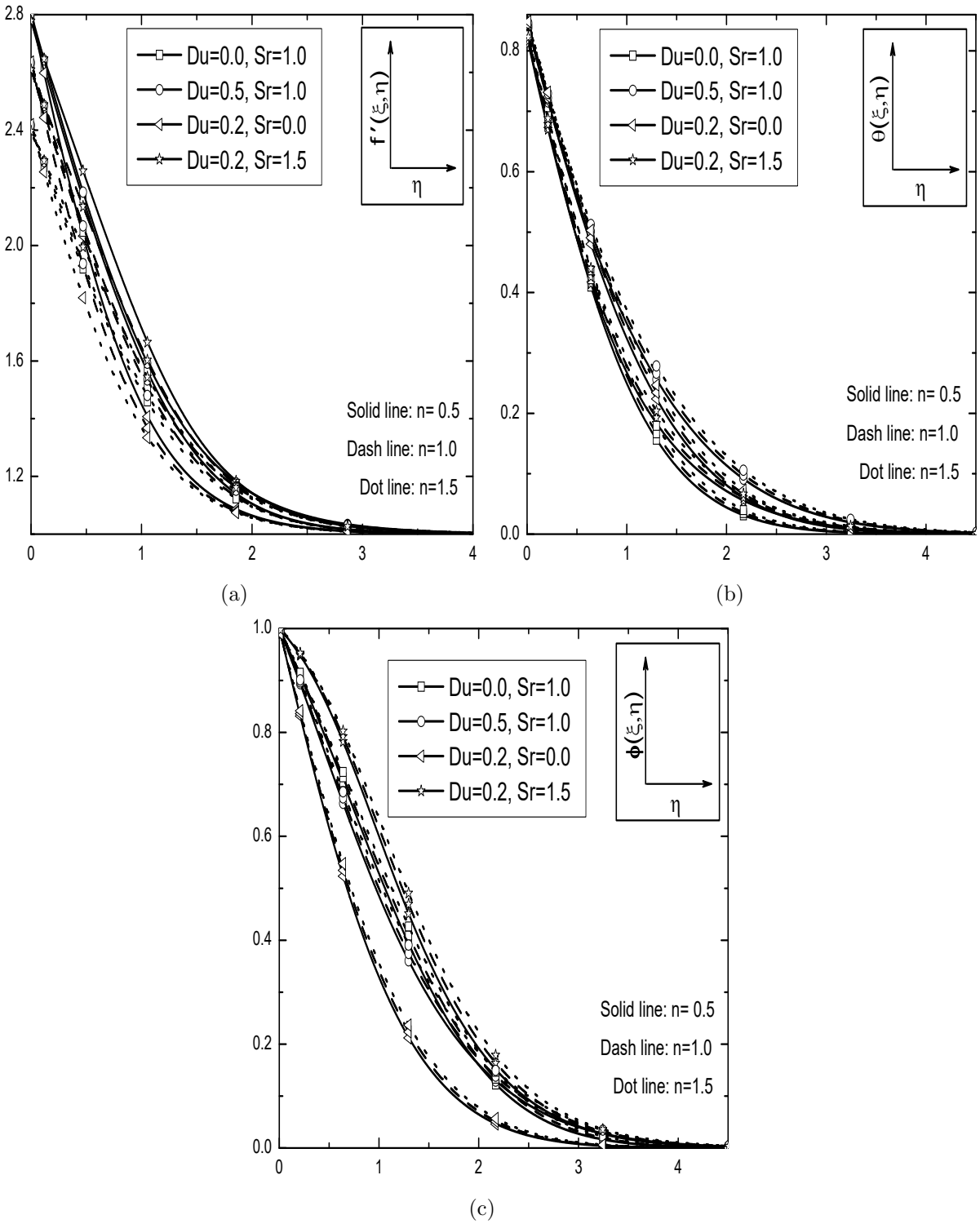

Figure 6.8: *Effects of Du and Sr for different values of n on the (a) velocity, (b) temperature and (c) concentration with the fixed values of* $Bi = 0.5$, $\alpha_1 = 1$, $\alpha_2 = 1$, $\Omega = 30^0$ *and* $\xi = 0.5$.

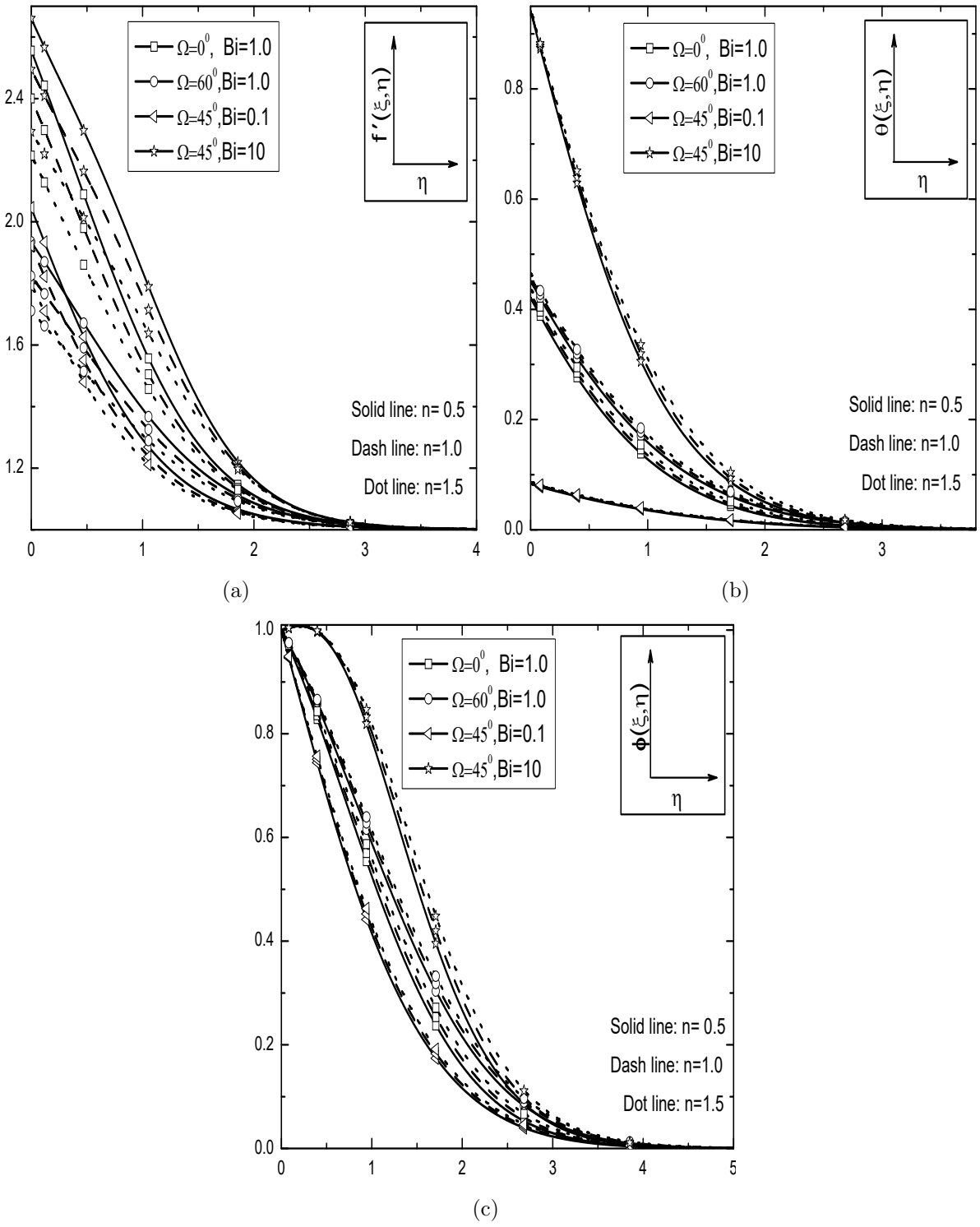

Figure 6.9: *Effects of* Ω *and* Bi *for different values of* n *on the (a) velocity, (b) temperature and (c) concentration with the fixed values of* $\alpha_1 = 1$, $\alpha_2 = 1$, $Du = 0.03$, $Sr = 2.0$ *and* $\xi = 0.5$.

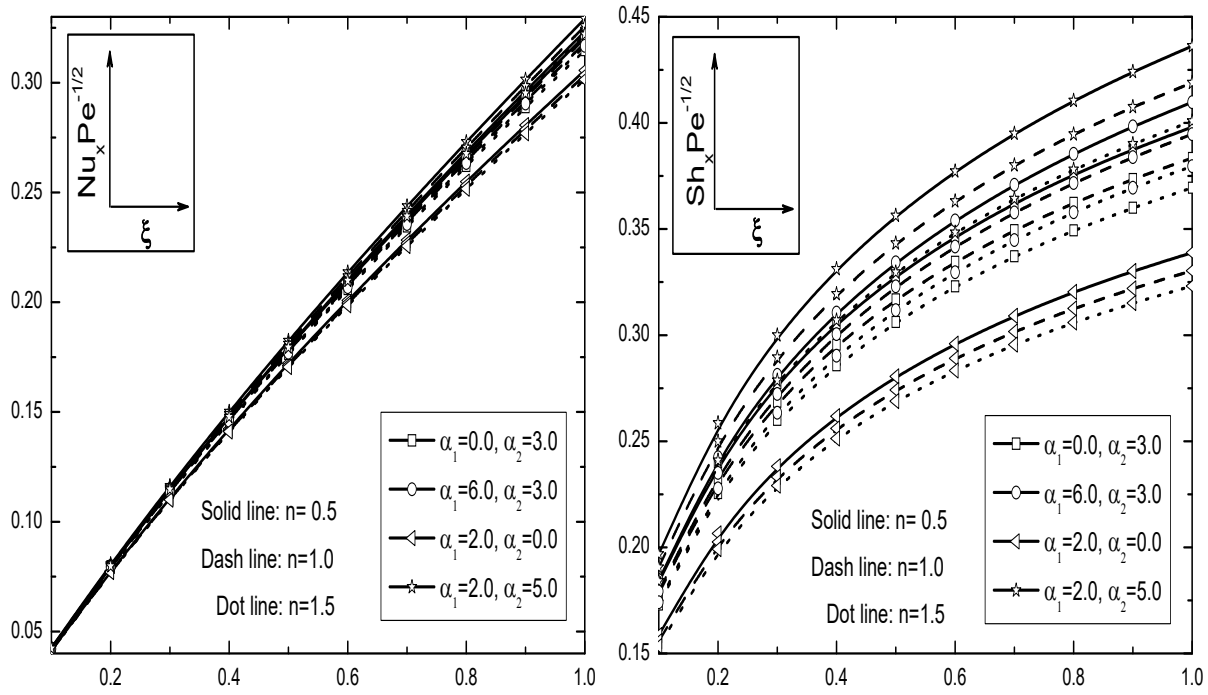

(a) (b)

Figure 6.10: *Effects of α_1 and α_2 for different values of n on the (a) heat transfer rate and (b) mass transfer rate against ξ with the fixed values of $Bi = 1$, $Du = 0.03$, $Sr = 2.0$ and $\Omega = 30^0$.*

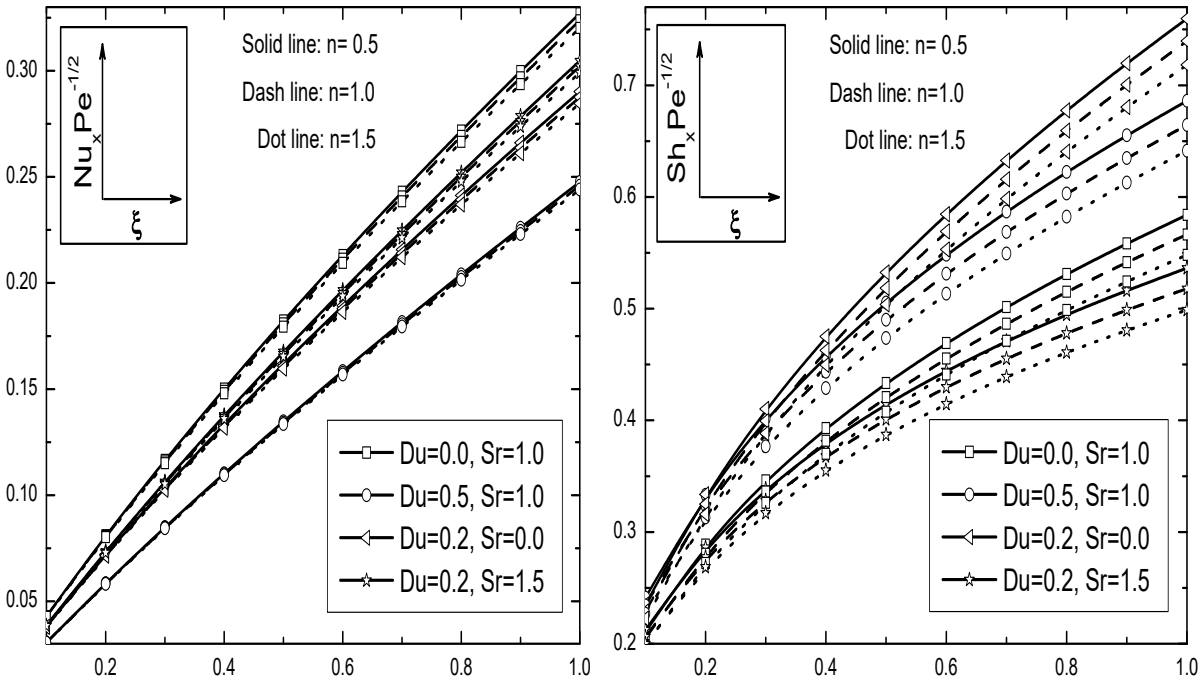

Figure 6.11: *Effects of Du and Sr for different values of n on the (a) heat transfer rate and (b) mass transfer rate against ξ with the fixed values of $Bi = 1$, $\alpha_1 = 1$, $\alpha_2 = 1$ and $\Omega = 30^0$.*

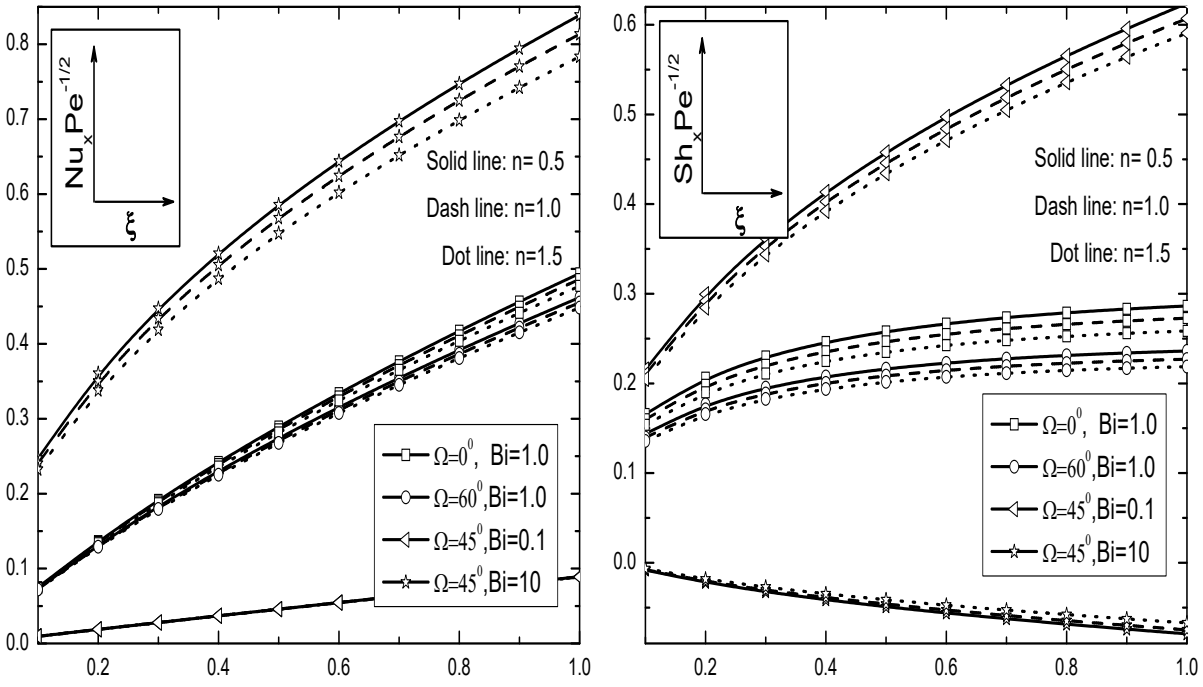

(a) (b)

Figure 6.12: *Effects of* Ω *and* Bi *for different values of* n *on the (a) heat transfer rate and (b) mass transfer rate against* ξ *with the fixed values of* $\alpha_1 = 1$, $\alpha_2 = 1$, $Du = 0.03$ *and* $Sr = 2.0$.

6.3 Conclusions

In this chapter, the non-similarity solution is obtained to analyze the effects of cross-diffusion and convective boundary condition on the nonlinear convective flow of a power-law fluid along the inclined plate in a non-Darcy porous medium. From this analysis, the main findings are drawn in both cases (a) and (b) as follows:

An increase in nonlinear convection parameters leads to increase the local Nusselt and Sherwood numbers, but it decreases the temperature and concentration in both case (a) and case (b). Further, the tangential velocity increases at the wall in both the cases (a) and (b), but it shows opposite trend in case (b) far away from the inclined plate. With the increase of Biot number, the tangential velocity, temperature and local Nusselt number enhance, but the local Sherwood number reduces in both case (a) and case (b). As the angle of inclination increases, the local Nusselt and Sherwood numbers reduce, but the temperature and concentration enhance. In addition, the tangential velocity decreases in the cases (a) and (b) at the wall, while it shows a reverse trend far away from the inclined plate in the case (b). The presence of Soret parameter increases the local heat transfer rate but decreases the local mass transfer rate. The local heat transfer rate is decreased and local mass transfer rate is increased due to the presence of Dufour parameter. Moreover, the higher Nusselt and lower Sherwood numbers are found for the case (b) when compared to those of the case (a).

Chapter 7

Effects of Double Dispersion in a Non-Darcy Porous Medium Saturated with a Power-law Fluid subject to Convective Boundary Condition [1]

7.1 Introduction

Power-law fluid flow through porous media has gained immense importance as a consequence of its wide range of applications in energy and geophysical industries, for example, thermal insulation, filtration processes, geophysical flows, petroleum resource, polymer processing and so forth. Extensive research has been considered on free/mixed convective flow of a power-law fluid through different geometries embedded in a Darcy/non-Darcy porous medium by [29, 49, 73]. Several works have been made in recent years to investigate the problem of convective flow over an inclined plate in various Newtonian and non-Newtonian fluids due to its geophysical and industrial applications. These applications include chemical processing, electrical systems, iron removal, brine clarification, etc. In view of the above said applications, Pal and Chatterjee [78] analyzed non-Newtonian fluid

[1]Case(a): Published in "**Journal of Nanofluids**" 7(6) (2018) 1247–1257, Case(b): Accepted by "**4th Thermal and Fluids Engineering Conference (TFEC) April 14–17, 2019 Las Vegas, NV, USA**".

flow characteristics along an inclined plate under variable thermal conductivity.

The thermal and solutal transport due to the hydrodynamic mixing is called thermal and solutal dispersions or double dispersion effects. The effects of thermal and solutal dispersions in a porous medium is necessary due to the presence of inertial effects [75]. Kairi *et al.* [53] examined importance of these effects on the natural convective flow of a power-law fluid in a non-Darcy porous medium (see also, the references therein). Narayana and Sibanda [74] analyzed the double dispersion effects on MHD mixed convective flow along a vertical flat plate embedded in a non-Darcy porous medium. The combined convective heat and mass transfers along a vertical surface in a non-Darcy porous medium in the presence of double dispersion effects, has been discussed by Afify and Elgazery [2].

Survey on earlier studies reveals that the effect of double dispersion on the convective heat and mass transfer in non-Newtonian fluids saturated non-Darcy porous medium has been investigated by very few authors. Also, the concept of natural and mixed convective flows of a power-law fluid over an inclined plate in a non-Dary porous medium with convective heating and double dispersion effects, is not examined so far. Hence, the present chapter aims to analyze the influence of double dispersion effects on the nonlinear convective flow over an inclined plate in a non-Darcy porous medium saturated with a power-law fluid. The effects of pertinent parameters on the physical quantities are studied, and the results are displayed graphically.

7.2 Mathematical Formulation

Consider an incompressible power-law fluid flow along an inclined plate embedded in a non-Darcy porous medium and flow is assumed to be two-dimensional, steady and laminar. The semi-infinite plate is inclined about vertical direction with an angle Ω as shown in Fig.(2.1). It is known from the literature that in a non-Darcy medium where the inertial effects are prevalent, the thermal and solutal dispersion effects will become significant in natural and mixed convective flows [75]. Due to this importance, the thermal and solutal dispersion effects are incorporated in the governing equations of the power-law fluid. Further, this chapter is an extension of chapter-5 by considering the double dispersion effects.

Under the consideration of assumptions made in chapter-5 along with the nonlinear Boussinesq approximation, the governing equations for the power-law fluid flow in a homogeneous and isotropic

non-Darcy porous medium (Forchheimer model), are given by

$$\frac{\partial u}{\partial x}+\frac{\partial v}{\partial y}=0 \tag{7.1}$$

$$\frac{\partial u^n}{\partial y}+\frac{b\sqrt{K_p}}{\nu}\frac{\partial u^2}{\partial y}=\frac{K_p g^*}{\nu}\left\{\left[\beta_0+2\beta_1(T-T_\infty)\right]\frac{\partial T}{\partial y}+\left[\beta_2+2\beta_3(C-C_\infty)\right]\frac{\partial C}{\partial y}\right\}\cos\Omega \tag{7.2}$$

$$u\frac{\partial T}{\partial x}+v\frac{\partial T}{\partial y}=\frac{\partial}{\partial y}\left[\alpha_e\frac{\partial T}{\partial y}\right] \tag{7.3}$$

$$u\frac{\partial C}{\partial x}+v\frac{\partial C}{\partial y}=\frac{\partial}{\partial y}\left[D_e\frac{\partial C}{\partial y}\right] \tag{7.4}$$

along with the boundary conditions

$$\begin{aligned} v=0,\ \ -k_f\frac{\partial T}{\partial y}=h_f(T_f-T),\ \ C=C_w \quad \text{at} \quad y=0 \\ u=u_\infty,\ \ T=T_\infty,\ \ C=C_\infty \quad \text{as} \quad y\to\infty \end{aligned} \tag{7.5}$$

where α is the molecular thermal diffusivity, D is the molecular solutal diffusivity, χ is the thermal dispersion coefficient, d is the pore diameter and ζ is the solutal dispersion coefficient. Further, the effective thermal and solutal diffusivities are defined as $\alpha_e=\alpha+\chi\,d\,u$ and $D_e=D+\zeta\,d\,u$ (Telles and Trevisan [104], Murthy [67]), respectively.

In this chapter also, two types (cases) of problems are considered: (a) free/natural convection and (b) mixed convection.

7.2.1 Case(a): Natural Convection

As in the earlier chapters, the flow is assumed to be a natural convective flow which is caused by only buoyancy forces and without any external agent. Hence, the velocity of the external flow becomes zero. To convert the system of dimensional equations (7.1) - (7.4) into the non-dimensional form, we considered the following dimensionless transformations

$$\begin{aligned} \xi=\frac{x}{L},\ \ \eta=\frac{y}{L}\,Ra^{\frac{1}{2}}\,\xi^{\frac{-1}{2}},\ \ \psi(\xi,\eta)=\alpha\,\xi^{\frac{1}{2}}\,Ra^{\frac{1}{2}}\,f(\xi,\eta) \\ T(\xi,\eta)=T_\infty+(T_f-T_\infty)\,\theta(\xi,\eta),\quad C(\xi,\eta)=C_\infty+(C_w-C_\infty)\,\phi(\xi,\eta) \end{aligned} \tag{7.6}$$

Substituting the stream function (2.7) and the transformations (7.6) into Eqs.(7.2) - (7.4), we obtain the following momentum, energy and concentration equations

$$n\,\left(f'\right)^{n-1}f''+2Gr^{*}f'f''=\left[(1+2\,\alpha_1\theta)\theta'+\mathcal{B}(1+2\,\alpha_2\phi)\phi'\right]\cos\Omega \tag{7.7}$$

$$\theta''+\,D_s\,\left(f'\,\theta'\right)'+\frac{1}{2}f\theta'=\xi\left(f'\frac{\partial\theta}{\partial\xi}-\frac{\partial f}{\partial\xi}\theta'\right) \tag{7.8}$$

$$\frac{1}{Le}\phi''+\,D_c\,\left(f'\,\phi'\right)'+\frac{1}{2}f\phi'=\xi\left(f'\frac{\partial\phi}{\partial\xi}-\frac{\partial f}{\partial\xi}\phi'\right) \tag{7.9}$$

Boundary conditions (7.5) in terms of f, θ, and ϕ can be written as

$$\begin{aligned} f(\xi,0)=-2\,\xi\left(\frac{\partial f}{\partial\xi}\right)_{\eta=0},\ \theta'(\xi,0)=-Bi\,\xi^{\frac{1}{2}}\left[1-\theta(\xi,0)\right],\phi(\xi,0)=1,\\ f'(\xi,\infty)=0,\ \theta(\xi,\infty)=0,\ \phi(\xi,\infty)=0. \end{aligned} \tag{7.10}$$

In the above equations, $Ra_d=\dfrac{d\,Ra}{L}$ is the modified pore-diameter-dependent Rayleigh number, $D_s=\chi Ra_d$ is the thermal dispersion parameter and $D_c=\zeta\,Ra_d$ is the solutal dispersion parameter.

The physical quantities of present interest such as heat and mass transfer rates, are defined as

$$Nu_x=-\frac{x}{k_f(T_f-T_\infty)}\left[k_e\frac{\partial T}{\partial y}\right]_{y=0},\ Sh_x=-\frac{x}{D(C_w-C_\infty)}\left[D_e\frac{\partial C}{\partial y}\right]_{y=0} \tag{7.11}$$

The non-dimensional local Nusselt number Nu_x and the Sherwood number Sh_x, are given by

$$Nu_xRa^{\frac{1}{2}}=-\xi^{\frac{1}{2}}\,\left[1\,+\,D_s\,f'(\xi,\,0)\right]\theta'(\xi,\,0),\ Sh_xRa^{\frac{-1}{2}}=-\xi^{\frac{1}{2}}\,\left[1\,+\,D_c\,f'(\xi,\,0)\right]\,\phi'(\xi,\,0). \tag{7.12}$$

Results and Discussion

The reduced governing Eqs.(7.7)-(7.9) along with the boundary conditions (7.10) are solved numerically by using the successive linearization method together with the local similarity and non-similarity approaches, as explained in the case (a) of Chapter-2. In the absence of double dispersion effects, this case reduces to the case (a) problem of the chapter-5. Validation of the present problem in this case, can be done on comparison as it was done in the case (a) of chapter-5.

The numerical computations are carried out by following the fixed values of parameters: $Gr^* = 0.5$, $\mathcal{B} = 0.5$, $Le = 1$ and $\xi = 0.5$. These values are continued same throughout this study, unless otherwise specified. The impacts of pertinent parameters such as nonlinear convection parameters (α_1, α_2), double dispersion parameters (D_s, D_c), inclination angle (Ω) and the Biot number (Bi) are discussed through the Figs.7.1(a)-7.6(b) for the boundary layer profiles along with the physical quantities of the flow.

Variations in the fluid flow profiles (such as f', θ and ϕ) for α_1(0, 6), α_2 (0, 5) and n (0.5, 1.0, 1.5) with the fixed values: $D_s = 0.6$, $D_c = 0.3$, $Bi = 0.5$, $\xi = 0.5$ and $\Omega = 30^0$, are considered in the first set of Figs.7.1(a)-7.1(c). With respect to α_1, the dimensionless velocity increases more at the surface of the inclined plate and then it satisfies the free stream condition far away from the wall as portrayed in Fig.7.1(a). Additionally, Figs.7.1(a) displays the influence of α_2 on the behavior of velocity for different values of the power-law index. The results of α_2 repeat the same kind of behavior as α_1 in all three kinds of fluids. The thermal and solutal boundary layer thicknesses diminish with the rise of α_1 or α_2, as displayed in Figs.7.1(b) and 7.1(c) respectively. Evidently, the differences between wall and ambient temperature and concentration increase for larger α_1 and α_2, due to which higher velocity in Figs.7.1(a), and smaller temperature and concentration are noticed in Figs.7.1(b)-7.1(c) respectively. Further, the dominance of α_2 is more on these three boundary layer profiles and in all three kinds of fluids (pseudo-plastic, Newtonian and dilatant fluid) compared to the influence of α_1.

The influences of $\Omega(0^0, 60^0)$ and $Bi(0.05, 0.5)$ on the fluid flow profiles are depicted in the second set of Figs.7.2(a)-7.2(c) for $D_s = 0.3$, $D_c = 0.3$, $\alpha_1 = 1$, $\alpha_2 = 1$ and $\xi = 0.5$ in three instances of power-law index ($n = 0.5, 1.0, 1.5$), separately. An expansion in the value of Ω reduces the velocity distribution inside the boundary layer region as shown in Fig.7.2(a). Also, maximum velocity is noticed near the plate with the rise of Bi and this is due to the reduction in the thermal resistance of the inclined plate. From Figs.7.2(b) and 7.2(c), one can notice that the temperature and concentration enhance with an increase in Ω. Fig.7.2(b) depicts the impact of Bi on the temperature distribution, it shows that the isothermal condition is a limiting case of convective boundary condition. Also, the temperature distribution accelerates on the surface of the plate when Bi increases from the thermally thin case to the thermally thick case. Further, Fig.7.2(c) reveals that the influence of Biot number is considerable on the concentration profile.

The third set of Figs.7.3(a)-7.3(c) exhibits the significance of double dispersion parameters D_s

(0, 5) and D_c (0, 4) on f', θ and ϕ in all three kinds of fluids (pseudo-plastic, Newtonian and dilatant fluids) for the fixed value: $\alpha_1 = 1$, $\alpha_2 = 1$, $Bi = 0.1$, $\xi = 0.5$ and $\Omega = 30^0$. From Fig.7.3(a), it is observed that when either of the dispersion parameters is increased with the other one held fixed (i.e when D_s varies, D_c is fixed and if D_c varies, D_s should be fixed) thickness of the momentum boundary layer increases. An addition in D_s leads to enhance the temperature gradient and decreases solutal boundary layer thickness. Introducing the thermal dispersion effect to the energy equation gives thermal conduction more dominance. That is, thermal dispersion increases the transport of heat along the normal direction to the inclined plate when compared to the case $D_s = 0$. It can be found from Figs.7.3(b)-7.3(c) that, the results of D_c are opposite to D_s influence on these two boundary layer profiles.

The significance of $\alpha_1(0, 6)$ and $\alpha_2(0, 5)$ on the Nusselt number ($Nu_x Ra^{-1/2}$) and Sherwood number ($Sh_x Ra^{-1/2}$) against the stream wise coordinate ξ, are depicted in the fourth set of Figs.7.4(a)-7.4(b) with $D_s = 0.6$, $D_c = 0.3$, $Bi = 0.5$ and $\Omega = 30^0$ for three kinds of fluids. The rise in α_1 or α_2 improves all the pertinent characteristics of the pseudo-plastic fluid flow for the fixed value of α_2 or α_1 individually. Moreover, these quantities have same effect in the Newtonian and dilatant fluid flows. Additionally, the changes in $Nu_x Ra^{-1/2}$ is reverse to the changes of $Sh_x Ra^{-1/2}$ along the stream wise coordinate ξ. However, both heat and mass transfer rates fall down in the presence of both α_1 and α_2 when power-law index changes from $n < 1$ to $n > 1$. But, both heat and mass transfer rates are considerably enhanced in the absence of either α_1 or α_2, when the power-law index varies from $n < 1$ to $n > 1$.

The fifth set of Figs.7.5(a)-7.5(b) describes the impact of $Bi(0.5, 2.0)$ and $\Omega(0^0, 60^0)$ on $Nu_x Ra^{-1/2}$ and $Sh_x Ra^{-1/2}$ for the three fluid cases with $D_s = 0.6$, $D_c = 0.3$, $\alpha_1 = 1$ and $\alpha_2 = 1$. With the increment of Ω, there is a decrement in g^* component and this degrades the buoyancy force. Hence, the reduction in the buoyancy will lead to diminish the heat and mass transfer rates when the inclined plate displaced from the vertical to horizontal position. One can notice that, an enhancement in the Biot number causes an increase in both $Nu_x Ra^{-1/2}$ and $Sh_x Ra^{-1/2}$.

The effects of $D_s(0, 5)$ and $D_c(0, 4)$ on the heat and mass transfer rates are displayed in the sixth set of Figs.7.6(a)-7.6(b) for the fixed values: $\alpha_1 = 1$, $\alpha_2 = 1$, $Bi = 0.1$ and $\Omega = 30^0$. With respect to above said variation in the temperature and concentration variations, higher values of D_s give large expansion in $Nu_x Ra^{-1/2}$ and less change in $Sh_x Ra^{-1/2}$ as shown in Figs.7.6(a)-7.6(b). But, with the expanding D_c, these figures show a reverse trend. That is, an increase in D_c leads to

enhance $Sh_x Ra^{-1/2}$ and shows a nominal influence on $Nu_x Ra^{-1/2}$ as displayed in Figs.7.6(a)-7.6(b). However, the influence of power-law index n is nominal for heat transfer rate and considerable for mass transfer rate, as shown in Figs.7.6(a)-7.6(b).

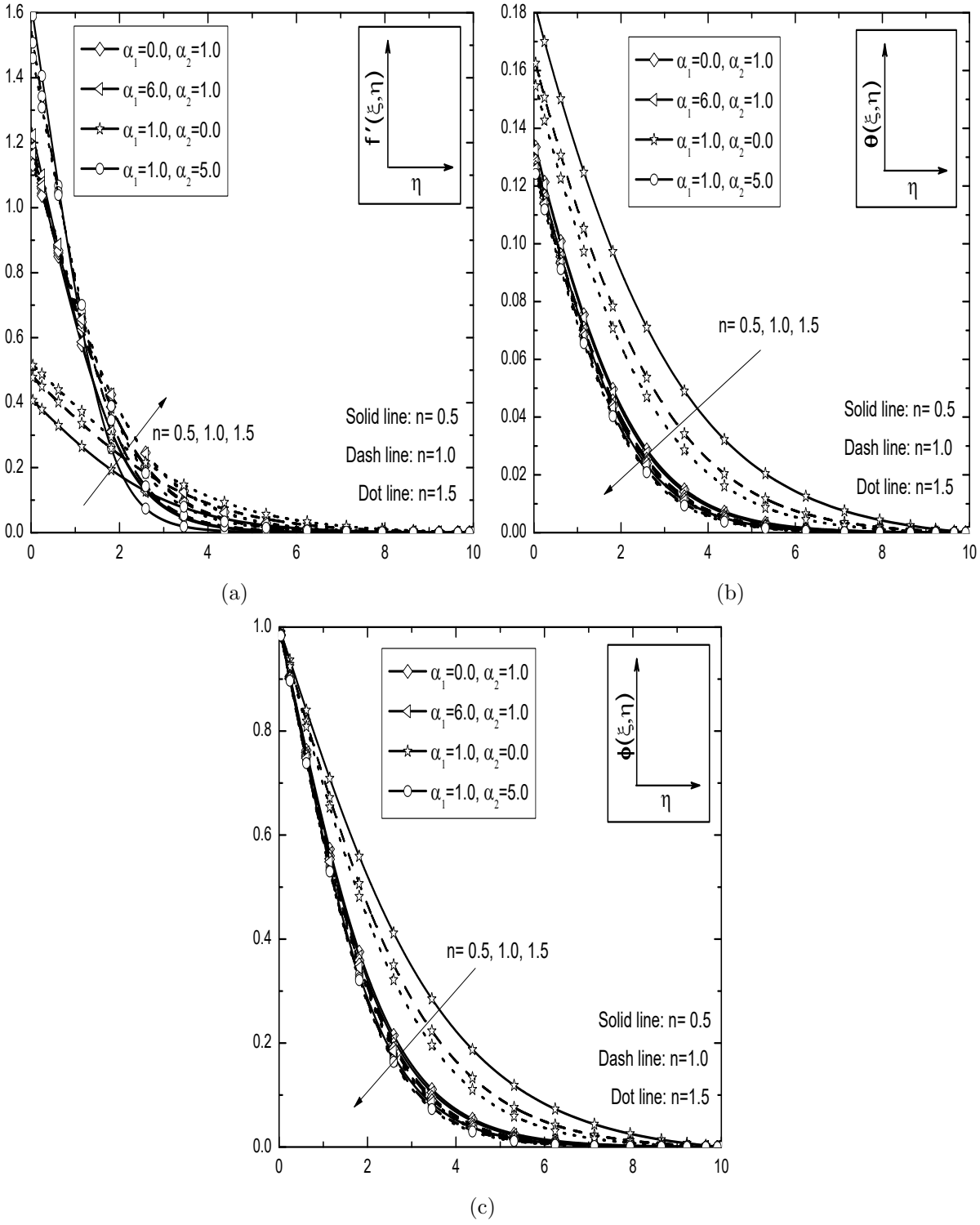

Figure 7.1: *Effects of* α_1 *and* α_2 *for different values of* n *on the (a) velocity, (b) temperature and (c) concentration with the fixed values of* $Bi = 0.5$, $D_s = 0.6$, $D_c = 0.3$, $\Omega = 30^0$ *and* $\xi = 0.5$.

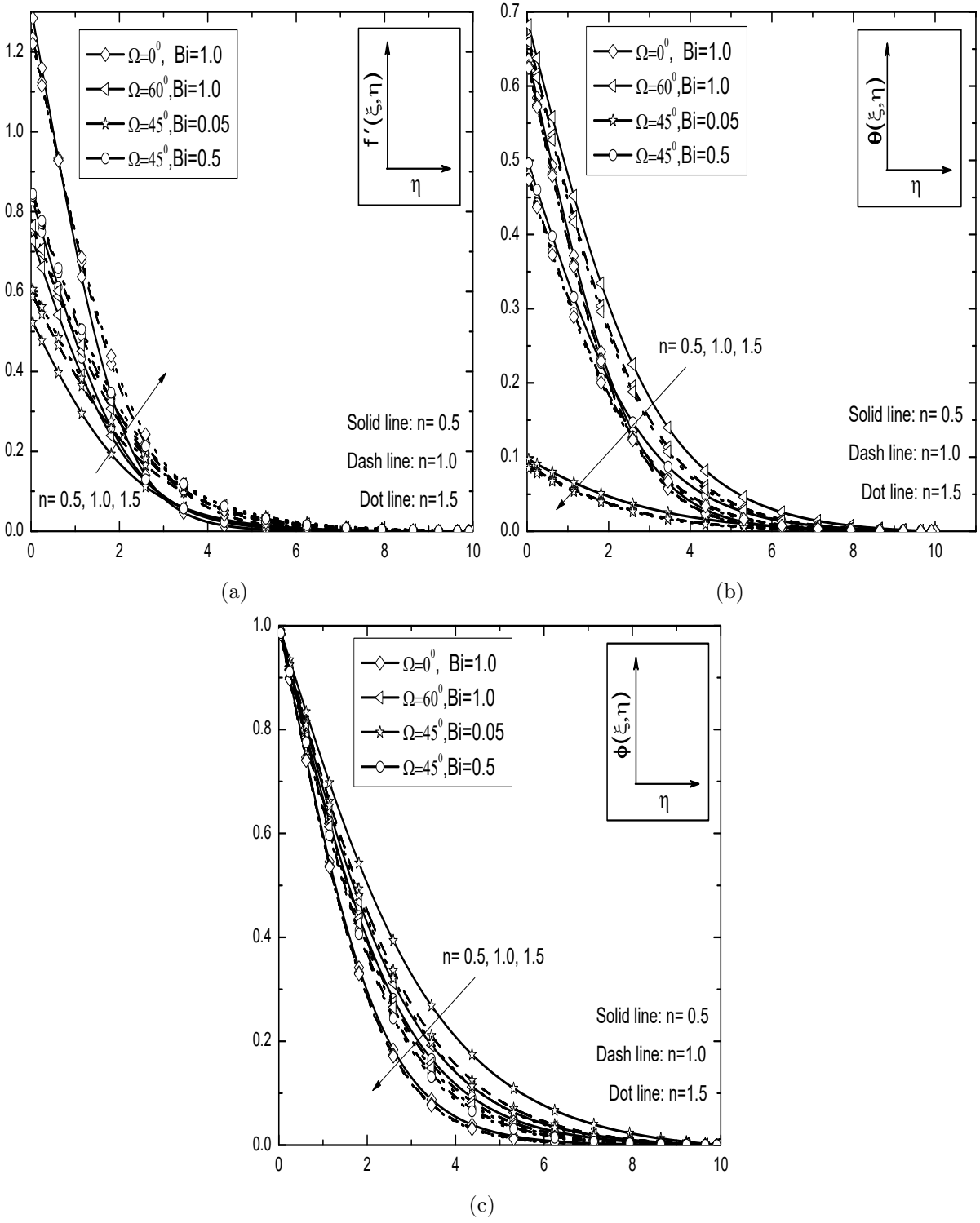

Figure 7.2: *Effects of* Ω *and* Bi *for different values of* n *on the (a) velocity, (b) temperature and (c) concentration with the fixed values of* $\alpha_1 = 1$, $\alpha_2 = 1$, $D_s = 0.6$, $D_c = 0.3$ *and* $\xi = 0.5$.

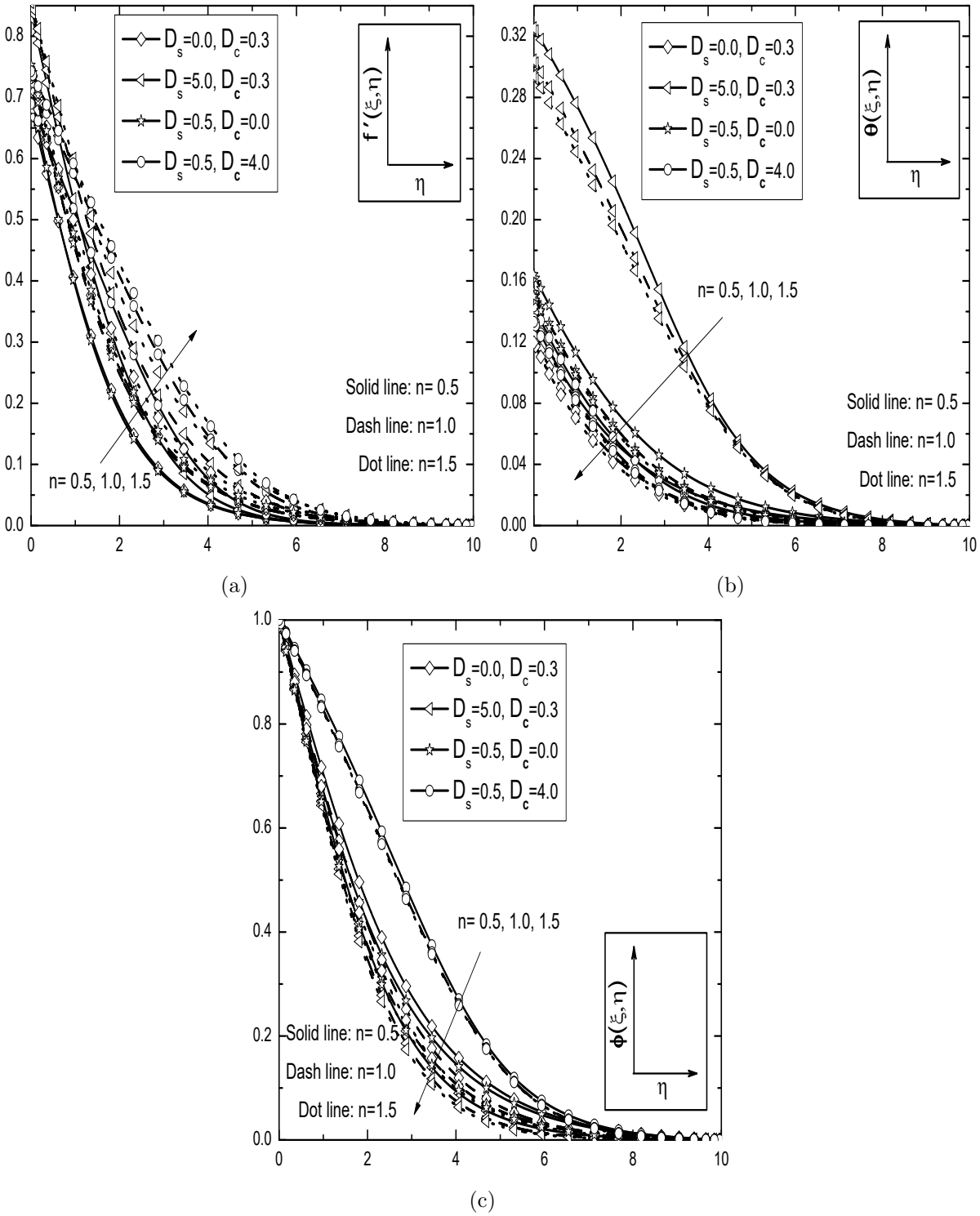

Figure 7.3: *Effects of D_s and D_c for different values of n on the (a) velocity, (b) temperature and (c) concentration with the fixed values of $Bi = 0.1$, $\alpha_1 = 1$, $\alpha_2 = 1$, $\Omega = 30^0$ and $\xi = 0.5$.*

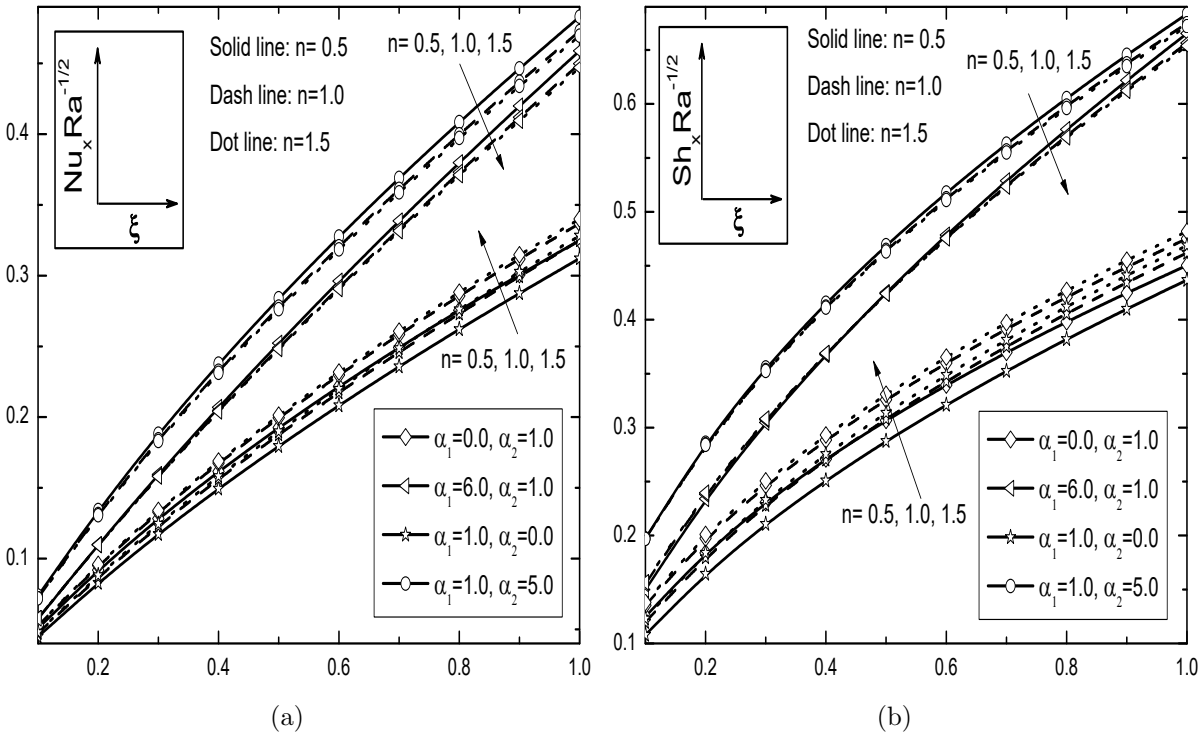

Figure 7.4: *Effects of* α_1 *and* α_2 *for different values of* n *on the (a) Nusselt number and (b) Sherwood number against* ξ *with the fixed values of* $Bi = 0.5$, $D_s = 0.6$, $D_c = 0.3$ *and* $\Omega = 30^0$.

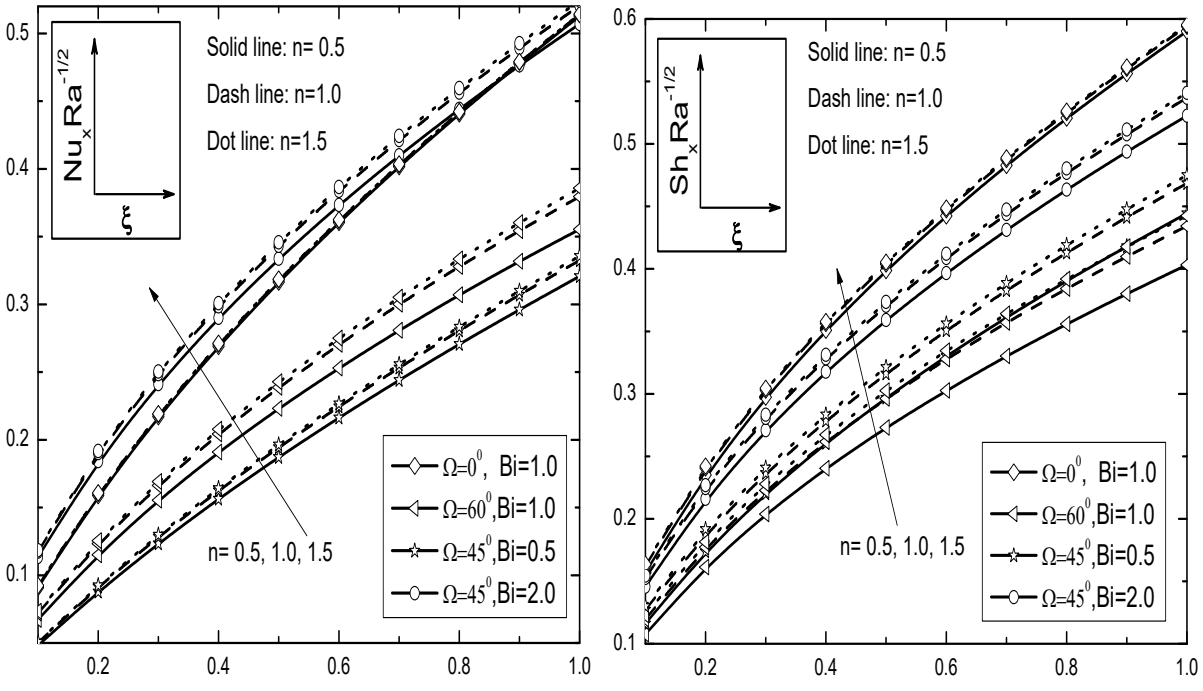

(a) (b)

Figure 7.5: *Effects of* Ω *and* Bi *for different values of* n *on the (a) Nusselt number and (b) Sherwood number against* ξ *with the fixed values of* $\alpha_1 = 1$, $\alpha_2 = 1$, $D_s = 0.6$ *and* $D_c = 0.3$.

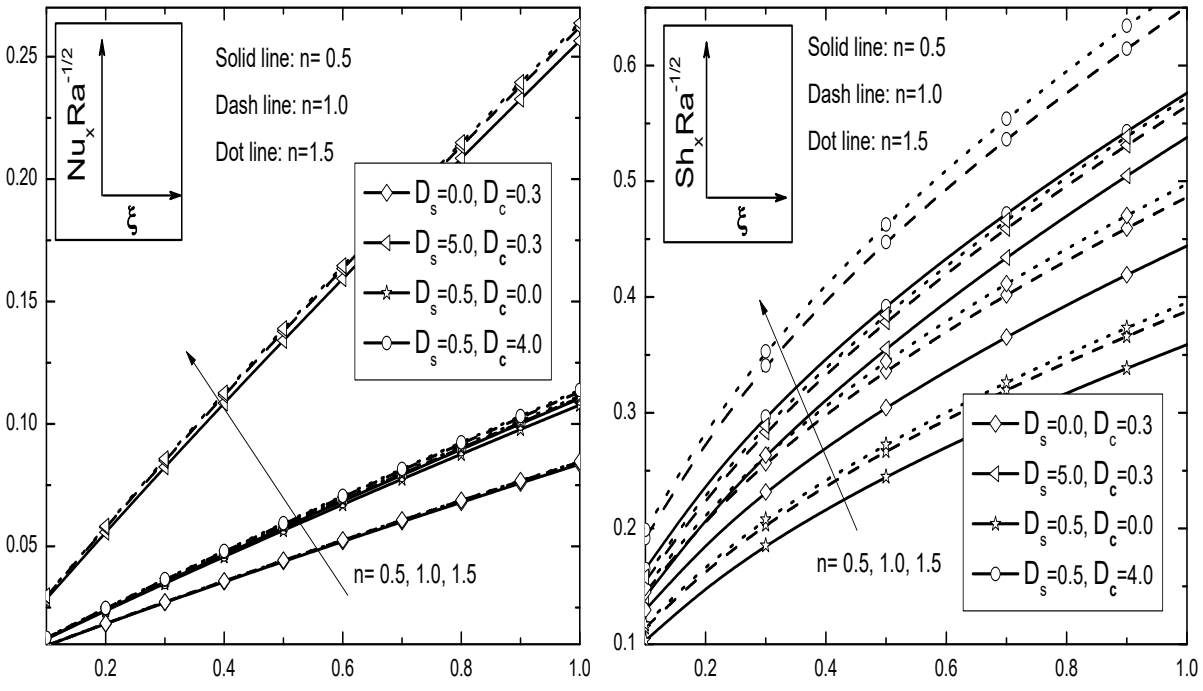

(a) (b)

Figure 7.6: *Effects of* D_s *and* D_c *for different values of* n *on the (a) Nusselt number and (b) Sherwood number against* ξ *with the fixed values of* $Bi = 0.1$, $\alpha_1 = 1$, $\alpha_2 = 1$ *and* $\Omega = 30^0$.

7.2.2 Case(b): Mixed Convection

It is assumed that the mixed convective flow arises from an external flow with the velocity u_∞ and buoyancy forces. We introduce the non-dimensional transformations in the following form

$$\begin{gathered}\xi = \frac{x}{L},\ \ \eta = \frac{y}{L}\, Pe^{\frac{1}{2}}\, \xi^{\frac{-1}{2}}, \psi(\xi,\eta) = \alpha\, \xi^{\frac{1}{2}}\, Pe^{\frac{1}{2}}\, f(\xi,\eta), \\ T(\xi,\eta) = T_\infty + (T_f - T_\infty)\ \theta(\xi,\eta),\ \ \ C(\xi,\eta) = C_\infty + (C_w - C_\infty)\ \phi(\xi,\eta)\end{gathered} \tag{7.13}$$

Substituting stream function (2.7) and the transformations (7.13) into Eqs.(7.1)-(7.4), then the dimensionless form of boundary layer equations can be written as

$$n\ \left(f'\right)^{n-1} f'' + 2Fs f' f'' = (Ri)^n \left[(1 + 2\,\alpha_1\theta)\theta' + \mathcal{B}(1 + 2\,\alpha_2\phi)\phi'\right] \cos\Omega \tag{7.14}$$

$$\theta'' +\ D_s \left(f'\,\theta'\right)' + \frac{1}{2} f\theta' = \xi \left(f' \frac{\partial\theta}{\partial\xi} - \frac{\partial f}{\partial\xi}\theta'\right) \tag{7.15}$$

$$\frac{1}{Le}\phi'' +\ D_c \left(f'\,\phi'\right)' + \frac{1}{2} f\phi' = \xi \left(f' \frac{\partial\phi}{\partial\xi} - \frac{\partial f}{\partial\xi}\phi'\right) \tag{7.16}$$

Boundary conditions (7.5) in terms of f, θ, and ϕ can be written as

$$\begin{gathered}f(\xi,0) = -2\,\xi \left(\frac{\partial f}{\partial\xi}\right)_{\eta=0},\ \ \theta'(\xi,0) = -Bi\,\xi^{\frac{1}{2}}\left[1 - \theta(\xi,0)\right], \phi(\xi,0) = 1, \\ f'(\xi,\infty) = 1,\ \ \theta(\xi,\infty) = 0,\ \ \phi(\xi,\infty) = 0.\end{gathered} \tag{7.17}$$

Here, $D_s = \dfrac{\chi\, d\, u_\infty}{\alpha}$ is the thermal dispersion parameter and $D_c = \dfrac{\zeta\, d\, u_\infty}{\alpha}$ is the solutal dispersion parameter.

The physical quantities of present interest, namely, the non-dimensional Nusselt and Sherwood numbers are given by

$$Nu_x Pe^{\frac{-1}{2}} = -\xi^{\frac{1}{2}}\ \left[1 + D_s\, f'(\xi,\,0)\right] \theta'(\xi,\,0),\ \ \ Sh_x Pe^{\frac{-1}{2}} = -\xi^{\frac{1}{2}}\ \left[1 + D_c\, f'(\xi,\,0)\right]\ \phi'(\xi,\,0). \tag{7.18}$$

Results and Discussion

As explained in the Chapter-2 for case (a) problem, in this chapter also, the numerical solution for the highly nonlinear coupled partial differential equations (7.14)-(7.16) subject to the boundary conditions (7.17) is obtained by using the successive linearization together with local similarity and non-similarity approaches. In the absence of double dispersion effects, this case reduces to the case (b) problem of the chapter-5. Validation of the present problem in this case, can be done on comparison as it was done in the case (b) of chapter-5.

The numerical computations are carried out by following the fixed values of parameters: $\mathcal{B} = 1$, $Fs = 1$, Pr $= 1$, $Le = 1$, $Ri = 0.5$ and $\xi = 0.5$. These values remains unchanged in this study, unless otherwise specified. The influences of the pertinent parameters α_1, α_2, D_s, D_c, Ω and Bi are determined through Figs.7.7(a)-7.12(b) for the boundary layer profiles (such as f', θ and ϕ) and the physical quantities of the fluid flow such as the Nusselt and Sherwood numbers (i.e, $Nu_x\, Pe^{\frac{-1}{2}}$ and $Sh_x\, Pe^{\frac{-1}{2}}$).

Influences of $\alpha_1(0,\, 6)$, α_2 $(0,\, 5)$ and n $(0.5,\, 1.0,\, 1.5)$ on the velocity, temperature and concentration profiles, are depicted through Figs.7.7(a)-7.7(c) with the fixed values: $D_s = 0.5$, $D_c = 0.2$, $Bi = 0.5$, $\xi = 0.5$ and $\Omega = 30^0$. It is observed that, the dimensionless velocity increases more at the surface of the inclined plate and it reaches unity to satisfy the free stream boundary condition for η_{max} value with the increase α_1, as shown in Fig.7.7(a). Additionally, Fig.7.7(a) displays the impact of α_2 on the behavior of velocity. The results of this figure repeat the same kind of behavior just like α_1 in all three kinds of fluids. The thermal and solutal boundary layer thicknesses diminish with the rise of either α_1 or α_2 and the same effect is displayed in Figs.7.7(b) and 7.7(c). Obviously, the nonlinear temperature and concentration differences between the wall and ambient medium increase for larger values of α_1 and α_2, due to which higher velocity, smaller temperature and concentration are obtained. Further, the influence of α_2 is more on these three boundary layer profiles in all three kinds of fluids (pseudo-plastic, Newtonian and dilatant fluid) compared with α_1 influence.

The influences of $\Omega(0^0, 60^0)$ and $Bi(0.1, 10)$ on the profiles of f', θ and ϕ are plotted through Figs.7.8(a)-7.8(c) for three instances of power-law index ($n = 0.5, 1.0, 1.5$). Due to the reduction in the thermal and solutal buoyancy effect in Eq.(7.2) caused by an increase in Ω, there is a reduction in the velocity distribution f' within the boundary layer, as shown in Fig.7.8(b). In other words,

an increase in the inclination angle leads to reduce the velocity distribution within the boundary layer and the most extreme buoyancy force occur for the vertical plate ($\Omega = 0^0$). Also, one can see from Fig.7.8(a) that, the velocity of the power-law fluid increases with a rise in Bi and this is due to the reduction in the thermal resistance of the inclined plate ($\Omega = 60^0$). From Figs.7.8(b) and 7.8(c), one can notice that the temperature θ and concentration ϕ enhance with a rise in Ω. Fig.7.8(b) shows the impact of Bi on the temperature distribution and shows two results mainly for the wall condition and non-isothermal condition. The convective thermal condition is changes into wall condition when $Bi \to \infty$ (i.e for a larger value of Bi) as given by Aziz [13] and the same result is observed in Fig.7.8(b). Also, the temperature distribution accelerates on the surface of the plate when Bi increases from the thermally thin case ($Bi < 0.1$) to the thermally thick case ($Bi > 0.1$). Further, Fig.7.8(c) reveals that the concentration profile decreases with the increase of Biot number.

Figures 7.9(a)-7.9(c) exhibit the significance of double dispersion parameters $D_s(0, 4)$ and $D_c(0, 6)$ on f', θ and ϕ in all three kinds of fluids (pseudo-plastic, Newtonian and dilatant fluids) for the fixed values: $\alpha_1 = 1$, $\alpha_2 = 1$, $Bi = 0.3$, $\xi = 0.5$ and $\Omega = 30^0$. From Fig.7.9(a), it is significant that, for an individual improvement of double dispersion parameters (i.e., when D_s varies, D_c is fixed and if D_c varies, D_s should be fixed), thickness of the momentum boundary layer increases. The addition in D_s leads to enhance the temperature extensively and decreases solutal boundary layer thickness nominally, while the results of D_c are opposite to D_s for these two boundary layer profiles. However, in the absence or presence of double dispersion parameters, the temperature and concentration profiles increase for power-law index n.

Figures 7.10(a)-7.10(b) show the effects of $\alpha_1(0, 6)$ and $\alpha_2(0, 5)$ on the Nusselt number ($Nu_x Pe^{-1/2}$) and Sherwood number ($Sh_x Pe^{-1/2}$) against the stream-wise coordinate ξ. The rise in either α_1 or α_2 improves all the pertinent characteristics of the pseudo-plastic fluid flow for the fixed value of other parameters. Also, these quantities have the same change in the Newtonian and dilatant fluid flows. It is observed that, these two quantities are qualitatively equal with the findings of Partha [79] in Newtonian fluid (for $n = 1$) case. However, both heat and mass transfer rates fall down for the fixed values of either α_1 or α_2 when power-law index moves from $n < 1$ to $n > 1$.

Figures 7.11(a)-7.11(b) delineate the impact of $Bi(0.1, 10)$ and $\Omega(0^0, 60^0)$ on $Nu_x Pe^{-1/2}$ and $Sh_x Pe^{-1/2}$ for three fluid cases with $D_s = 0.6$, $D_c = 0.3$, $\alpha_1 = 1$, $\alpha_2 = 1$. When the inclined plate is displaced from vertical to horizontal position, there is a decrement in $g^* cos\Omega$ component

and this degrades the buoyancy force. Hence, the reduction in the buoyancy will lead to diminish $Nu_x Pe^{-1/2}$ and $Sh_x Pe^{-1/2}$. However, the heat and mass transfer rates are increase with the rise of Bi and decrease with power-law index n.

The effects of $D_s(0,4)$ and $D_c(0,6)$ on the heat and mass transfer rates are displayed in Figs.7.12(a)-7.12(b) with $\alpha_1 = 1$, $\alpha_2 = 1$, $Bi = 0.2$ and $\Omega = 30^0$. With respect to above-said variation in the temperature and concentration profiles, thermal dispersion favors the heat transfer and solutal dispersion favors the mass transfer as shown in Figs.7.12(a)-7.12(b). However, these two transfer rates are more in pseudo-plastic fluids when compared with Newtonian and dilatant fluids. Also, the variation of the power-law index is extensive and diminishes the momentum boundary layer thickness, whereas it enhances thermal and solutal boundary layer thicknesses as displayed in the profiles (see. Figs. 7.9(a)-7.9(c)).

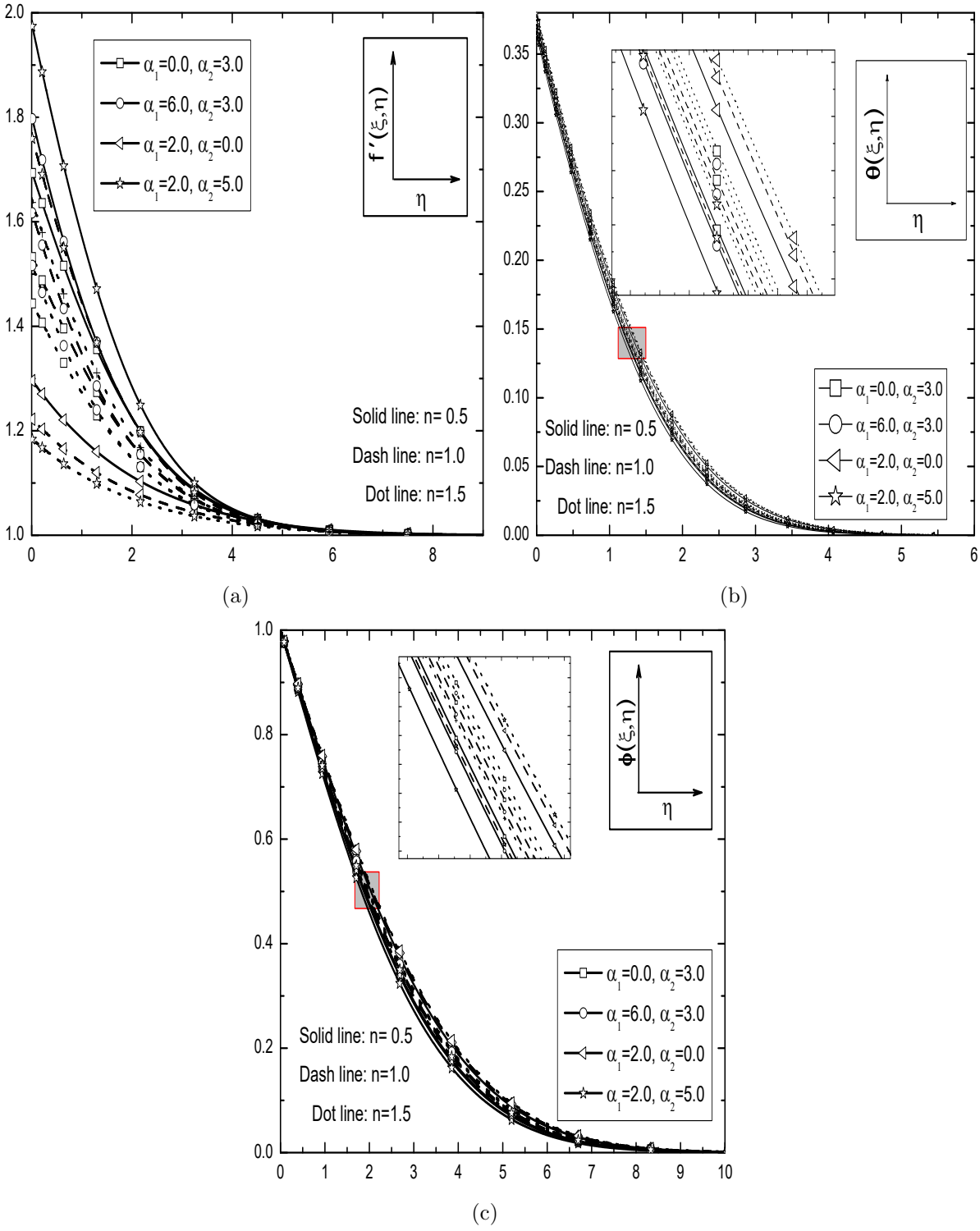

Figure 7.7: *Effects of* α_1 *and* α_2 *for different values of* n *on the (a) velocity, (b) temperature and (c) concentration with the fixed values of* $Bi = 0.5$, $D_s = 0.6$, $D_c = 0.3$, $\Omega = 30^0$ *and* $\xi = 0.5$.

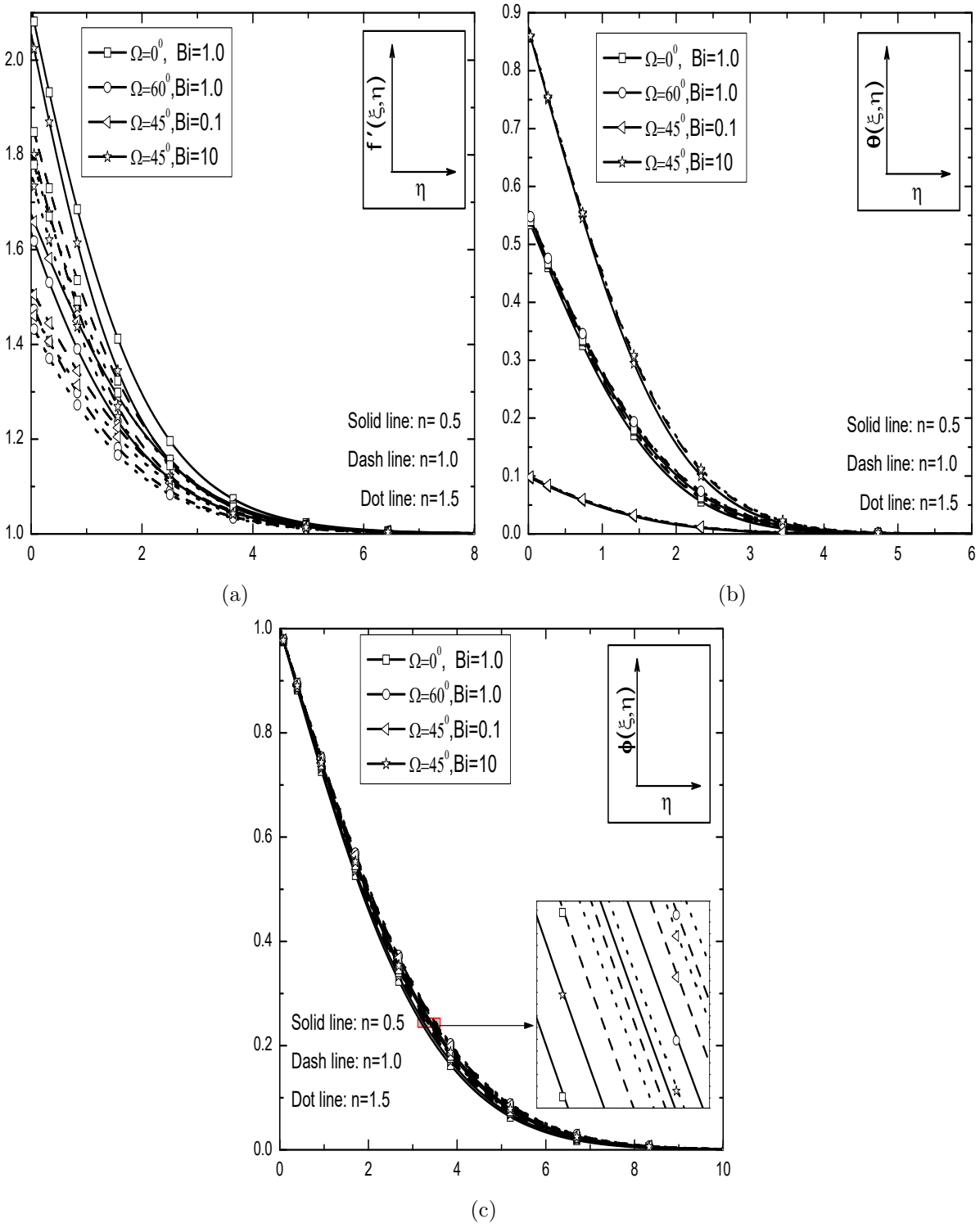

Figure 7.8: *Effects of* Ω *and* Bi *for different values of* n *on the (a) velocity, (b) temperature and (c) concentration with the fixed values of* $\alpha_1 = 1$, $\alpha_2 = 1$, $D_s = 0.6$, $D_c = 0.3$ *and* $\xi = 0.5$.

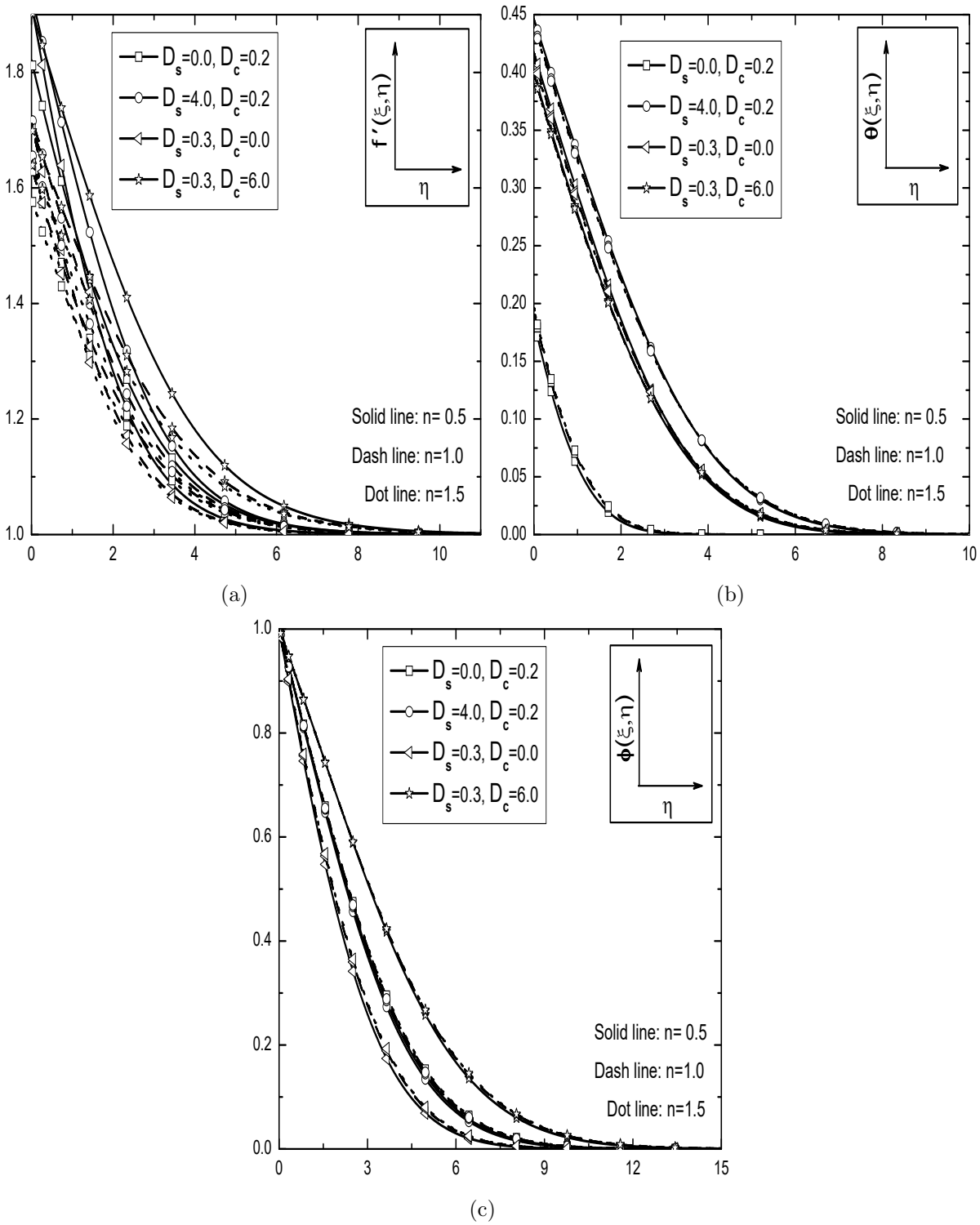

Figure 7.9: *Effects of D_s and D_c for different values of n on the (a) velocity, (b) temperature and (c) concentration with the fixed values of $Bi = 0.1$, $\alpha_1 = 1$, $\alpha_2 = 1$, $\Omega = 30^0$ and $\xi = 0.5$.*

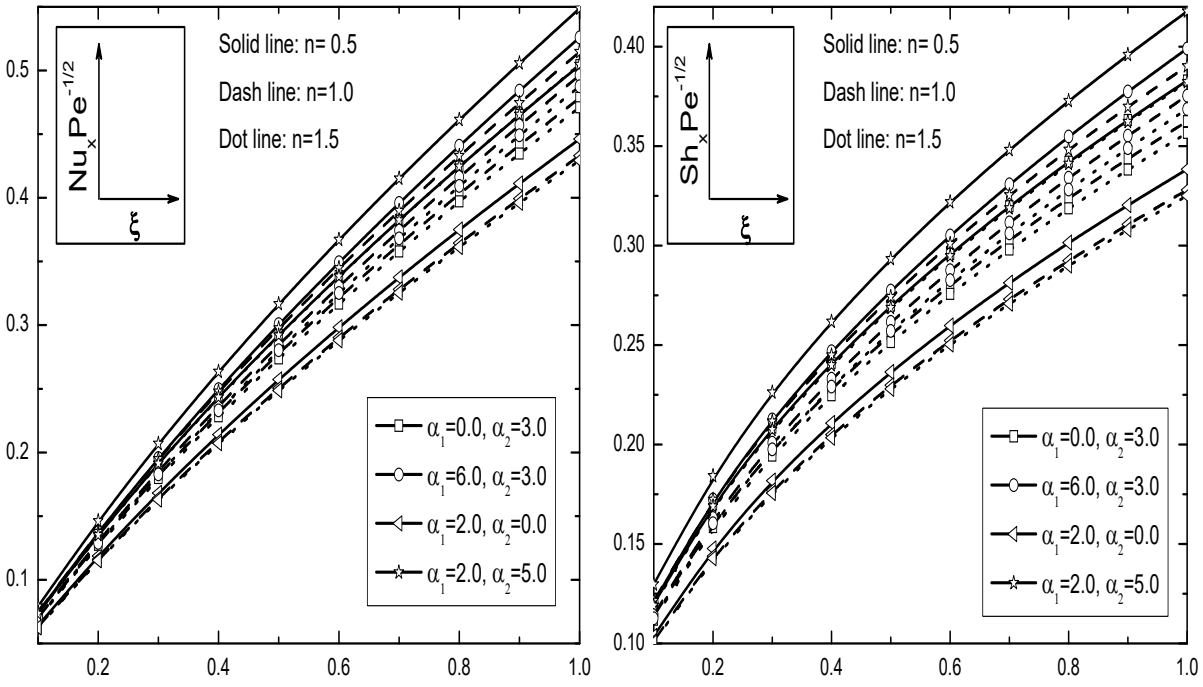

Figure 7.10: *Effects of* α_1 *and* α_2 *for different values of* n *on the (a) Nusselt number and (b) Sherwood number against* ξ *with the fixed values of* $Bi = 0.5$, $D_s = 0.6$, $D_c = 0.3$ *and* $\Omega = 30^0$.

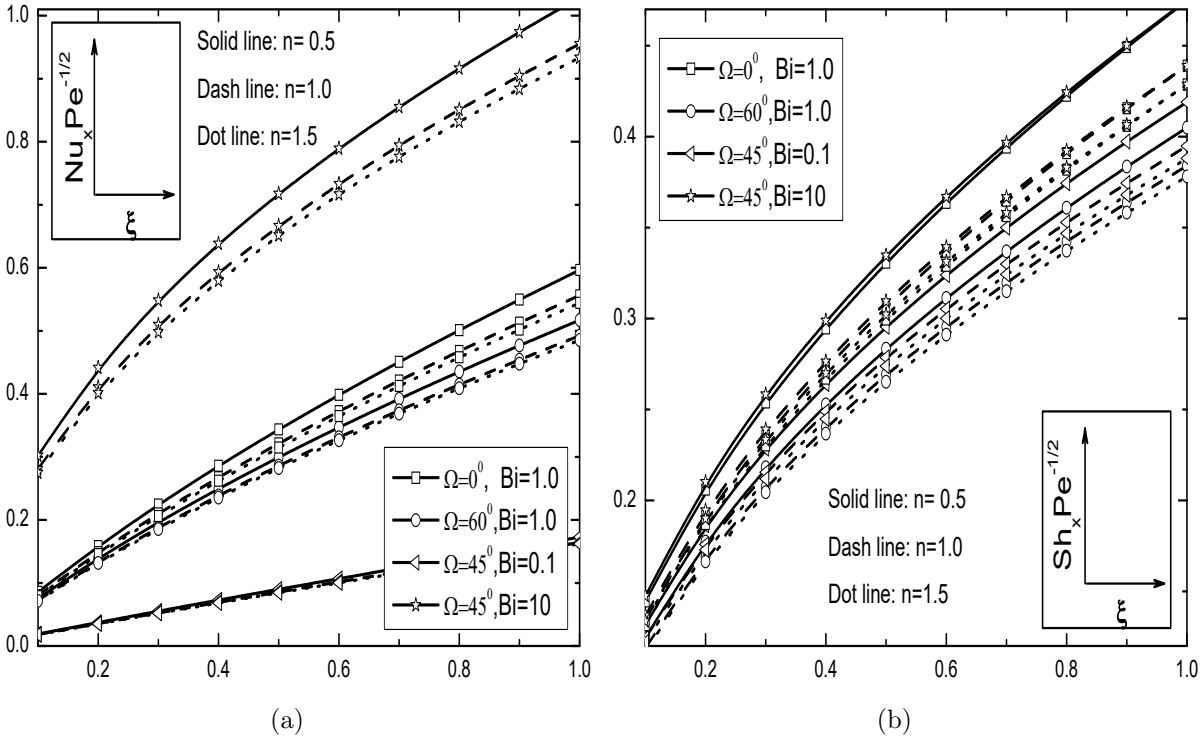

(a) (b)

Figure 7.11: *Effects of* Ω *and* Bi *for different values of* n *on the (a) Nusselt number and (b) Sherwood number against* ξ *with the fixed values of* $\alpha_1 = 1$, $\alpha_2 = 1$, $D_s = 0.6$ *and* $D_c = 0.3$.

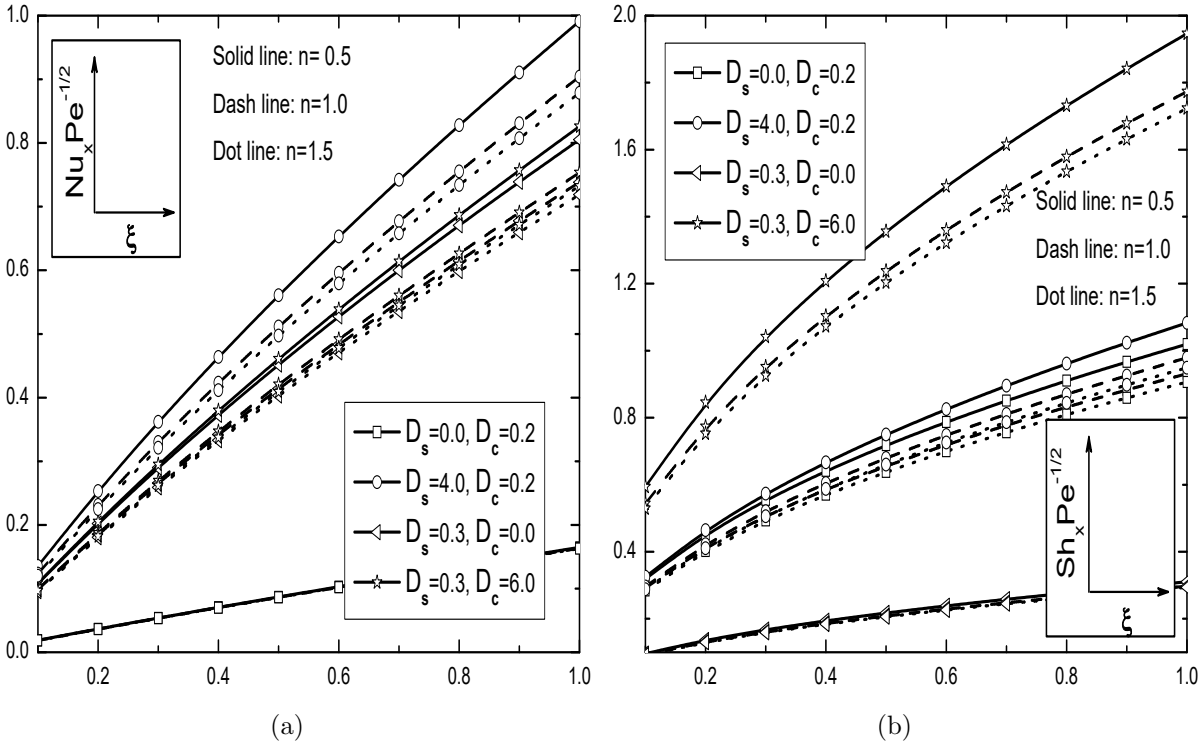

(a) (b)

Figure 7.12: *Effects of* D_s *and* D_c *for different values of* n *on the (a) Nusselt number and (b) Sherwood number against* ξ *with the fixed values of* $Bi = 0.1$, $\alpha_1 = 1$, $\alpha_2 = 1$ *and* $\Omega = 30^0$.

7.3 Conclusions

The influence of double dispersion on the nonlinear convective flow of an incompressible power-law fluid over an inclined plate in a non-Darcy porous medium subject to the convective boundary condition, is investigated in this chapter. The resultant non-similarity equations are solved using the successive linearization method together with the local similarity and local non-similarity procedures. Based on the analysis carried out, the main conclusions drawn for both case (a) and case (b) are given below:

The behavior of nonlinear convection parameters (α_1 and α_2) on the various profiles, Nusselt and Sherwood numbers in both case (a) and case (b), is similar to the results of chapter-5. As Biot number enhances, the velocity and temperature profiles along with the heat transfer rate enhance, whereas the mass transfer rate diminishes for both the cases (a) and (b). The temperature and concentration increase, but the velocity, heat and mass transfer rates decrease, with an increase in inclination angle in both the cases (a) and (b). Further, it is found that the velocity and local Nusselt number increase, whereas the concentration decrease with the increase of thermal dispersion parameter. As the solutal dispersion parameter enhances, the velocity, concentration and local Sherwood number enhance, whereas the temperature decreases in both case (a) and case (b).

Part IV

SUMMARY AND CONCLUSIONS

Chapter 8

Summary and Conclusions

In this thesis, analysis of convective heat and mass transfer over an inclined plate in micropolar and power-law fluids saturated non-Darcy porous medium subject to convective boundary condition is discussed. Additionally, the effect of nonlinear Boussinesq approximation (also known as nonlinear convection) is considered in the momentum equation to address the heat and mass transfer phenomena of some thermal systems which are operated at moderate to very high temperatures. The study of convective boundary condition has significant importance in heat transfer problems because it is more realistic and general, particularly in various engineering and industrial processes.

The non-similarity solution for a convective flow along an inclined plate immersed in a micropolar fluid saturated non-Darcy porous medium is analyzed in part-II. The objective of this part is to study the effects of Biot number, micropolar parameter, non-Darcy parameter, Soret number, Dufour number, nonlinear convection parameters, and the thermal and solutal dispersion parameters on the free and mixed convective flows of a micropolar fluid. The governing coupled nonlinear partial differential equations of the considered problem are cast into a sequence of nonlinear ordinary differential equations by the local similarity and local non-similarity techniques. Then the successive linearization method (SLM) is used to solve these transformed set of nonlinear ordinary differential equations. The main conclusions of the analysis carried out in part-II for both case (a) and case (b) are given below:

- An increase in coupling number, increases the temperature, concentration, skin friction and wall couple stress but reduces the heat and mass transfer rates for both free and mixed

convective flows in the presence of cross-diffusion and double dispersion parameters. In the absence of cross-diffusion and double dispersion parameters, wall couple stress decreases in both free and mixed convective flows. Moreover, the velocity increases near the plate and far away from the plate, it shows reverse behavior in case of free convection, while in mixed convective flow the velocity increases and reaches free stream velocity for both opposing and aiding flows.

- For free convective flows, the velocity, temperature, skin friction, wall couple stress and heat transfer rates increase and concentration decreases with the increase of Biot number. Meanwhile, for mixed convective flows, the velocity, skin friction, wall couple stress and heat transfer rate increase. But, concentration decreases in aiding flow of case (b) whereas in opposing flow these all show a reverse trend.

- Higher values of both the NDT and NDC parameters results higher velocity and microrotation, but lower temperature and concentration in both cases (a) and (b). Also, the surface drag, wall couple stress, heat and mass transfer rates increase in both cases (a) and (b). Further, the presence of cross-diffusion and double dispersion effects has unaltered the influence of nonlinear convection parameters in this study.

- As the Forchheimer number increases, the velocity and microrotation decrease near the plate and away from the plate in case (a) and case (b). But the local heat and mass transfer rates decrease in case (a). The behaviors of physical quantities of the flow in case (b) show an opposite nature.

- In the presence or absence of cross-diffusion and double dispersion effects, a rise in inclination angle reduces the velocity and microrotation whereas temperature and concentration decreased in case (a) and aiding flow of case (b). But, in opposing flow of case (b) it shows opposite trend.

- A rise in Dufour number increases the temperature of the micropolar fluid and decrease the concentration in both the free and mixed convective flows. But, Soret number shows the opposite influence on these profiles. Further, the heat transfer rate increases with Dufour number in case (a) and decreases in case (b), whereas Soret number has opposite influence on heat transfer rate as compared with Dufour number results in both cases.

- In case (a), the mass transfer rate increases with Soret number and decrease with Dufour number, whereas in case (b) mass transfer has opposite influence with both Soret and Dufour numbers when compared with the results of case (a).

- Soret and Dufour effects has nominal influence on the microrotation and wall couple stress in both case (a) and (b), whereas considerable variation is noticed in velocity and skin friction.

- An increase in the thermal dispersion parameter decreases the temperature and increases the rate of heat transfer in case (a) and aiding flow of case (b). On the other hand, both the concentration and mass transfer rate increase with an increase in the solutal dispersion parameter. But, both wall couple stress and skin friction decrease for thermal dispersion parameter whereas these increase for solutal dispersion parameter in both case (a) and aiding flow of case (b).

Part-III deals with a non-similarity solution for the nonlinear convective flow of a power-law fluid along an inclined plate in a non-Darcy porous medium with convective boundary condition. Additionally, the influences of cross-diffusion and double dispersion effects are analyzed in some of the chapters. To study the influence of pertinent parameters like Biot number, Soret number, Dufour number, inclination angle, viscosity index, thermal and solutal dispersions on velocity, temperature and concentration profiles along with heat and mass transfer rates are the objectives of this section. Using the non-dimensional variables, the governing equations are transformed into nonlinear partial differential equations. These equations are solved using the successive linearization method along with local similarity and non-similarity procedures. The important observations from these investigations are as following:

- In the presence and absence of both double dispersion and cross-diffusion, the velocity decreases with viscosity index, but the temperature and concentration increase in both free and mixed convective flows. The heat and mass transfer rates increases with viscosity index in the absence of both double dispersion and cross-diffusion effects, whereas these transfer rates show the opposite trend when only one of these effects are present.

- An enhancement in the Biot number, the velocity, temperature, and heat transfer rate enhance but, concentration reduces for both case (a) and case (b). Further, the mass transfer rate increases in the absence of Soret number but decreases in the presence of Soret number.

- The changes in inclination angle reduces the velocity and increases both temperature and concentration for both case (a) and case (b), and also in the presence or absence of dispersion and cross-diffusion parameters. Further, the heat and mass transfer rates decrease for higher values of inclination angle, but the influence of viscosity index depends on inclination angle.

- The higher values of nonlinear convection parameters result in lower temperature and concentration, but higher velocity, heat, and mass transfer rates. The physical quantities of the flow in case (a) and case (b) show the same behavior and also in the presence or absence of cross-diffusion and dispersion parameters.

- The velocity, concentration and local heat transfer rate enhance, whereas the temperature and local mass transfer rates reduce with the increase of Soret number in both case (a) and case (b).

- In both case (a) and case (b), the velocity, temperature and mass transfer rate increase, but the concentration and heat transfer rate decrease with the increase of Dufour number.

- Soret and Dufours numbers have an opposite influence on Nusselt and Sherwood number and these two transfer rates are more in pseudo-plastic fluid when compared with Newtonian and dilatant fluids.

- The velocity, temperature and local heat transfer rate increase, whereas the concentration decrease with the increase of thermal dispersion parameter in both free and mixed convective flows.

- As the solutal dispersion parameter increases, the velocity, concentration and local mass transfer rate enhances, whereas temperature decreases in both free and mixed convective flows. However, the presence of dispersion parameters can change the influence of viscosity index on the heat transfer rate in case (a).

Comparison between the Part-II and Part-III results

- Changes in different profiles with stream-wise coordinate proved that the present results are non-similar and hence, the present solutions are not unique for different values of the stream-wise coordinate in both the problems of micropolar and power-law fluids.

- By the experience of these two NDT and NDC parameters, one can conclude that the influence of NDC parameter is more prominent compared with that of NDT parameter in both free and mixed convective flows. This is due to the presence of Biot number which controls the influence of NDT parameter.

- Influence of nonlinear convection parameters is more in the presence of cross-diffusion and dispersion effects in both free and mixed convective flows of both micropolar and power-law fluids.

- In both micropolar and power-law fluids, the nonlinear differences between the wall and ambient medium improve with bigger estimations of NDT and NDC parameters, and in view of this, there is tremendous addition in the velocity, microrotation (in the case of micropolar fluid) and little change in temperature and concentration is obtained. However, the changes in velocity and angular velocity (in the case of micropolar fluid) of the fluid are more in the Darcy porous medium when compared with non-Darcy porous medium results.

- Influence of Biot number is unaffected in the presence of cross-diffusion and double dispersion effects in both micropolar and power-law fluids. Also, the presence of cross-diffusion and double dispersion effects does not control the influence of inclination angle in both micropolar and power-law fluids.

The work presented in this thesis can be extended to investigate the effects of Joule heating, MHD, Hall and Ion slip, heat source/sink, first and second order slip, etc. Further, this work can be extended with the analysis for various non-Newtonian fluids like nanofluids, Casson fluids, Jeffrey fluids, etc. Moreover, stability analysis has attracted the curiosity of many researchers in the recent past. Thus, the work presented in this thesis can be extended to study the stability and convergence analysis. Such an exhaustive study can be a rewarding experience though it is challenging as well as time-consuming.

Bibliography

[1] E.M. Abo-Eldahab and M.A. El Aziz. Flow and heat transfer in a micropolar fluid past a stretching surface embedded in a non-Darcian porous medium with uniform free stream. *Applied Mathematics and Computation*, 162(2):881–899, 2005.

[2] A.A. Afify and N.S. Elgazery. Effect of double dispersion on non-Darcy mixed convective flow over vertical surface embedded in porous medium. *Applied Mathematics and Mechanics*, 34(10):1247–1262, 2013.

[3] G. Ahmadi. Self-similar solution of incompressible micropolar boundary layer flow over a semi-infinite plate. *Internationl Journal of Engineering Science*, 14:639–646, 1976.

[4] J. Ahmed, A. Begum, A. Shahzad, and R. Ali. MHD axisymmetric flow of power-law fluid over an unsteady stretching sheet with convective boundary conditions. *Results in Physics*, 6:973–981, 2016.

[5] M.S. Alam and M.M. Rahman. Dufour and Soret effects on mixed convection flow past a vertical porous flat plate with variable suction. *Nonlinear Analysis: Modelling and Control*, 11(1):3–12, 2006.

[6] M.S. Alam, M.M. Rahman, and M.A. Sattar. Effects of variable suction and thermophoresis on steady MHD combined free-forced convective heat and mass transfer flow over a semi-infinite permeable inclined plate in the presence of thermal radiation. *International Journal of Thermal Sciences*, 47(6):758–765, 2008.

[7] F. Aman, A. Ishak, and I. Pop. MHD stagnation point flow of a micropolar fluid toward a vertical plate with a convective surface boundary condition. *Bulletin of the Malaysian Mathematical Sciences Society*, 36(4), 2013.

[8] T. Ariman, M.A. Turk, and N.D. Sylvester. Microcontinuum fluid mechanics–A review. *International Journal of Engineering Science*, 11(8):905–930, 1973.

[9] T. Ariman, M.A. Turk, and N.D. Sylvester. Applications of microcontinuum fluid mechanics. *International Journal of Engineering Science*, 12(4):273–293, 1974.

[10] F. Awad and P. Sibanda. Dufour and Soret effects on heat and mass transfer in a micropolar fluid in a horizontal channel. *WSEAS Transanctions Heat Mass Transfer*, 5:165–177, 2010.

[11] F.G. Awad, P. Sibanda, S.S. Motsa, and O.D. Makinde. Convection from an inverted cone in a porous medium with cross-diffusion effects. *Computers & Mathematics with Applications*, 61(5):1431–1441, 2011.

[12] F.G. Awad, P. Sibanda, and P.V.S.N. Murthy. A note on double dispersion effects in a nanofluid flow in a non-Darcy porous medium. *Journal of Heat Transfer*, 137(10):104501, 2015.

[13] A. Aziz. A similarity solution for laminar thermal boundary layer over a flat plate with a convective surface boundary condition. *Communications in Nonlinear Science and Numerical Simulation*, 14(4):1064–1068, 2009.

[14] M. Bandaru, M.M. Rashidi, and S.H. Raju. Influence of non-linear convection and thermophoresis on heat and mass transfer from a rotating cone to fluid flow in porous medium. *Thermal Science*, 21:2781–2793, 2017.

[15] H. Barrow and T.L. Sitharamarao. Effect of variation in volumetric expansion coefficient on free convection heat transfer. *British Chemical Engineering*, 16(8):704–709, 1971.

[16] O.A. Bég, R. Bhargava, S. Rawat, and E. Kahya. Numerical study of micropolar convective heat and mass transfer in a non-Darcy porous regime with Soret and Dufour diffusion effects. *Emirates Journal for Engineering Research*, 13(2):51–66, 2008.

[17] O.A. Bég, V.R. Prasad, B. Vasu, N.B. Reddy, Q. Li, and R. Bhargava. Free convection heat and mass transfer from an isothermal sphere to a micropolar regime with Soret/Dufour effects. *International Journal of Heat and Mass Transfer*, 54(1-3):9–18, 2011.

[18] O.A. Bég, M.J. Uddin, M.M. Rashidi, and N. Kavyani. Double-diffusive radiative magnetic mixed convective slip flow with Biot and Richardson number effects. *Journal of Engineering Thermophysics*, 23(2):79–97, 2014.

[19] A. Bejan. *Convection heat transfer*. John Wiley & Sons, 2013.

[20] A.J. Benazir and R. Sivaraj. Influence of double dispersion on non-Darcy free convective Magnetohydrodynamic flow of Casson fluid. In *Proceedings of Fifth International Conference on Soft Computing for Problem Solving*, pages 537–551. Springer, 2016.

[21] C. Canuto, M.Y. Hussaini, A. Quarteroni, and T.A. Zang. *Spectral Methods*. Springer, 2006.

[22] A.J. Chamkha, S. Abbasbandy, and A.M. Rashad. Non-Darcy natural convection flow for non-Newtonian nanofluid over cone saturated in porous medium with uniform heat and volume fraction fluxes. *International Journal of Numerical Methods for Heat & Fluid Flow*, 25(2):422–437, 2015.

[23] A.J. Chamkha, C. Issa, and K. Khanafer. Natural convection from an inclined plate embedded in a variable porosity porous medium due to solar radiation. *International Journal of Thermal Sciences*, 41(1):73–81, 2002.

[24] C. Chang and Z. Lee. Free convection on a vertical plate with uniform and constant heat flux in a thermally stratified micropolar fluid. *Mechanics Research Communications*, 35(6):421–427, 2008.

[25] C.L. Chang. Numerical simulation of micropolar fluid flow along a flat plate with wall conduction and buoyancy effects. *Journal of Physics D: Applied Physics*, 39(6):1132, 2006.

[26] W. Chaoyang, T. Chuanjing, and Z. Xiaofen. Mixed convection of non-Newtonian fluids from a vertical plate embedded in a porous medium. *Acta Mechanica Sinica*, 6(3):214–220, 1990.

[27] C.H. Chen. Heat and mass transfer in MHD flow by natural convection from a permeable, inclined surface with variable wall temperature and concentration. *Acta Mechanica*, 172(3-4):219–235, 2004.

[28] H.T. Chen. Free convection flow of non-Newtonian fluids along a vertical plate embedded in a porous medium. *Journal of Heat Transfer*, 110(1), 1988.

[29] H.T. Chen. Natural convection of a non-Newtonian fluid about a horizontal cylinder and a sphere in a porous medium. *International Communications in Heat and Mass Transfer*, 15(5):605–614, 1988.

[30] C.Y. Cheng. Natural convection heat and mass transfer near a vertical wavy surface with constant wall temperature and concentration in a porous medium. *International Communications in Heat and Mass Transfer*, 27(8):1143–1154, 2000.

[31] C.Y. Cheng. Combined heat and mass transfer in natural convection flow from a vertical wavy surface in a power-law fluid saturated porous medium with thermal and mass stratification. *International Communications in Heat and Mass Transfer*, 36(4):351–356, 2009.

[32] P. Cheng. Combined free and forced boundary layer flows about inclined surfaces in a porous medium. *NASA STI/Recon Technical Report N*, 77, 1976.

[33] S.C. Cowin. Polar fluids. *The Physics of Fluids*, 11(9):1919–1927, 1968.

[34] H. Darcy. *The Flow of Homogeneous Fluids Through Porous Media*. Victor Dalmont, Paris, 1856.

[35] A. De Waele. Viscometry and plastometry. *Oil Color Chem Assoc J*, 6(33):e88, 1923.

[36] Z. Dursunkaya and M. William Worek. Diffusion-thermo and thermal-diffusion effects in transient and steady natural convection from a vertical surface. *International Journal of Heat and Mass Transfer*, 35(8):2060–2065, 1992.

[37] E.R.G. Eckert and R.M. Drake Jr. Analysis of heat and mass transfer. 1987.

[38] M.F. El-Amin. Combined effect of magnetic field and viscous dissipation on a power-law fluid over plate with variable surface heat flux embedded in a porous medium. *Journal of Magnetism and Magnetic Materials*, 261(1-2):228–237, 2003.

[39] V.A. Eremeyev, L.P. Lebedev, and H. Altenbach. *Foundations of Micropolar Mechanics*. Springer Science & Business Media, 2012.

[40] A. Eringen. Theory of micropolar fluids. *Journal of Mathematics and Mechanics*, pages 1–18, 1966.

[41] T. Hayat, Z. Abbas, and T. Javed. Mixed convection flow of a micropolar fluid over a non-linearly stretching sheet. *Physics Letters A*, 372:637–647, 2008.

[42] T. Hayat, M. Mustafa, and S. Obaidat. Soret and Dufour effects on the stagnation-point flow of a micropolar fluid toward a stretching sheet. *Journal of Fluids Engineering*, 133(2):021202, 2011.

[43] T. Hayat, M. Waqas, S.A. Shehzad, and A. Alsaedi. Mixed convection radiative flow of Maxwell fluid near a stagnation point with convective condition. *Journal of Mechanics*, 29(3):403–409, 2013.

[44] K.A. Helmy, H.F. Idriss, and S.E. Kassem. MHD free convection flow of a micropolar fluid past a vertical porous plate. *Canadian Journal of Physics*, 80(12):1661–1673, 2002.

[45] M. Huang, J. Huang, Y. Chou, and C. Chen. Effects of prandtl number on free convection heat transfer from a vertical plate to a non-Newtonian fluid. *Journal of Heat Transfer*, 111(1), 1989.

[46] F.S. Ibrahim, S.M. Abdel-Gaid, and R. Subba Reddy Gorla. Non-Darcy mixed convection flow along a vertical plate embedded in a non-Newtonian fluid saturated porous medium with surface mass transfer. *International Journal of Numerical Methods for Heat & Fluid Flow*, 10(4):397–408, 2000.

[47] D.B. Ingham and I. Pop. *Transport Phenomena in Porous Media III*, volume 3. Elsevier, 2005.

[48] S.K. Jena and M.N. Mathur. Mixed convection flow of a micropolar fluid from an isothermal vertical plate. *Computers & Mathematics with Applications*, 10(3):291–304, 1984.

[49] R.Y. Jumah and A.S. Mujumdar. Free convection heat and mass transfer of non-Newtonian power law fluids with yield stress from a vertical flat plate in saturated porous media. *International Communications in Heat and Mass Transfer*, 27(4):485–494, 2000.

[50] R.R. Kairi and P.V.S.N. Murthy. Free convection in a thermally stratified non-Darcy porous medium saturated with a non-Newtonian fluid. *International Journal of Fluid Mechanics Research*, 36(5), 2009.

[51] R.R. Kairi and P.V.S.N. Murthy. Effect of double dispersion on mixed convection heat and mass transfer in a non-Newtonian fluid-saturated non-Darcy porous medium. *Journal of Porous Media*, 13(8), 2010.

[52] R.R. Kairi and P.V.S.N. Murthy. Effect of viscous dissipation on natural convection heat and mass transfer from vertical cone in a non-Newtonian fluid saturated non-Darcy porous medium. *Applied Mathematics and Computation*, 217(20):8100–8114, 2011.

[53] R.R. Kairi, P.A.L. Narayana, and P.V.S.N. Murthy. The effect of double dispersion on natural convection heat and mass transfer in a non-Newtonian fluid saturated non-Darcy porous medium. *Transport in Porous Media*, 76(3):377–390, 2009.

[54] P.K. Kameswaran, P. Sibanda, M.K. Partha, and P.V.S.N. Murthy. Thermophoretic and nonlinear convection in non-Darcy porous medium. *Journal of Heat Transfer*, 136(4):042601, 2014.

[55] W.A. Khan and R.S.R. Gorla. Heat and mass transfer in power-law nanofluids over a non-isothermal stretching wall with convective boundary condition. *Journal of Heat Transfer*, 134(11):112001, 2012.

[56] A.A. Khidir, M. Narayana, P. Sibanda, and P.V.S.N. Murthy. Natural convection from a vertical plate immersed in a power-law fluid saturated non-Darcy porous medium with viscous dissipation and Soret effects. *Afrika Matematika*, 26(7-8):1495–1518, 2015.

[57] Y.J. Kim. Heat and mass transfer in MHD micropolar flow over a vertical moving porous plate in a porous medium. *Transport in Porous Media*, 56(1):17–37, 2004.

[58] M. Kumari and G. Nath. Non-Darcy mixed convection in power-law fluids along a non-isothermal horizontal surface in a porous medium. *International Journal of Engineering Science*, 42(3-4):353–369, 2004.

[59] J.R. Lloyd and E.M. Sparrow. Combined forced and free convection flow on vertical surfaces. *International Journal of Heat and Mass Transfer*, 13(2):434–438, 1970.

[60] G. Lukaszewicz. *Micropolar fluids: theory and applications*. Springer Science & Business Media, 1999.

[61] A. Mahdy. Soret and Dufour effect on double diffusion mixed convection from a vertical surface in a porous medium saturated with a non-Newtonian fluid. *Journal of Non-Newtonian Fluid Mechanics*, 165(11-12):568–575, 2010.

[62] O.D. Makinde and A. Aziz. MHD mixed convection from a vertical plate embedded in a porous medium with a convective boundary condition. *International Journal of Thermal Sciences*, 49(9):1813–1820, 2010.

[63] O.D. Makinde, K. Zimba, and O.A. Bég. Numerical study of chemically-reacting hydromagnetic boundary layer flow with Soret/Dufour effects and a convective surface boundary condition. *International Journal of Thermal and Environmental Engineering*, 4(1):89–98, 2012.

[64] Z.G. Makukula, P. Sibanda, and S.S. Motsa. A novel numerical technique for two-dimensional laminar flow between two moving porous walls. *Mathematical Problems in Engineering*, 2010, 2010.

[65] W.J. Minkowycz and E.M. Sparrow. Local nonsimilar solutions for natural convection on a vertical cylinder. *Journal of Heat Transfer*, 96(2):178–183, 1974.

[66] S.S. Motsa, F.G. Awad, Z.G. Makukula, and P. Sibanda. The spectral homotopy analysis method extended to systems of partial differential equations. *Abstract and Applied Analysis*, 2014:1–11, 2014.

[67] P.V.S.N. Murthy. Effect of double dispersion on mixed convection heat and mass transfer in non-Darcy porous medium. *Journal of Heat Transfer*, 122(3):476–484, 2000.

[68] P.V.S.N. Murthy, Ch. RamReddy, A.J. Chamkha, and A.M. Rashad. Magnetic effect on thermally stratified nanofluid saturated non-Darcy porous medium under convective boundary condition. *International Communications in Heat and Mass Transfer*, 47:41–48, 2013.

[69] P.V.S.N. Murthy and P. Singh. Heat and mass transfer by natural convection in a non-Darcy porous medium. *Acta Mechanica*, 138(3-4):243–254, 1999.

[70] P.V.S.N. Murthy, A. Sutradhar, and Ch. RamReddy. Double-diffusive free convection flow past an inclined plate embedded in a non-Darcy porous medium saturated with a nanofluid. *Transport in Porous Media*, 98(3):553–564, 2013.

[71] A.S.N. Murti, P.K. Kameswaran, and T.P. Kantha. Radiation, chemical reaction, double dispersion effects on heat and mass transfer in non-Newtonian fluids. *International Journal of Engineering*, 4(1):13–25, 2010.

[72] A. Nakayama and A.V. Shenoy. Combined forced and free convection heat transfer in power-law fluid-saturated porous media. *Applied Scientific Research*, 50(1):83–95, 1993.

[73] M. Narayana, A.A. Khidir, P. Sibanda, and P.V.S.N. Murthy. Soret effect on the natural convection from a vertical plate in a thermally stratified porous medium saturated with non-Newtonian liquid. *Journal of Heat Transfer*, 135(3):032501, 2013.

[74] P.A.L. Narayana and P. Sibanda. Influence of the Soret effect and double dispersion on MHD mixed convection along a vertical flat plate in non-Darcy porous medium. *International Journal of Nonlinear Science*, 12:352–364, 2011.

[75] D.A. Nield and A. Bejan. *Convection in Porous Media, 4th Ed.* Springer-Verlag, New York, 2013.

[76] W. Ostwald and R. Auerbach. Ueber die viskosität kolloider lösungen im struktur-, laminar- und turbulenzgebiet. *Kolloid-Zeitschrift*, 38(3):261–280, 1926.

[77] D. Pal, G. Mandal, and K. Vajravalu. Soret and Dufour effects on MHD convective–radiative heat and mass transfer of nanofluids over a vertical non-linear stretching/shrinking sheet. *Applied Mathematics and Computation*, 287:184–200, 2016.

[78] Dulal Pal and Sewli Chatterjee. Soret and dufour effects on mhd convective heat and mass transfer of a power-law fluid over an inclined plate with variable thermal conductivity in a porous medium. *Applied Mathematics and Computation*, 219(14):7556–7574, 2013.

[79] M.K. Partha. Nonlinear convection in a non-Darcy porous medium. *Applied Mathematics and Mechanics*, 31(5):565–574, 2010.

[80] I. Pop and T. Na. Free convection from an arbitrarily inclined plate in a porous medium. *Heat and Mass Transfer*, 32(1-2):55–59, 1996.

[81] M.M. Rahman, M.J. Uddin, and A. Aziz. Effects of variable electric conductivity and non-uniform heat source (or sink) on convective micropolar fluid flow along an inclined flat plate with surfaceheat flux. *International Journal of Thermal Sciences*, 48(12):2331–2340, 2009.

[82] Ch RamReddy and T Pradeepa. Spectral quasi-linearisation method for nonlinear thermal convection flow of a micropolar fluid under convective boundary condition. *Nonlinear Engineering*, 5(3):193–204, 2016.

[83] Ch. RamReddy, T. Pradeepa, and D. Srinivasacharya. Similarity solution for free convection flow of a micropolar fluid under convective boundary condition via lie scaling group transformations. *Advances in High Energy Physics*, 2015, 2015.

[84] M. Ramzan, M. Farooq, T. Hayat, and J.D. Chung. Radiative and Joule heating effects in the MHD flow of a micropolar fluid with partial slip and convective boundary condition. *Journal of Molecular Liquids*, 221:394–400, 2016.

[85] S. Rawat, R. Bhargava, R. Bhargava, and O.A. Bég. Transient magneto-micropolar free convection heat and mass transfer through a non-Darcy porous medium channel with variable thermal conductivity and heat source effects. *Proceedings of the Institution of Mechanical Engineers, Part C: Journal of Mechanical Engineering Science*, 223(10):2341–2355, 2009.

[86] S. Rawat, S. Kapoor, and R. Bhargava. MHD flow heat and mass transfer of micropolar fluid over a nonlinear stretching sheet with variable micro inertia density, heat flux and chemical reaction in a non-Darcy porous medium. *Journal of Applied Fluid Mechanics*, 9(1), 2016.

[87] G.V.R. Reddy and Y. Hari Krishna. Soret and Dufour effects on MHD micropolar fluid flow over a linearly stretching sheet, through a non-Darcy porous medium. *International Journal of Applied Mechanics and Engineering*, 23(2):485–502, 2018.

[88] S. Shafie. Heat and mass transfer in a MHD non-Darcian micropolar fluid over an unsteady stretching sheet with non-uniform heat source/sink and thermophoresis. *Heat TransferAsian Research*, 41(7):601–612, 2012.

[89] A. Shahzad and A. Ramzan. MHD flow of a non-Newtonian power law fluid over a vertical stretching sheet with the convective boundary condition. *Walailak Journal of Science and Technology (WJST)*, 10(1):43–56, 2012.

[90] S.A. Shehzad, M. Waqas, A. Alsaedi, and T. Hayat. Flow and heat transfer over an unsteady stretching sheet in a micropolar fluid with convective boundary condition. *Journal of Applied Fluid Mechanics*, 9(3), 2016.

[91] A.V. Shenoy. Darcy-Forchheimer natural, forced and mixed convection heat transfer in non-Newtonian power-law fluid-saturated porous media. *Transport in Porous Media*, 11(3):219–241, 1993.

[92] A.V. Shenoy. Non-Newtonian fluid heat transfer in porous media. *Advances in Heat Transfer*, 24:102–191, 1994.

[93] P. Singh and K. Tewari. Non-Darcy free convection from vertical surfaces in thermally stratified porous media. *International Journal of Engineering Science*, 31(9):1233–1242, 1993.

[94] S. Sivasankaran, H. Niranjan, and M. Bhuvaneswari. Chemical reaction, radiation and slip effects on MHD mixed convection stagnation-point flow in a porous medium with convective boundary condition. *International Journal of Numerical Methods for Heat & Fluid Flow*, 27(2):454–470, 2017.

[95] E.M. Sparrow and H.S. Yu. Local non-similarity thermal boundary-layer solutions. *Journal of Heat Transfer*, 93(4):328–334, 1971.

[96] D. Srinivasacharya and Ch. RamReddy. Heat and mass transfer by natural convection in a doubly stratified non-Darcy micropolar fluid. *International Communications in Heat and Mass Transfer*, 37(7):873–880, 2010.

[97] D Srinivasacharya and Ch RamReddy. Mixed convection in a doubly stratified micropolar fluid saturated non-darcy porous medium. *The Canadian Journal of Chemical Engineering*, 90(5):1311–1322, 2012.

[98] D. Srinivasacharya and Ch. RamReddy. Mixed convection heat and mass transfer in a doubly stratified micropolar fluid. *Computational Thermal Sciences*, 5(4):273–287, 2013.

[99] D. Srinivasacharya, Ch. RamReddy, J. Pranitha, and A. Postelnicu. Soret and Dufour effects on non-Darcy free convection in a power-law fluid in the presence of a magnetic field and stratification. *Heat Transfer–Asian Research*, 43(7):592–606, 2014.

[100] D. Srinivasacharya and G. Swamy Reddy. Mixed convection heat and mass transfer over a vertical plate in a power-law fluid-saturated porous medium with radiation and chemical reaction effects. *Heat Transfer–Asian Research*, 42(6):485–499, 2013.

[101] J. Sui, L. Zheng, X. Zhang, and G. Chen. Mixed convection heat transfer in power law fluids over a moving conveyor along an inclined plate. *International Journal of Heat and Mass Transfer*, 85:1023–1033, 2015.

[102] G. Swapna, L. Kumar, O.A. Bég, and B. Singh. Finite element analysis of radiative mixed convection magneto-micropolar flow in a Darcian porous medium with variable viscosity and convective surface condition. *Heat Transfer–Asian Research*, 44(6):515–532, 2015.

[103] B. Tai and M. Char. Soret and Dufour effects on free convection flow of non-Newtonian fluids along a vertical plate embedded in a porous medium with thermal radiation. *International Communications in Heat and Mass Transfer*, 37(5):480–483, 2010.

[104] R.S. Telles and O.V. Trevisan. Dispersion in heat and mass transfer natural convection along vertical boundaries in porous media. *International Journal of Heat and Mass Transfer*, 36(5):1357–1365, 1993.

[105] K. Vafai. *Handbook of porous media*. CRC Press, 2015.

[106] K. Vajravelu and K.S. Sastri. Fully developed laminar free convection flow between two parallel vertical wallsi. *International Journal of Heat and Mass Transfer*, 20(6):655–660, 1977.

[107] T. Wang. The coupling of conduction with mixed convection of micropolar fluids past a vertical flat plate. *International Communications in Heat and Mass Transfer*, 25(8):1075–1084, 1998.

[108] N.A. Yacob and A. Ishak. Stagnation point flow towards a stretching/shrinking sheet in a micropolar fluid with a convective surface boundary condition. *The Canadian Journal of Chemical Engineering*, 90(3):621–626, 2012.